

70-15,465

SCHWARTZ, Leon Joseph, 1943-
INTERACTIONS OF REFRACTORY METAL SILICIDE
COATINGS WITH SUBSTRATES.

The City University of New York, Ph.D., 1970
Engineering, metallurgy

University Microfilms, A XEROX Company, Ann Arbor, Michigan

INTERACTIONS OF REFRACTORY
METAL SILICIDE COATINGS WITH SUBSTRATES

by

LEON J. SCHWARTZ

A dissertation submitted to the Graduate
Faculty in Engineering in partial
fulfillment of the requirements for the
degree of Doctor of Philosophy, The City
University of New York.

1969

This manuscript has been read and accepted
for the Graduate Faculty in Engineering in
satisfaction of the dissertation requirement
for the degree of Doctor of Philosophy.

January 7, 1970
date

Morris Kolodney
Chairman of Examining Committee

Jan 7, 1970
date

Lynne Greene
Executive Officer

Prof. Morris Ettenberg

Prof. Robert A. Graff

Prof. Morris Kolodney (Chairman)

Prof. Miriam Sarachik

Supervisory Committee

PLEASE NOTE:

Not original copy.
Some pages have very
light type. Filmed
as received.

University Microfilms

Acknowledgements

The author gratefully acknowledges and thanks the following people:

The National Aeronautics and Space Administration for their support through NASA Grant 33-013-017 to Professors M. Kolodney and R.A. Graff. The NASA Grant Administrator was Mr. Robert Oldrieve of the Lewis Research Center.

Professor Morris Kolodney of the Department of Chemical Engineering, The City University of New York, my mentor for five years, without whose guidance this work would have been impossible.

Professor Robert A. Graff of the Department of Chemical Engineering, The City University of New York, for his advice and encouragement.

Professor Clarence Anderson of the Department of Mechanical Engineering, The City University of New York, for his helpfulness with the statistical planning and analysis of this experimentation.

The entire Shop of the Department of Chemical Engineering, The City University of New York, for their assistance; particularly, Mr. David Marden.

My colleagues whose interest in this work provided a stimulating environment: Dr. Stanley Levine, Mr. Andrew Mueller and Dr. Frederic Schweitzer.

Finally, Mrs. Harlene Schrek, for her fine job of typing.

The author was supported initially by an NDEA Title IV Fellowship and later by a City University Fellowship.

Abstract

The growth rate of Ta_5Si_3 in the Ta/TaSi₂ system has been accurately measured. This was accomplished by contacting dense TaSi₂ wafers and wafers of Ta, holding the couple at a controlled temperature for the desired time and later measuring the thickness of the resultant intermediate zone. In the Arrhenius form the parabolic growth constant is:

$$k = 5e^{-77,000/RT}$$

where the activation energy is known with 95% confidence to be between 74,000 and 80,000 cal/mole and the pre-exponential constant is known with the same confidence to be between 2 and 11 cm²/sec. The rate of degradation of TaSi₂ in the Ta/TaSi₂ system has been measured separately and may be expressed as

$$k_1 = 2e^{-81,000/RT}.$$

The 95% confidence intervals are 74,000 to 88,000 cal/mole for the activation energy and 0.2 to 16 cm²/sec for the pre-exponential constant. Marker experiments indicated that only silicon diffuses.

Six metals were tested as barriers to the degradation of TaSi₂. They were: tungsten, rhenium, molybdenum, niobium (columbium), zirconium and titanium. None of the metals tested was effective in lowering the rate of loss of TaSi₂. In all but the Ti/TaSi₂ system, Si alone was

shown to diffuse. Incompatibility in the W/TaSi₂ and Re/TaSi₂ systems interrupted solid state diffusion and resulted in the vapor transport of Si, particularly during the early stages of the diffusion anneal. Fundamental activation energies for diffusion of silicon in four silicides have been determined. The four compounds are:

Ta₅Si₃; Q_{Si} = 77,000 cal/mole

Mo₃Si ; Q_{Si} = 58,000 cal/mole

Nb₅Si₃; Q_{Si} = 49,000 cal/mole

and Ti₅Si₃; Q_{Si} = 44,000 cal/mole.

Table of Contents

	<u>Page</u>
Acknowledgements	i
Abstract	iii
Table of Contents	v
List of Tables	ix
List of Figures	xi
List of Plates	xiv
I. Background	
A. General	
1. Introduction	1
2. Nature of Silicides	2
B. Theory	
1. Basic	5
2. Diffusion in Solids	5
3. Mechanisms	9
C. Diffusion Equations	13
1. Ta/TaSi ₂ System	14
2. Markers in the Ta/TaSi ₂ System	19
3. M/TaSi ₂ System	22
4. Markers in the M/TaSi ₂ System	29
5. Basis of Δx_1 Comparisons	31
D. Previous Work	31
II. Experimental	
A. General	34

	<u>Page</u>
B. TaSi ₂ Wafer Fabrication	
1. Powder Metallurgy and Sintering	35
2. Successful Procedures	36
3. Quality of TaSi ₂ Wafers	37
4. Natural Markers	40
C. Experimental Schedule	40
D. Apparatus	45
E. Measuring Techniques	48
III Experimental Results	
A. General Description	52
B. Specific Systems	
1. Ta/TaSi ₂	56
2. Diffusion Barrier Systems	62
a. Nb/TaSi ₂	62
b. Zr/TaSi ₂	69
c. Ti/TaSi ₂	75
d. W/TaSi ₂	81
e. Mo/TaSi ₂	86
f. Re/TaSi ₂	90
C. Comparative Results and Effect of Temperature	92
D. Results of Marker Experiments	
1. Ta/TaSi ₂ System	98
2. M/TaSi ₂ Systems	99
E. Plots of Experimental Results	

	<u>Page</u>
1. Parabolic Plots	101
2. Zone Profile/Concentration Change Profile Plots	104
3. Temperature Dependence (Arrhenius) Plots	124
IV Photomicrographs (Plates)	129
V Discussion	
A. The Ta/TaSi ₂ Couple	
1. Comparison of Results	143
2. Significance of Results	145
B. Barriers	
1. Effectiveness of Metals Tested	147
2. Factors Influencing the Effective- ness of Test Metals	148
a. Phases Formed	148
b. Compatibility	156
C. Relationship of D's to k's	157
D. Unusual Behavior	164
1. Atypical Diffusion Zone in the Ta/TaSi ₂ System	164
2. Cusps in the Ti/TaSi ₂ System	165
VI Conclusion	167
VII Areas of Further Investigation	168
Appendix I: Phase Diagrams	169
Appendix II: Materials and Etching Reagents	175
Appendix III: Details of TaSi ₂ Wafer Production	177

	<u>Page</u>
Appendix IV: Details of X-Ray Diffraction Analysis	181
Appendix V: Plan for the Statistical Analysis of the Data	195
Bibliography	199

List of Tables

<u>Table</u>	<u>Title</u>	<u>Page</u>
I	Ratio of Silicon Atom Radius to Radii of Some Refractory Metal Atoms	3
II	Resistivities of Silicides Compared to Metals	4
III	Ta/TaSi ₂ System - Parabolic Rate Constants	57
IV	Nb/TaSi ₂ System - Parabolic Rate Constants	64
V	Zr/TaSi ₂ System - Parabolic Rate Constants	71
VI	Ti/TaSi ₂ System - Parabolic Rate Constants	78
VII	W/TaSi ₂ System - Parabolic Rate Constants	82, 82a
VIII	Mo/TaSi ₂ System - Parabolic Rate Constants	87
IX	Arrhenius Expressions for Growth Rates (Complete Data)	93
X	Arrhenius Expressions for Growth Rates (Incomplete Data)	94
XI	Results of Marker Experiments for Ta/TaSi ₂	99
XII	Calculated Times to Grow a 1 Mil Layer of Ta ₅ Si ₃ and Lose 1 Mil TaSi ₂	145
XIII	Summary of Intermediate Phases Found	150
XIV	Thermodynamically Stable Phases	154
XV	Structural Correlation of Silicide Formation	155

<u>Table</u>	<u>Title</u>	<u>Page</u>
XVI	Elastic Moduli of Some Refractory Metals	157
XVII	Comparison of Activation Energies	163
IV-I	X-Ray Analysis of Good TaSi ₂ Wafers at Different Stages ² of Fabrication	186
IV-II	X-Ray Analysis of TaSi ₂ Surfaces After Sintering	187
IV-III	X-Ray Analysis at Ta ₅ Si ₃ Zones Near the Original Interface in Different M/TaSi ₂ Couples	188
IV-IV	X-Ray Analysis of the Re Side of a Re/TaSi ₂ Couple Annealed at 2100°F for 7 Hours	191
IV-V	Results of X-Ray Analysis on a Powder Sample Removed from the Surface of a Zr Wafer After Annealing Against TaSi ₂ for 72 hours at 2100°F	192
IV-VI	X-Ray Data for the Zr Side of a Zr/TaSi ₂ Couple Annealed at 2100°F	193
IV-VII	X-Ray Data for the Zr Side of a Zr/TaSi ₂ Couple Annealed at 2500°F	194

List of Figures

<u>Figure</u>	<u>Title</u>	<u>Page</u>
1	Ta/TaSi ₂ System	15
2	Markers in the Ta/TaSi ₂ System	20
3	M/TaSi ₂ System	23
4	Markers in the M/TaSi ₂ System	29
5	Flowsheet for TaSi ₂ Manufacture	37
6	Experimental Schedule	42
7	Diffusion Anneal Apparatus	46
8	Diffraction Scans Within the Ta/TaSi ₂ Diffusion Zone	51
9a	Parabolic Rate $\sim \Delta x = k' \sqrt{t}$: Ta/TaSi ₂ System. Total Zone. Complete - All Data	101
9b	Parabolic Rate $\sim \Delta x = k' \sqrt{t}$: Ta/TaSi ₂ System. Total Zone. Incomplete - Good Wafers Only (•)	102
10	Parabolic Rate $\sim \Delta x = k' \sqrt{t}$: W/TaSi ₂ System. Total Zone. Complete Data	103
11	ZP/CCP: Ta/TaSi ₂ Couple Annealed at 2100°F for 4 Hours	104
12	ZP/CCP: Ta/TaSi ₂ Couple Annealed at 2100°F for 100 Hours	105
13	ZP/CCP: Ta/TaSi ₂ Couple Annealed at 2500°F for 4 Hours	106
14	ZP/CCP: Ta/TaSi ₂ Couple Annealed at 2500°F for 100 Hours	107
15	ZP/CCP: Nb/TaSi ₂ Couple Annealed at 2100°F for 4 Hours	108
16	ZP/CCP: Nb/TaSi ₂ Couple Annealed at 2100°F for 100 Hours	109

<u>Figure</u>	<u>Title</u>	<u>Page</u>
17	ZP/CCP: Nb/TaSi ₂ Couple Annealed at 2500°F for 4 Hours	110
18	ZP/CCP: Nb/TaSi ₂ Couple Annealed at 2500°F for 48 Hours	111
19	ZP: Zr/TaSi ₂ Couple Annealed at 2100°F for 4 Hours	112
20	ZP: Zr/TaSi ₂ Couple Annealed at 2500°F for 72 Hours	113
21	ZP/CCP: Ti/TaSi ₂ Couple Annealed at 2100°F for 4 Hours	114
22	ZP/CCP: Ti/TaSi ₂ Couple, 72 Hours at 2400°F	115
23	ZP/CCP: W/TaSi ₂ Couple Annealed at 2100°F for 48 Hours	116
24	ZP/CCP: W/TaSi ₂ Couple, 100 Hours at 2100°F	117
25	ZP/CCP: W/TaSi ₂ Couple, 48 Hours at 2500°F	118
26	ZP/CCP: W/TaSi ₂ Couple Annealed at 2500°F for 100 Hours	119
27	CCP: Mo/TaSi ₂ Couple Annealed at 2100°F for 24 Hours	120
28	ZP/CCP: Mo/TaSi ₂ Couple, 72 Hours at 2100°F	121
29	ZP/CCP: Mo/TaSi ₂ Couple Annealed at 2500°F for 4 Hours	122
30	ZP/CCP: Mo/TaSi ₂ Couple Annealed at 2500°F for 100 Hours	123
31	Temperature Dependence of the Parabolic Rate Constant: Ta/TaSi ₂ System. Total Zone, Complete Data	124

<u>Figure</u>	<u>Title</u>	<u>Page</u>
32a	The Effect of Temperature on Parabolic Rate Constants: Total Zones, Complete Data	125
32b	The Effect of Temperature on Parabolic Rate Constants: Total Zones, Incomplete - Good Wafers Only	126
33a	The Effect of Temperature on Parabolic Rate Constants: Δx_1 (Ta_5Si_3) Zones, Complete Data	127
33b	The Effect of Temperature on Parabolic Rate Constants: Δx_1 (Ta_5Si_3) Zones, Incomplete - Good Wafers Only	128
34	Comparison of k_0 and $D \Delta N$ Values in a Coupled System: Nb/ $TaSi_2$ System	161
35	Comparison of k_0 and $D \Delta N$ Values for a Coupled System: Mo/ $TaSi_2$ System	162
I-1	Ta-Si Phase Diagram	169
I-2	Nb-Si Phase Diagram	170
I-3	Zr-Si Phase Diagram	171
I-4	Ti-Si Phase Diagram	172
I-5	W-Si Phase Diagram	173
I-6	Mo-Si Phase Diagram	174

List of Plates

<u>Plate</u>	<u>Title</u>	<u>Page</u>
I	Ta/TaSi ₂ Couple after 48 Hours at 2300°F	129
II	Ta/TaSi ₂ Couple Employing *-type TaSi ₂ Wafer after 48 Hrs. at 2500°F	129
III	Atypical Ta/TaSi ₂ Couple Employing "A" Type TaSi ₂ Wafers after 72 Hours at 2500°F	130
IV	Surface of "A" type TaSi ₂ Wafer	130
V	Ta/TaSi ₂ Couple Employing "B" type TaSi ₂ Wafer after 72 Hours at 2500°F	131
VI	Surface of "B" type TaSi ₂ Wafer	131
VII	Ta/TaSi ₂ Couple after 4 Hours at 2100°F	132
VIII	Ta/TaSi ₂ Couple after 100 Hours at 2400°F	132
IX	Nb/TaSi ₂ Couple after 4 Hours at 2100°F	133
X	Nb/TaSi ₂ Couple after 4 Hours at 2500°F	133
XI	Nb/TaSi ₂ Couple After 24 Hours at 2200°F	134
XII	Nb/TaSi ₂ Couple After 48 Hours at 2200°F	134
XIII	Nb/TaSi ₂ Couple After 72 Hours at 2200°F	134
XIV	Zr/TaSi ₂ Couple After 4 Hours at 2100°F	135
XV	Zr/TaSi ₂ Couple After 48 Hours at 2200°F	135

<u>Plate</u>	<u>Title</u>	<u>Page</u>
XVI	Zr/TaSi ₂ Couple after 4 Hours at 2400°F	136
XVII	Zr/TaSi ₂ Couple after 72 Hours at 2500°F	136
XVIII	Ti/TaSi ₂ Couple after 4 Hours at 2100°F	137
XIV	Ti/TaSi ₂ Couple after 24 Hours at 2400°F	137
XX	W/TaSi ₂ Couple after 48 Hours at 2100°F	138
XXI	W/TaSi ₂ Couple after 100 Hours at 2400°F	138
XXII	Mo/TaSi ₂ Couple after 48 Hours at 2100°F	139
XXIII	Mo/TaSi ₂ Couple after 100 Hours at 2500°F	139
XXIV	Re/TaSi ₂ Couple after 100 Hours at 2100°F	140
XXV	Re/TaSi ₂ Couple after 100 Hours at 2500°F	140
XXVI	Appearance of Ti/Ti ₅ Si ₃ Eutectoid in a Ti/TaSi ₂ Couple Annealed at 2100°F for 72 Hours	141
XXVII	Appearance of Ti/Ti ₅ Si ₃ Eutectoid Formed from the Melt in a Ti/TaSi ₂ Couple Annealed at 2500°F	141
XXVIII	Attack of Eutectic on Ti in a Ti/TaSi ₂ Couple after Annealing at 2500°F	142
XXIX	Example of Cusp Formation in the Ti/TaSi ₂ System	142

I. BACKGROUND

A. General

1. Introduction

The Supersonic Transport will ultimately require turbine materials capable of operating at temperatures as high as 2400°F. Alloys based on tantalum and columbium possess the requisite high temperature strength but are readily oxidized unless protected by coatings. Reasonably protective coatings embodying the disilicides of the metals have been empirically developed. The protective mechanism is based upon the ability of the coating to generate a silica-based glassy oxide at the interface with the oxidizing atmosphere. This film is self-healing because it is supplied with silicon from the bulk of the coating.

The service lifetimes of disilicide coatings are shortened because they interact by diffusion with metallic substrates to form lower silicides, such as Ta_5Si_3 . The latter is unable to form the protective glassy oxide, presumably because of the simultaneous formation of the substrate metal oxide. Therefore, an understanding of the mechanism of growth of the lower silicide layer and its inhibition is essential to increasing the coating life.

It has been empirically discovered that additives of elements such as titanium to the coating or substrate can substantially increase coating life. This

can be due to either or both of two mechanisms.

a. The participation of the additive in the oxidation reaction to form a more resistant glass.

b. The performance of the additive as a diffusion barrier to inhibit the growth of the less protective lower silicide.

Therefore an understanding of additive behavior as a barrier to lower silicide growth can help to separate the two mechanisms as well as set up criteria for the selection of additive elements which will act as good diffusion barriers.

2. Nature of Silicides

Silicides are classified as intermetallic compounds. They possess high electrical conductivity and the ability to pass into the superconductive state; their thermal-EMF behavior when paired with metals is similar to that of metals and they show the metallic luster typical of metals. Unlike carbides and borides, silicides are not interstitial-phase compounds. Interstitial compounds are produced when non-metals with small atomic radii dissolve into the crystal structure voids of the metal lattice. In order for this to occur, the ratio of interstitial atom radius to the radius of the metal atom should be less than 0.59. This requirement is called Hägg's condition. In silicides the silicon atom radius is 1.17Å and inspection

of Table I will show that $r_{Si}/r_{Me} > 0.59$; therefore, when silicides are formed the silicon atoms must substitute for metallic atoms in the lattice positions.

TABLE I
RATIO OF SILICON ATOM RADIUS TO RADII OF SOME REFRACTORY METAL
ATOMS (1)

<u>Metal</u>	<u>r_{Si}/r_{Me}</u>
Re	0.85
W	0.84
Ta	0.80
Mo	0.84
Nb	0.80
Zr	0.73
Ti	0.79

While metal-silicon bonds are metallic in nature, silicide structures also contain covalent Si-Si bonds. Therefore, the metallic nature of a silicide is generally not as strong as the metal from which it forms, as is evidenced in Table II. Nonetheless, silicides are definitely metallic and compare with borides, carbides and nitrides in electrical resistance.

TABLE II
RESISTIVITIES OF SILICIDES COMPARED TO METALS (1)

Metal	ρ ($\mu\Omega$ -cm)	Silicide	ρ ($\mu\Omega$ -cm)	$\rho_{\text{MeSi}_2}/\rho_{\text{Me}}$
Ti	55.0	TiSi ₂	123	2.59
		TiSi ₂	16.7	0.35
		TiSi ₂	18	0.33
Zr	41.0	ZrSi ₂	161	3.94
		ZrSi ₂	106.2	2.6
Nb	13.1	NbSi ₂	6.3	0.48
		NbSi ₂	24.5	1.85
Mo	5.2	MoSi ₂	21.5	3.46
Ta	12.4	TaSi ₂	8.5	0.68
		TaSi ₂	38.0	3.1
W	5.03	WSi ₂	33.4	6.6
		WSi ₂	38.2	7.5

As the silicon content of a silicide increases, the metallic bonds are weakened and the higher silicides exhibit higher resistivities (1).

Cr ₃ Si	Cr ₃ Si ₂	CrSi	CrSi ₂
45.5 $\mu\Omega$ -cm	114 $\mu\Omega$ -cm	143 $\mu\Omega$ -cm	> 250 $\mu\Omega$ -cm

The higher silicides are also very hard and brittle, and many silicides have extremely narrow homogeneity ranges. Silicides can, therefore, be thought of as stoichiometric, intermetallic compounds which derive their unusual properties from their hybrid type of bonding.

B. Theory

1. Basic

Diffusion is the transport of matter by atomic motion. The driving force is a difference in free energy from one region to another. This difference, ΔG , may be a function of composition, temperature and pressure. Generally, in experimentation, only one parameter is allowed to vary across the region in question, the others being held constant, giving rise to chemical diffusion, thermal diffusion and stress-induced diffusion respectively. By far, the most widely studied diffusional processes are those in which the concentration (or activity) varies.

These general definitions pertain to all states of matter and Fick's first law, relating the flux or motion of the diffusing species to its concentration gradient, can be applied to gaseous, liquid or solid systems.

2. Diffusion in Solids

In solids the carriers in diffusional processes may be electrically charged ions or effectively neutral atoms. In ionic and covalent compounds the breaking of bonds necessary to the motion of atoms produces both positively and negatively charged ions. Rules of electrical neutrality must be obeyed as these ions move, adding restrictions to the solution of the diffusion equations and aiding in the determination of the diffusing species. In metals and metallic

compounds, on the other hand, positively charged metal ions moving through the equi-potential "electron cloud" constituting the metallic bond are effectively neutral atoms. Balances on the electrical charges of the diffusing species cannot be made.

When two different metals with extensive solid solubility are interdiffused an alloyed intermediate grows between them. There is a continuous change in concentration from pure A to pure B. This concentration can be followed by means of lattice parameter changes, microhardness profiles, electron microprobe analysis or by radioactive counter methods (if half of the couple is a radioactive isotope). Various mathematical expressions have been derived for such cases. Most of these employ the Matano interface, which is a plane of reference embodying a material balance so that Fick's second law may be solved using a transformation known as the Matano-Boltzman method. Castleman (2) and Kidson (3) give a variety of solutions for different types of systems. These approaches yield an interdiffusion coefficient, \tilde{D} .

Darken (4), in a classic paper, using a non-mechanistic approach to the data of Smigelskas and Kirkendall (5), has derived the relationship between this interdiffusion coefficient and the actual diffusivities of the two diffusing species in a binary system with no compound

formation. Darken's main contribution was to separate diffusion from gross motion based on relative motion considerations, using Smigelskas and Kirkendall's revolutionary marker experiment results. He also succeeded in relating \tilde{D} to impurity diffusivities from radioactive tracer experiments.

With the formation of an intermediate compound, discontinuities arise in the concentration profile and Fick's second law cannot be explicitly solved. Instead, the stoichiometric nature of the compound adds the needed condition to Fick's first law. In conjunction with material balances, this leads to the parabolic rate law, relating the thickness of the growing phase to time of diffusion. The method of following this growth is simple (microscopic, X-ray diffraction, electron microprobe) and is called the "moving boundary" technique. The difficulty lies with the more empirical, less basic nature of the parabolic rate constant, k , where k is defined as $(\Delta x)^2/t$, or the thickness of the phase grown in time t squared divided by the time. This constant must be defined in terms of \tilde{D} to have fundamental significance. This is particularly true when more than one compound grows simultaneously. Janssen and Rieck (6), in studying compound formation in the Ni-Al system, used both a "moving boundary" technique and Boltzman-Matano method to calculate D values for four aluminides. Gibbs (7), in a general treatment, considered the total zone of n intermediate

phases, assigning an "effective diffusivity", D_{β} , to the system. He concluded that "only if the n phases have similar diffusion parameters and small miscibility gaps at the intermediate interfaces will D_{β} approximate some true average diffusivity". Kidson (3) showed that each phase layer obeys the parabolic rate. Roy (8) found D 's and k 's coupled in a treatment of interstitial systems; and Resnick, Steinitz and Seigle (9) in determining the diffusivity of C in Ta and Cb carbides found the diffusivities in the two growing phases coupled.

In the treatment of substitutional compound growth in the Ni/U system, Kimmel, Bar-or and Rosen (10) concluded that the relation between D and k for any growing layer depends only on the homogeneity range or ΔC , the concentration difference, and not on the growth constant (or diffusivity) of any other phase growing in the same couple. Arzamasov (11), in a more general argument, arrives at the same conclusion. Wagner (12), recently derived k values for three types of systems. For an intermediate with narrow homogeneity range growing between one compound of higher stoichiometry and one of lower stoichiometry, his k (called k_{III}) value is related to the average diffusivity in a manner similar to the above-mentioned substitutional cases, but is also a function of the mole fractions of the diffusing species in the three compounds. Silicides, being substitutional intermetallics

of narrow homogeneity ranges, should fall into the category analyzed by Wagner as long as the silicide grows in a stable fashion.

3. Mechanisms

There are three types of diffusion to consider in polycrystalline solids; bulk or volume diffusion, grain boundary and surface diffusion. Both grain boundary and surface diffusion are local effects caused by differences in free energy between the grains and grain boundaries and along the surface of the material respectively. Single crystal diffusion experiments completely eliminate grain boundary effects. Careful study of the shape of accurately made penetration curves can aid in deducing the effect of grain boundary or surface diffusion. Generally, all three types of diffusion occur simultaneously in any couple, but if the concentration gradient across the couple is substantial, diffusion through the bulk of the solid greatly predominates and the grain boundary and surface diffusion contributions may be neglected. Therefore, in couples with a definite concentration gradient, conformity of the growth to the parabolic rate indicates that the smaller effects of grain boundary and surface diffusion are negligible.

Volume diffusion can be thought of as being generated by three different types of defects: interstitial and substitutional defects and vacancies. The interstitial

mechanism proceeds by motion of atoms (impurity or solute), within the interstices of the parent lattice. This mechanism predominates in interstitial compounds in which the smaller atom (e.g. C, N) alone diffuses. In the substitutional mechanism, a foreign atom occupying a lattice site in the parent lattice must be displaced by the diffusing atom. This requires an exchange of atoms from stable lattice positions and the requisite energy is high. The energy required for vacancy diffusion is considerably less. All solids have a certain concentration of vacancies or empty lattice positions. In vacancy diffusion, an atom occupying a lattice site adjacent to a vacancy can jump into the vacancy, leaving its previous lattice site unoccupied. This effectively creates a vacancy one atomic distance away from the original position in a direction opposite to the motion of the diffusing atom. This mechanism requires the least net amount of broken bonds and the increase in entropy upon filling in the vacant lattice site makes vacancy diffusion the most energetically favored mechanism (13). Therefore, binary diffusion via vacancy mechanism can be thought of as resulting from the motion of the two atomic species and vacancies. The overall flow of the vacancies is opposite to the net flow of the two atomic species. In fact, if one component diffuses at a much higher rate than the other, vacancies moving in the opposite direction tend to accumulate and form

voids. Observation of this void formation is experimental evidence of vacancy-type diffusion.

In order to understand the complete diffusion process, three questions must be answered:

- 1) By what path does the diffusion proceed?
- 2) How fast does the process take place?
- 3) What is diffusing?

Diffusion paths may be estimated by proposing a sequence of jumps and then minimizing the required energy. This is a complicated and lengthy procedure. It has only been attempted for the simplest cases and with little success (14, 15, 16).

The diffusivity may be evaluated experimentally. By measuring the intermediate rate of growth at constant temperature, one can obtain k from the parabolic rate, $k = \frac{(\Delta x)^2}{t}$. Adherence to this form of growth indicates the predominance of volume diffusion. The constant k is a measure of diffusivity. The fundamental quantity, \tilde{D} , may be computed from k .

As with any rate process, the temperature dependence of k (or \tilde{D}) should be of the Arrhenius form: $\tilde{D} = \tilde{D}_0 e^{-Q/RT}$, where R is the gas constant and Q is the activation energy for diffusion. Any deviation from this type of dependence would indicate a mechanism consisting of more than

one thermally activated step. Q is the activation energy which measures the effect of temperature on diffusivity. In vacancy diffusion Q can be thought of as the sum of the energy necessary to form vacancies and the energy needed to move vacancies. In order to form vacancies, bonds must be broken and the energy to do this should be related to the melting point. The energy to move the vacancy depends on crystal structure and electronic factors. Therefore, Q should bear some relationship to absolute melting point for a particular structure (17). In the same vein, the relationship could also exist with heat of vaporization (18). Many empirical expressions have been formulated showing these relationships. In pure BCC metals, Q is directly related to melting point; $Q = 34T_M$ (19). Sherby and Simnad (20) characterized volume self-diffusion in metals by: $D = D_0 e^{-(K_0+V)T_M/T}$ where K_0 = crystal structure factor (14 for BCC, 17 for FCC and HCP and 21 for diamond), V = valence and T_M is absolute melting point. In complex structures such relationships probably do not hold.

To determine the diffusing species, markers may be used. This method is based on marking the original interface in the diffusion couple and measuring the growth on either side of it. Since different reactions are taking place at the interfaces to the left and right of the original interface, a ratio of the diffusivities of the two species

in a binary system results. Any material being used as a marker must be completely inert to its environment. It must not be displaced by any mechanism so that it can be used as a reference plane. Previous experience is useful in helping to predict which species should predominate in the diffusion process. In a review on diffusion in intermetallic compounds, Hagel (17) clearly states "Many correlations were tried to aid in predicting which component of a binary compound would be the faster moving species, and almost without exception it is the element possessing the lower melting point."

Books by Jost (21), Crank (22) and Baarer (23) give fundamentals of diffusion mechanisms and the mathematics associated with them, as well as good overall coverage of the field.

C. Diffusion Equations

Reaction kinetics in the solid state are usually diffusion controlled. Because of the high temperatures at which the studies are made, reactions occur very quickly compared to the time required for the reacting species to migrate through an ordered solid to the reaction interface. Therefore, it is a good assumption that diffusion through a growing layer controls the growth rate of that layer. Experimental observation of a parabolic rate supports this assumption. If two components, A and B, are coupled and heated to a temperature at which diffusion can proceed at a measurable rate,

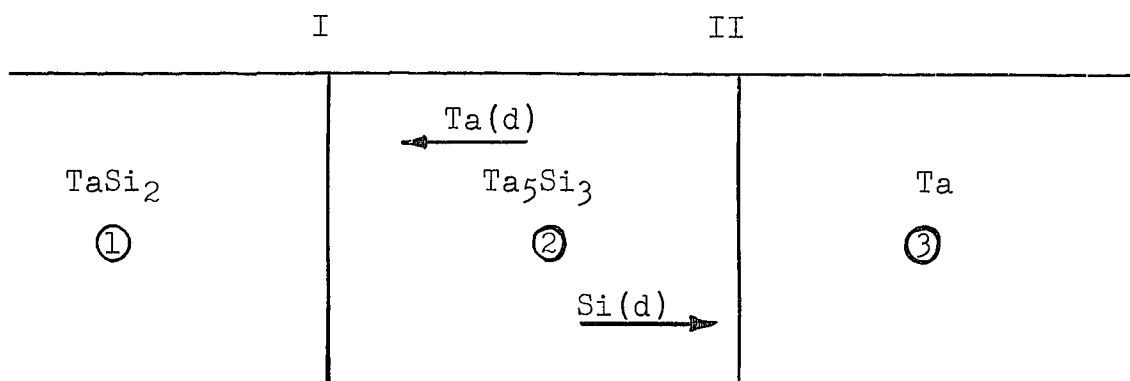
one would expect to find every phase between A and B that exists at the diffusion temperature. Therefore, knowledge of the phase diagrams is invaluable in solid state diffusion experiments. Frequently, some of the phases predicted from the diagram do not appear in measurable amounts. This can be caused by slow nucleation of the missing phases or by a balance between the formation of a phase at one interface and its destruction at another interface or by extremely low diffusion rates through the phases. A phase that is slow to nucleate can be found simply by increasing the length of the diffusion experiment. The other two factors can be coupled in complicated systems, but generally quickly growing phases indicate high diffusivity in the growing phase. From steric considerations it may be argued that reactions forming new compounds must occur only at the phase interfaces.

1. Ta/TaSi₂ System

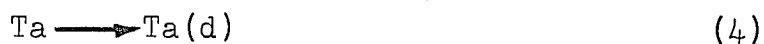
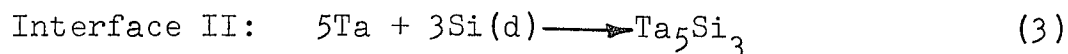
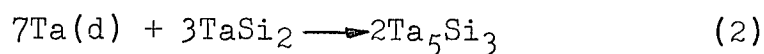
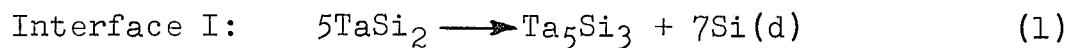
From consideration of the Ta-Si phase diagram (Appendix I) it would be expected that three intermediate silicides would grow between TaSi₂ and Ta: Ta₅Si₃, Ta₂Si and Ta_{4.5}Si. The phase of Ta containing a very small concentration of silicon is considered pure Ta. It has been found, in this investigation and others (24), that as long as TaSi₂ is available to supply Si to the growing system, only the trisilicide, Ta₅Si₃, grows in discernible amounts. An analysis including the lower silicides, Ta₂Si and Ta_{4.5}Si,

assuming that their rate of formation is zero, yields the same result that their exclusion from the analysis predicts. Therefore, it may be considered that the system is Ta_5Si_3 alone growing between $TaSi_2$ and Ta.

FIGURE 1



In the figure above ①, ② and ③ represent the phases and I and II the interfaces. Si(d) indicates Si diffusing from interface I to interface II through phase ②; and Ta(d) indicates Ta diffusing from interface II to interface I through phase ②. The reactions that may take place at the interfaces are:



During the growth of the intermediate phase the reactions are diffusion-controlled and the growth rate of any compound is dependent upon the fluxes, J (moles/cm²sec), of the diffusing components across the phase boundaries.

Therefore, taking the flux toward the right as positive, the rate of growth of the trisilicide at interface I is

$$J_I = \frac{1}{7} J_{Si} - \frac{2}{7} J_{Ta} \quad (5)$$

and its rate of growth at interface II is

$$J_{II} = \frac{1}{3} J_{Si}. \quad (6)$$

The total rate of growth of the layer of Ta_5Si_3 is the sum of J_I and J_{II} .

$$J_{total} = \frac{10}{21} J_{Si} - \frac{2}{7} J_{Ta} \quad (7)$$

The fluxes J_{Si} and J_{Ta} may be expressed in terms of their diffusivities (cm^2/sec) and concentration gradients (moles/ cm^3/cm).

$$J_{Si} = - D_{Si} \frac{dC_{Si}}{dx} \quad (8)$$

$$J_{Ta} = - D_{Ta} \frac{dC_{Ta}}{dx} \quad (9)$$

It is more convenient to express the concentrations in terms of mole fractions. For example:

$$C_{Si} = \frac{N_{Si}}{V_m} \alpha$$

where N_{Si} = moles Si / (moles Si + moles metal)

$$V_m = cm^3 / \text{mole of compound}$$

and α = (moles Si + moles metal) / mole of compound.

Hence, restating Fick's first law

$$J_{Si} = \frac{-D_{Si}}{V_m} \frac{dN_{Si}}{dx} \alpha \quad (10)$$

$$J_{Ta} = \frac{-D_{Ta}}{V_m} \frac{dN_{Ta}}{dx} \alpha \quad (11)$$

Inserting these fluxes in equation (7)

$$J_{total} \frac{V_m}{\alpha} = \frac{-10}{21} D_{Si} \frac{dN_{Si}}{dx} + \frac{2}{7} D_{Ta} \frac{dN_{Ta}}{dx} \cdot \quad (12)$$

Let $J_{total} V_m = r$ (cm/sec, a velocity of growth of the Ta_5Si_3) and note that for a binary system

$$N_{Si} = 1 - N_{Ta} \text{ and}$$

$$-dN_{Si} = dN_{Ta}.$$

Now for the Ta_5Si_3 , the concentration change across the almost stoichiometric phase is very small* and may be assumed independent of thickness. Therefore, following the usual convention regarding signs,

$$\frac{dN_{Si}}{dx} = \frac{-\Delta N_{Si}}{\Delta x}$$

and

$$\frac{dN_{Ta}}{dx} = \frac{-dN_{Si}}{dx} = \frac{\Delta N_{Si}}{\Delta x} \cdot$$

Rewriting equation (12) yields

$$r = \frac{2\alpha}{21} (5 D_{Si} + 3 D_{Ta}) \frac{\Delta N_{Si}}{\Delta x} \cdot \quad (13)$$

Defining the interdiffusion coefficient \tilde{D} according to Darken (4),

$$\tilde{D} = N_2 D_1 + N_1 D_2$$

$$\tilde{D} Ta_5Si_3 = \frac{5}{8} D_{Si} + \frac{3}{8} D_{Ta}$$

*It should be emphasized that diffusion occurs down a thermodynamic activity gradient rather than down a concentration gradient. A large activity difference may exist despite a very small concentration difference.

and inserting into equation (13) results in

$$r = \frac{16d}{21} \tilde{D} \frac{\Delta N_{Si}}{\Delta x} . \quad (14)$$

The rate of growth can also be expressed as a rate of change in thickness, Δx , of the growing phase.

$$r = \frac{d(\Delta x)}{dt} = \frac{16(8)}{21} \tilde{D} \frac{\Delta N_{Si}}{\Delta x} \quad (15)$$

On integration of equation (15) the parabolic rate expression is obtained.

$$(\Delta x)^2 = \frac{256}{21} \tilde{D} \Delta N_{Si} t \quad (16)$$

Since accurate solvus lines have not been determined for the silicides, the values of ΔN are unknown and cannot be separated from \tilde{D} . Then solving for the product $\tilde{D}\Delta N_{Si}$,

$$\tilde{D}\Delta N_{Si} = \frac{21}{256} \frac{(\Delta x)^2}{t} = \frac{21}{256} k \quad (17)$$

where k is the experimentally determined parabolic rate constant.

The interdiffusion coefficient is directly related to the measured parabolic rate constant by a constant and ΔN . One can be fairly assured that ΔN does not vary significantly over the temperature range of interest and the activation energy from $k = k^0 e^{-Q/RT}$ should be the same as the activation energy from $\tilde{D} = \tilde{D}_0 e^{-Q/RT}$. But $\tilde{D} = N_2 D_1 + N_1 D_2 = N_2 D_0^1 e^{-Q_1/RT} + N_1 D_0^2 e^{-Q_2/RT}$. Therefore an apparent activation energy, \tilde{Q} , results from a plot of $\ln ((\Delta x)^2/t)$ vs. $1/T_{abs}$, which involves both of the fundamental activation energies,

Q_1 and Q_2 , and may be temperature dependent. Only if the diffusivity of one species is much greater than the other or if Q_1 and Q_2 are almost equal will \tilde{Q} represent a true activation energy. Therefore, if only silicon diffuses \tilde{D} and \tilde{Q} will represent the actual diffusivity and activation energy for diffusion of Si in Ta_5Si_3 .

2. Markers in the Ta/TaSi₂ System

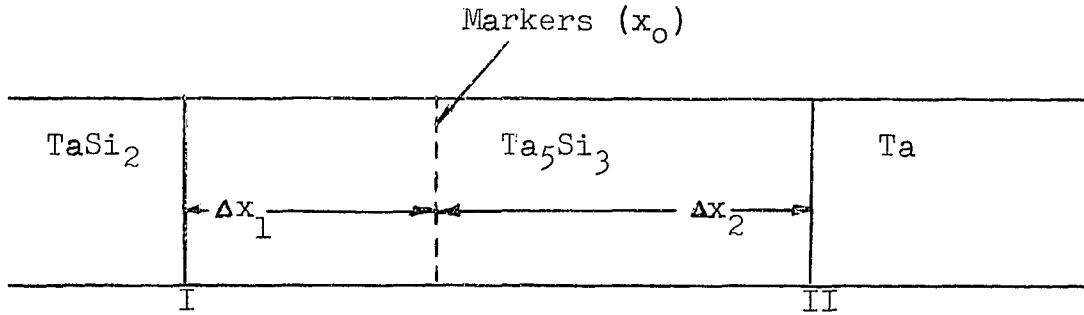
In order to ascertain which of the components predominates in the diffusion process the original interface must be marked. This is the purpose of a marker experiment in which small inert particles or wires are inserted between the halves of the diffusion couple before the couple is annealed. If these markers do not react with the surroundings, they act as a reference plane, pinning the original interface.

The marker technique has been frequently used in oxidation studies, where the marker is attached to a clean metal surface and the metal then oxidized. If oxygen is the diffusing species, the marker will remain at the gas-solid interface. If only the metal diffuses, the marker will become embedded at the solid-solid interface.

In the Ta/TaSi₂ system, as the intermediate layer grows a marker at the original interface will indicate the relative fluxes of the diffusing species Ta and Si. In this case, the relationship is not as simple as in oxidation

experiments because the trisilicide is formed both by loss of Si from the disilicide and by reaction of Si with Ta and of Ta with $TaSi_2$.

FIGURE 2



In this analysis, it will be assumed that Ta does not diffuse. Since the markers do not participate in any reactions, the reactions (1) and (3) occur at interfaces I and II, and it is possible to measure the rates of formation at each of the interfaces separately. The following pair of equations result in which k_1 and k_2 are the growth constants for the Δx_1 and Δx_2 zones respectively.

$$(\Delta x_1)^2/t = 2/7 \alpha (D_{Si} \Delta N_{Si})_1 = k_1 \quad (18)$$

$$(\Delta x_2)^2/t = 2/3 \alpha (D_{Si} \Delta N_{Si})_2 = k_2 \quad (19)$$

A simple material balance using reactions (1) and (3) shows that if Ta does not diffuse the thicknesses of the growing phases are stoichiometrically related when molar density is taken into account.

$$\frac{\Delta x_2/V_{m2}}{\Delta x_1/V_{m1}} = \frac{7}{3} \quad (20)$$

Since the molecular weights of the compound (Ta_5Si_3) are nearly the same in both zones,

$$\frac{\Delta x_2}{\Delta x_1} = \frac{7}{3} \frac{\rho_1}{\rho_2} \quad (21)$$

where ρ_1 and ρ_2 are the densities (gms/cc) of Ta_5Si_3 in the Δx_1 and Δx_2 zones respectively. Therefore, if measured values of $\Delta x_2 / \Delta x_1$ conform to equation (21), it may be said that Ta does not appreciably diffuse.

Dividing equation (19) by equation (18) results in

$$\frac{k_2}{k_1} = \left(\frac{\Delta x_2}{\Delta x_1} \right)^2 = \frac{7}{3} \frac{(D_{Si} \Delta N_{Si})_2}{(D_{Si} \Delta N_{Si})_1} \quad (22)$$

The following relationship between ΔN and Δx results from solving equations (21) and (22) together.

$$\frac{\rho_2}{\rho_1} \frac{(D_{Si} \Delta N_{Si})_2}{(D_{Si} \Delta N_{Si})_1} = \frac{\Delta x_2}{\Delta x_1} \quad (23)$$

Therefore, if the diffusivities of silicon in Ta_5Si_3 on both sides of the original interface are the same, the ratio of the stoichiometry ranges across the zones is proportional to the ratio of the thicknesses of the zones because ρ_2/ρ_1 is a constant close to unity. Since the ratio $\Delta x_2/\Delta x_1$ is known, under the assumptions stated, $\Delta N_2/\Delta N_1$ is known explicitly from

$$\frac{(\Delta N_{Si})_2}{(\Delta N_{Si})_1} = \frac{7}{3} \left(\frac{\rho_1}{\rho_2} \right)^2 \quad (24)$$

Therefore, if it can be shown experimentally that Ta does

not diffuse (equation (21) is satisfied) and that the diffusivities in both zones are close (equations (18) and (19)), the ratio of the ΔN_{Si} values is established by stoichiometry.

3. M/TaSi₂ System

As previously mentioned, TaSi₂ on Ta is protective by virtue of the formation of a silica glass at the air interface. If this protective glass is impaired, the TaSi₂ acts as a reservoir of silicon for the formation of additional glass. However, the lower silicide, Ta₅Si₃, is not protective, so that the diffusion of silicon out of TaSi₂ into the tantalum diminishes the coating life. The thickness of the Δx_1 layer is a measure of the extent of this loss. If it were possible to interpose a silicon-impermeable barrier between the TaSi₂ and the Ta, the coating life would be greatly increased. The interpolation of a barrier that merely reduced the flow of silicon would also be desirable. Hence, the measure of the effectiveness of any barrier, M, may be determined from the growth rate of the Δx_1 layer.

In testing the barrier effect of certain additive metals, the growth kinetics of the intermediate zone depends on the fluxes of components in

and out of Ta_5Si_3 and one or more M silicides. The system is not truly binary any more and complete analysis is considerably complicated. The growth of the total zone is therefore not easily related to fundamental diffusivities or activation energies. Analysis leads to an apparent activation energy which is related to the activation energies for the growth of each of the separate phases. Therefore, each of the growing zones will be analyzed separately yielding an activation energy for that phase.

FIGURE 3

I	II	III	IV	V	VI	
$TaSi_2$	Ta_5Si_3 ②	Ta_2Si ③	MSi_x ④	MSi_y ⑤	MSi_z ⑥	M

Figure 3 is a generalized picture of the results obtained from a diffusion couple of the metal M against $TaSi_2$. The silicides MSi_x , MSi_y and MSi_z are of decreasing silicon content in the order $x > y > z$. In specific cases, some of the phases shown in Figure 3 may be absent. When present, Ta_2Si and MSi_x are generally found in only small amounts and show no observable growth rate.

An analysis of this system is developed below based on the following assumptions:

- 1) Since the diffusion of Ta was not observed in the Ta/TaSi₂ system, it is assumed that no Ta diffusion occurs.
- 2) No complex silicides containing Ta and M are observed, therefore M does not diffuse through regions ② and ③.
- 3) Adjacent phases are in equilibrium with Si at interface I. Adjacent phases are in equilibrium with Si and M at interfaces V and VI.
- 4) The growth rates of Ta₂Si and MSi_x are negligible.
- 5) Phase equilibria (but not reaction equilibria) exist at interfaces II, III and IV, and the Si concentrations on either side of these interfaces are directly related by a solubility constant, K.

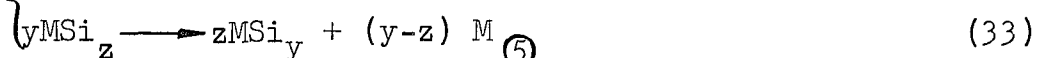
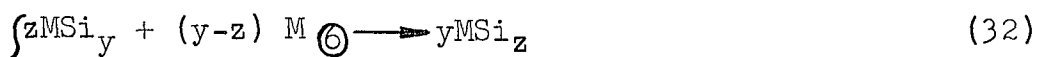
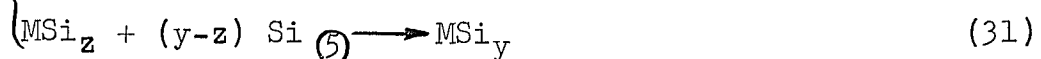
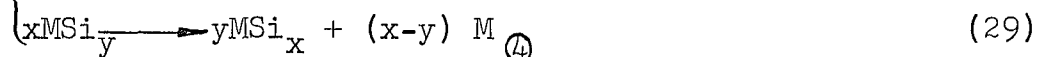
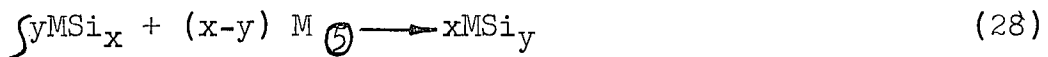
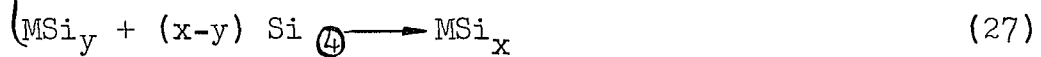
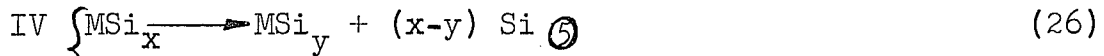
It can be shown that under these assumptions the growth in phases ②, ⑤ and ⑥ is parabolic. Therefore, the range of stoichiometry in these phases, ΔC (or ΔN), must be independent of thickness, as in the Ta/TaSi₂ system.

Then the reactions occurring at each interface are:



II No net reaction

III No reaction



In the above equations $\text{Si} \textcircled{i}$ and $\text{M} \textcircled{i}$ represent Si or M respectively diffusing through phase \textcircled{i} in opposite directions. From the previously stated assumptions $J_{\text{Si} \textcircled{2}} = J_{\text{Si} \textcircled{3}} = J_{\text{Si} \textcircled{4}}$ and $J_{\text{M} \textcircled{4}} = J_{\text{M} \textcircled{3}} = J_{\text{M} \textcircled{2}} = 0$. Since there are no net reactions at interfaces II and III, a material balance on region $\textcircled{3}$ produces the same result as if the phase were neglected. Material balances on the remaining regions produce the following results:

$$J_{\text{Ta}_5\text{Si}_3} = \frac{1}{V \textcircled{2}} \frac{d \Delta x \textcircled{2}}{dt} = \frac{1}{7} J_{\text{Si} \textcircled{2}} \quad (36)$$

$$J_{\text{MSi}_x} = \frac{1}{V \textcircled{4}} \frac{d \Delta x \textcircled{4}}{dt} = \frac{1}{x-y} (J_{\text{Si} \textcircled{4}} - J_{\text{Si} \textcircled{5}}) + \frac{y}{x-y} J_{\text{M} \textcircled{5}} \quad (37)$$

$$J_{\text{MSi}_y} = \frac{1}{V \textcircled{5}} \frac{d \Delta x \textcircled{5}}{dt} = \frac{1}{y} (J_{\text{Si} \textcircled{4}} - J_{\text{Si} \textcircled{5}}) + \frac{1}{y-z} (J_{\text{Si} \textcircled{5}} - J_{\text{Si} \textcircled{6}}) + \frac{z}{y-z} (J_{\text{M} \textcircled{6}} - J_{\text{M} \textcircled{5}}) \quad (38)$$

$$J_{MSi_z} = \frac{1}{V_6} \frac{d \Delta x_6}{dt} = \frac{1}{y-z} (J_{Si_6} - J_{Si_5}) + \frac{y}{y-z} (J_{M_5} - J_{M_6}) + \frac{1}{z} J_{Si_6} \quad (39)$$

From assumption 4) J_{MSi_x} can be set to zero resulting in:

$$\frac{1}{y} (J_{Si_4} - J_{Si_5}) = - J_{M_5} \quad (40)$$

When this is substituted into equation (38) the result contains fluxes of Si and M only through phases 5 and 6.

Applying Fick's first law as in the Ta/TaSi₂ system and defining the interdiffusion constants according to Darken

$$\tilde{D}_5 = \tilde{D}_{MSi_y} = \frac{1}{1+y} D_{Si_5} + \frac{y}{1+y} D_{M_5} \text{ and}$$

$$\tilde{D}_6 = \tilde{D}_{MSi_z} = \frac{1}{1+z} D_{Si_6} + \frac{z}{1+z} D_{M_6}$$

the following three rate equations result.

$$\frac{d \Delta x_2}{dt} = \frac{\alpha_2}{7} \frac{D_{Si_2} \Delta N_{Si_2}}{\Delta x_2} \quad (41)$$

$$\frac{d \Delta x_5}{dt} = \frac{1+y}{y-z} \alpha_5 \frac{\tilde{D}_5 \Delta N_{Si_5}}{\Delta x_5} - \frac{1+z}{y-z} \frac{V_5}{V_6} \alpha_6 \frac{\tilde{D}_6 \Delta N_{Si_6}}{\Delta x_6} \quad (42)$$

$$\frac{d \Delta x_6}{dt} = \frac{y(1+z)}{z(y-z)} \alpha_6 \frac{\tilde{D}_6 \Delta N_{Si_6}}{\Delta x_6} - \frac{1+y}{y-z} \frac{V_6}{V_5} \alpha_5 \frac{\tilde{D}_5 \Delta N_{Si_5}}{\Delta x_5} \quad (43)$$

Equation (41) is of the same form as equation (12) and is easily solved for $D \Delta N$ of the Ta₅Si₃ phase.

$$D_{Si_2} \Delta N_{Si_2} = \frac{7}{2\alpha_2} \frac{(\Delta x_2)^2}{t} = \frac{7}{16} k_2 \quad (44)$$

Equations (42) and (43) represent a pair of coupled differential equations of the form

$$\frac{d \Delta x_{(5)}}{dt} = \frac{A}{\Delta x_{(5)}} - \frac{B}{\Delta x_{(5)}} \quad (45)$$

$$\frac{d \Delta x_{(6)}}{dt} = \frac{C}{\Delta x_{(6)}} - \frac{D}{\Delta x_{(6)}} \quad (46)$$

where $A = \frac{1+y}{y-z} \alpha_{(5)} \tilde{D}_{(5)} \Delta N_{Si_{(5)}}$

$$B = \frac{1+z}{y-z} \frac{V_{(5)}}{V_{(6)}} \alpha_{(6)} \tilde{D}_{(6)} \Delta N_{Si_{(6)}}$$

$$C = \frac{y(1+z)}{z(y-z)} \alpha_{(6)} \tilde{D}_{(6)} \Delta N_{Si_{(6)}}$$

and $D = \frac{1+y}{y-z} \frac{V_{(6)}}{V_{(5)}} \alpha_{(5)} \tilde{D}_{(5)} \Delta N_{Si_{(5)}}$.

To solve the equations, assume a solution of the form

$$\Delta x_{(5)} = k' t^n$$

$$\Delta x_{(6)} = k' t^m$$

where $k' = \sqrt{k}$ and k is the experimentally determined parabolic rate constant. Substituting this into equations (45) and (46) and equating powers results in $n = m = \frac{1}{2}$, which mathematically substantiates the parabolic rate. Solving the equation yields

$$\frac{k'_{(5)}}{2} = \frac{A}{k'_{(5)}} - \frac{B}{k'_{(5)}} \quad (47)$$

$$\frac{k'_{(6)}}{2} = \frac{C}{k'_{(6)}} - \frac{D}{k'_{(6)}} \quad (48)$$

Replacing the values for A, B, C and D and solving for

$\tilde{D}_{(5)} \Delta N_{Si_{(5)}}$ and $\tilde{D}_{(6)} \Delta N_{Si_{(6)}}$ results in a pair of equations showing

that the diffusion constants in the two growing phases are

coupled through the rate constants, $k_{(5)}$ and $k_{(6)}$.

$$\begin{aligned} \tilde{D}_{\text{Si}} \Delta N_{\text{Si}} &= \frac{y}{1+y} \frac{k_{\text{Si}}'}{2\alpha_{\text{Si}}} \left(k_{\text{Si}}' + \frac{z}{y} \frac{V_{\text{Si}}}{V_{\text{M}}} k_{\text{M}}' \right) \\ &= \frac{N_{\text{Si}}}{2\alpha_{\text{Si}}} \left(k_{\text{Si}} + \frac{z}{y} \frac{V_{\text{Si}}}{V_{\text{M}}} \sqrt{k_{\text{Si}} k_{\text{M}}} \right) \end{aligned} \quad (49)$$

$$\begin{aligned} \tilde{D}_{\text{M}} \Delta N_{\text{Si}} &= \frac{z}{1+z} \frac{k_{\text{M}}'}{2\alpha_{\text{M}}} \left(k_{\text{M}}' + \frac{V_{\text{M}}}{V_{\text{Si}}} k_{\text{Si}}' \right) \\ &= \frac{N_{\text{Si}}}{2\alpha_{\text{M}}} \left(k_{\text{M}} + \frac{V_{\text{M}}}{V_{\text{Si}}} \sqrt{k_{\text{Si}} k_{\text{M}}} \right) \end{aligned} \quad (50)$$

Therefore, although the relationship between diffusion constant and parabolic growth constant for the Ta_5Si_3 zone is the same in the M/TaSi_2 and Ta/TaSi_2 systems, when two M silicide layers grow simultaneously the diffusivities of the two zones are coupled through the experimentally determined k values. The Mo/TaSi_2 system is an example of one in which two M silicide phases grow simultaneously: Mo_3Si and Mo_5Si_3 . In such a system the $\ln k$ versus $1/T$ plot is not necessarily a straight line since each growth constant involves at least two activation energies: one from \tilde{D}_{M} and one from \tilde{D}_{Si} , even if there is no M diffusion. If only one M silicide grows J_{MSi_z} can be set equal to zero and only one equation results.

$$\frac{d(\Delta x_{\text{Si}})}{dt} = \frac{1+y}{y\alpha_{\text{Si}}} \frac{\tilde{D}_{\text{Si}} \Delta N_{\text{Si}}}{\Delta x_{\text{Si}}} \quad (51)$$

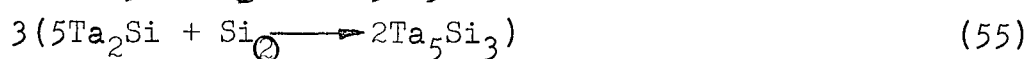
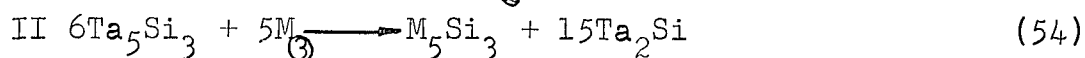
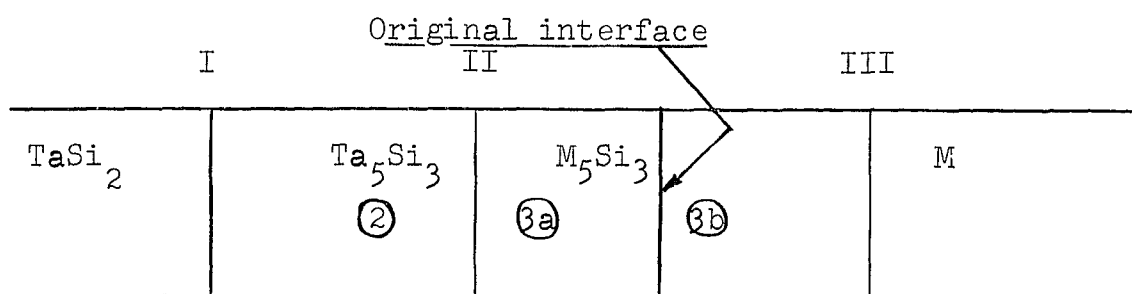
and

$$\tilde{D}_{\text{Si}} \Delta N_{\text{Si}} = \frac{1}{2\alpha_{\text{Si}}} \frac{y}{1+y} \frac{(\Delta x_{\text{Si}})^2}{t} = \frac{N_{\text{Si}}}{2\alpha_{\text{Si}}} k_{\text{Si}} \quad (52)$$

4. Markers in the M/TaSi₂ Systems

In the M/TaSi₂ systems, if M diffusion is negligible the original interface, as indicated by markers, will coincide with the Ta silicide-M silicide interface (III in Figure 3). Therefore, one should observe only one phase (Ta₅Si₃), corresponding to the Δx_1 of Figure 2, and there should be no phase boundaries between the original interface and the TaSi₂/Ta₅Si₃ interface. If this is not the case and the original interface is positioned within a M silicide phase, M atoms are diffusing. The relative fluxes of M and Si diffusion can then be calculated as in the Ta/TaSi₂ case. As an example, a simple system consisting of one M silicide will be considered.

FIGURE 4



Because the molar volumes, V_m , cancel out in this analysis they will be omitted for clarity.

$$\text{I } J_{\text{Ta}_5\text{Si}_3} = \frac{1}{7} J_{\text{Si}_2} \quad (58)$$

$$\text{II } J_{\text{Ta}_5\text{Si}_3} = \frac{6}{5} J_{\text{M}_3} + 2J_{\text{Si}_2} \quad (59)$$

$$J_{\text{Ta}_2\text{Si}} = -3J_{\text{M}_3} - 5J_{\text{Si}_2} \quad (60)$$

$$J_{\text{M}_5\text{Si}_3} = -\frac{1}{5} J_{\text{M}_3} \quad (61)$$

$$\text{III } J_{\text{M}_5\text{Si}_3} = \frac{1}{3} J_{\text{Si}_2} \quad (62)$$

If no Ta_2Si grows

$$3J_{\text{M}_3} + 5J_{\text{Si}_2} = 0 = \frac{5}{2} J_{\text{Ta}_5\text{Si}_3} \quad (\text{III})$$

and $J_{\text{Ta}_5\text{Si}_3} \text{ (II)} = 0$.

Therefore,

$$J_{\text{Ta}_5\text{Si}_3} = \frac{1}{7} J_{\text{Si}_2} \quad (63)$$

$$J_{\text{M}_5\text{Si}_3(a)} = -\frac{1}{5} J_{\text{M}_3} \quad (64)$$

$$J_{\text{M}_5\text{Si}_3(b)} = \frac{1}{3} J_{\text{Si}_2} \quad (65)$$

and

$$D_{\text{Si}_2} \Delta N_{\text{Si}_2} = \frac{7}{2\alpha} \frac{(\Delta x_{2a})^2}{t} = \frac{7}{2\alpha} k_{2a} \quad (66)$$

$$D_{\text{M}_3} \Delta N_{\text{M}_3} = \frac{5}{2\alpha} \frac{(\Delta x_{3a})^2}{t} = \frac{5}{2\alpha} k_{3a} \quad (67)$$

and

$$D_{\text{Si}_2} \Delta N_{\text{Si}_2} = \frac{3}{2\alpha} \frac{(\Delta x_{3b})^2}{t} = \frac{3}{2\alpha} k_{3b} \quad (68)$$

5. Basis of Δx_1 Comparisons

As can be seen from the previous analysis, $\bar{D}_{Si} \Delta N_{Si}$ is directly related to k_2 for all cases of diffusion under the assumptions stated. These values for the growth of Ta_5Si_3 (Δx_1 zones) can be compared with the Δx_1 growth in the Ta/TaSi₂ system directly by comparison of the growth constants k . As previously mentioned, this is exactly the comparison needed to describe the effect of barrier metals on the degradation of TaSi₂. Therefore, one can determine the rate of degradation of TaSi₂ directly from the rate constants of the Δx_1 zones in any of the systems investigated. Since both the diffusing species (Si) and the medium (Ta_5Si_3) through which it is lost are the same in all cases, differences in growth rates depend on the activities of Si in the M silicides adjacent to the growing Ta_5Si_3 .

D. Previous Work

The only previous comparable work is that by Bartlett (24) and Lavendel and Elliot (25). Both of these used silicide-coated Ta specimens. The TaSi₂ coatings were deposited on the Ta substrates by vapor deposition and the coated system was then diffusion-annealed to form the lower silicide, Ta_5Si_3 . The TaSi₂ had cracks, defects and compositional impurities which could affect the results of the studies. Diffusing

times were limited by the thickness of the original TaSi₂ layer. Bartlett's experiments done in a nitrogen-argon atmosphere resulted in an activation energy of 58,000 cal/mole for the growth of Ta₅Si₃. Lavendel and Elliot performed their diffusion anneal in helium and at higher temperatures. They observed the growth of Ta₂Si as well as Ta₅Si₃ at 3000°F and above, and derived an activation energy of 49,000 cal/mole for the process.

Other diffusion results relevant to this investigation are not directly comparable. Both of the above-mentioned studies included a similar investigation of the Cb/CbSi₂ system and both found the activation energy for the growth of Cb₅Si₃ to be the same as for Ta₅Si₃ in the Ta/TaSi₂ system. Koffman and Ogilvie (26) calculated the interdiffusion coefficients in Cb containing small amounts of Si and in Cb₃Si, using a Wagner analysis based on the coupling of two-phase, arc-melted wafers both of which contained the growing phase. Due to technical difficulties they were not able to determine \bar{D} for the higher silicides. The resulting activation energies are 88,000 cal/mole for Cb/Si solid solution, 166,000 cal/mole for Cb₃Si and 89,000 cal/mole for W/Si solid solution (which was analyzed by the Grube analysis).

Bartlett, Gage and Larssen (27) also investigated the W/Si system and the Mo/Si system by coating WSi₂ and MoSi₂ on W and Mo respectively. The method and analysis are

similar to those used for Ta/TaSi₂ and Cb/CbSi₂. The results were: $Q = 86,000$ cal/mole for both W₅Si₃ and Mo₅Si₃ and 78,000 cal/mole for Mo₃Si.

Bartlett and Gage (28) also measured the growth rate of WSi₂ and MoSi₂ during vapor deposition. Although Si reaches the surface of the substrate by vapor transport, it is solid-state diffusion through the silicide that controls the rate of formation. Marker experiments using ZrO₂ spray indicated that only Si diffused appreciably. The activation energy for the growth of both MoSi₂ and WSi₂ was determined to be 25,000 cal/mole. Hashimoto (29) grew WSi₂ on a Si substrate and obtained a Q equal to 22,000 cal/mole for the process. Samsonov, et.al. (30) reported activation energies for deposition of Si on Ta, Mo and Ti as 22,000, 14,000 and 5,000 cal/mole respectively. A general survey of diffusion in inter-metallic compounds has been presented by Hagel (17). Although no data for silicides are offered, the wide range of values for Q (4 to 240 kcal/mole) indicates how much variation one can expect in the diffusion properties.

No data on the actual effect of coating-substrate interaction on coating performance or the effect of barriers on service life have been found. Many empirical studies have been made on the effect of certain additives on oxidation resistance of the refractory silicide coatings. Passmore, et.al. (31, 32) have investigated diffusion barriers in refractory metals, but not silicides.

II. EXPERIMENTAL

A. General

The main reason for lack of reliability in diffusion results is poor control of experimental variables: temperature, pressure (contact), composition. In addition, physical defects such as cracks and pores affect the results. Temperature and pressure can be controlled in the usual manner during the diffusion anneal and contact between halves of the couple can be ensured by careful cleaning, degreasing and deoxidizing of mating surfaces. In the present study, diffusion couples consisted of a refractory metal wafer and a TaSi_2 wafer. This has several advantages over the coating method used by Bartlett. First, TaSi_2 can be coupled with any metal to test the barrier effect, whereas the coating method can only yield a M/M silicide couple. Markers can be placed in the couple at the investigator's discretion. The TaSi_2 phase can be as thick as necessary to ensure that it is not depleted during the anneal. Lastly, the composition and physical defect variables can be better controlled. The metals were obtained commercially as high purity, high density rods or sheets (Appendix II) with very few physical defects. TaSi_2 , on the other hand, is commercially available only in the powder form. In order to obtain reliable diffusion data, TaSi_2 had to be fabricated into a high density, high purity form with a low level of physical defects. Moreover, this fabrication must be reproducible so that these variables will be constant

in order to produce consistent results. Therefore, the first experimental efforts in this research involved the development of a technique for reproducibly fabricating high density, high purity TaSi₂ wafers.

B. TaSi₂ Wafer Fabrication

1. Powder Metallurgy and Sintering

Because the melting point of TaSi₂ is very high ($\sim 2200^{\circ}\text{C}$) it was decided to use powder metallurgical techniques rather than melting to densify TaSi₂ powder. This involves first pressing the powder into the desired shape in a die at room temperature and then sintering at elevated temperatures. Sintering is a surface phenomenon based on producing a high rate of mass flux across contacting surfaces of the powder particles. The temperature needed to effect sintering is usually taken as around three-quarters of the absolute melting point. The temperature dependence and rates of shrinkage can be shown to follow an Arrhenius expression. Pressure is necessary to increase contact between the particle surfaces. High pressures can mechanically deform most metals so that as pressure is increased, spherical particle surfaces flatten against each other increasing contact area.

Sintering aids may also be used to hasten the process. They may operate by increasing the effective area for diffusion, or by activating the surfaces or by inhibiting grain growth. Reducing particle size also increases contact

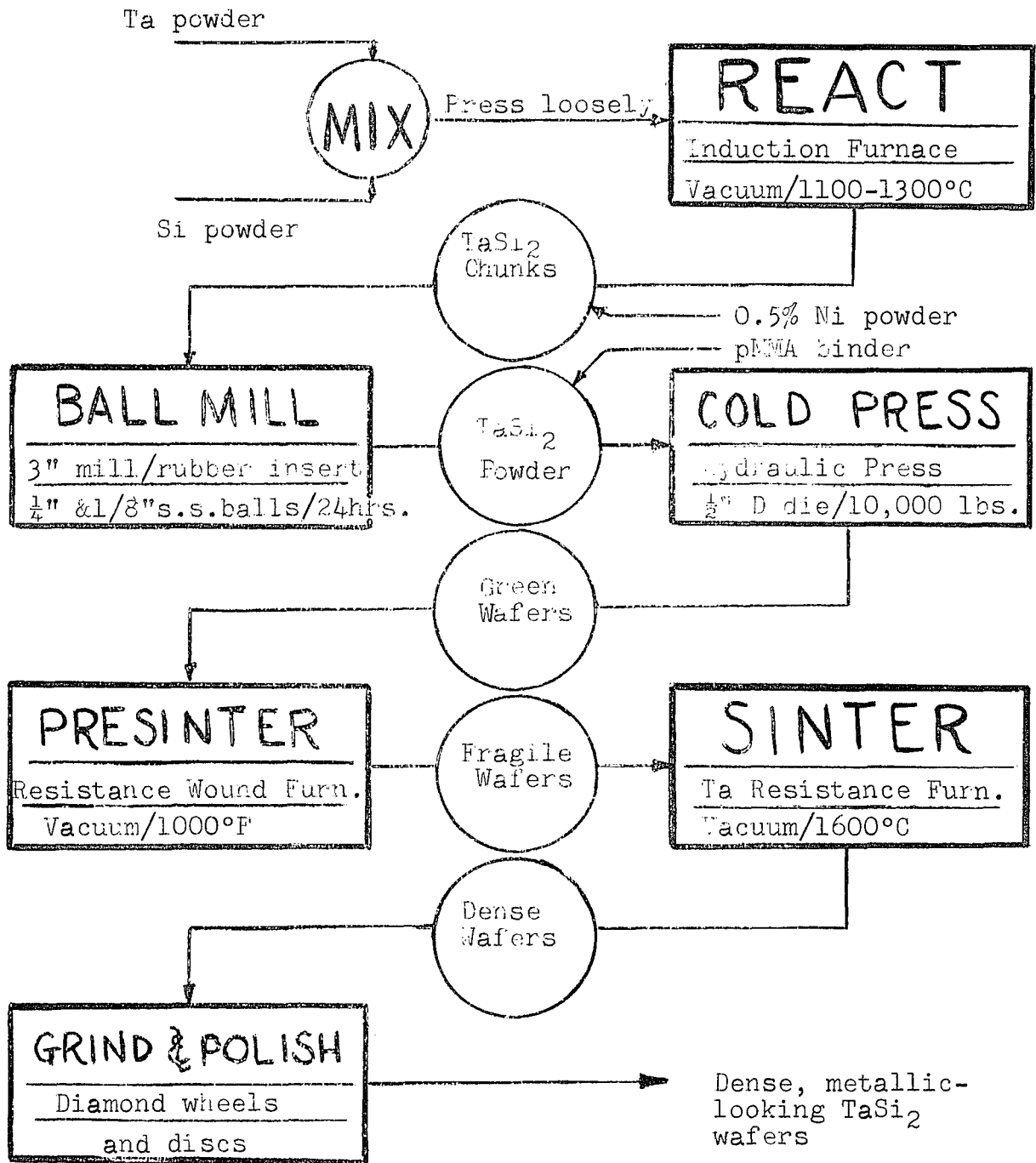
area. Minute amounts of impurities, especially adsorbed on the surfaces of the particles, can have an extremely adverse effect on the sintering process.

2. Successful Procedures

Initially, commercially available TaSi₂ powders were cold-pressed and sintered in an effort to densify the material. The aim was to produce $\frac{1}{2}$ " diameter x 0.05" thick wafers with densities exceeding 90% of theoretical (X-ray) density. The resulting product had no strength and large amounts of various sintering aids did not produce densities in excess of 80% of theoretical. For this reason, the commercial TaSi₂ powders were abandoned and the material was synthesized from the elements. Using the same techniques, our TaSi₂ yielded final densities over 90% of theoretical.

The manufacturing process shown by the flow diagram (Figure 5) is the result of refinements and scale-up of the initial crude fabrication technique. Complete description of each of the steps, the equipment and conditions used can be found in Appendix III. In the reaction step, loosely pressed wafers of the Ta-Si mixture were placed in a pile atop an alumina ring. In this way, only a very small area of the reaction mixture was in contact with any contaminating material. It was necessary to add a nickel sintering aid to hasten sintering and to introduce a plastic binder to the TaSi₂ powder before cold-pressing to facilitate pressing and handling. TaSi₂

FIGURE 5
FLOWSHEET FOR TaSi₂ WAFER MANUFACTURE



being much less ductile than most metals does not flow readily when pressed and small faults are formed, which develop into large cracks upon sintering. The use of a binder eliminated the problem of cracking. To minimize contamination by the binder, a presintering step was added to remove the binder very slowly at a low temperature. During sintering in vacuum an outer layer of Ta_5Si_3 formed by evaporation of Si from the surfaces. This was ground off on a diamond disc. Successive grinding and polishing on diamond discs produced a final $TaSi_2$ wafer with a mirror finish.

3. Quality of $TaSi_2$ Wafers

Fabrication of $TaSi_2$ wafers using the above techniques produced densities in excess of 95% of theoretical. Although the finished wafers had a mirror finish, small pores were visible microscopically. The concentration of pores was small and reproducible (Plate I). X-ray diffraction results showed the wafers to be almost pure $TaSi_2$ with trace amounts of Ta_5Si_3 (<5%). Under high magnification (1250X), the trisilicide was found to be uniformly dispersed across the wafer. (The trisilicide appears pinkish against the gray disilicide background.) No free Si or Ta was found nor were any other phases detected. The microstructure consisted of small, irregular, rounded grains. About 150 such wafers were produced at various times from five different starting batches.

After 60% of the diffusion anneal runs had

been completed, the fabricating techniques which had previously been successful could not be reproduced. Visual inspection of the new wafers indicated a high concentration of large pores. A substantial effort was made to study the effects of binder concentration, pressing load, mixing time, sintering conditions and starting materials.

Since there was already enough data with reliable wafers to test for effects due to wafer porosity or impurity level, it was decided to use various types of wafers in the remaining diffusion anneals. Good wafers were used as controls in the same runs to test for any effects caused by the use of the more porous wafers.

Three types of wafers had been produced during the attempt to reproduce the original technique.

a. Very dense (close to 100% theoretical) wafers containing a high concentration of Ta_5Si_3 with hardly any pores. X-ray diffraction yielded a concentration of about 40-50% Ta_5Si_3 . Microscopic examination showed the Ta_5Si_3 dispersed as a web throughout the $TaSi_2$. These were designated * type (Plate II).

b. Dense ($\sim 95\%$ theoretical) wafers containing a high concentration of extremely small pores. No traces of Ta_5Si_3 could be found in these wafers. These were designated "A" type (Plates III and IV).

c. Low density ($< 90\%$ theoretical) wafers containing an average concentration of large pores with trace amounts of Ta_5Si_3 similar to the original wafers. The grain size was considerably larger and more angular than in any other wafers. These were called "B" type (Plates V and VI).

4. Natural Markers

From thermodynamic calculations it was found that at the temperatures used in the diffusion anneals many prospective marker materials would be expected to be unstable in the silicide system. This problem was overcome when it was noticed during trial diffusion anneals that a line of natural markers appeared in the diffusion couple. These markers are partly the result of "dirt" remaining on the mating surfaces even after careful cleaning. In addition, the $TaSi_2$ wafers have more pores than the metal wafers. This coupled with the low deformability of the $TaSi_2$ wafer tends to pin a row of these pores along the original interface (Plate I). Similar markers were observed by other investigators (19b) who noticed the same effect and tested it by using wire markers and observing them to be along this line of defects. Therefore, no foreign markers were needed to locate the original interface.

C. Experimental Schedule

An initial series of trial diffusion anneals were made to check out equipment and bonding requirements and to

become familiar with techniques and with the appearance of annealed couples. Thereafter, an experimental schedule was set up to retrieve the most information in an allotted time. Figure 6 is a diagram of the schedule followed. The temperature range of interest, as determined by service conditions of the silicides, is up to 2500°F. The lower limit of 2100°F was chosen because bonding between Ta and TaSi₂ was poor below this temperature. The range of times was chosen as the widest practical to ensure stability of diffusion zones at the long times and observation of any non-equilibrium effects for the short times.

Each box then represents one run made at a particular temperature for a particular time. Therefore, the schedule called for 25 runs. The circled number at the top of the box represents the chronological order of the runs. This order was chosen at random so that statistical analysis would be meaningful. The number 1 or 2 in the lower right-hand corner of the box identifies the diffusion anneal furnace for the runs.

The criteria for selection of barrier metals were:

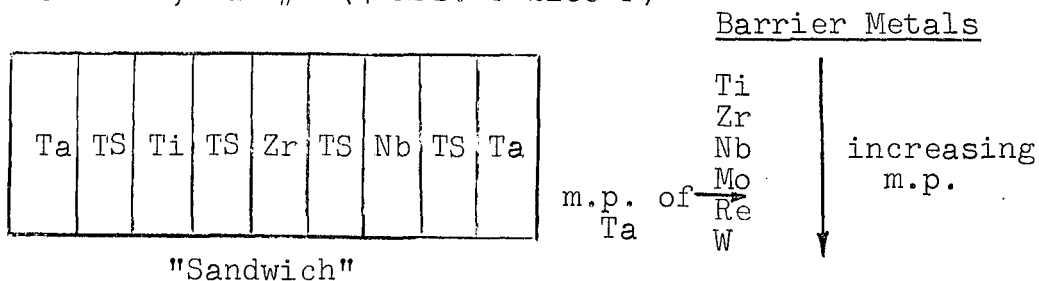
1. Metals that were known to improve oxidation resistance of silicide coatings.
2. Metals with a wide range of melting points bracketing the melting point of tantalum.
3. Metals available in high purity in rods or sheet.

FIGURE 6
EXPERIMENTAL SCHEDULE

Time (Hrs.)	Temperature (°F)				
	2100	2200	2300	2400	2500
4	⑥ Ti, Zr, Nb 1	⑱ Ti, Zr, Mo 2	⑰ Ti, Zr, Nb 1	⑳ Ti, Zr, Mo, Nb 1	⑪ Ti, Zr, Mo, Nb 2
24	⑱ Zr, Nb, Mo 2	⑧ Re, Mo, Nb 2	⑰ W, Zr, Nb, Mo 2	⑤ Re, Ti, Mo, Nb 2	② W, Ti, Zr, Nb 2
48	⑦ W, Re, Zr, Mo 1	⑫ W, Ti, Zr, Nb 1	① Re, Ti, Nb, Mo 1	⑬ W, Re, Zr 1	⑮ W, Re, Ti, Nb 1
72	⑳ W, Re, Ti, Mo 2	⑩ W, Re, Zr, Nb 1	④ W, Re, Ti 2	㉕ W, Ti, Mo, Nb 2	㉑ Re, Zr, Mo 1
100	㉔ W, Re, Ti, Nb 1	⑭ W, Re, Ti, Mo 2	㉒ W, Re, Zr, Mo 2	③ W, Re, Zr 1	⑨ W, Re, Mo 2

Each cell contains Ta.

Cell 1-1, Run #6 (4 hrs. @ 2100°F)



These criteria led to the selection of six barrier metals: tungsten, rhenium, molybdenum, niobium, zirconium and titanium. Rhenium is of particular interest because, besides having a higher melting point than Ta, it is the densest of the selected metals and has a hexagonal crystal structure at the annealing temperatures.

Since Ta/TaSi₂ was the system of primary interest, each of the 25 runs contained a Ta/TaSi₂ couple. Three runs at each of the temperatures were made for each of the barrier metals. A group of couples to be annealed were stacked in a sandwich arrangement and run under exactly the same conditions. Therefore, the three or four metals listed in the center of each box on the schedule indicate which M/TaSi₂ couples were run together with Ta/TaSi₂ at that particular time and temperature. The distribution of barrier metal couples throughout the schedule is semi-random, the restriction being that the higher melting point metals (W, Re and Mo) be run for long times at low temperatures. This was necessary because these materials exhibited poor bonding at the lower temperatures.

An example of how the wafers are stacked in sandwich form is shown below the schedule in Figure 6, which is for couples run at 2100°F for four hours. All couple sandwiches were stacked in the same way: Ta wafers at the ends and four or five TaSi₂ wafers (TS on sketch) alternating with three or four barrier metal wafers. Each wafer measured

approximately $\frac{1}{2}$ " diameter by $1/16$ " thick; therefore, the total sandwich was a cylinder about $\frac{1}{2}$ " in diameter by $\frac{1}{2}$ " high. The use of this procedure in making runs has two advantages.

1. In any run the variables are exactly the same for each of the couples.

2. There are always duplicate couples within any batch.

These advantages allowed analysis of the data for random or unexpected effects. It permitted variations whose effects could be simply tested. For instance, any metal wafer could be coupled with a dense $TaSi_2$ wafer on one side and a porous $TaSi_2$ wafer on the other side. Differences due to porosity were then compared to random differences obtained when the metal was coupled on both sides by one type of $TaSi_2$ wafer. Tests of this kind could be used to study effects of $TaSi_2$ wafer quality and surface preparation of both metal and $TaSi_2$ wafers. Since each $TaSi_2$ wafer is coupled to two different metal wafers, differences on either side of the $TaSi_2$ may be attributed to differences in the metals.

Before the diffusion anneal the various wafers to be used in the sandwich had their surfaces ground flat and parallel and polished. They were then mechanically or chemically fine polished, cleaned with water and acetone and immediately immersed in acetone. The wafers were then, one at a time, taken out of the acetone, dried and stacked in a

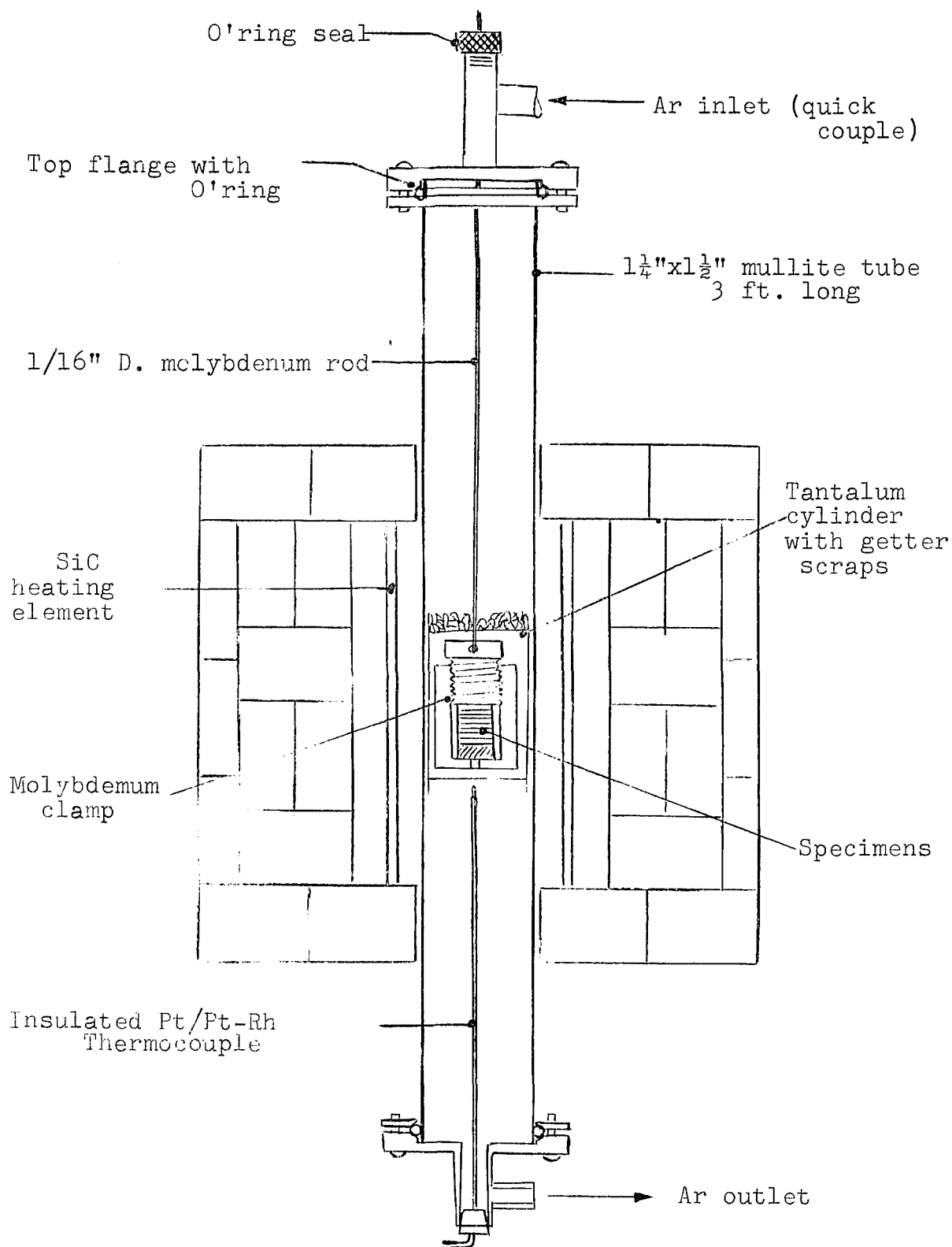
Ta sheet basket. The basket consisted of a bottom circle through which two ribbons were laced and upon which the bottom Ta wafer rested. After the wafers had been stacked to form the sandwich, the four ends of the ribbons were fed through holes in an upper circle of Ta sheet and twisted to hold the wafers in place. The excess ribbon was snipped off and flattened down and the sandwich lowered into a molybdenum clamp. This was a device that applied pressure by differential thermal expansion. The top of the clamp was screwed down tightly against the wafers and the assembly was ready for diffusion annealing.

D. Apparatus

The diffusion annealing was done in two identical SiC resistance furnaces diagrammed in Figure 7. The temperature was controlled to within $\pm 10^\circ\text{F}$ by a powerstat through an on-off controller and accurately measured by a potentiometer connected to a calibrated Pt/Pt-10%Rh thermocouple. The same thermocouple was used for control and measurement. The furnaces were heated over a weekend before the annealing to assure thermal steady state, and the temperature monitored on a Leeds and Northrup recorder.

The Mo clamp was tightened down on the wafer sandwich and the entire assembly, consisting of the clamp suspended on a molybdenum rod was fed through a small O-ring seal connected to the top flange positioned on top of the

FIGURE 7
DIFFUSION ANNEAL APPARATUS



mullite tube. At this stage the rod had been drawn up so that the clamp and top flange were in contact. The flange was then sealed at the top of the tube by an O-ring seal and the argon inlet quickcoupled to the argon line.

Annealing took place in an argon atmosphere to prevent oxidation. The system was flushed by first drawing a vacuum and then releasing argon through the tube. This was repeated at least five times before the argon flow rate was set and the pressure in the tube made slightly above atmospheric. To further protect the specimens from any leaks that might develop, the clamp was completely surrounded by a cylinder of tantalum sheet. This cylinder had a recess near the top into which scraps of Ta, Ti and Zr were placed to provide more gettering action. Five minutes was allowed for temperature adjustment. The specimens at the top of the tube were relatively cold even when the furnace temperature was 2500°F. After the furnace had returned to temperature, the clamp and specimens were rapidly lowered to the center of the furnace. As the result of heating, the wafers inside the molybdenum clamp expanded more than the clamp itself because of the low thermal coefficient of expansion of molybdenum. Consequently, pressure was applied to the couples. The clamp was designed for a minimum required pressure.

After the diffusion anneal, the specimens were pulled up to the top of the tube and quickly cooled with the

aid of a blower. Since the time for the furnace to return to its steady-state control after injection of the clamp was about five minutes and the time for the specimens to cool to below diffusion temperature was also about five minutes, time control was within ± 5 minutes and no corrections need be applied. Within twenty minutes the clamp was cool enough to be disassembled. A high temperature lubricant, MoS_2 , was used to prevent sticking of threads and sandwich.

E. Measuring Techniques

After the specimen sandwich was removed from the clamp, it was mounted in a room temperature-curing resin and sectioned using a small high speed circular saw. The section was taken as close to a diameter of the cylinder of couples as possible and perpendicular to the mating surfaces. One-half of the sandwich was stored for later X-ray diffraction analysis and the other was ground, polished and etched. Great care was taken in grinding to ensure perpendicularity of ground surfaces and coupled surfaces so that false positive errors were not incurred. Polishing and etching techniques proved to present a challenge since the sandwich contained both hard, non-reactive and softer, very reactive materials. Regular metallurgical polishing techniques together with no load SiC grinding proved to be most satisfactory. However, etching of couples consisting of non-reactive TaSi_2 and very reactive metals (such as Ti and Zr) proved more of a problem. Techniques

based on masking the reactive metal while etching TaSi₂ were satisfactorily developed to overcome this difficulty. A list of etching reagents used is in Appendix II.

The appearance of the final microstructures of the diffusion zones appears in Section IV. Measurements of zone thicknesses were made using a Kentron microhardness tester equipped with a 12.5X filar eyepiece and regular 20X and 40X and oil-immersion 100X objectives. The filar was calibrated for each objective using a stage micrometer with 0.001" divisions and the calibration converted to microns. Errors in zone thicknesses resulting from filar calibration were not more than ± 1 micron.

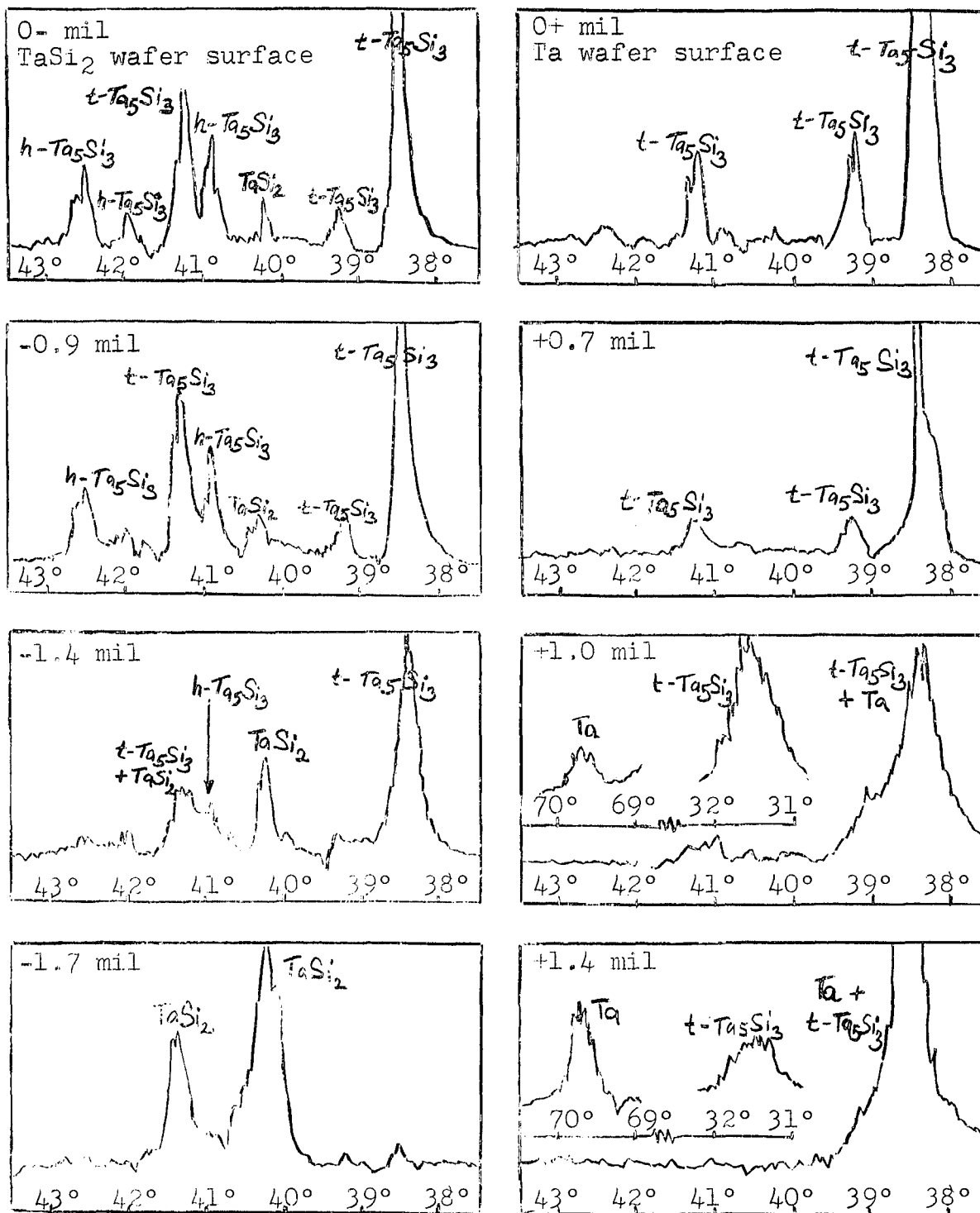
Whenever possible, at least five equally spaced measurements were taken along each side of the couple. As previously mentioned, there were duplicate diffusion zones in each run; one zone was called side (A) and the other side (B) of the couple. Comparison of the two sides of a particular couple was a check of reproducibility within the run and differences due to surface preparation, TaSi₂ wafer quality and poor contact could be readily observed and recorded. Distances from the original interface, indicated by a row of holes, were generally easily measurable.

In order to determine the composition of the growing phases, the couples were subjected to X-ray diffraction analysis. The general method was to analyze and grind successively through the diffusion zone in steps, starting with pure

metal and ending with pure $TaSi_2$. First, the half of the couple sandwich set aside after sectioning was broken out of the mount. Different techniques for analyzing the zones were tried, but one proved most practical and reliable. Since the original interface is marked by a line of defects and holes, this is the line of least resistance to mechanical stress. Therefore, when the couple is mechanically split, the wafers separate at or near the original interface. This was accomplished by applying a torque to the wafers. In most cases the wafers split without much stress. All indications were that when the wafers split cleanly they did so at the original interface. Failure to achieve this condition was easily observed. After splitting, the separated surfaces were subjected to full scans ($17-72^\circ$) in a Norelco diffractometer using $CuK\alpha$ radiation to determine the phases present near the original interface by comparison with the ASTM file (33). Full details of diffraction conditions appear in Appendix IV. If the composition of the zones were well determined, a short scan was chosen to include the high intensity peaks of the phases present. Each wafer was then successively ground and analyzed until pure metal was reached in one wafer, and pure $TaSi_2$ in the other. Measurements of amount of material ground off were made with a micrometer to ± 0.0001 ". Figure 8 is an example of a series of scans made on a $Ta/TaSi_2$ couple showing how the peaks for Ta , $TaSi_2$ and two forms of Ta_5Si_3 vary as the diffusion zone is traversed. Although the method of splitting the wafers and grinding was relatively crude, the results obtained proved very satisfactory.

FIGURE 8

DIFFRACTOMETER SCANS WITHIN THE Ta/TaSi₂ DIFFUSION ZONE



III. EXPERIMENTAL RESULTS

A. General Description

Photomicrographs of microstructures encountered in this investigation appear in Section IV. These indicate how interfaces were located during zone thickness measurements. The appearance of the microstructures and bonding defects adds much to the qualitative understanding of the phenomena. Generally the most difficult interface to identify accurately was the $\text{TaSi}_2/\text{Ta}_5\text{Si}_3$ interface. This was because the appearance of the trisilicide closely resembles that of the disilicide and grows on the grains of the disilicide. Therefore, the $\text{TaSi}_2/\text{Ta}_5\text{Si}_3$ interface generally appears as a wavy, non-uniform line running along grain boundaries, rather than as a sharp, straight line as with the M/M silicide interface. The $\text{TaSi}_2/\text{Ta}_5\text{Si}_3$ interface was actually more noticeable than is indicated in the black and white photomicrographs presented here, since the trisilicide appeared pinkish against the gray disilicide.

Besides yielding quantitative kinetic results, the zone thickness measurements can be analyzed qualitatively for other effects. Since measurements were made at equally spaced intervals along an interface, the first and last measurements are results for the ends of the measurable zone length toward the periphery of the wafers. The center of the zone corresponds to a point either at the middle measurement (if there are

an odd number of readings) or between the two middle measurements (for an even number of readings). Therefore, a plot of zone thickness vs. distance along a diameter indicates variations other than random fluctuations in the growth of diffusion zones. These may be due to the effects of differences in pressure or surface condition. These plots are called Zone Profiles (ZP) and appear together with the appropriate X-ray diffraction data in part E of this section, Figures 11 through 30. The data have been plotted using arbitrary units so that zone thicknesses (X-axis) have been expanded about 1000 times. Thus, fluctuations are greatly exaggerated so that trends may be readily observed. The center line of the wafer is indicated in each plot and since the M/M silicide interface was always most clearly and accurately defined, all thicknesses have been shown relative to that interface.

The X-ray diffraction data shown with the Zone Profiles appears in a plot called Concentration Change Profile (CCP). These profiles are drawn by recording the absolute intensities above background of the strongest (or second strongest) peaks of the phases in the diffusion zone as a function of distance from the original interface. The experimental technique has been previously described. Although the absolute intensity of a particular peak in a mixture of solids does not relate directly to concentration, a qualitative relationship may be assumed. Therefore, by noting the changes

in intensities, changes in concentration can be observed and the composition of the diffusion zones may be deduced.

Parabolic growth constants, k , are tabulated in Tables III through VIII for each of the systems investigated. In each table, k values are listed for isothermal growth at each of the experimental temperatures. They are given for the total diffusion zone and for each of the partial zones composing it. The data were analyzed by performing a least-squares analysis on the equations

$$(\Delta x)^2 = k_0 t$$

and $(\Delta x)^2 = k_s t + b.$

Details of statistical analysis applied to the data appear in Appendix V. The variance is expressed as a 95% confidence interval (C.I.) and therefore the first two values tabulated are:

$$\text{Parabolic constant (through origin)} = k_0 \pm 95\%$$

C.I. of k_0 and

$$\text{Parabolic constant (best straight line)} = k_s \pm 95\%$$

C.I. of k_s ; $\sqrt{b} \pm 95\%$ C.I. of \sqrt{b}

where k 's are in cm^2/sec and \sqrt{b} values are in microns.

The second equation (best straight line) was tested to ascertain if there were delay times for the formation of any phases. This would correspond to a negative value for b . Positive values of b have no physical significance since this would require a finite thickness of the growing phase to

be present before the diffusion anneal was started. The sign of b was retained before the \sqrt{b} for this purpose.

The third value, C_{test} , is a result of a linear regression analysis performed on the equation : $(\Delta x)^2 = kt$. This analysis yields a linear regression factor, F_L , which if significant indicates that a straight line should be fitted to the plot of $(\Delta x)^2$ versus t . A departure from linearity factor, F_D , if significant, indicates that a higher order curve can be fitted. Using standard statistical practices, F_D as well as F_L frequently proved to be significant even when F_L was very much greater than F_D and it seemed evident that the best fit should be a straight line. A ratio of the linear factor (or contribution) to the total contribution (linear plus higher order factors) was used and called the C_{test} . Therefore, $C_{\text{test}} = \frac{F_L}{F_L + F_D}$ and varies between 0 and 1. The approach of the C_{test} to unity then indicates the relative strength of the linear factor and measures the reliability of the assumption of linearity.

The three values described above are the result of the analysis of all the data recorded for a particular temperature. The three values appearing immediately below these (designated k_O^* , k_S^* and C_{test}^*) are the results of the same analysis performed on data omitting the poorer wafers. This was done to determine the effects of the use of these poorer wafers on the reliability of the data. All of the statistical

analyses were performed on an IBM 360 computer using a program written in Fortran IV.

B. Specific Systems

1. Ta/TaSi₂

Plates I and VIII show the appearance of typical Ta/TaSi₂ diffusion zones in the unetched and etched state respectively. The Ta/Ta₅Si₃ interface (x_M) and the original interface (x_0) are easily identifiable in the unetched couple as well as in the etched couple; but the TaSi₂/Ta₅Si₃ interface (x_{TS}) can be located only after etching. On the other hand, Plate VII indicates the appearance of a couple in which the junction was broken. In this couple the adhesion was very weak because annealing was at the lowest experimental temperature for only four hours. In this instance, mounting of the sample was enough to rupture the intermediate zone. However, readings were taken for total zone thickness for such a couple because, as is shown in the ZP for this couple (Figure 11), the total thicknesses did not vary greatly from the one reliable point at which the couple was well joined.

The results of the thickness measurements in the Ta/TaSi₂ system are shown in Table III and in Figures 9a and 9b. It will be observed from Table III that the parabolic growth constants, k , for the total zone have been measured within fairly narrow confidence limits (approximately $\pm 5\%$ to $\pm 15\%$ of the average value). (The Ta/TaSi₂ system is the only

TABLE III

Ta/TaSi₂ SYSTEM - PARABOLIC RATE CONSTANTS

TEMP. (°F)	TOTAL ZONE	PARTIAL ZONES	
	K's in (cm ² /sec); T ₅ (μ)	Ax ₁ (Ta ₅ Si ₃) TaSi ₂ Side	Ax ₂ (Ta ₅ Si ₃) Ta Side
2100 k ₀ = k _S = k _S '= C _{test} = 0.973	(7.5±0.8) x10 ⁻¹² (6.7±0.8) x10 ⁻¹² ; 4±4 C _{test} = 0.974	(4±4) x10 ⁻¹³ (-1±4) x10 ⁻¹³ ; 4±3 0.387	(5±1) x10 ⁻¹² (4±1) x10 ⁻¹² ; 5±4 0.855
	(7.5±0.9) x10 ⁻¹² (6.6±0.8) x10 ⁻¹² ; 4±4 C _{test} = 0.973	same	(4.6±0.9) x10 ⁻¹² (4.1±0.8) x10 ⁻¹² ; 3±5 0.945
2200	(1.5±0.3) x10 ⁻¹¹ (1.1±0.2) x10 ⁻¹¹ ; 8±4 0.949	(3±2) x10 ⁻¹² (1±8) x10 ⁻¹³ ; 4±2 0.492	(7.7±0.9) x10 ⁻¹² (6.3±0.8) x10 ⁻¹² ; 3±2 0.940
	(1.5±0.3) x10 ⁻¹¹ (1.0±0.2) x10 ⁻¹¹ ; 9±7 0.932	(3±2) x10 ⁻¹² (-1±1) x10 ⁻¹² ; 6±3 0.377	(8±1) x10 ⁻¹² (6±1) x10 ⁻¹² ; 4±3 0.924
2300	(5.5±0.5) x10 ⁻¹¹ (6.0±0.4) x10 ⁻¹¹ ; -10±10 0.990	(6±2) x10 ⁻¹² (7±2) x10 ⁻¹² ; -5±7 0.934	(2.6±0.2) x10 ⁻¹¹ (2.7±0.2) x10 ⁻¹¹ ; -4±7 0.993
	(5.2±0.7) x10 ⁻¹¹ (6.5±0.6) x10 ⁻¹¹ ; -17±12 0.955	(4±1) x10 ⁻¹² (6±1) x10 ⁻¹² ; 5±6 0.912	(2.7±0.3) x10 ⁻¹¹ (3.2±0.2) x10 ⁻¹¹ ; -10±7 0.973
2400	(1.27±0.08) x10 ⁻¹⁰ (1.31±0.08) x10 ⁻¹⁰ ; -9±9 0.994	(1.3±0.3) x10 ⁻¹¹ (1.8±0.3) x10 ⁻¹¹ ; -11±8 0.879	(6.2±0.3) x10 ⁻¹¹ (5.6±0.3) x10 ⁻¹¹ ; 10±8 0.997
	(1.27±0.09) x10 ⁻¹⁰ (1.34±0.09) x10 ⁻¹⁰ ; -12±15 0.992	same	(6.1±0.4) x10 ⁻¹¹ (5.8±0.4) x10 ⁻¹¹ ; 8±9 0.999
2500	(2.5±0.3) x10 ⁻¹⁰ (2.0±0.2) x10 ⁻¹⁰ ; 28±16 0.973	(2.3±0.6) x10 ⁻¹¹ (1.5±0.5) x10 ⁻¹¹ ; 12±11 0.922	(1.21±0.09) x10 ⁻¹⁰ (1.07±0.08) x10 ⁻¹⁰ ; 16±13 0.983
	(2.5±0.3) x10 ⁻¹⁰ (2.1±0.2) x10 ⁻¹⁰ ; 26±23 0.962	(2.2±0.5) x10 ⁻¹¹ (1.6±0.5) x10 ⁻¹¹ ; 10±10 0.870	(1.21±0.09) x10 ⁻¹⁰ (1.05±0.08) x10 ⁻¹⁰ ; 17±13 0.982

system in which the growth of the total zone has basic significance.) For instance, the first value for k , $k_0 = (7.5 \pm 0.8) \times 10^{-12}$ cm²/sec means that one has 95% confidence that the true value for k_0 lies between 8.3×10^{-12} cm²/sec and 6.7×10^{-12} cm²/sec. The values for k_s and b indicate that variations of the best straight line through the data about the origin are random, and a line through the origin can be accepted as the best line. In other words, there is no incubation period for the formation of Ta₅Si₃. The C_{test} values are very close to unity indicating that the growth rate is truly parabolic. Comparing the data for the partial zones, it is clear that the values of the Δx_2 zones (Ta side) are more accurate than those for the Δx_1 zones (TaSi₂ side). This stems from the extra difficulty in identifying the TaSi₂/Ta₅Si₃ interface. Comparing the complete and the incomplete (●) values, it is obvious that the inclusion of data from couples employing poorer TaSi₂ wafers has a negligible effect on the overall reliability.

Figures 9a and 9b are examples of the parabolic plots obtained. The Ta/TaSi₂ system represents a relatively simple growth mechanism. Each point represents an average of about ten pieces of data. The lines drawn are the least-squares lines through the origin utilizing all of the data. The scatter for individual points is shown in Figure 9a as $\pm\sigma$, but is omitted on the other parabolic plots for purposes of clarity. The overall quality of the data may best be inferred from the k values in Table III.

The Arrhenius plot of the data for the total zone growth in the Ta/TaSi₂ system is shown in Figure 31. The line drawn is the least-squares fit of all the data (not the k₀ values alone) and each point represents an average of approximately fifty pieces of data. The slope and intercept of the line were computed using the same statistical approach applied in the determination of parabolic growth constants, and the statistical limits of the values expressed as a 95% confidence interval. The expression for the least-squares line is $k = 5e^{-77,000/RT}$ where Q (the activation energy) = 77,000 ± 3,000 calories/mole and the pre-exponential constant = $5 \frac{+6}{-3}$ cm²/sec.

The ZP (Figure 11) for the couple corresponding to the microstructure shown in Plate VII has already been discussed. It can also be observed from this plot and ZPs for Ta/TaSi₂ couples annealed at different conditions (Figures 12 through 14) that fluctuations along the diameter indicate nothing more than random variations since no trends can be observed. They also clearly depict which sides of the couples exhibit poor bonding by the relative paucity of data points.

The CCP in Figure 11 shows some interesting features. First, Ta₅Si₃ was found to grow in two different crystallographic forms: tetragonal and hexagonal. Bartlett (21) found only tetragonal Ta₅Si₃ in his couples, but Nowotny, et.al. (34) reported Ta₅Si₃ as having a hexagonal structure. On the other hand, Knapton (35) and Parthe, et.al. (36, 37)

reported that pure Ta_5Si_3 is normally tetragonal and that the hexagonal form is an impurity-stabilized phase. In this research, when Ta_5Si_3 formed in small amounts during the synthesis of $TaSi_2$, it was found to be hexagonal; whereas the trisilicide formed by loss of Si from the $TaSi_2$ wafer surface during sintering was found to be tetragonal. In Figure 11, hexagonal Ta_5Si_3 can be seen to form only on the $TaSi_2$ side of the original interface (the negative directions toward the sides of the CCP, designated Δx_1 in the ZP. The Ta or metal part of the couple is located in the center of both ZP and CCP plots with $TaSi_2$ on either side, forming side (A) and side (B) for a couple as it appears in the wafer sandwich.) The ratio of hexagonal Ta_5Si_3 to tetragonal Ta_5Si_3 was always higher in the Δx_1 zone ($TaSi_2$ is hexagonal) than in the Δx_2 zone (growing from Ta (cubic)) as evidenced in Figures 12 through 14.

Figure 14 is a good example of how well the CCP discloses the compositions of the growing zones. (There is a small amount of overlapping of phases growing in adjacent zones due to diffraction of X-rays by different depths within the couple. Using a relationship given by Cullity (38), 95% of X-ray diffraction in Ta_5Si_3 takes place within a layer approximately 0.3 mils thick. (Appendix IV)). Notice that the amounts of hexagonal and tetragonal Ta_5Si_3 in the Δx_1 zone are about equal. The ratio of the two crystallographic forms of trisilicide varied from practically pure tetragonal

in Figure 11 to an intermediate condition in Figures 12 and 13 and finally to a state in which the two forms are present in equal amounts (Figure 14). This is a general trend noted in the diffusion couples as the zone grows. That is, the ratio of hexagonal Ta_5Si_3 to tetragonal Ta_5Si_3 on the $TaSi_2$ side of the original interface increases from a small number for thin diffusion zones to about unity for the thickest zone observed as depicted in Figure 14. On the other hand, in the Δx_2 zone, the ratio increases only slightly from its low thin-zone value as the zone thickness increases. Therefore, not only are there different concentrations of the two forms of trisilicide on each side of the original interface, but the relative concentrations change differently as a function of time and temperature.

Another interesting feature of Figure 11 is that it indicates that a lower silicide (Ta_2Si) is growing. This phase does not appear as a differentiated zone under the microscope, which means that either it is dispersed within the trisilicide or present in very small amounts. Lavendel and Elliot (25) found this phase growing only at high temperatures. Although there is no microscopic evidence of Ta_2Si in any of the data, the phase does grow apparently as a dispersed phase at low temperatures when local deficiencies of Si occur due to low rates of diffusion. This is illustrated in Figures 11 and 12. Figures 13 and 14 indicate that at higher temperatures

Ta_2Si can also grow; now as thin layers and only under certain unusual conditions. By comparing sides (A) and (B) in both high temperature CCPs, it can be seen that the Ta_2Si layer forms only when there is a poor junction between the Ta and $TaSi_2$ wafers. This is because the silicon activity in Ta_2Si is low and therefore appears only when it can be in equilibrium with a low concentration of Si, as when a barrier to diffusion such as an empty space is interposed in the growing zone.

2. Diffusion Barrier Systems

As stated earlier, this research had two main aims. First was the measurement of the rate of loss of silicon to tantalum from $TaSi_2$. The second purpose was the search for a diffusion barrier to minimize this loss. For the latter, it was preferable to examine the behavior of a substantial number of candidate metals rather than make precise measurements on a few. Therefore, the number of couples tested in the M/ $TaSi_2$ systems were fewer and the results less reliable. Nevertheless, they were more than adequate for the purpose. In addition, the nature of the intermediate layers was investigated.

a. Nb/ $TaSi_2$

Niobium resembles tantalum in its properties and forms similar silicides; $NbSi_2$ (hexagonal crystal structure), hexagonal and tetragonal Nb_5Si_3 . Although the metal-rich side of the Nb-Si phase diagram is not as clearly defined as that of the Ta-Si phase diagram and Nb and its

silicides melt at considerably lower temperatures, the similarities between Nb and Ta make analysis of the Nb/TaSi₂ system imperative. Plates IX and X show the microstructure of the Nb/TaSi₂ diffusion zone after annealing at low and high temperatures respectively. Plates XI, XII and XIII show an isothermal sequence, revealing the appearance of the growing zones at 2200°F. From the photomicrographs it is noticed that there are two zones growing on the Nb side of the original interface (Δx_a and Δx_2) as well as the Ta₅Si₃ zone (Δx_1) on the TaSi₂ side of the original interface. The appearance of the zones is the same for all of the experimental conditions and even under the condition furthest from equilibrium (Plate IX) the zones exhibit the same microstructure. The columnar growth of the Δx_2 zone is an interesting feature brought out by proper etching of the sample and is a frequent phenomenon in solid state surface reactions. All of the interfaces were readily identifiable and the results of the thickness measurements in the Nb/TaSi₂ system appear in Table IV.

The first item to be noticed in Table IV is the values of the parabolic growth constants, k . They are generally an order of magnitude larger than the corresponding values in the Ta/TaSi₂ system for both total and Δx_1 (Ta₅Si₃) zones. This indicates that niobium would probably make a poor barrier material. The confidence limits for the parabolic growth constants listed in Table IV are somewhat

TABLE IV

Nb/TaSi₂ SYSTEM - PARABOLIC RATE CONSTANTS

TEMP. (°F)	TOTAL ZONE	PARTIAL ZONES		
	k's in (cm ² /sec): \bar{V} (μ)	Δx_1 (Ta ₅ Si ₃)	Δx_2	Δx_3
2100 k _o = k _s =	(1.3±0.2) x10 ⁻¹⁰ (0.9±0.1) x10 ⁻¹⁰ ; 23±17 C _{test} = 0.867	(3.3±0.9) x10 ⁻¹¹ (1.5±0.7) x10 ⁻¹¹ ; 17±12 0.642	(1.4±0.1) x10 ⁻¹¹ (1.5±0.1) x10 ⁻¹¹ ; -4±5 0.991	(4.0±0.7) x10 ⁻¹² (2.5±0.5) x10 ⁻¹² ; 5±3 0.847
	(1.02±0.08) x10 ⁻¹⁰ (1.03±0.08) x10 ⁻¹⁰ ; -4±14 C _{test} = x (2 points)	(2.1±0.3) x10 ⁻¹¹ (2.1±0.3) x10 ⁻¹¹ ; -3±9 x (2 points)	(1.5±0.2) x10 ⁻¹¹ (1.5±0.2) x10 ⁻¹¹ ; -3±7 x (2 points)	(3.3±0.5) x10 ⁻¹² (2.8±0.4) x10 ⁻¹² ; 3±3 x (2 points)
2200	(1.8±0.2) x10 ⁻¹⁰ (1.6±0.2) x10 ⁻¹⁰ ; 20±20 0.982	(4.0±0.8) x10 ⁻¹¹ (3.3±0.8) x10 ⁻¹¹ ; 11±12 0.968	(1.7±0.6) x10 ⁻¹¹ (0.8±0.5) x10 ⁻¹¹ ; 12±10 0.625	(7±1) x10 ⁻¹² (5±1) x10 ⁻¹² ; 6±4 0.914
	same	same	same	same
2300	(3.8±0.8) x10 ⁻¹⁰ (2.3±0.7) x10 ⁻¹⁰ ; 36±28 0.754	(1.6±0.7) x10 ⁻¹⁰ (-2±2) x10 ⁻¹¹ ; 40±14 0.439	(4±2) x10 ⁻¹¹ (-0.9±0.5) x10 ⁻¹¹ ; 20±10 0.400	(2.6±0.8) x10 ⁻¹¹ (6±4) x10 ⁻¹² ; 13±7 0.581
	2.7x10 ⁻¹⁰	6.6x10 ⁻¹¹	1.6x10 ⁻¹¹	1.9x10 ⁻¹¹
2400	Only 1 Point	Only 1 Point	Only 1 Point	Only 1 Point
	(5.4±0.7) x10 ⁻¹⁰ (5.0±0.7) x10 ⁻¹⁰ ; 21±32 0.993	(1.0±0.3) x10 ⁻¹⁰ (0.9±0.3) x10 ⁻¹⁰ ; 12±21 0.970	(8±1) x10 ⁻¹¹ (10±1) x10 ⁻¹¹ ; -13±12 0.954	(2.0±0.4) x10 ⁻¹¹ (1.1±0.3) x10 ⁻¹¹ ; 10±6 0.798
2500	(5.3±0.9) x10 ⁻¹⁰ (4.9±0.8) x10 ⁻¹⁰ ; 24±38 0.992	(1.0±0.3) x10 ⁻¹⁰ (0.8±0.3) x10 ⁻¹⁰ ; 15±24 0.962	(8±1) x10 ⁻¹¹ (10±1) x10 ⁻¹¹ ; 15±14 0.943	(2.0±0.5) x10 ⁻¹¹ (1.0±0.3) x10 ⁻¹¹ ; 11±7 0.773
	(6±1) x10 ⁻¹⁰ (5±1) x10 ⁻¹⁰ ; 37±33 0.941	(1.1±0.4) x10 ⁻¹⁰ (0.9±0.3) x10 ⁻¹⁰ ; 16±20 0.943	(3.3±0.7) x10 ⁻¹¹ (1.9±0.5) x10 ⁻¹¹ ; 11±7 0.843	(6.6±0.8) x10 ⁻¹¹ (5.7±0.8) x10 ⁻¹¹ ; 9±9 0.985
2500	(7±1) x10 ⁻¹⁰ (4.5±0.5) x10 ⁻¹⁰ ; 37±20 0.904	(1.1±0.3) x10 ⁻¹⁰ (5±2) x10 ⁻¹¹ ; 20±12 0.745	(3.9±0.8) x10 ⁻¹¹ (2.3±0.5) x10 ⁻¹¹ ; 10±6 0.850	(7.1±0.7) x10 ⁻¹¹ (6.4±0.7) x10 ⁻¹¹ ; 7±8 0.987

higher than those obtained in the Ta/TaSi₂ system; ranging between approximately $\pm 10\%$ and $\pm 20\%$ of the average value. This is to be expected because 40% fewer runs were made in the Nb/TaSi₂ than in the Ta/TaSi₂ system. Again, the values of b indicate that there is no incubation period for any of the zones. By comparing the results for each of the partial zones, it is evident that each zone has been measured with approximately the same accuracy. Most of the C_{test} values are close to unity indicating parabolic growth, but there are some exceptions. For example, the values at 2300°F using complete data are quite low (the corresponding confidence limits are higher than for the other temperatures). The reason for this is that two of the three runs made at this temperature used a poorer type of TaSi₂ wafer. When this type of wafer was diffusion-annealed using a good TaSi₂ wafer as a control at the same conditions, it was found that the poorer wafers yielded larger diffusion zones in the Nb/TaSi₂ and Zr/TaSi₂ systems. Therefore, the data obtained using these types of TaSi₂ wafers in the Nb/TaSi₂ couples are of questionable reliability; and by comparing the complete data with the incomplete data (•) at 2300°F it can be seen that exclusion of the questionable data lowers the average values for k considerably. Since (after omitting this data), the results depend on only one couple, confidence intervals and C_{test} values have no meaning and statistical methods cannot be used. Nonetheless,

the effect of omitting poor data can be observed at 2100°F for the Δx_1 zone. In this case, the confidence interval was reduced to one-third of its previous value. In the tables of k values for the M/TaSi₂ systems, when all the data for one particular run are omitted (because poor TaSi₂ wafers were incorporated in the couple) no value for C_{test}° can be computed and this is designated by "X (2 points)". If two runs are omitted as at 2300°F in Table IV, the value of the confidence interval also has no meaning and only an average k_0 value is entered and the notation "Only 1 point". One other low value for C_{test} is noted in Table IV. This is the result for Δx_2 at 2200°F. In this case, only good TaSi₂ wafers were used, but close inspection of Plate XIII will indicate that the Δx_2 zone is unusual. This is the only one of the fifteen Nb/TaSi₂ couples to exhibit a region in Δx_2 close to the original interface in which the columnar grain structure is lost. Since the Δx_2 zone grew in a non-typical manner, this is reflected in the quality of the data. The Arrhenius plots and results of temperature dependence for the M/TaSi₂ systems will be presented comparatively in parts C and E of this section.

The ZP and CCP plots for Nb/TaSi₂ couples appear in Figures 15 through 18. As in the Ta/TaSi₂ couples two crystallographic forms of the trisilicide appear: tetragonal Nb₅Si₃ and hexagonal Nb₅Si₃. Knapton (35) assigns a tetragonal structure to the pure trisilicide and calls the

hexagonal Nb_5Si_3 an impurity-stabilized phase. In this work it was found that both forms of trisilicide grew with the hexagonal phase increasing in amount relative to the tetragonal phase as the zone grew. This can be observed in Figures 15 through 18. In Figure 15 (thinnest zone) only the tetragonal Nb_5Si_3 appears. After 100 hours at the same temperature (Figure 16) the hexagonal phase is also evident. At 2500°F (Figure 17) the amount of hexagonal Nb_5Si_3 increases until, for the thickest zone (Figure 18), the hexagonal trisilicide becomes predominant. In the same sequence, it can be seen that as hexagonal Nb_5Si_3 becomes prominent, NbSi_2 appears near the original interface. NbSi_2 should be unstable between Ta_5Si_3 and Nb_5Si_3 (if Si activities in Ta and Nb silicides of the same stoichiometry are close, as assumed); but X-ray diffraction analysis indicates a thin layer of NbSi_2 existing close to the original interface. This is observed only at high temperatures when rapid Si transport can produce the unstable highest silicide. The formation of NbSi_2 (which is hexagonal) could account for the stabilization of the hexagonal Nb_5Si_3 phase.

Besides NbSi_2 and two forms of Nb_5Si_3 another phase (labeled X) is drawn on the CCP. This represents one unidentified X-ray peak not characteristic of any Nb silicides in the ASTM file. The shapes of the X profiles closely follow the shapes of the tetragonal Nb_5Si_3

profiles and one might therefore infer that the unidentified peak is a usually negligible Nb_5Si_3 peak enhanced by preferred orientation. But this would not explain the appearance of two distinct microscopic zones in the ZP of Figure 15, where, if X and $t\text{-Nb}_5\text{Si}_3$ were the same phase, the CCP would predict only one phase. Therefore, if one accepts the microscopic evidence, the X profile must be considered as a phase separate from the trisilicide.

The difficulty in identifying the X phase is that the ASTM file contains only the diffraction data for NbSi_2 and three Nb_5Si_3 's. The phase diagram, Figure I-2 (Appendix I), also presents a lower silicide, Nb_4Si . Another lower silicide, Nb_3Si , has also been proposed (26); but Alysmovskii, et.al. (39) were unable to establish the existence of either Nb_3Si or Nb_4Si . In addition, Lavendel and Elliot (25) found no evidences of lower silicides in Nb/ NbSi_2 couples at any of their experimental conditions. Hence the existence of lower silicides is in some doubt. On the other hand, the shape of the X profile in Figure 18 seems to indicate that the X phase corresponds to Δx_a and is therefore a lower silicide; but the other CCP plots give no indication as to which phase is growing in Δx_a and which phase is growing in Δx_2 . Therefore, the experimental evidence in this work is also inconclusive in determining the existence of a lower Nb silicide layer.

The X phase may be a silicide higher in Si content than Nb_5Si_3 for Koffman and Olgivie (26), in trying to grow Nb_5Si_3 between mixed couples of Nb_3Si/Nb_5Si_3 and $Nb_5Si_3/NbSi_2$, found two distinct layers growing. The appearance of their diffusion zone strikingly resembled that observed in this work. The zone adjacent to the high silicon concentration wafer had a columnar microstructure and was identified as Nb_3Si_2 by electron beam microprobe analysis. Parthe, et.al. (40) had assumed this composition for what is now accepted as tetragonal Nb_5Si_3 ; but Koffman and Olgivie showed both Nb_3Si_2 and Nb_5Si_3 to be growing side by side. Therefore, if Nb_3Si_2 and Nb_5Si_3 can be considered as having very similar crystal structures but very dissimilar microstructures, the Δx_a zone and the Δx_2 zone can be considered Nb_5Si_3 and Nb_3Si_2 respectively. It is possible that a slight change in stoichiometry results in a major change in the chemical behavior and physical appearance, but very little change in X-ray diffraction properties. In some instances a microscopic zone may be a mixture of more than one phase, e.g. tetragonal Nb_5Si_3 and hexagonal Nb_5Si_3 . In other cases, a phase may be found by X-ray analysis, but be too thin for microscopic detection.

b. $Zr/TaSi_2$

Zirconium is a very active metal and forms many silicides. Because it has been used as an additive

to help increase the protectiveness of silicide coatings, its effectiveness as a diffusion barrier has been studied. Zr metal goes through a phase transition from hexagonal to cubic crystal structure at 860°C and is therefore cubic at the diffusion anneal temperatures. Plates XIV through XVII show the intermediate zones in the Zr/TaSi₂ system as they grow thicker. It is apparent from these photomicrographs that the TaSi₂/Ta₅Si₃ interface (x_{TS}) is less distinguishable than in the previously cited plates. This is because of the high chemical activity of Zr and its silicides, so that proper etching of the TaSi₂ and Ta₅Si₃ would overetch the Zr side of the couple. Masking the highly active side with tape or wax while etching the Ta₅Si₃ helped in disclosing the total microstructure; but difficulty in exactly positioning the masking material made it necessary to compromise the etching procedure so that the Ta₅Si₃ was usually underetched. Another feature of the Zr/TaSi₂ couple is that at the higher temperatures the Zr silicides become cracked and porous (Plates XVI and XVII). This makes measurements of the thickest zones less accurate.

The results of the thickness measurements for the Zr/TaSi₂ system are listed in Table V, and the k values can be seen to be of the same order of magnitude as in the Nb/TaSi₂ system for both total and Δx_1 zones. Therefore, zirconium does not act as a diffusion barrier. The confidence intervals for k_0 are generally in the same range as for the

TABLE V

Zr/TaSi₂ SYSTEM - PARABOLIC RATE CONSTANTS

TEMP. (°F)	TOTAL ZONE	PARTIAL ZONES		
	k's in (cm ² /sec); \sqrt{b} (μ)	Δx_1 (Ta ₅ Si ₃)	Δx_2	Δx_a
2100	$k_o = (1.5 \pm 0.4) \times 10^{-10}$ $k_s = (1.0 \pm 0.3) \times 10^{-10}; 20 \pm 20$ $C_{test} = 0.714$	$(3 \pm 2) \times 10^{-11}$ $(1 \pm 1) \times 10^{-11}; 14 \pm 12$ 0.377	$(3.5 \pm 0.6) \times 10^{-11}$ $(4.3 \pm 0.5) \times 10^{-11}; -8 \pm 7$ 0.938	$(3 \pm 1) \times 10^{-12}$ $(2 \pm 1) \times 10^{-12}; 1 \pm 3$ 0.971
	$k_o = (1.1 \pm 0.1) \times 10^{-10}$ $k_s = (1.0 \pm 0.1) \times 10^{-10}; 5 \pm 12$ $C_{test} = x$ (2 points)	$(1.5 \pm 0.4) \times 10^{-11}$ $(1.2 \pm 0.3) \times 10^{-11}; 5 \pm 7$ \bar{x} (2 points)	$(3.8 \pm 0.6) \times 10^{-11}$ $(4.2 \pm 0.6) \times 10^{-11}; -6 \pm 8$ \bar{x} (2 points)	$(3 \pm 1) \times 10^{-12}$ $(2 \pm 1) \times 10^{-12}; 2 \pm 3$ x (2 points)
2200	$(1.6 \pm 0.2) \times 10^{-10}$ $(1.4 \pm 0.2) \times 10^{-10}; 17 \pm 19$ 0.952	$(2.3 \pm 0.7) \times 10^{-11}$ $(1.2 \pm 0.6) \times 10^{-11}; 12 \pm 10$ 0.646	$(4 \pm 1) \times 10^{-11}$ $(3 \pm 1) \times 10^{-11}; 8 \pm 15$ 0.876	$(1.2 \pm 0.4) \times 10^{-11}$ $(1.3 \pm 0.4) \times 10^{-11}; -4 \pm 8$ 0.985
	1.7×10^{-10} Only 1 Point	2.5×10^{-11} Only 1 Point	2.5×10^{-11} Only 1 Point	1.2×10^{-11} Only 1 Point
2300	$(4 \pm 1) \times 10^{-10}$ $(1.5 \pm 0.6) \times 10^{-10}; 70 \pm 40$ \bar{x} (2 points)	$(3 \pm 4) \times 10^{-11}$ $(-4 \pm 2) \times 10^{-11}; 40 \pm 21$ \bar{x} (2 points)	$(6 \pm 3) \times 10^{-11}$ $(2 \pm 3) \times 10^{-11}; 29 \pm 28$ \bar{x} (2 points)	$(1.5 \pm 0.8) \times 10^{-11}$ $(1.0 \pm 0.8) \times 10^{-11}; 10 \pm 14$ \bar{x} (2 points)
	6.2×10^{-10} Only 1 Point	7.3×10^{-11} Only 1 Point	1.3×10^{-10} Only 1 Point	2.6×10^{-11} Only 1 Point
2400	$(6.3 \pm 0.6) \times 10^{-10}$ $(5.2 \pm 0.6) \times 10^{-10}; 40 \pm 30$ 0.958	$(8 \pm 1) \times 10^{-11}$ $(6 \pm 1) \times 10^{-11}; 17 \pm 16$ 0.927	$(8 \pm 1) \times 10^{-11}$ $(5.4 \pm 0.6) \times 10^{-11}; 20 \pm 12$ 0.925	$(5.7 \pm 0.7) \times 10^{-11}$ $(5.3 \pm 0.6) \times 10^{-11}; 8 \pm 12$ 0.981
	same	same	same	same
2500	$(1.0 \pm 0.2) \times 10^{-9}$ $(6 \pm 2) \times 10^{-10}; 80 \pm 60$ 0.815	$(1.3 \pm 0.7) \times 10^{-10}$ $(-1 \pm 5) \times 10^{-11}; 45 \pm 29$ 0.488	$(1.5 \pm 0.3) \times 10^{-10}$ $(9 \pm 2) \times 10^{-11}; 29 \pm 15$ 0.916	$(1.1 \pm 0.1) \times 10^{-10}$ $(0.9 \pm 0.1) \times 10^{-10}; 16 \pm 14$ 0.966
	$(1.5 \pm 0.4) \times 10^{-9}$ $(1.0 \pm 0.2) \times 10^{-9}; 68 \pm 50$ 0.834	$(2.2 \pm 0.8) \times 10^{-10}$ $(1.1 \pm 0.5) \times 10^{-10}; 30 \pm 23$ 0.763	$(1.7 \pm 0.6) \times 10^{-10}$ $(0.8 \pm 0.4) \times 10^{-10}; 29 \pm 23$ 0.702	$(1.3 \pm 0.2) \times 10^{-10}$ $(1.2 \pm 0.2) \times 10^{-10}; 9 \pm 13$ 0.986

Nb/TaSi₂ system, with the values at 2300°F being somewhat higher. This is because data could only be recorded for two conditions at 2300°F. Comparison of the results for the partial zones indicates that the Δx_1 zone has been measured less accurately than the other zones. One reason for this is the already mentioned difficulty in measuring the TaSi₂/Ta₅Si₃ interface in these couples. Also, the Δx_1 results are improved by omitting the data employing poor TaSi₂ wafers. No such effect is noticed for the other partial zones. In other words, use of poor TaSi₂ wafers only affects the growth of the Δx_1 zone (as was corroborated by control runs with good TaSi₂).

The ZP plots for the thinnest and thickest intermediate zones in the Zr/TaSi₂ system are shown in Figures 19 and 20 respectively. No corresponding CCP plots were drawn because X-ray diffraction analysis was inconclusive in determining all of the phases present in the diffusion zones. At first glance, the variations along side \textcircled{B} in Figure 19 might seem to indicate a trend due to an unmeasured parameter such as pressure. In Plate XIV, which shows the microstructure of the same couple presented in Figure 19, it will be noticed that the Zr/Zr silicide interface (x_M) is not a straight line as in all of the other M/TaSi₂ couples, but instead the original interface (x_0) is considerably less wavy. Therefore, if x_0 is taken as the line of reference, the true appearance of the interfaces can be represented by the dotted

lines shown on side (B) of the ZP. The trend now appears somewhat improved. Comparing Figures 19 and 20 it can be seen that the Δx_1 zone grows considerably more slowly than both Δx_2 and Δx_a zones. Therefore, Zr is consumed in these couples at a higher rate than is TaSi_2 . But if the porous nature of the Δx_a zone at high temperatures (Plate XVII) is taken into account, the amount of Zr reacted would not be as high as indicated by the parabolic rate constants.

Although X-ray diffraction analysis fairly well determined the composition of the Δx_1 zone as Ta_5Si_3 , as in other couples, identification of the other two zones was not successful. There are a number of reasons for this difficulty. The Zr-Si phase diagram (Figure I-3) indicates the existence of seven Zr silicides. In addition to these, the ASTM Powder Diffraction File (33) gives X-ray diffraction data for two other Zr silicides and Karpinskii and Evseev (41) report even another Zr silicide, Zr_5Si_4 . Therefore, a total of ten Zr silicides have been reported to exist which are, in order of decreasing Si content: ZrSi_2 , ZrSi , $\underline{\text{Zr}_6\text{Si}_5}$, $\underline{\text{Zr}_5\text{Si}_4}^*$, $\underline{\text{Zr}_4\text{Si}_3}$, Zr_3Si_2^* , Zr_5Si_3 , Zr_2Si , Zr_3Si^* , and $\underline{\text{Zr}_4\text{Si}}$. Those silicides marked with an asterisk are not reported on the accepted phase diagram and those underlined are not found in the ASTM X-ray Diffraction File. X-ray diffraction studies on the diffusion couples showed no evidences of ZrSi_2 , ZrSi , Zr_3Si_2 or Zr_5Si_3 . Some of the X-ray peaks could be

associated with Zr_2Si and Zr_3Si , but most of them remained unidentified. This means that any or all of the underlined silicides could be present, either as thin layers, mixtures or in solid solution. Also because of the data recorded near the original interface, it was assumed that ternary Ta, Zr silicides or solid solutions of Ta silicides and Zr silicides might exist. It was later found that the $Zr/TaSi_2$ couples were at times being split within the porous, fragile Zr silicide zone rather than at the original interface and, therefore, the unknown peaks as well as the shifted Ta silicide peaks were being recorded. The complexity of the X-ray patterns added to the difficulty of deducing the composition of the zones.

In one experiment a $Zr/TaSi_2$ couple was split and part of the intermediate layer was scraped off the Zr wafer. This layer was not very adherent and flaked off quite easily. It was ground to a powder and mounted into a film-type X-ray powder diffraction camera for complete diffraction analysis. Two sets of arcs appeared on the film strip. One set was composed of continuous arcs and proved to be Zr_3Si and the other set had the spotty appearance accompanying large grain size and was identified as the α -Zr-Si solid solution. Therefore, the existence of Zr_3Si in the diffusion zone was fairly well established; but there is X-ray evidence that this does not grow in the early stages of diffusion. This

work also appears to indicate a much higher solubility of silicon in zirconium than is shown in the phase diagram derived from earlier X-ray measurements. Full details of the X-ray diffraction data recorded for the Zr/TaSi₂ system appear in Appendix IV.

c. Ti/TaSi₂

The additive which has been empirically shown to be most effective in increasing the protectiveness of silicide coatings is titanium. The results of this work should be conclusive in determining if this effectiveness is a result of Ti acting as a diffusion barrier. Ti goes through the same phase transition at the same temperature as zirconium. Typical microstructures of thin and thick diffusion zones in the Ti/TaSi₂ couples appear in Plates XVIII and XIX respectively. The only interface which was always easily located was Ti/silicide (x_M). Problems in properly etching the Ti/TaSi₂ couples were similar to those encountered in etching the Zr/TaSi₂ couples. Masking of the Ti side of the couple was employed to avoid overetching of the highly active Ti metal and Ti silicides. This was particularly difficult when the intermediate zone thickness was very small, as illustrated in Plate XVIII. Not only was the TaSi₂/Ta₅Si₃ interface difficult to identify under these circumstances, but the original interface was also not easily located. Polarized light was helpful in ascertaining the positions of these interfaces. For the thicker zones the TaSi₂/Ta₅Si₃ interface (x_{TS})

was readily identified where the masking technique was used (Plate XIX). The position of the original interface (x_0) was still not certain, now because of the extreme amount of porosity developed during diffusion. Therefore, there is some doubt about the true position of x_0 ; but various micrographic techniques were helpful in locating x_0 and indicated that the Δx_1 zone represented a larger percentage of the total thickness than in other couples. (This is opposite to the effect noticed in the Zr/TaSi₂ couples). It proved helpful to locate x_0 by high magnification prior to measurement at normal magnification. Plate XXVI indicates the appearance of the Ti side of the couple under high magnification. A slight change in microstructure as well as initiation of porosity were used to locate x_0 . The zone measured as Δx_2 is also visible in this photomicrograph. At normal magnifications this appeared as a dark non-uniform strip running along the Ti interface. At the high magnification shown in Plate XXVI the eutectoid nature of the zone, as well as its non-uniformity, is evident. The eutectoid is predicted from the Ti-Si phase diagram (Figure I-4) which shows the eutectoid reaction occurring at about 860°C and about 1 atomic percent Si. In addition, there is a eutectic which forms from the melt at 1330°C (2426°F) and contains 13.7 atomic percent Si. Therefore, the upper limit of use of titanium as a barrier with TaSi₂ is 2400°F because of liquid formation. The appearance of the eutectic is shown

in Plate XXVII which shows a Ti/TaSi₂ couple annealed at 2500°F. Plate XXVIII shows this Ti/TaSi₂ couple at lower magnification and indicates the severe attack on titanium by the formation of a liquid phase. The results for Ti/TaSi₂ at 2500°F obviously have no significance in a study of solid-state reaction kinetics. One other unique effect in the Ti/TaSi₂ system is shown in Plate XXIX. In this photomicrograph the lower part is near the edge of the sample and the upper region is toward the center of the sample. Toward the edge of the sample the Δx_2 zone is considerably thicker than near the center of the sample where the thickness measurements are usually made. It is also noticed that there is an abrupt change in the position of x_M starting a cusp near the center of the photomicrograph. Generally, one such cusp was found beginning near each edge of the sample with a long continuous region, in which all thickness measurements were made.

The results of the thickness measurements for the Ti/TaSi₂ system are presented in Table VI. From the values for k it can be seen that the total zone grows at a rate close to that for both the Nb/TaSi₂ and Zr/TaSi₂ systems, but the Δx_1 zone grows at a much higher rate on a comparative scale. Therefore, titanium's effectiveness as an additive in commercial coatings is not a result of diffusion barrier action. The confidence limits listed for the data that have been recorded are in the same range as the previously mentioned

TABLE VI

T₁/T_{as1} SYSTEM - PARABOLIC RATE CONSTANTS

TEMP. (°F)	TOTAL ZONE	PARTIAL ZONES		
	k's in (cm ² /sec); T _b (μ)	Δx ₁ (T _{as1}) ₃	Δx ₂	Δx ₃
2100 k ₀ = k _s =	(1.0±0.2)x10 ⁻¹⁰ (1.1±0.2)x10 ⁻¹⁰ ; -14±24 C _{test} = 0.778	(3+1)x10 ⁻¹¹ (4±1)x10 ⁻¹¹ ; -12±17 0.551	(1.0±0.2)x10 ⁻¹¹ (1.0±0.2)x10 ⁻¹¹ ; -2±8 0.960	(1.2±0.5)x10 ⁻¹² (0.7±0.5)x10 ⁻¹² ; 3±3 0.465
	(1.2±0.2)x10 ⁻¹⁰ (1.2±0.2)x10 ⁻¹⁰ ; 10±20 C _{test} = x (2 points)	(4.8±0.7)x10 ⁻¹¹ (4.7±0.7)x10 ⁻¹¹ ; 5±13 x (2 points)	(1.1±0.2)x10 ⁻¹¹ (1.1±0.2)x10 ⁻¹¹ ; 2±8 x (2 points)	(7+1)x10 ⁻¹³ (4±1)x10 ⁻¹³ ; 2±2 x (2 points)
2200	(1.8±0.2)x10 ⁻¹⁰ (2.0±0.2)x10 ⁻¹⁰ ; -18±21 0.974	(8+2)x10 ⁻¹¹ (8±2)x10 ⁻¹¹ ; -9±22 0.998	(1.2±0.4)x10 ⁻¹¹ (1.4±0.4)x10 ⁻¹¹ ; -6±10 0.960	(1.3±0.4)x10 ⁻¹² (1.1±0.4)x10 ⁻¹² ; 2±3 0.913
	(1.8±0.3)x10 ⁻¹⁰ (2.0±0.2)x10 ⁻¹⁰ ; -22±25 0.965	Same	Same	(1.2±0.5)x10 ⁻¹² (1.2±0.5)x10 ⁻¹² ; 1±3 0.895
2300	(5.0±0.8)x10 ⁻¹⁰ (5.1±0.8)x10 ⁻¹⁰ ; -16±36 0.863	(2.6±0.4)x10 ⁻¹⁰ (2.4±0.4)x10 ⁻¹⁰ ; 17±27 0.910	(2.7±0.9)x10 ⁻¹¹ (3.5±0.8)x10 ⁻¹¹ ; -11±12 0.639	(1.2±0.3)x10 ⁻¹² (0.9±0.3)x10 ⁻¹² ; 2±2 0.858
	(5+3)x10 ⁻¹⁰ (10±1)x10 ⁻¹⁰ ; 100±50 x (2 points)	(2+1)x10 ⁻¹⁰ (4±1)x10 ⁻¹⁰ ; -63±45 x (2 points)	(3+3)x10 ⁻¹¹ (8±2)x10 ⁻¹¹ ; -33±20 x (2 points)	(1+1)x10 ⁻¹² (-1±9)x10 ⁻¹³ ; 5±4 x (2 points)
2400	(1.1±0.1)x10 ⁻⁹ (1.2±0.1)x10 ⁻⁹ ; -40±40 0.964	(4.9±0.4)x10 ⁻¹⁰ (4.5±0.4)x10 ⁻¹⁰ ; 21±24 0.993	(1.0±0.3)x10 ⁻¹⁰ (1.3±0.2)x10 ⁻¹⁰ ; -21±20 0.781	(1+5)x10 ⁻¹¹ (1±5)x10 ⁻¹¹ ; -11±36 x (2 points)
	(1.1±0.2)x10 ⁻⁹ (1.3±0.1)x10 ⁻⁹ ; -52±48 0.953	(4.9±0.5)x10 ⁻¹⁰ (4.5±0.5)x10 ⁻¹⁰ ; 23±29 0.992	(1.0±0.4)x10 ⁻¹⁰ (1.4±0.3)x10 ⁻¹⁰ ; -26±23 0.737	Same
2500	Melting	Melting	Melting	Melting

M/TaSi₂ systems. The results for the total zone fit the theoretical parabolic rate equation better than would be expected for a ternary system as indicated by the values for C_{test}. Two noticeably low values for C_{test} at 2100°F occur for Δx₁ and Δx_a. Omission of the poorer specimens (* values) reduces the confidence interval for these zones, indicating improvement of accuracy, but has little effect on other zones. In fact omission of data employing poor TaSi₂ wafers considerably worsens results for 2300°F. The results for Δx_a seem better than might be expected from the microscopic appearance of the zone.

The ZP and CCP plots for the thinnest and thickest Ti/TaSi₂ diffusion zones are presented in Figures 21 and 22. Although variations of zone thicknesses seem to be random, the fluctuations of the Δx_a zone appear to be much more pronounced than in any of the other M/TaSi₂ systems, in which the Δx_a zone is generally the best behaved zone. Micrography also appears to indicate that the Δx_a zone is not a simple compound, but rather a eutectoid mixture which may grow in a complex manner. X-ray diffraction analysis tends to confirm this. Difficulty in drawing CCP plots for Ti/TaSi₂ couples was caused by problems associated with preparing the samples for analysis rather than difficulty in identifying the phases present in the intermediate zone. Titanium metal bonded so well to TaSi₂ that most of the couples could not be

properly split. Most often, the couple broke apart within the TaSi_2 wafer. This made it impossible to be sure of the position of the original interface. Fortunately, the two specimens which did split cleanly were the thinnest and the thickest zones produced, presented in Figures 21 and 22 respectively. In these couples only one side could be properly split and therefore CCP plots have been drawn for only one side in each couple. The phase diagram for the Ti-Si system (Figure I-4) is known accurately and predicts the existence of three silicides: TiSi_2 , Ti_5Si_3 , and TiSi . However, only Ti_5Si_3 was found in any of the Ti/ TaSi_2 couples. The distribution of phases according to the CCP in Figure 21 is unusual. Ti_5Si_3 is shown as growing on the TaSi_2 side of the original interface. This is the only system in which this was found, but the lack of silicides on the Ti side (only solid solubility of Si in Ti was indicated by the shifting of the X-ray parameters of Ti near x_0) seemed to indicate that perhaps this was observed because the wafers actually split near x_M rather than x_0 . However, the results of the CCP in Figure 22 strongly confirmed the presence of Ti_5Si_3 in the Δx_1 zone. Visual evidence after splitting substantiated the position of x_0 as indicated. Moreover, Ti_5Si_3 grew as a separate layer (0- to \sim -2.0 mil) within Δx_1 rather than in mixture with Ta_5Si_3 . Unfortunately, because of the porosity of the Δx_1 zone, no interface between Ti_5Si_3 and Ta_5Si_3

could be found. The small region (+1.5 to +2.0 mil) in which the intensities of Ti_5Si_3 and Ti peaks are relatively constant may be considered the eutectoid composition.

d. W/TaSi₂

Tungsten has the highest melting point of all true metals. This property alone makes it a candidate barrier material. Plates XX and XXI show the microscopic appearance of the two types of diffusion zones encountered in the W/TaSi₂ system. Plate XX is typical of short time, low temperature runs and shows only two porous zones; whereas Plate XXI exhibits four distinct microscopic zones and is typical of high temperature, long-time runs. Although the thickness of the diffusion zone in Plate XXI should be much greater than that of the porous zone in Plate XX, the porous zone is actually thicker. This indicates that the intermediate growth in the W/TaSi₂ couple is not simply solid state diffusion, at least at low temperatures and short times.

From the results of the thickness measurements, presented in Table VII, it should be noted that the values for k (total and Δx_1), although an order of magnitude higher than in the Ta/TaSi₂ system at low temperatures, are close to the values for Ta/TaSi₂ at high temperatures. Most noticeable are the low values for C_{test} which show that the parabolic growth rate is not followed. Confidence limits

TABLE VII

W/TaSi₂ SYSTEM - PARABOLIC RATE CONSTANTS

TEMP. (°F)	TOTAL ZONE	PARTIAL ZONES (to be continued)	
	k's in (cm ² /sec); \bar{x} (μ)	Δx_1 (Ta ₅ Si ₃)	
2100	$k_o = (2+3) \times 10^{-10}$ $k_s = (-4+1) \times 10^{-10}; 120+60$ $C_{test} = 0.112$	$(4+8) \times 10^{-11}$ $(-4+7) \times 10^{-11}; 47+46$ \bar{x} (2 points)	
	$k_o = (2+3) \times 10^{-10}$ $k_s = (-4+1) \times 10^{-10}; 130+50$ $C_{test} = 0.130$	$(4+11) \times 10^{-11}$ $(-10+9) \times 10^{-11}; 66+52$ \bar{x} (2 points)	
2200	$(4+3) \times 10^{-10}$ $(-3+2) \times 10^{-10}; 130+70$ 0.177	2×10^{-11} Only 1 Point	
	Same	Same	
2300	$(5+3) \times 10^{-10}$ $(6+3) \times 10^{-10}; -60+80$ 0.696	$(9+3) \times 10^{-11}$ $(6+3) \times 10^{-11}; 22+22$ \bar{x} (2 points)	
	$(3+1) \times 10^{-10}$ $(2+1) \times 10^{-10}; 43+48$ \bar{x} (2 points)	$(9+4) \times 10^{-11}$ $(6+3) \times 10^{-11}; 24+27$ \bar{x} (2 points)	
2400	$(3+3) \times 10^{-10}$ $(1+3) \times 10^{-10}; 70+90$ 0.243	$(5+8) \times 10^{-11}$ $(0.7+8.0) \times 10^{-11}; 35+47$ 0.139	
	$(1.7+0.9) \times 10^{-10}$ $(1.0+0.8) \times 10^{-10}; 43+48$ 0.815	$(3+2) \times 10^{-11}$ $(1+2) \times 10^{-11}; 20+19$ 0.761	
2500	$(2.4+0.4) \times 10^{-10}$ $(2.3+0.4) \times 10^{-10}; 10+30$ 0.986	$(4+2) \times 10^{-11}$ $(0.8+1.5) \times 10^{-11}; 26+19$ 0.602	
	$(2.5+0.5) \times 10^{-10}$ $(2.3+0.5) \times 10^{-10}; 23+35$ \bar{x} (2 points)	$(4+2) \times 10^{-11}$ $(0.7+1.0) \times 10^{-11}; 27+16$ \bar{x} (2 points)	

TABLE VII
W/TaSi₂ SYSTEM - PARABOLIC RATE CONSTANTS - CONTINUED

TEMP. (°F)	PARTIAL ZONES (Continued)		
	Δx_2	Δx_1	Δx_2
2100 $k_0 =$ $k_s =$	(4+6)x10-11 (-7+4)x10-11; 56+41 C _{test} = x (2 points)	(6+12)x10-14 (1.5+0.9)x10-13; -2+2 0.214	0
	(3+8)x10-11 (-8+5)x10-11; 60+40 C _{test} = x (2 points)	Same	0
2200	2x10-11	(4+2)x10-13 (7+2)x10-13; -3+2 0.382	3x10-13
	Only 1 Point	0.382	Only 1 Point
2300	Same	Same	Same
	(5+2)x10-11 (5+2)x10-11; 2+18 x (2 Points)	(6+2)x10-13 (5+2)x10-13; 1+2 x (2 Points)	(1.0+0.4)x10-12 (1.2+0.4)x10-12; -2+3 x (2 Points)
2400	(5+2)x10-11 (4+2)x10-11; 18+21 x (2 Points)	(6+2)x10-13 (6+2)x10-13; -1+2 x (2 Points)	(1.0+0.6)x10-12 (1.2+0.5)x10-12; -2+3 x (2 Points)
	(5+8)x10-11 (2+4)x10-12; 35+46 0.106	(2+1)x10-12 (2+1)x10-12; -3+5 0.419	(4+1)x10-12 (4+1)x10-12; 4+6 x (2 Points)
2500	(2+2)x10-11 (8+16)x10-12; 20+21 0.551	(1.9+0.8)x10-12 (2.0+0.8)x10-12; -2+5 0.753	Same
	(2.1+0.7)x10-11 (2.4+0.6)x10-11; -8+12 0.786	(3.7+0.6)x10-12 (2.6+0.4)x10-12; 5+3 0.902	(1.4+0.5)x10-11 (1.3+0.5)x10-11; 6+12 x (2 Points)
2500	(2.5+6.6)x10-11 (2.2+0.6)x10-11; 8+13 x (2 Points)	(3.5+0.6)x10-12 (2.6+0.4)x10-12; 4+3 x (2 Points)	1.4x10-11 Only 1 Point

on k_0 reflect a large amount of scatter about a straight line through the origin; but in most cases, the limits on k_s are considerably better indicating that a straight line through the origin is a poor fit of the data. The quality of the results improves at higher temperatures. Omission of poor data does not improve the quality of the results except at 2400°F. At this temperature, data were recorded for one couple in which the junction between the wafers had been ruptured. A control couple run at the same time showed that good contact had never been established in the ruptured zone and therefore, the data recorded were erroneous. Because each run involved other couples with good behavior, it may be assumed that the poor quality of the data is a result of the properties of W and its silicides. Because of the hardness and stiffness of W metal, the junctions between the wafers in W/TaSi₂ couples were poor, particularly at low temperatures and short diffusion times. This may result in silicon being transferred by vapor transport as well as solid state diffusion and, therefore, simple parabolic behavior would not be expected.

In this system the parabolic plot, Figure 10, can be helpful in interpreting the results. The lines drawn for 2300°F, 2400°F and 2500°F are the least-squares lines obtained from the k_0 values in Table VII. At 2100°F and 2200°F the solid lines were drawn by eye through the three

average data points for each temperature and the dotted lines extended to the origin, assuming that vapor transport controlled growth in this region. If it is remembered that the growth of the total zone, represented in Figure 10, was controlled by the growth and shrinkage of different partial zones, three stages of growth can be seen in the parabolic plot. At low temperatures (2100°F and 2200°F) vapor transport of silicon caused the total zone to grow very quickly at first and when contact later improved, solid state diffusion became the controlling mechanism. In addition to slowing the rate of Si transport, different phases might be caused to grow by depletion of those previously grown, resulting in thinner total zones. In the second stage (2300°F, 2400°F), although zone thickness increased with time, the temperature dependence was not followed. Only in the third stage (2400°F, 2500°F) did solid state diffusion control growth after each experimental condition.

The ZP and CCP for the couple shown in Plate XX are presented in Figure 23. Because of the wide space between the two growing zones, no significant data could be recorded for the position of the original interface. The CCP shows the composition of the growing phases to be WSi_2 and Ta_5Si_3 . WSi_2 was the only W silicide growing. Figures 24, 25 and 26 show how the number and composition of the microconstituents in the complete zone changed with increasing time and temperature. In Figure 24 another phase, W_5Si_3 , forming a new microconstituent zone, Δx_{a1} , appears. Because of the porosity of the low temperature zones, both

W_5Si_3 and W metal seem to be present near the original interface in the CCP. This was caused by diffraction of X-rays which penetrate deep into the porous zone. In the ZP Δx_{a1} is not a continuous zone but only grew near the center of the couple. Associated with the growth of Δx_{a1} was a decrease in thickness of the other two zones near the center line. This is just such a trend that the ZP was designed to disclose. Clearly the growth of a thin Δx_{a1} (W_5Si_3) zone and the decreased growth rate of the other zones, as a result of less vapor transport, caused the total zone to be considerably thinner near the center than toward the edges of the measured zone. The thickness of the total zone varied dramatically, exhibiting symmetry about the center line. This same effect is noticed (somewhat less dramatically) in the ZP plots in Figures 25 and 26, representing the high temperature appearance of the diffusion zones. Although the variation in total thickness became more subdued as the Δx_{a1} layer thickened and became more uniform, it can still be seen how small decreases in the size of the W_5Si_3 zones enlarged the total zone to a much greater extent. In Figure 25 another new zone has grown, Δx_{a2} , between Ta_5Si_3 and WSi_2 . This can be seen to be WSi_2 and W_5Si_3 from the CCP below. The compositions of all four diffusion zones, grown under conditions most closely resembling steady state, are clearly defined in the CCP of Figure 26. The phase compositions were determined by X-ray

diffraction analysis. The W-Si phase diagram (Figure I-5) is well established and indicates only two silicides: WSi_2 and W_5Si_3 . All X-ray data were clearly defined. The ZP and CCP plots for the W/ $TaSi_2$ couples, by showing that the number and composition of growing phases changes as a function of time and temperature, confirm the existence of more than one growth mechanism.

e. $Mo/TaSi_2$

Molybdenum silicides are the best known and most carefully studied compounds in the silicide family. The melting point of molybdenum is between those of Ta and Nb. These qualifications make Mo a choice candidate to be tested as a barrier material. Microstructures of $Mo/TaSi_2$ diffusion zones formed under low and high diffusion conditions appear in Plates XXIII and XXVIII respectively. At first the appearance of these diffusion zones might be considered similar to the zones encountered in W/ $TaSi_2$ couples (W and Mo are in the same group in the periodic chart), but there are two major differences. A small but measureable Δx_a zone (next to Mo) appeared in the $Mo/TaSi_2$ couple at 2100°F even after short diffusion anneals. The Δx_{a1} (W_5Si_3) zone in W/ $TaSi_2$ couples run at 2100°F was not measurable except after the 100 hour anneal. Also, whereas Plate XXI represents the appearance of W/ $TaSi_2$ diffusion zones in many of the high diffusion conditions, the $Mo/TaSi_2$ zone in Plate XXVIII does not.

TABLE VIII

Mo/TaSi₂ SYSTEM - PARABOLIC RATE CONSTANTS

TEMP. (°F)	TOTAL ZONE	PARTIAL ZONES		
	k's in (cm ² /sec); \bar{v} (μ)	Δx_1 (Ta ₅ Si ₃)	Δx_2	Δx_a
2100	$k_o = (7+18) \times 10^{-10}$ $k_s = (-1.3+0.4) \times 10^{-9}; 200+90$ $C_{test} = x$ (2 points)	$(2+4) \times 10^{-10}$ $(-4+1) \times 10^{-10}; 112+54$ x (2 points)	$(1+3) \times 10^{-10}$ $(-2.8+0.4) \times 10^{-10}; 93+31$ x (2 points)	$(1.3+0.9) \times 10^{-12}$ $(1.6+0.7) \times 10^{-12}; -3+4$ x (2 points)
	$k_{o } = 1 \times 10^{-9}$ $C_{test} = \text{Only 1 Point}$	3×10^{-10} Only 1 Point	2×10^{-10} Only 1 Point	1.2×10^{-12} Only 1 Point
2200	$(1.0+0.1) \times 10^{-9}$ $(1.0+0.1) \times 10^{-9}; -14+52$ $\bar{v} = 0.999$	$(2.3+0.4) \times 10^{-10}$ $(2.5+0.4) \times 10^{-10}; -18+28$ $\bar{v} = 0.990$	$(1.6+0.2) \times 10^{-10}$ $(1.6+0.2) \times 10^{-10}; 3+20$ $\bar{v} = 0.997$	$(3.2+0.5) \times 10^{-12}$ $(2.6+0.4) \times 10^{-12}; 3+3$ $\bar{v} = 0.963$
	$(1.0+0.2) \times 10^{-9}$ $(1.0+0.2) \times 10^{-9}; 25+75$ \bar{x} (2 points)	$(2.3+0.6) \times 10^{-10}$ $(2.5+0.6) \times 10^{-10}; -22+40$ \bar{x} (2 points)	$(1.6+0.3) \times 10^{-10}$ $(1.5+0.3) \times 10^{-10}; 15+29$ \bar{x} (2 points)	$(3.1+0.8) \times 10^{-12}$ $(2.4+0.7) \times 10^{-12}; 4+4$ \bar{x} (2 points)
2300	$(1.6+0.2) \times 10^{-9}$ $(1.4+0.2) \times 10^{-9}; 50+80$ $\bar{v} = 0.956$	$(5+1) \times 10^{-10}$ $(4+1) \times 10^{-10}; 58+47$ $\bar{v} = 0.894$	$(2.9+0.9) \times 10^{-10}$ $(3.7+0.9) \times 10^{-10}; -42+46$ $\bar{v} = 0.862$	$(1.1+0.8) \times 10^{-11}$ $(1.1+0.8) \times 10^{-11}; 3+11$ $\bar{v} = 0.438$
	$(1.4+0.3) \times 10^{-9}$ $(1.1+0.2) \times 10^{-9}; 69+70$ $\bar{v} = 0.950$	$(4+1) \times 10^{-10}$ $(4+1) \times 10^{-10}; 43+48$ $\bar{v} = 0.957$	$(2.2+0.6) \times 10^{-10}$ $(2.5+0.6) \times 10^{-10}; -21+30$ $\bar{v} = 0.891$	$(1+1) \times 10^{-11}$ $(1+1) \times 10^{-11}; 7+14$ $\bar{v} = 0.338$
2400	$(1.8+0.2) \times 10^{-9}$ $(1.4+0.1) \times 10^{-9}; 70+50$ $\bar{v} = 0.950$	$(4.0+0.4) \times 10^{-10}$ $(3.5+0.4) \times 10^{-10}; 26+27$ \bar{x} (2 points)	$(2.9+0.6) \times 10^{-10}$ $(2.7+0.6) \times 10^{-10}; 14+32$ \bar{x} (2 points)	$(1.7+0.4) \times 10^{-11}$ $(1.3+0.3) \times 10^{-11}; 7+7$ $\bar{v} = 0.905$
	Same	Same	Same	Same
2500	$(1.5+0.8) \times 10^{-9}$ $(8+7) \times 10^{-10}; 140+140$ $\bar{v} = 0.387$	$(2+1) \times 10^{-10}$ $(9+13) \times 10^{-11}; 59+60$ $\bar{v} = 0.313$	$(3+3) \times 10^{-10}$ $(1+2) \times 10^{-10}; 72+81$ $\bar{v} = 0.240$	$(6+2) \times 10^{-11}$ $(7+1) \times 10^{-11}; -16+20$ $\bar{v} = 0.767$
	$(8+1) \times 10^{-10}$ $(6.2+0.5) \times 10^{-10}; 62+42$ \bar{x} (2 points)	$(1.0+0.2) \times 10^{-10}$ $(6+1) \times 10^{-11}; 30+20$ \bar{x} (2 points)	$(1.0+0.2) \times 10^{-10}$ $(0.7+0.1) \times 10^{-10}; 26+19$ \bar{x} (2 points)	$(6.9+0.7) \times 10^{-11}$ $(7.0+0.7) \times 10^{-11}; -5+14$ \bar{x} (2 points)

The results of the thickness measurements are presented in Table VIII for the Mo/TaSi₂ system. Low temperature values for k are the highest of any of the systems tested being two orders of magnitude higher than the results for Ta/TaSi₂. At high temperatures, however, the k values are only one order of magnitude higher than in the Ta/TaSi₂ system, or about the same as in most of the other M/TaSi₂ systems. The high confidence limits on the 2100°F results can be attributed to paucity of data at this temperature and the results are consequently in considerable doubt. Results at 2200°F, 2300°F and 2400°F are almost as good as those for the Ta/TaSi₂ system. Confidence limits are generally low and the high values for C_{test} indicate that up to 2400°F growth follows the parabolic rate. At 2500°F, the result for one of the runs was not reliable.

Figures 27 through 30 show ZP and CCP plots for the Mo/TaSi₂ system. Mo itself becomes very brittle after heat treatment causing many Mo/TaSi₂ couples to crack and making measurements impossible. Therefore, three of the ZP plots contain data for only one side of the couple, whereas there is no ZP data for the couple represented in Figure 27. The CCP for this couple, nonetheless, shows that there should be two zones growing: Mo₅Si₃ and Mo₃Si. Although the Mo-Si phase diagram (Figure I-6) predicts the existence of these two silicides, as well as MoSi₂, it was

not evident at first that Mo_3Si was growing in the diffusion couple. Many of the X-ray diffraction peaks for Mo_3Si coincide with those for Mo_5Si_3 , making the diffraction data difficult to interpret. Identification of Mo_3Si was made on the basis of one abnormally high peak which corresponded to the 200 diffractometer reflection for Mo_3Si . This same peak is listed in the ASTM Powder Diffraction File as being very low and, therefore, the enhancement of the reflection would have to be a result of preferred orientation. The argument for defining Mo_3Si (cubic crystal structure) by virtue of its 200 reflection alone would not have been acceptable had not the type of preferred orientation responsible for the enhancement of this peak (called "cube texture") been found to be common in many cubic metals as a result of recrystallization. The intensity recorded for Mo_3Si must be considered abnormally high, and when identifying zones using the CCP, it must be remembered that the relationship between concentration and X-ray peak intensity is considerably more strained than for other compounds and metals. Therefore, in comparing the ZP and CCP in Figure 28, Mo_5Si_3 was assigned to the thicker, Δx_2 zone and Mo_3Si to the Δx_a zone. It must also be remembered that at 2100°F the Δx_2 zone is quite porous, and the enhanced reflection from the Mo_3Si below (and the high amount of background scatter associated with it) causes the Mo_5Si_3 peaks to be more subdued. These effects are more noticeable in

Figures 29 and 30, in which the intensity of the Mo_3Si peak is so high that a separate scale had to be used. It is noticed that MoSi_2 is also growing in Δx_2 similar to the growth of NbSi_2 in the Nb/Ta Si_2 couples at high temperatures. Even in these diffusion couples the CCP plots cause some confusion. In Figure 30 the CCP seems to indicate the sequence: Ta Si_2 , Ta $_5\text{Si}_3$, MoSi_2 (Mo_5Si_3), Mo_3Si , Mo_5Si_3 and Mo metal. This seems unreasonable from the standpoint of thermodynamics. Also, the microstructure in Plate XXIII shows the two regions in Δx_2 on the ZP as being very similar. This would hardly be expected if these two zones were MoSi_2 (Mo_5Si_3) and Mo_3Si . Therefore, from microscopic evidence, thermodynamic considerations as well as the results of the thickness measurements compositions were assigned as in the ZP for Figure 30, realizing that the CCP could be misleading due to the extreme orientation of the Mo_3Si phase.

f. Re/Ta Si_2

Rhenium was chosen for testing as a diffusion barrier because of its high melting point and high density. Re is the densest metal and has a melting point between W and Ta. It was also of interest to investigate a metal with a hexagonal crystal structure as a barrier. (Re was the only metal tested which was not cubic at the annealing conditions.) Plates XXIV and XXV show Re/Ta Si_2 couples run at 2100°F and 2500°F respectively. In fact, the diffusion

zone shown in Plate XXIV was the most consolidated of all those run. Because of cracking and loss of material from the diffusion zones, only a few pieces of data could be recorded and, therefore, no results for the growth kinetics in the Re/TaSi₂ system were obtained. The reason for the incompatibility in the Re/TaSi₂ couples is probably mechanical and a result of the properties of both Re metal and its silicides at the temperatures of interest. Mechanical compatibility should be improved at higher temperatures and, therefore, runs made above the temperatures of interest should produce results. There is not much data available on the Re silicides, and the Re-Si phase diagram has not yet been resolved. Three silicides of Re have been reported in the literature: ReSi₂ (tetragonal), ReSi (cubic) and Re₃Si (cubic) (42, 43). X-ray diffraction analysis of Re/TaSi₂ couples indicated ReSi₂ growing initially and another phase appearing as the zone grew thicker. This new phase was not ReSi (the only other Re silicide reported in the ASTM X-ray file), and was assumed to be Re₅Si₃ by analogy with the W/TaSi₂ system. Knapton (44) reported a Re₅Si₃ having a tetragonal structure and lattice parameters of $a \approx 9.53$ and $c \approx 4.81$. This is not in agreement with the results of this investigation which are reported in detail in Appendix IV.

C. Comparative Results and Effect of Temperature

Tables IX and X list the results for the temperature dependence of the growth constants using all data and incomplete data with high quality specimens respectively. The Arrhenius relation of the form $k = k^0 e^{-Q/RT}$ is assumed. The parameters k^0 and Q are obtained by a least-squares analysis of the equation: $\ln k = \ln k^0 - Q/RT$, and R is the gas constant. The previously calculated parabolic rate constants (k) were not used; but rather the original thickness measurements themselves were used in the analysis. Therefore, at each temperature there are about fifty values of $(\Delta x)^2/t$ for the Ta/TaSi₂ system and about thirty for each M/TaSi₂ system. These data were analyzed by computer using the subroutines for least-squares and departure from linearity analyses employed previously in the computation of parabolic growth constants.

In Tables IX and X the Arrhenius expressions are listed for the total and partial zones for each system. Q , the activation energies for diffusion, are tabulated in the next column together with the 95% confidence intervals. Values for the pre-exponential constants, k^0 , appear with their 95% confidence limits in the next column; and C_{test} values are listed in the last column. High values for C_{test} in this case indicate that the data follow the expected exponential temperature dependence. Using C_{test} as a criteria

TABLE IX

ARRHENIUS EXPRESSIONS FOR GROWTH RATES (Complete Data)

System	$k = k^0 e^{-Q/RT}$	Q + CI (kcal/mole)	$-k^0 < k^0 < +k^0$ (cm ² /sec)	C _{test}
<u>Ta/TaSi₂</u> total Δx ₁ Δx ₂	k=5e ^{-77,000/RT} k=2e ^{-81,000/RT} k=0.6e ^{-73,000/RT}	77 ± 3 81 ± 7 73 ± 2	2<5<11 0.2<2<16 0.3<0.6<1.4	0.9998 0.979 0.996
<u>W/TaSi₂</u> total Δx ₁ Δx _{a2} Δx ₂ Δx _{a1}	k=(4x10 ⁻¹⁰)e ^{-2,000/RT} k=(1x10 ⁻⁹)e ^{-11,000/RT} k=(1.5x10 ⁵)e ^{-120,000/RT} k=(5x10 ⁻¹²)e ^{+5,000/RT} k=(1x10 ⁻⁹)e ^{-20,000/RT}	2 ± 13 11 ± 14 120 ± 10 -5 ± 17 20 ± 45	(0.3<4<52)x10 ⁻¹⁰ (0.1<1<23)x10 ⁻⁹ (0.1<1.5<20)x10 ⁵ (0.4<5<80)x10 ⁻¹² 10 ⁻¹⁵ <10 ⁻⁹ <10 ⁻³	0.033 0.374 0.996 0.163 0.110
<u>Mo/TaSi₂</u> total Δx ₁ Δx ₂ Δx _a	k=(4x10 ⁻⁶)e ^{-25,000/RT} k=(2x10 ⁻⁷)e ^{-20,000/RT} k=(1x10 ⁻⁶)e ^{-30,000/RT} k=0.4e ^{-75,000/RT}	25 ± 9 20 ± 10 30 ± 10 75 ± 7	(0.5<4<31)10 ⁻⁶ (0.1<2<60)x10 ⁻⁷ (0.1<1<16)x10 ⁻⁶ 0.04<0.4<3.6	0.873 0.547 0.923 0.998
<u>Nb/TaSi₂</u> total Δx ₁ Δx ₂ Δx _a	k=(1.4x10 ⁻⁴)e ^{-40,000/RT} k=(4x10 ⁻⁶)e ^{-30,000/RT} k=(4x10 ⁻⁶)e ^{-36,000/RT} k=(1.4x10 ⁻³)e ^{-55,000/RT}	40 ± 6 30 ± 10 36 ± 9 55 ± 7	(0.4<1.4<4.5)x10 ⁻⁴ (0.2<4<68)x10 ⁻⁶ (0.4<4<42)x10 ⁻⁶ (0.2<1.4<12)x10 ⁻³	0.987 0.770 0.883 0.954
<u>Zr/TaSi₂</u> total Δx ₁ Δx ₂ Δx _a	k=(4x10 ⁻³)e ^{-50,000/RT} k=(3x10 ⁻⁵)e ^{-40,000/RT} k=(1x10 ⁻⁴)e ^{-45,000/RT} k=1.2e ^{-76,000/RT}	50 ± 5 40 ± 10 45 ± 9 76 ± 6	(1<4<17)x10 ⁻³ (0.1<3<76)x10 ⁻⁵ (0.1<1<12)x10 ⁻⁴ 0.2<1.2<8.6	0.991 0.924 0.989 0.995
<u>Ti/TaSi₂</u> total Δx ₁ Δx ₂ Δx _a	k=0.8e ^{-66,000/RT} k=170e ^{-84,000/RT} k=(4x10 ⁻⁵)e ^{-44,000/RT} k=(1x10 ⁻¹¹)e ^{-6,000/RT}	66 ± 6 84 ± 9 44 ± 9 6 ± 20	0.1<0.8<5.4 10<170<2600 (0.3<4<57)x10 ⁻⁵ (0.01<1<150)x10 ⁻¹¹	0.978 0.982 0.911 0.254

TABLE X

ARRHENIUS EXPRESSIONS FOR GROWTH RATES (Incomplete Data)

System	$k = k^0 e^{-Q/RT}$	Q + CI (kcal/mole)	$-k^0 < k^0 < +k^0$ (cm ² /sec)	C _{test}
Ta/TaSi ₂ total	$k=6e^{-78,000/RT}$	78 ± 3	2<6<14	0.9996
	$k=3e^{-84,000/RT}$	84 ± 7	0.3<3<34	0.979
	$k=0.8e^{-74,000/RT}$	74 ± 2	0.4<0.8<1.4	0.998
W/TaSi ₂ total	$k=(1 \times 10^{-10}) e^{+2,000/RT}$	-2 ± 15	(0.1<1<21) x 10 ⁻¹⁰	0.038
	$k=(5 \times 10^{-10}) e^{-8,000/RT}$	8 ± 18	(0.1<5<13) x 10 ⁻¹⁰	0.188
	$k=(1.3 \times 10^5) e^{-120,000/RT}$	120 ± 10	(0.1<1.3<21) x 10 ⁵	0.996
	$k=(5 \times 10^{-11}) e^{-2,000/RT}$	2 ± 18	(0.3<5<80) x 10 ⁻¹¹	0.022
	$k=(3 \times 10^{-10}) e^{-20,000/RT}$	20 ± 50	(2 x 10 ⁻¹⁷ < 3 x 10 ⁻¹⁰ < 4 x 10 ⁻³)	0.063
Mo/TaSi ₂ total	$k=(1.3 \times 10^{-7}) e^{-14,000/RT}$	14 ± 12	(0.1<1.3<15) x 10 ⁻⁷	0.605
	$k=(1.3 \times 10^{-9}) e^{-5,000/RT}$	5 ± 19	(0.03<1.3<65) x 10 ⁻⁹	0.053
	$k=(2 \times 10^{-9}) e^{-6,000/RT}$	6 ± 17	(0.1<2<44) x 10 ⁻⁹	0.263
	$k=11e^{-86,000/RT}$	86 ± 9	(0.6<11<200)	0.997
Nb/TaSi ₂ total	$k=(1 \times 10^{-3}) e^{-46,000/RT}$	46 ± 5	(0.4<1<2.6) x 10 ⁻³	0.998
	$k=(7 \times 10^{-5}) e^{-43,000/RT}$	43 ± 8	(1<7<49) x 10 ⁻⁵	0.990
	$k=(8 \times 10^{-6}) e^{-39,000/RT}$	39 ± 9	(1<8<55) x 10 ⁻⁶	0.927
	$k=(2.5 \times 10^{-3}) e^{-58,000/RT}$	58 ± 6	(0.5<2.5<13) x 10 ⁻³	0.983
Zr/TaSi ₂ total	$k=0.08e^{-58,000/RT}$	58 ± 5	0.02<0.08<0.33	0.994
	$k=(4 \times 10^{-3}) e^{-55,000/RT}$	55 ± 7	(0.6<4<31) x 10 ⁻³	0.986
	$k=(8 \times 10^{-4}) e^{-50,000/RT}$	50 ± 9	(0.5<8<120) x 10 ⁻⁴	0.968
	$k=0.5e^{-72,000/RT}$	72 ± 5	(0.1<0.5<2.2)	0.9992
Ti/TaSi ₂ total	$k=0.03e^{-55,000/RT}$	55 ± 5	0.006<0.03<0.17	0.956
	$k=0.5e^{-66,000/RT}$	66 ± 6	0.1<0.5<4.1	0.964
	$k=(2.3 \times 10^{-5}) e^{-40,000/RT}$	40 ± 10	(0.1<2.3<53) x 10 ⁻⁵	0.895
	$k=(5 \times 10^{-11}) e^{-10,000/RT}$	10 ± 20	(0.01<5<2000) x 10 ⁻¹¹	0.394

for the quality of the data, it can be seen that the best results are those for the Ta/TaSi₂ system, and the worst are those for the W/TaSi₂ system. It can also be observed that the growth of the Δx_2 zone (Ta side) in the Ta/TaSi system is more accurately known than the growth of the Δx_1 zone (TaSi₂ side). This was noticed before and is a result of difficulty in measuring the TaSi₂/Ta₅Si₃ interface. The low values for C_{test} in the W/TaSi₂ system are another indication of more than one mechanism of growth. Interpretation of the growth rates based on a solid state diffusion mechanism produce results which have no meaning due to the extremely high confidence intervals and must therefore be disregarded. The remaining values of C_{test} , with two exceptions, are high indicating that there is only one controlling mechanism and the Arrhenius temperature dependence is observed. One of the exceptions is the Δx_1 zone in Mo/TaSi₂. Deviations due to poor data at 2100°F and 2500°F are strongly observed in the Δx_1 zone. Also, the Δx_2 zone in the Ti/TaSi₂ system does not show the expected temperature dependence. Microscopic evidence indicated that this zone was a eutectoid mixture and not a stoichiometric compound and, therefore, would not be expected to grow in the usual manner. These results, as well as the values in the W/TaSi₂ system, were not improved by the omission of poor TaSi₂ wafer data, as is evident by comparing Table X to Table IX. On the other hand, results

in the Nb/TaSi₂ and Zr/TaSi₂ systems were improved by omitting the poor wafer data. The reason has been previously discussed.

Comparison of the activation energies for the partial zones in the Ta/TaSi₂ system shows that their ranges overlap, although the extremes are substantially different. Hence, it may be concluded that the controlling process is the diffusion of silicon in Ta₅Si₃, even though the reaction producing the Ta₅Si₃ is different in the two zones. This is also true for the Δx_1 and Δx_2 zones in all of the other systems with the exception of the Ti/TaSi₂ system, where Q for Δx_1 is considerably greater than Q for Δx_2 . In the remaining systems it is the Δx_a zone (closest to the metal) which exhibits a higher activation energy (Δx_{a2} zone in the W/TaSi₂ system) than the other partial zones. The activation energies for total and Δx_1 zones in the Ta/TaSi₂ system are higher than in any of the other systems (with the exception of the Δx_1 zone in the Ti/TaSi₂ system reported in Table IX).

Comparison of data for barrier effects can best be accomplished by Arrhenius plots shown in Figures 32 through 33. Figures 32a and 32b are plots of total zone results for complete and incomplete data respectively; whereas Figures 33a and 33b show the Δx_1 zone results. In each figure, data for each of the barrier metal systems is plotted, together with the Ta/TaSi₂ results so that direct comparison may be made. Each point on the plot is an average of the number of

measurements recorded for the temperature of interest. The line is the least-squares line calculated from all the data. All of the plots indicate the same conclusion: none of the metals tested should make good barriers to the degradation of TaSi_2 in the temperature range of interest. This is because all the M/TaSi_2 systems tested show larger growth rates than the Ta/TaSi_2 system. The only competitor is tungsten at the highest temperature. Data at the lower temperatures was most probably a result of poor contact and vapor transport of silicon. At higher temperatures, the existence of a thick WSi_2 zone indicated that solid state diffusion did not control the rate during the initial stages of growth. Although it seems that W could act as a diffusion barrier for TaSi_2 at temperatures above those investigated, the system still contained WSi_2 (grown by vapor transport of Si) even at 2500°F and, therefore, no prediction could be made. The other unusual results are those for the Mo/TaSi_2 system. It can be seen that if the points at 2100°F (in doubt because of paucity of data) and 2500°F are ignored, a line through the other three points better fits the expected temperature dependence. Also, the slope of the line, indicating the value of Q , is closer to the slopes observed for the other lines.

Degradation of TaSi_2 is best observed by comparing the growth rates of the Δx_1 (Ta_5Si_3) zones repre-

sented in Figures 33a and 33b. Although the same conclusion concerning barriers is reached, deviations from the Arrhenius lines are more pronounced than for the total zones.

D. Results of Marker Experiments

1. Ta/TaSi₂ System

The results shown in Table XI are the simple averages of the ratio $\Delta x_2 / \Delta x_1$ for each run in the Ta/TaSi₂ system in which the partial zones were measurable. In Section IC, it was shown that in the Ta/TaSi₂ system

$$\frac{\Delta x_2}{\Delta x_1} = \frac{7}{3} \frac{P_1}{P_2} \quad (21)$$

if $D_{Ta} = 0$ (only Si diffuses). $\Delta x_2 / \Delta x_1$ should range from 2.3 to 2.45, depending on whether the Δx_1 zone is tetragonal or hexagonal Ta₅Si₃. X-ray diffraction analysis showed that the Δx_2 zone was ostensibly pure tetragonal Ta₅Si₃ at all conditions, whereas the Δx_1 zone contained varying amounts of hexagonal trisilicide of higher density. P_1/P_2 varied from unity (homogeneous Ta₅Si₃) to 1.05 (Δx_1 being pure hexagonal Ta₅Si₃) in the extreme. The values of $\Delta x_2 / \Delta x_1$ shown in Table XI are near the expected values. The low values may be expected when the Δx_1 zone develops extensive porosity as is sometimes the case after short diffusion anneals. Therefore, these results indicate that Ta does not diffuse.

TABLE XI
RESULTS OF MARKER EXPERIMENTS FOR Ta/TaSi₂
AVERAGE VALUES FOR $\Delta x_2 / \Delta x_1$

	2100°F	2200°F	2300°F	2400°F	2500°F
4 HRS.	1.6		1.8		1.9
24 HRS.		1.7	1.8	2.9	2.1
48 HRS.	2.2	2.6	2.6	2.4	2.9
72 HRS.			2.5		
100 HRS.				1.9	2.6

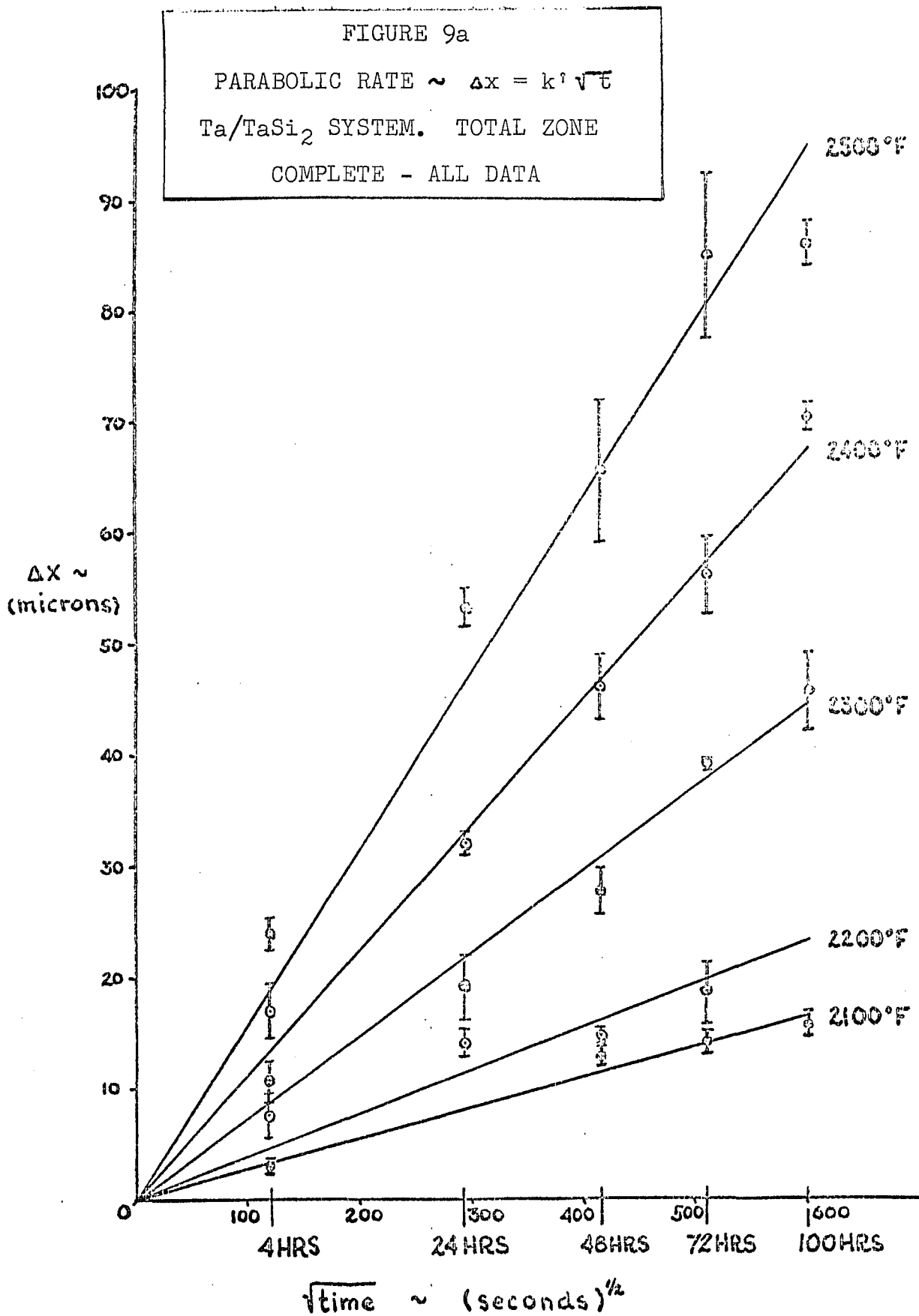
2. M/TaSi₂ Systems

In the M/TaSi₂ systems, it was of primary interest to ascertain whether the metal atom diffused. Marker experiments similar to those made on the Ta/TaSi₂ couples need not be made if the phases on each side of the original interface can be identified. In most cases, the original interface was easily located, and identification of the M silicides in the diffusion zone was accomplished. If metal atoms had diffused, M silicides or ternary M, Ta

silicides should have been found on the TaSi_2 side of the original interface (Δx_1). In all cases but one, only Ta_5Si_3 was found in Δx_1 , indicating that the metal did not diffuse appreciably. The one exception was the Ti/TaSi_2 system in which results clearly indicated Ti_5Si_3 growing in the Δx_1 zone.

E. PLOTS OF EXPERIMENTAL RESULTS

Page 101 follows



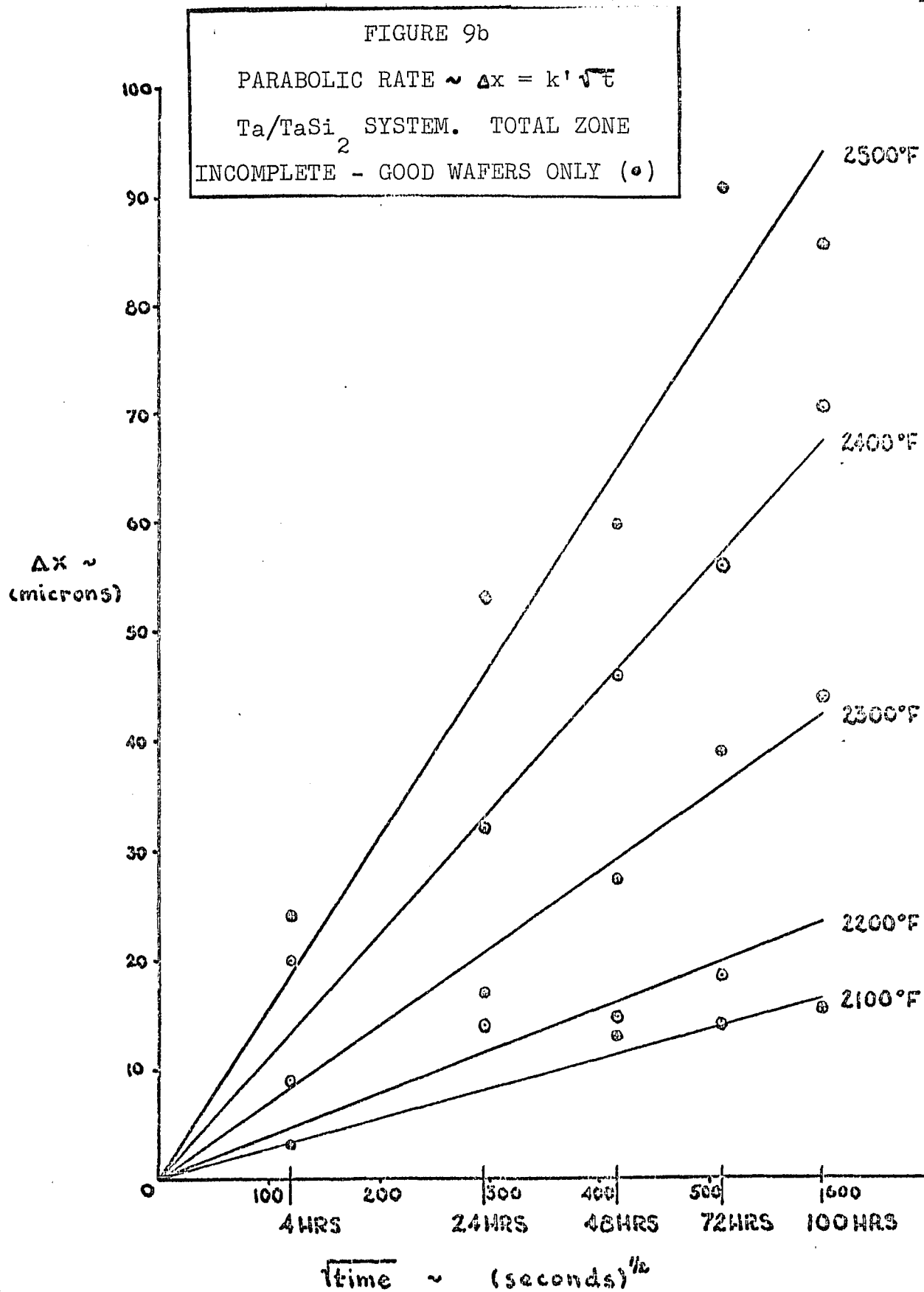
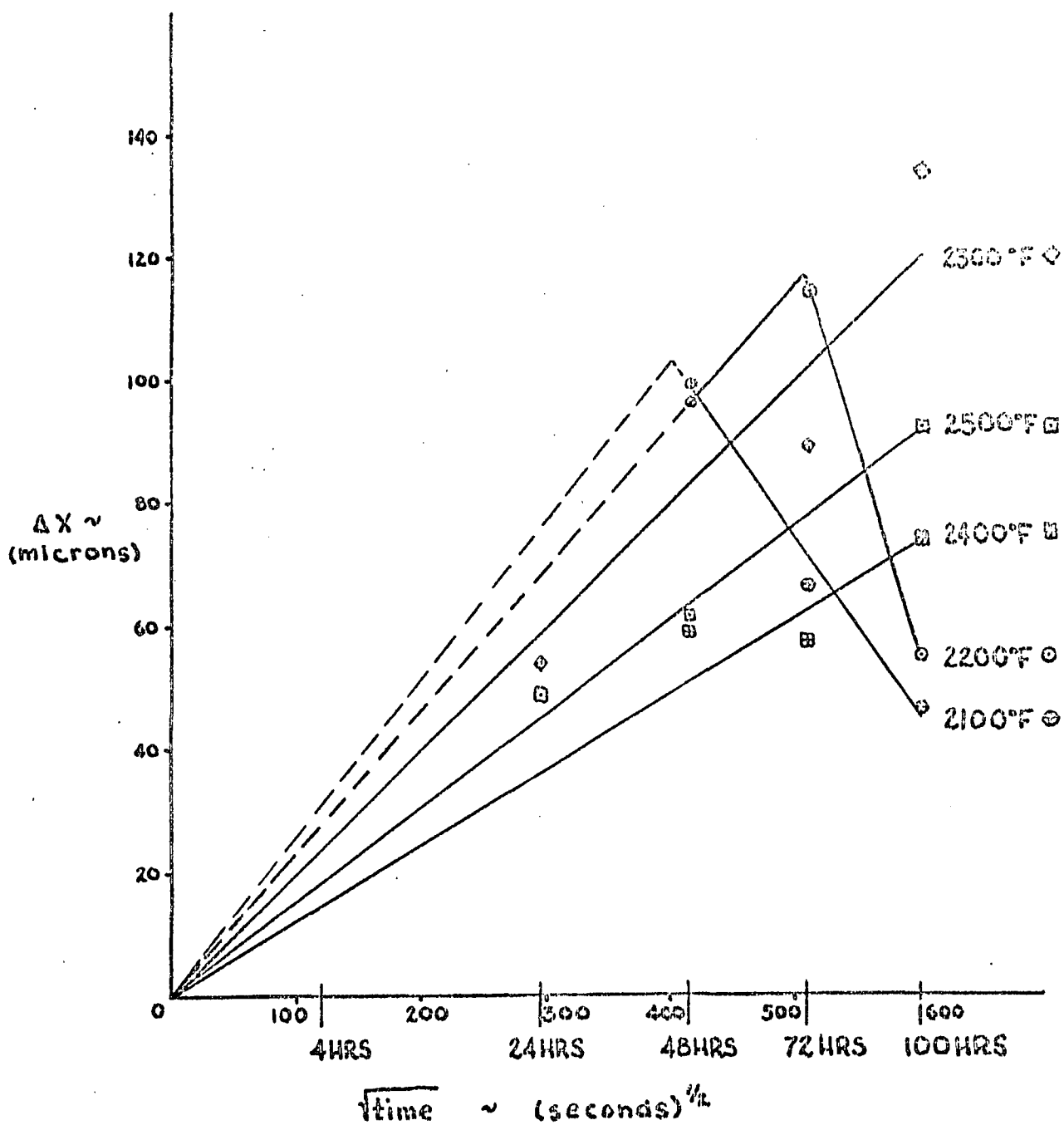


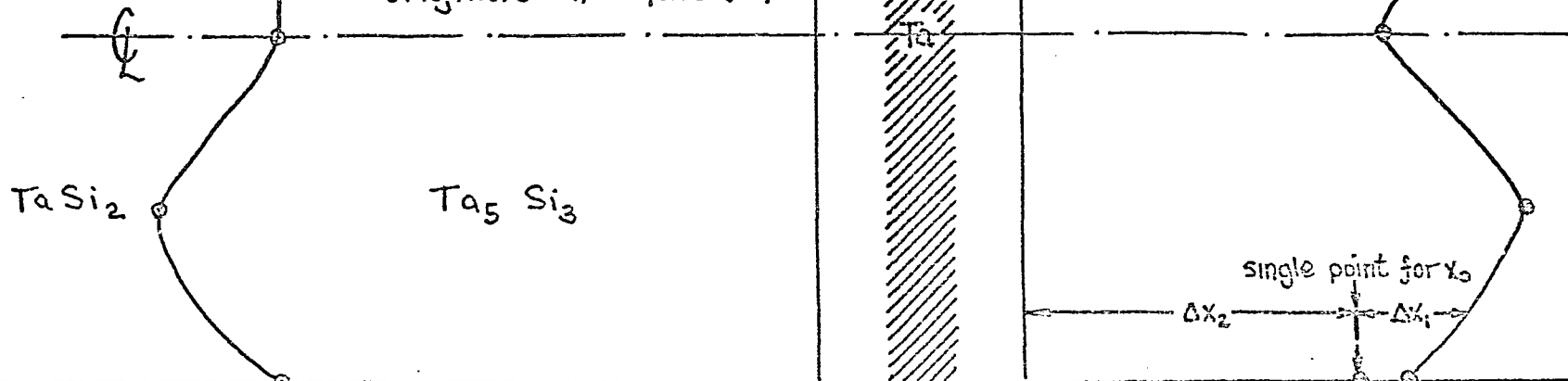
FIGURE 10
PARABOLIC RATE $\sim \Delta x = k'\sqrt{t}$
W/TaSi₂ SYSTEM. TOTAL ZONE
COMPLETE DATA



ZP

FIGURE 11
Ta/TaSi₂ COUPLE ANNEALED
AT 2100°F FOR 4 HOURS

no data for
original interface (x₀)



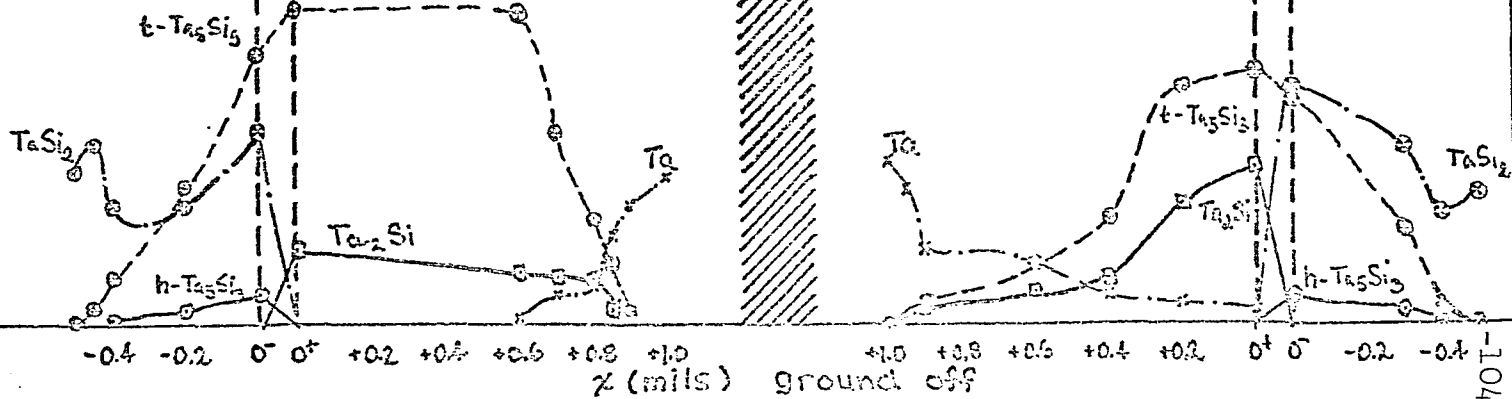
side (A)

original interface

side (B)

CCP

I_{abs.}
20
10

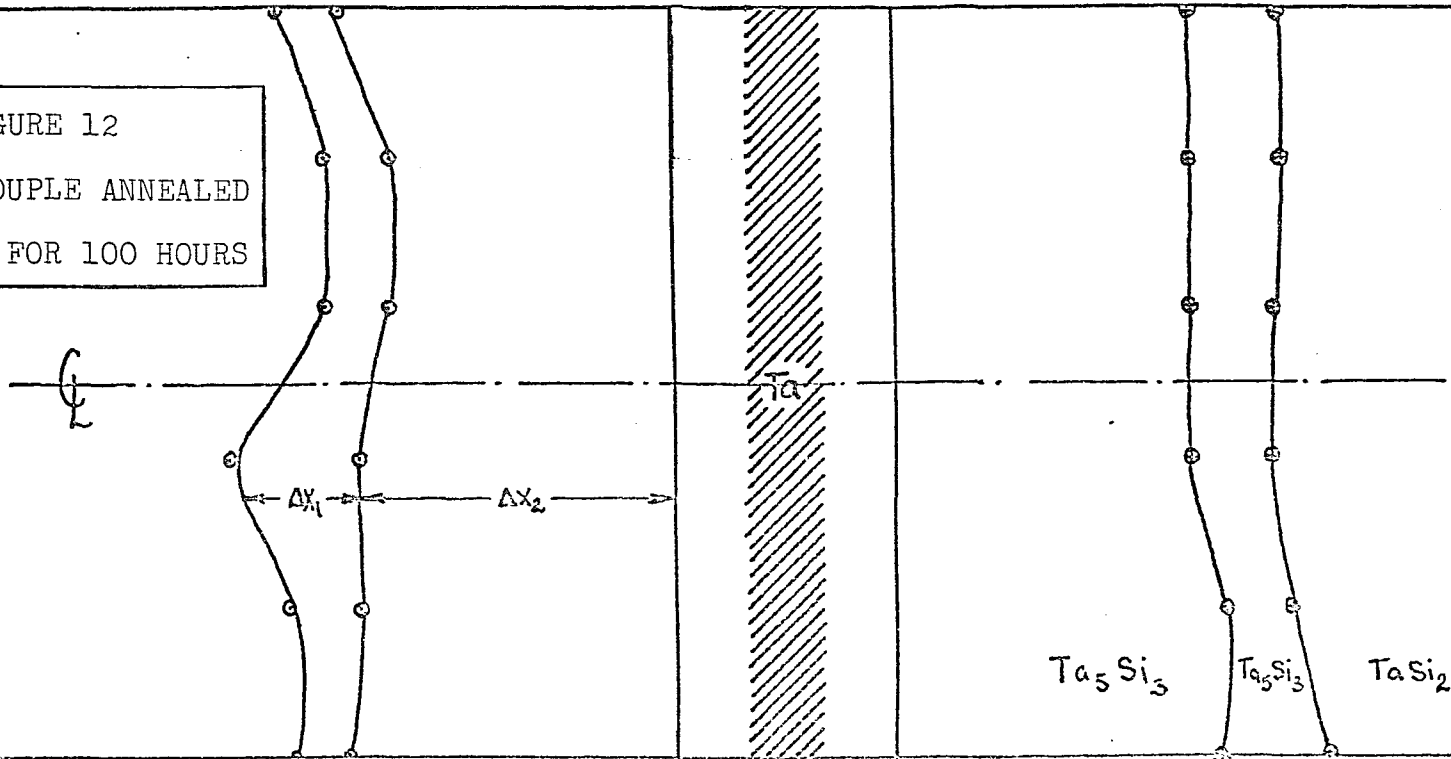


-101-

ZP

FIGURE 12

Ta/TaSi₂ COUPLE ANNEALED
AT 2100°F FOR 100 HOURS

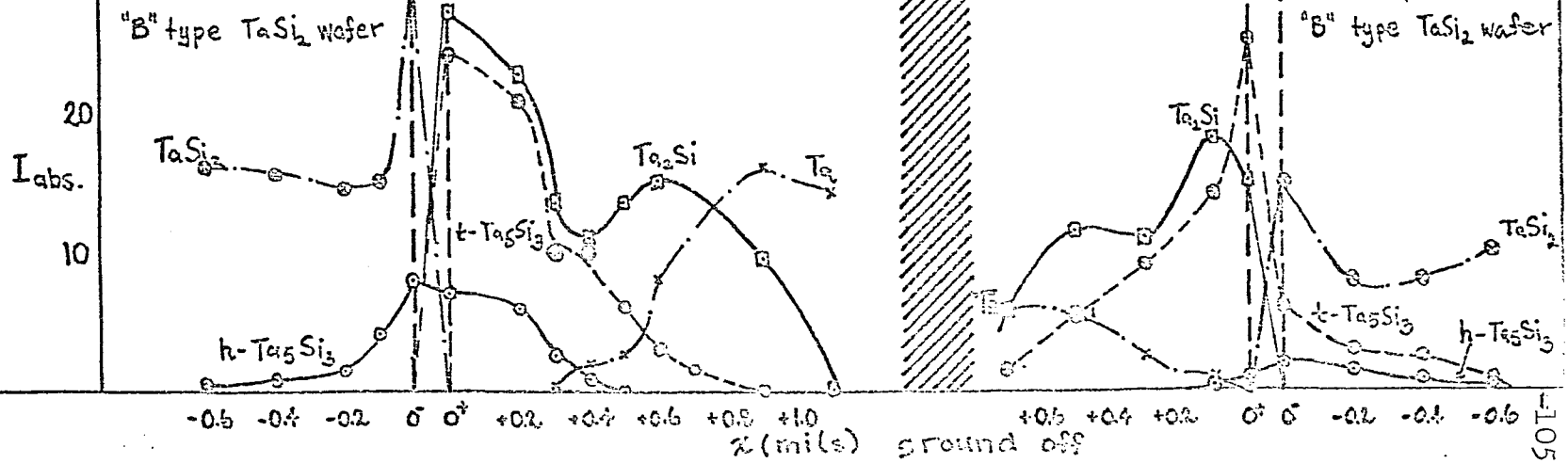


side A

original interface

side B

CCP

"B" type TaSi₂ wafer"B" type TaSi₂ waferI_{abs.}

-0.5 -0.4 -0.2

0

0.2

0.4

0.6

0.8

1.0

z (miles)

ground off

0.2

0.4

0.6

0.8

1.0

z (miles)

ground off

0.2

0.4

0.6

0.8

1.0

z (miles)

ground off

0.2

0.4

0.6

0.8

1.0

z (miles)

ground off

0.2

0.4

0.6

0.8

1.0

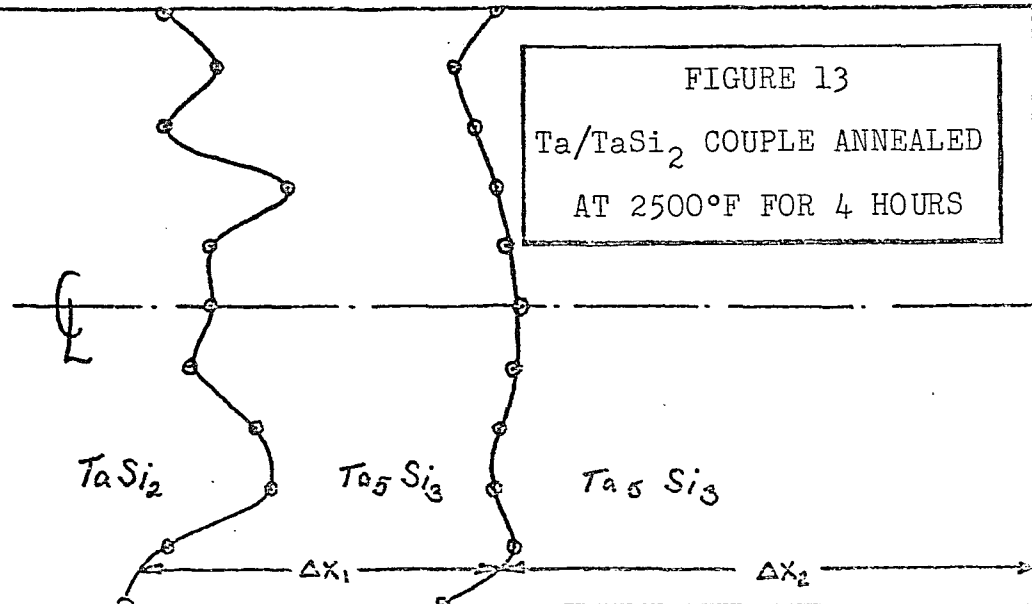
z (miles)

ground off

105-

ZP

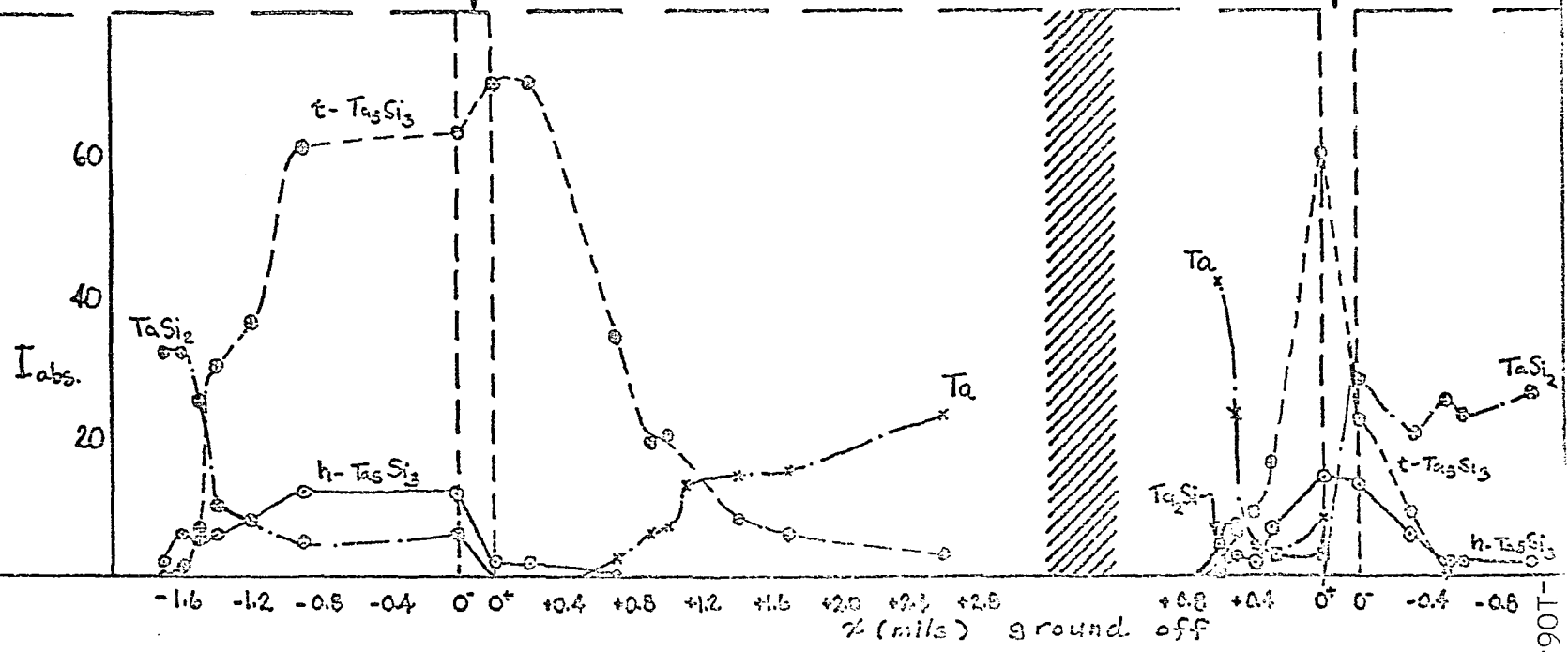
FIGURE 13
Ta/TaSi₂ COUPLE ANNEALED
AT 2500°F FOR 4 HOURS



no data
junction broken

side (A) original interface side (B)

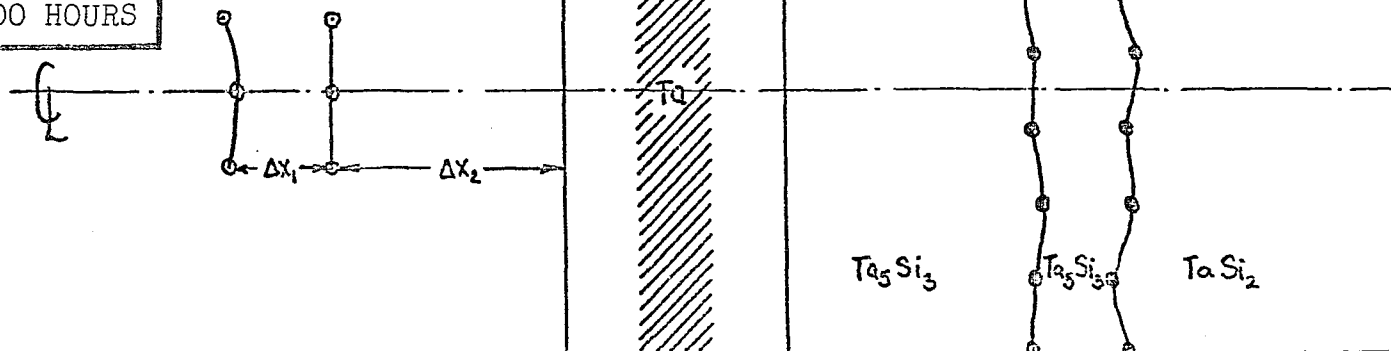
CCP



ZP

FIGURE 14

Ta/TaSi₂ COUPLE ANNEALED
AT 2500°F FOR 100 HOURS

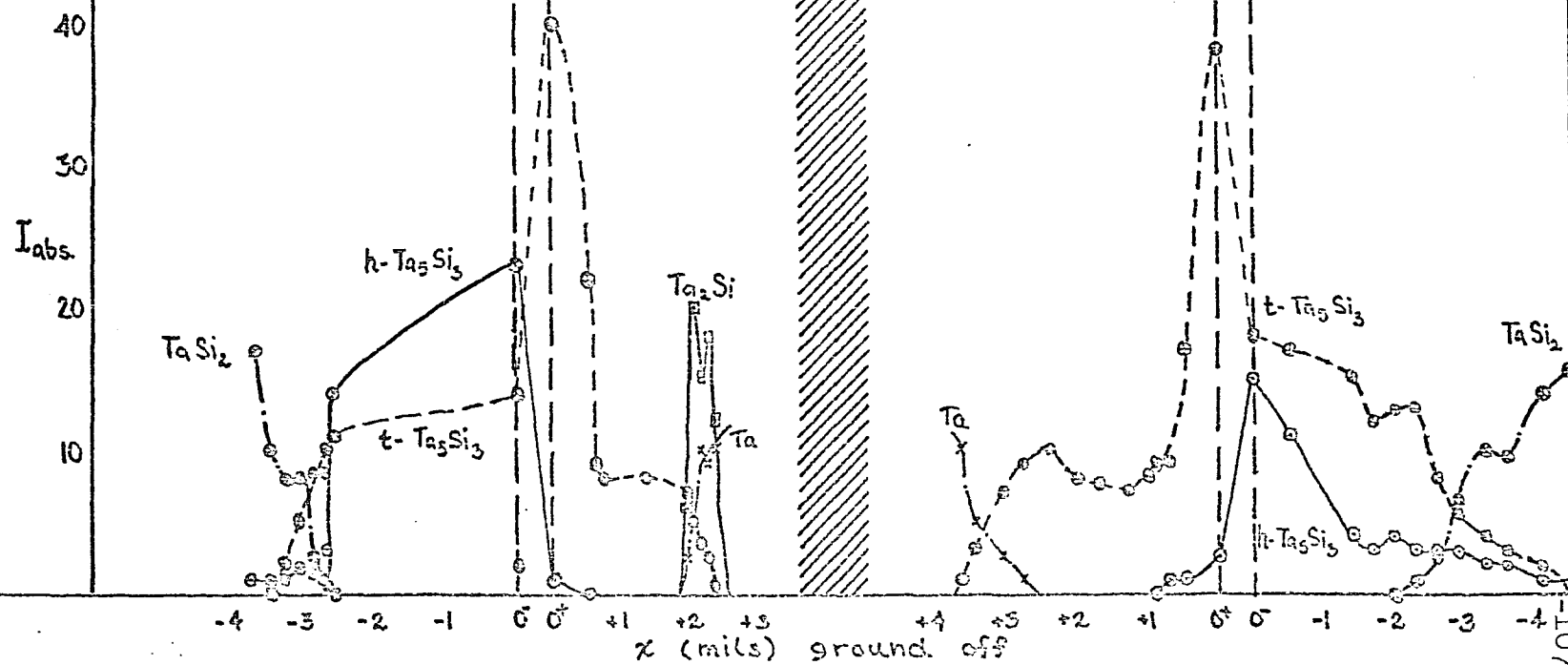


side (A)

original interface

side (B)

CCP



ZP

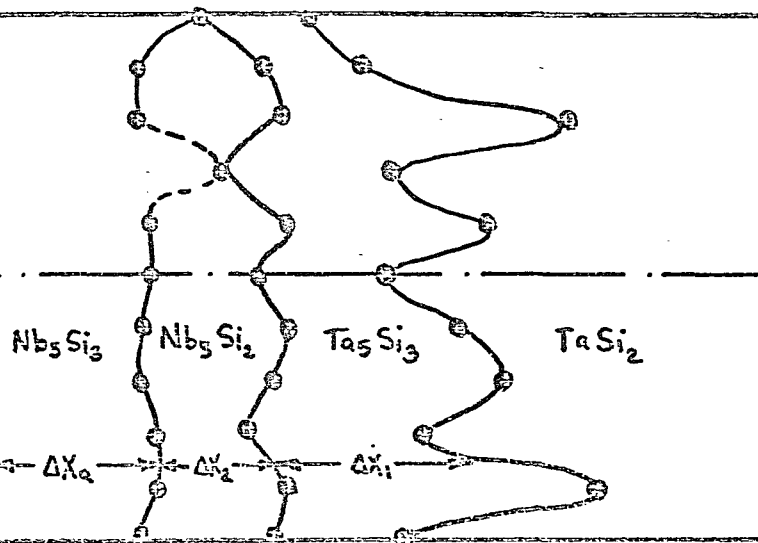
FIGURE 15

Nb/TaSi₂ COUPLE ANNEALED
AT 2100°F FOR 4 HOURS

zone broken



no data



side (A)

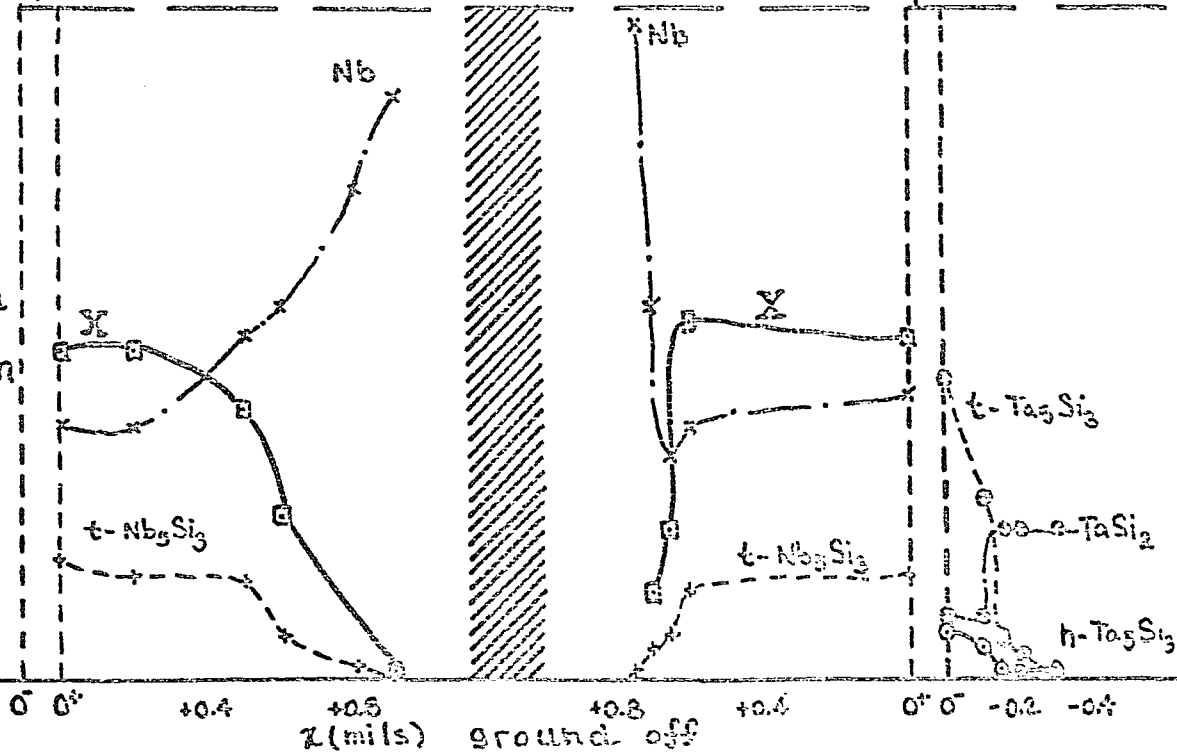
original interface

side (B)

CCP

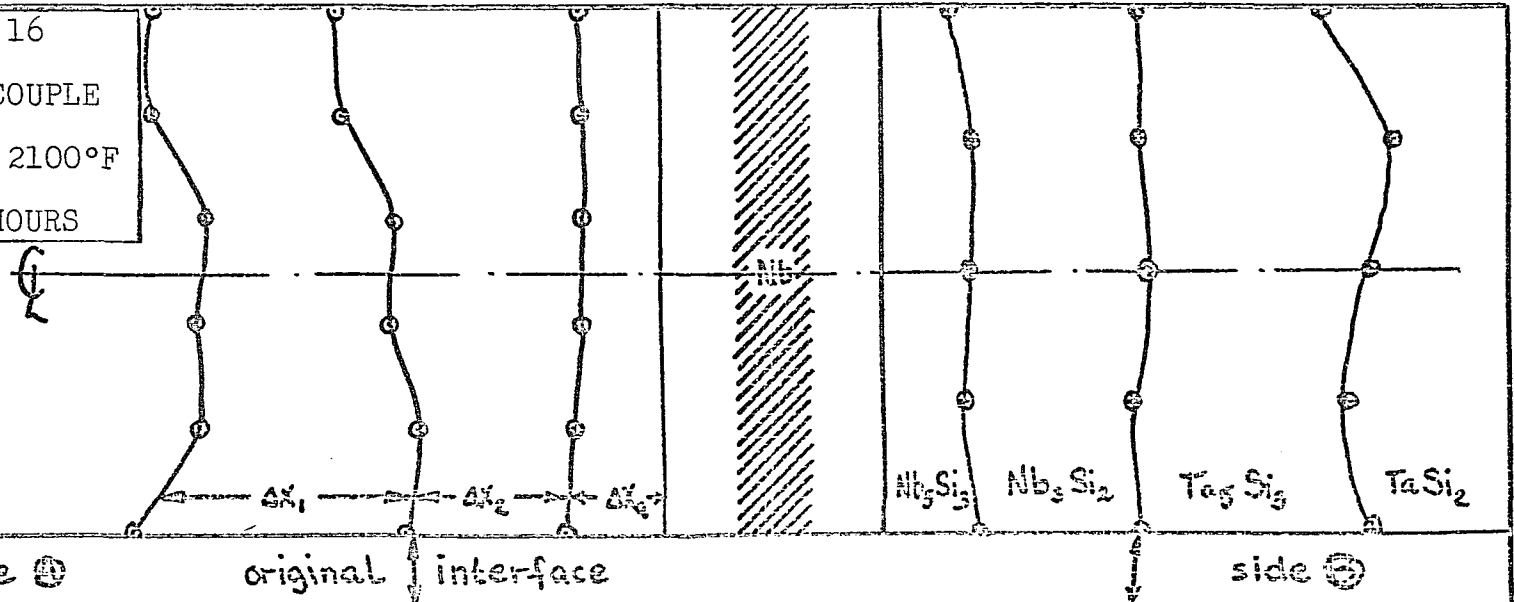
40
30
I. abs.
20
10

no
data
taken

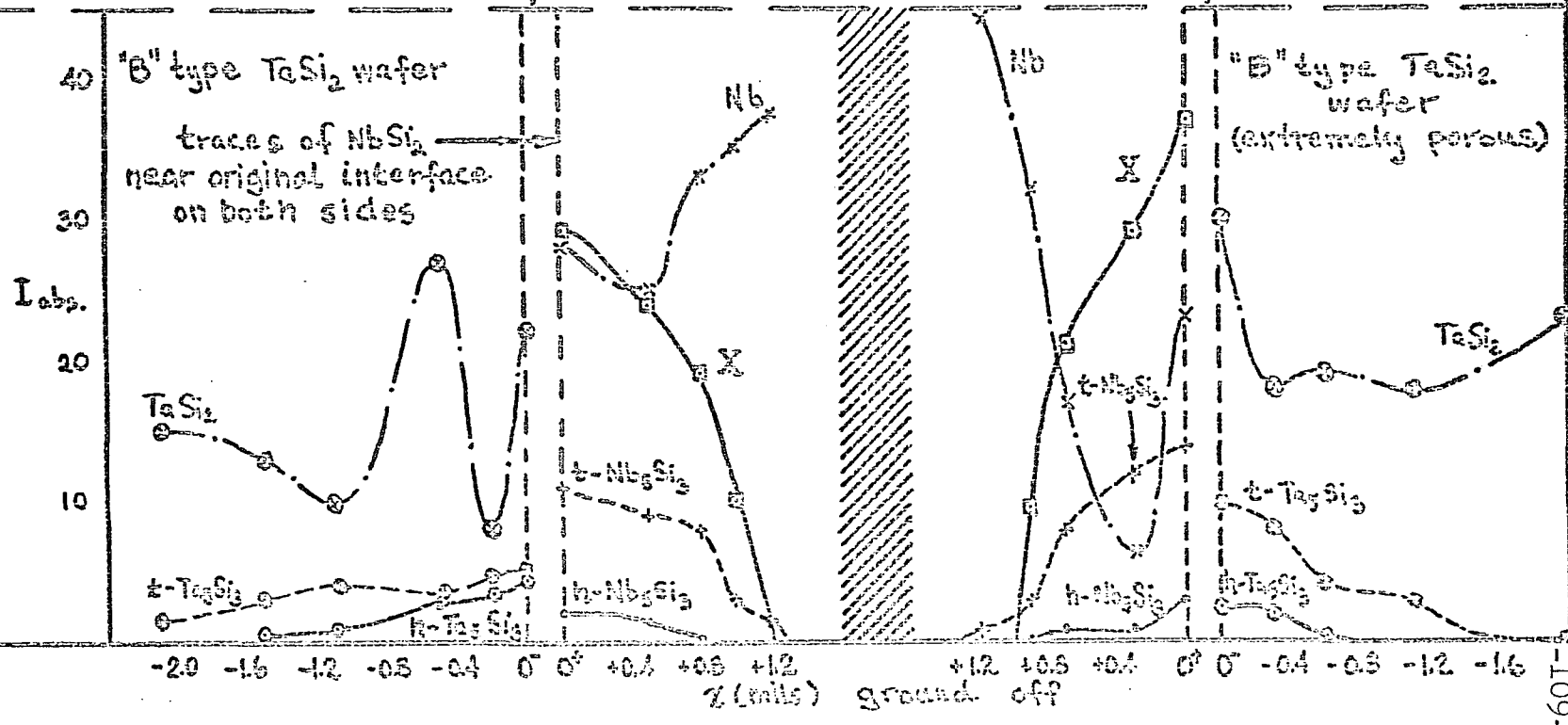


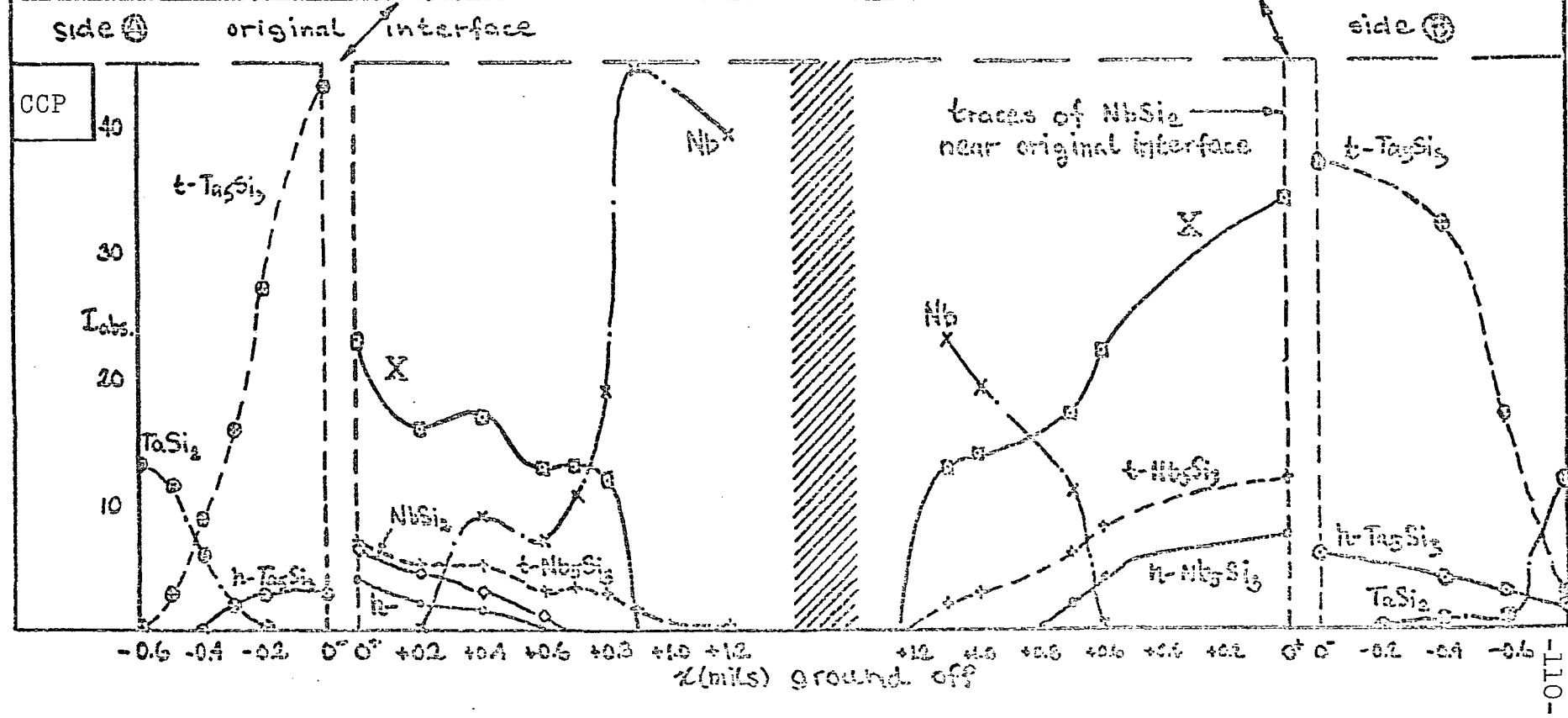
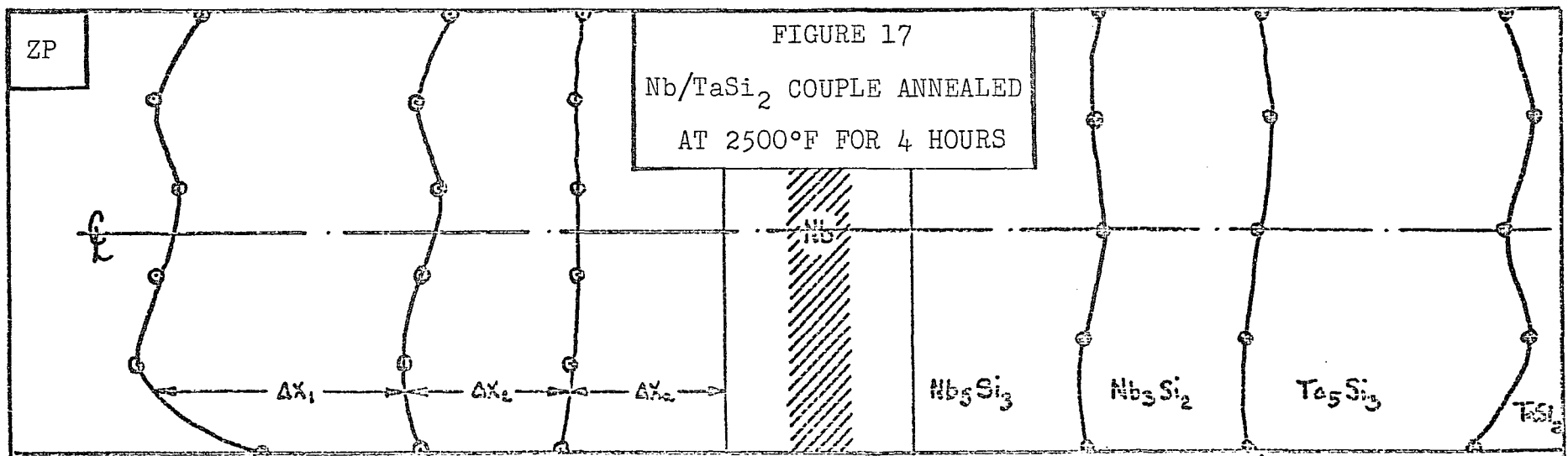
ZP

FIGURE 16
 Nb/TaSi₂ COUPLE
 ANNEALED AT 2100°F
 FOR 100 HOURS



GCP

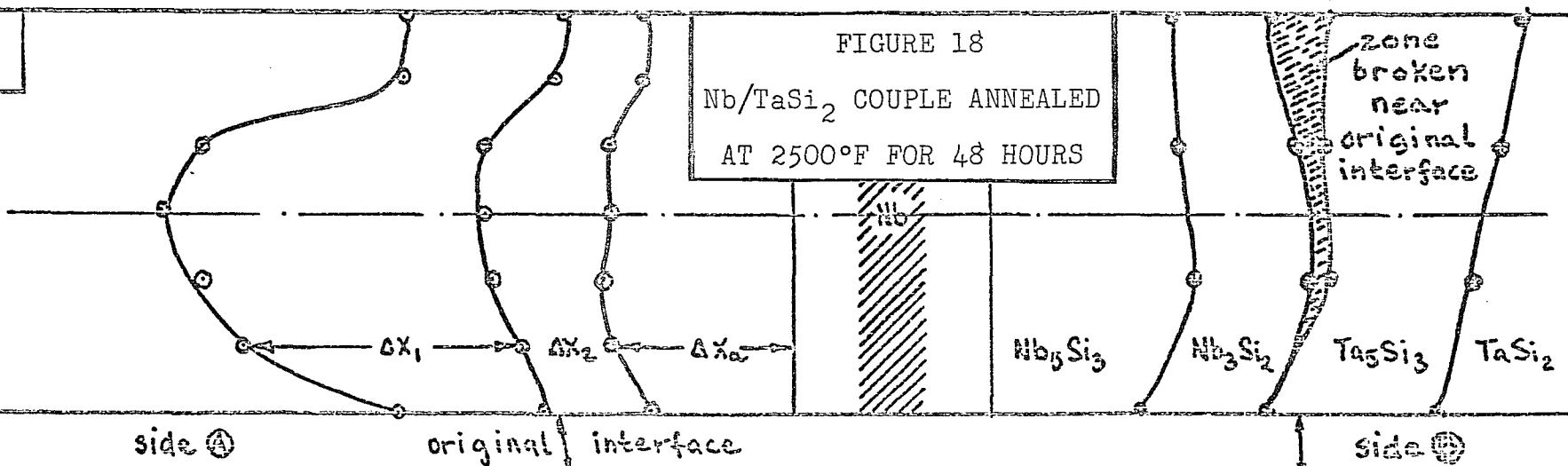




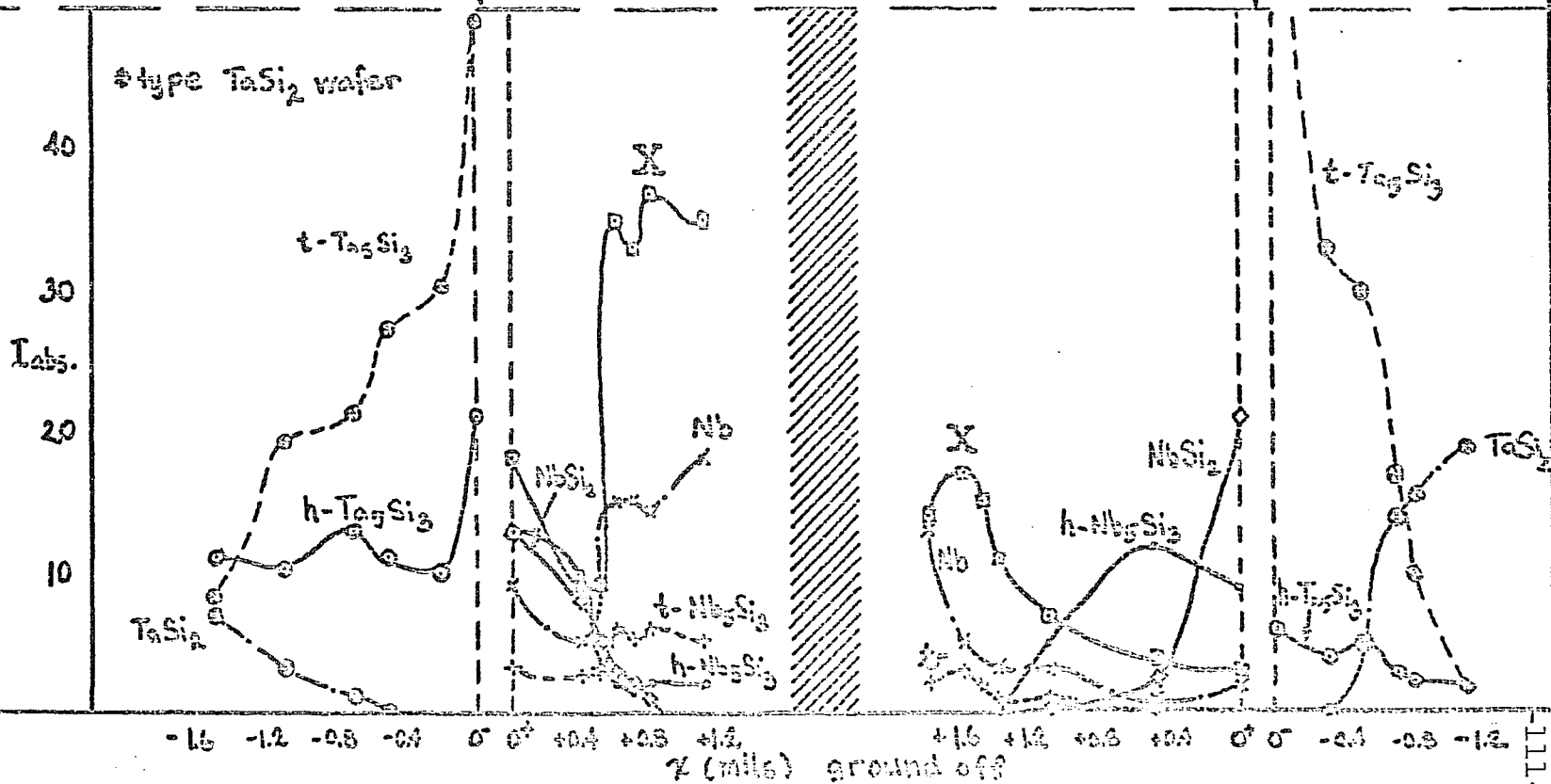
ZP

FIGURE 18

Nb/TaSi₂ COUPLE ANNEALED
AT 2500°F FOR 48 HOURS



CCP



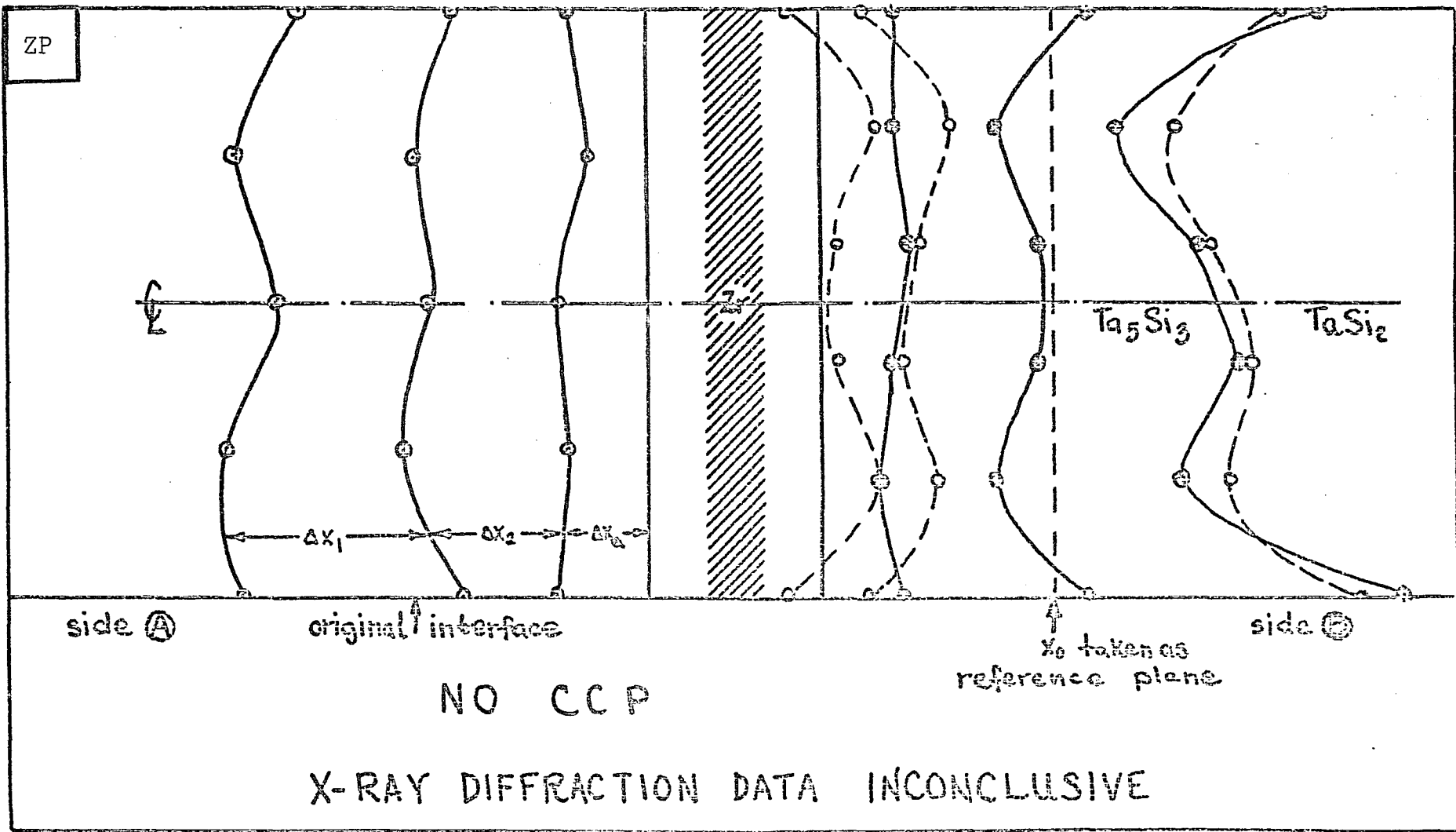


FIGURE 19

Zr/TaSi₂ COUPLE ANNEALED AT 2100°F FOR 4 HOURS

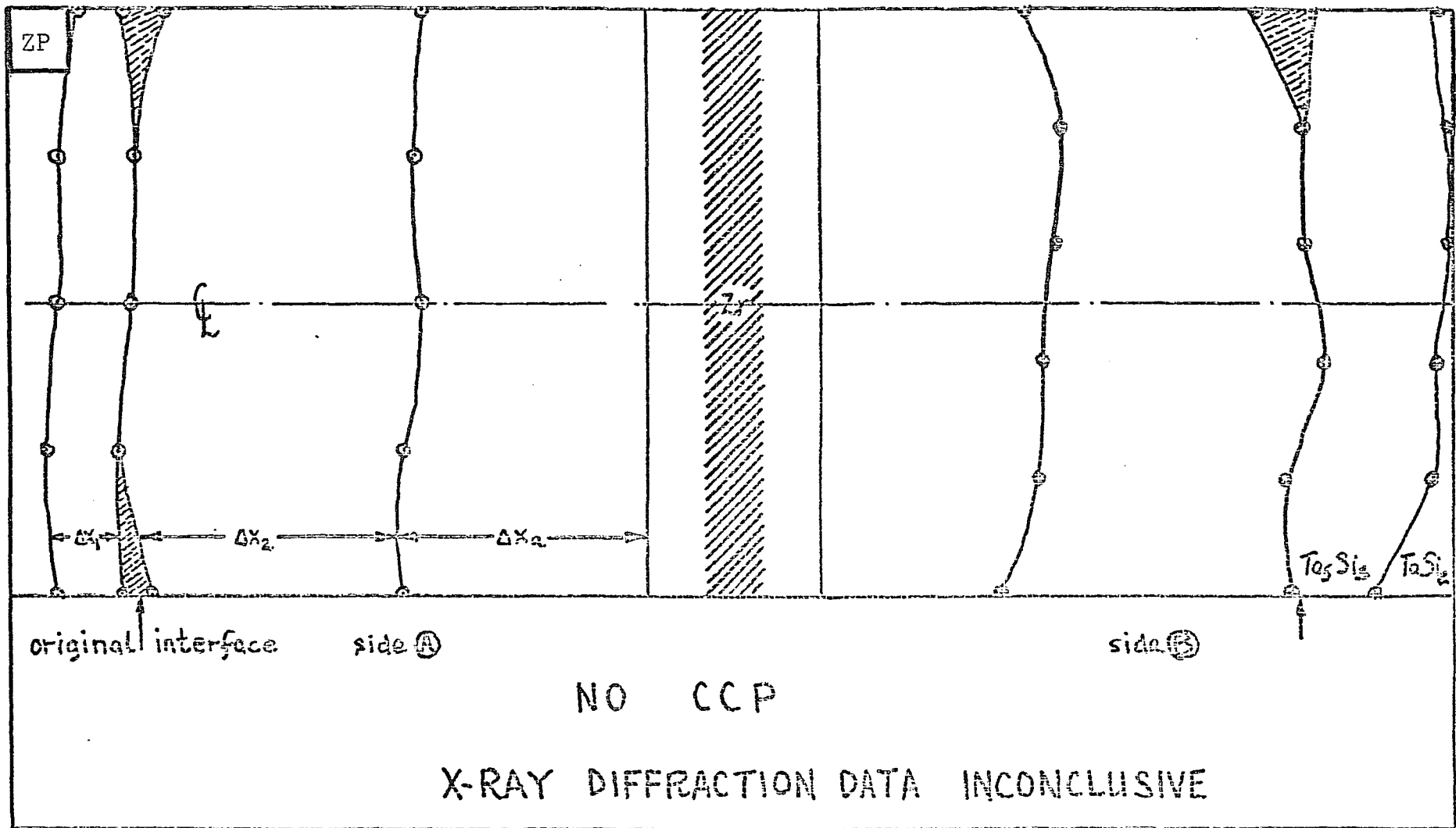
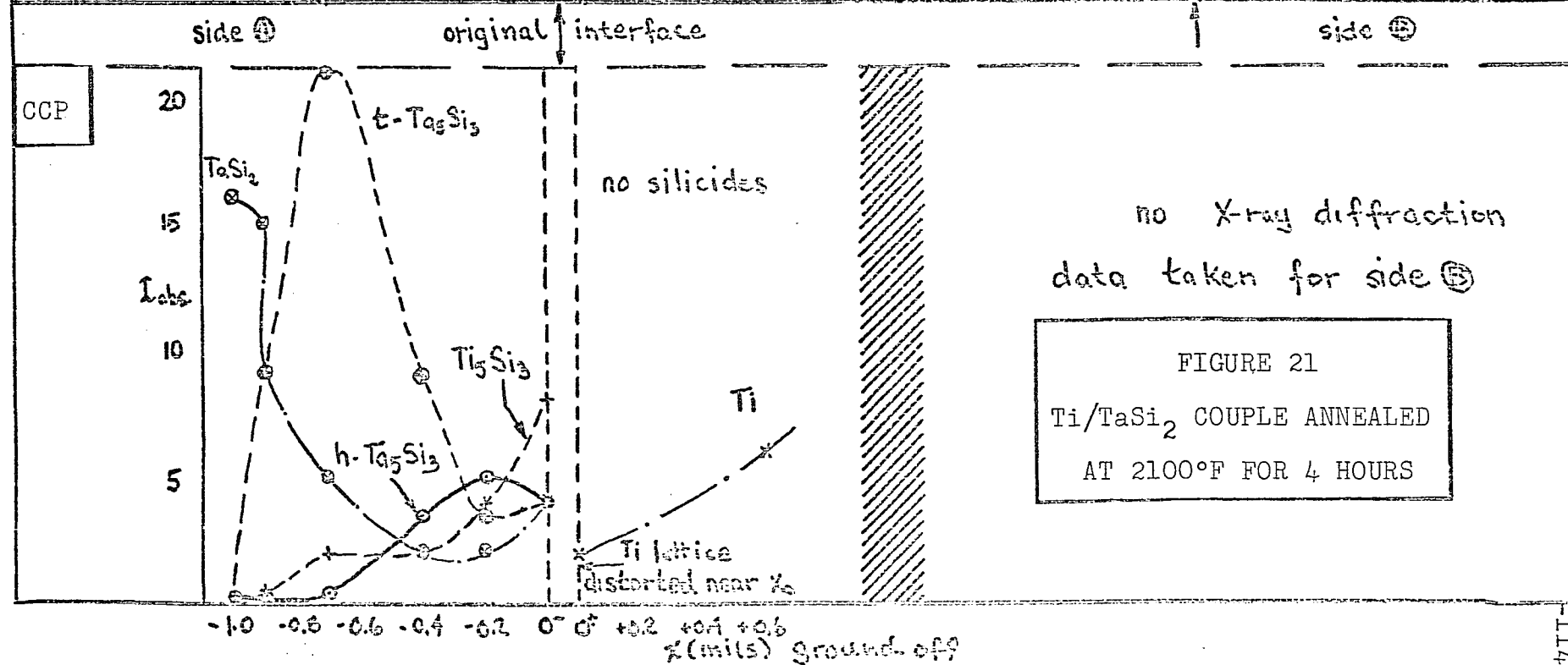
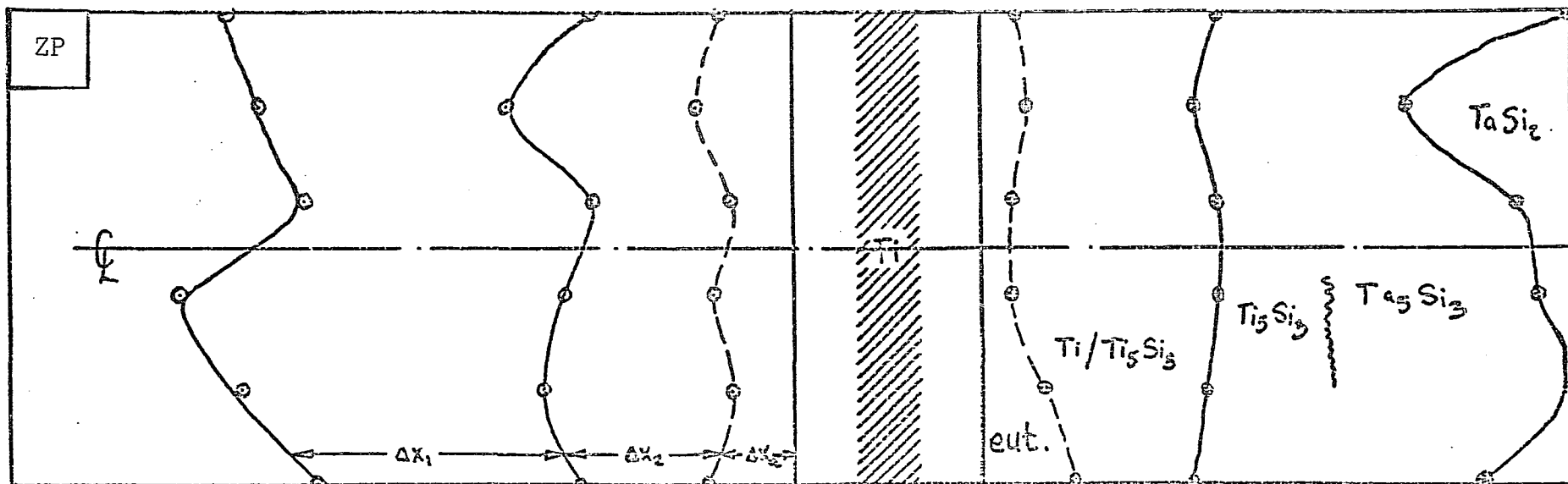
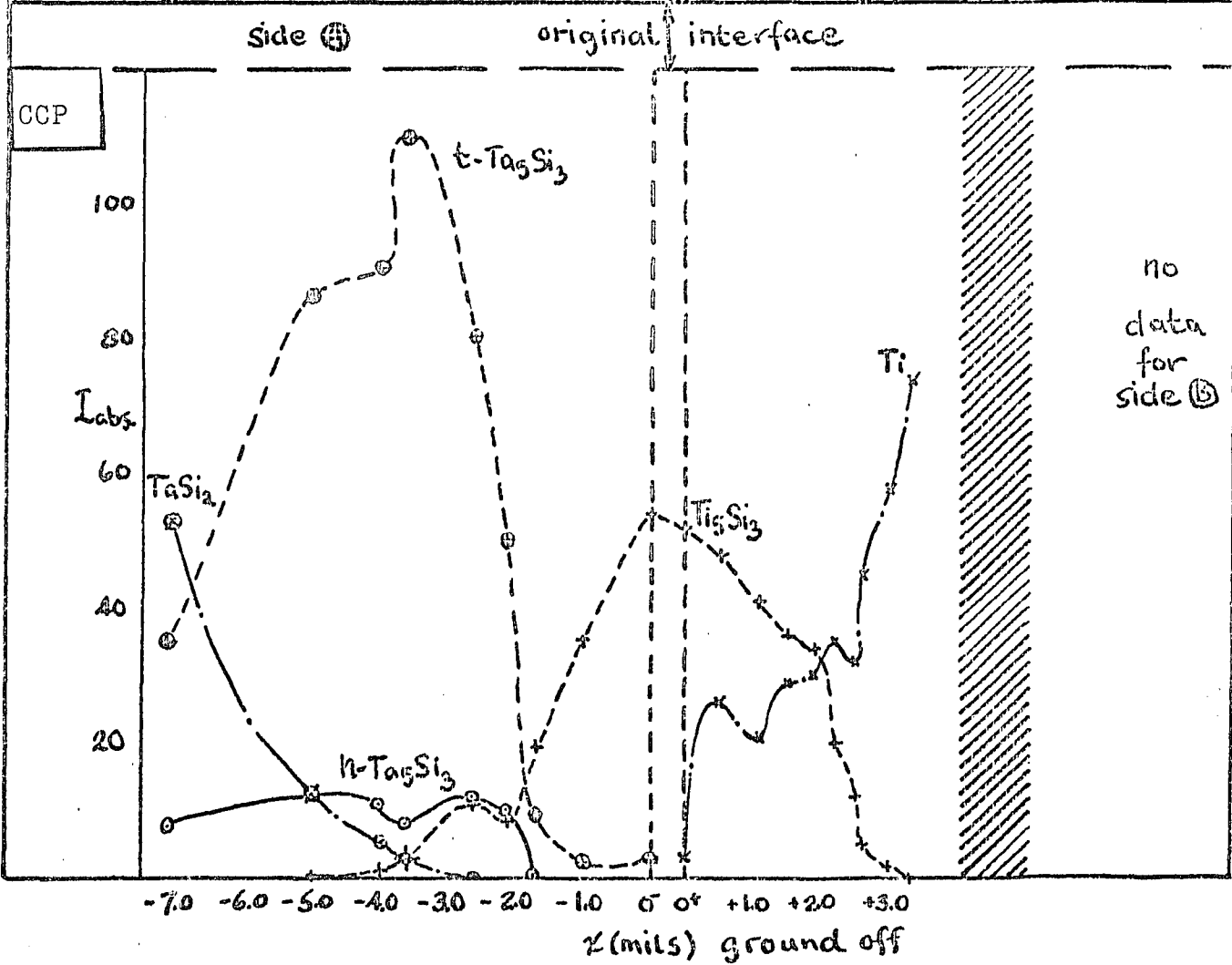
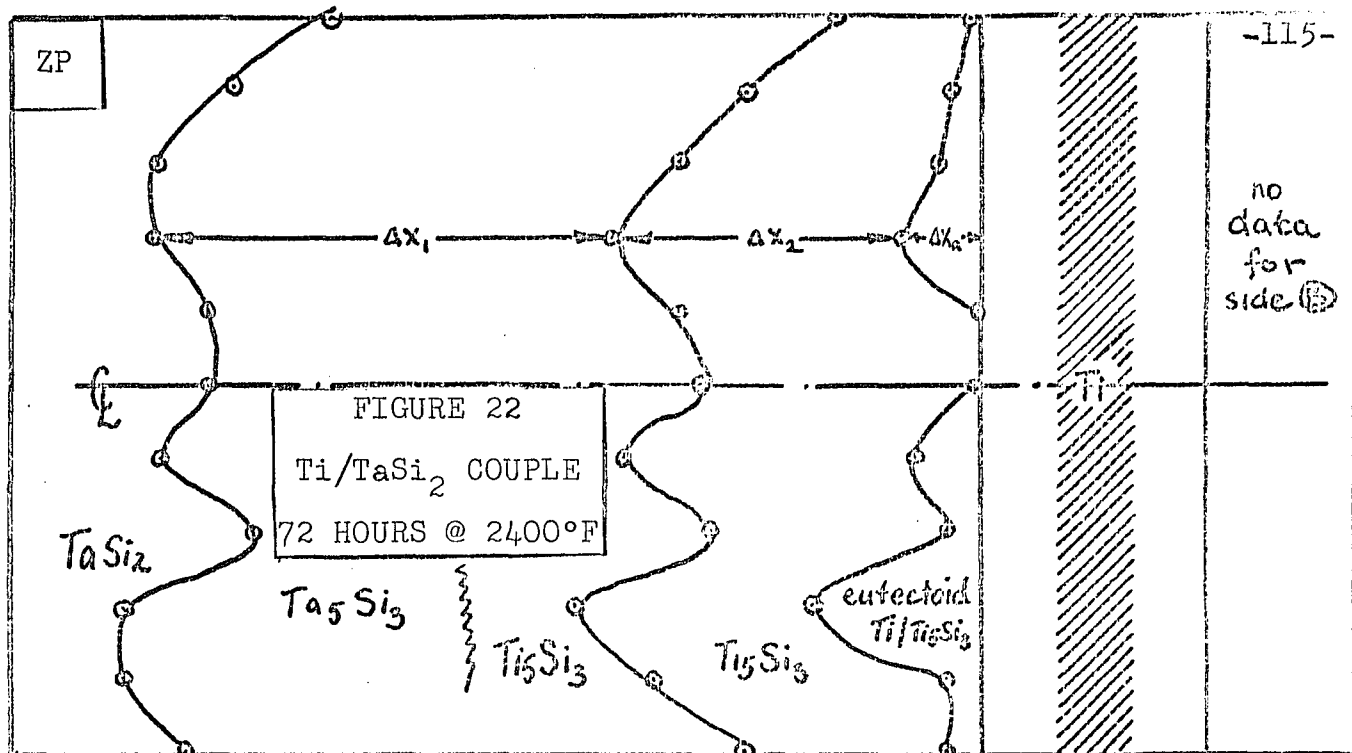
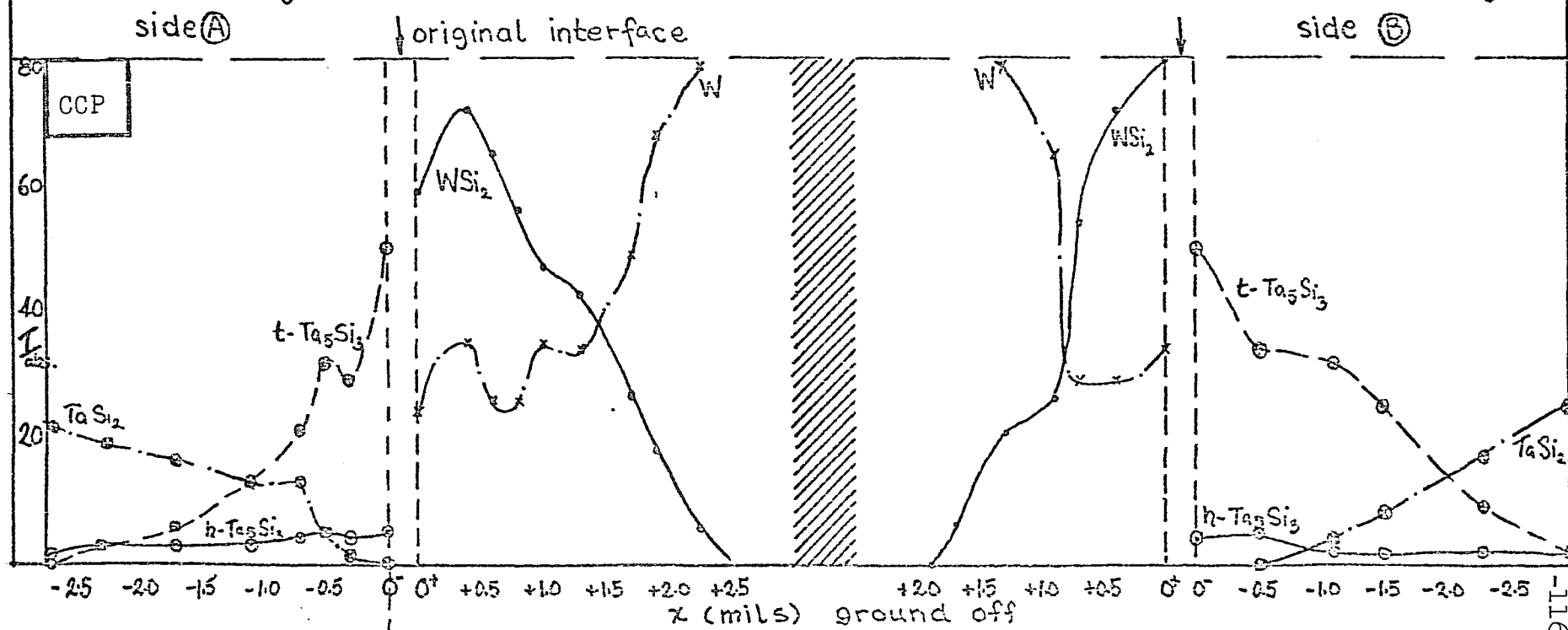
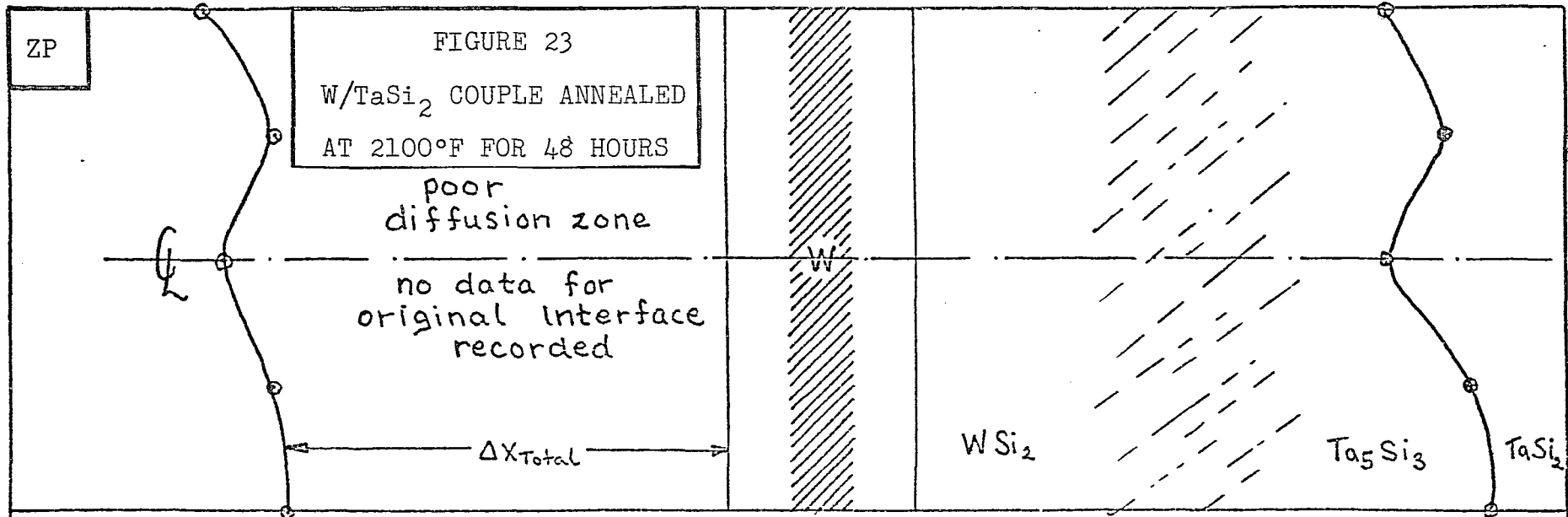
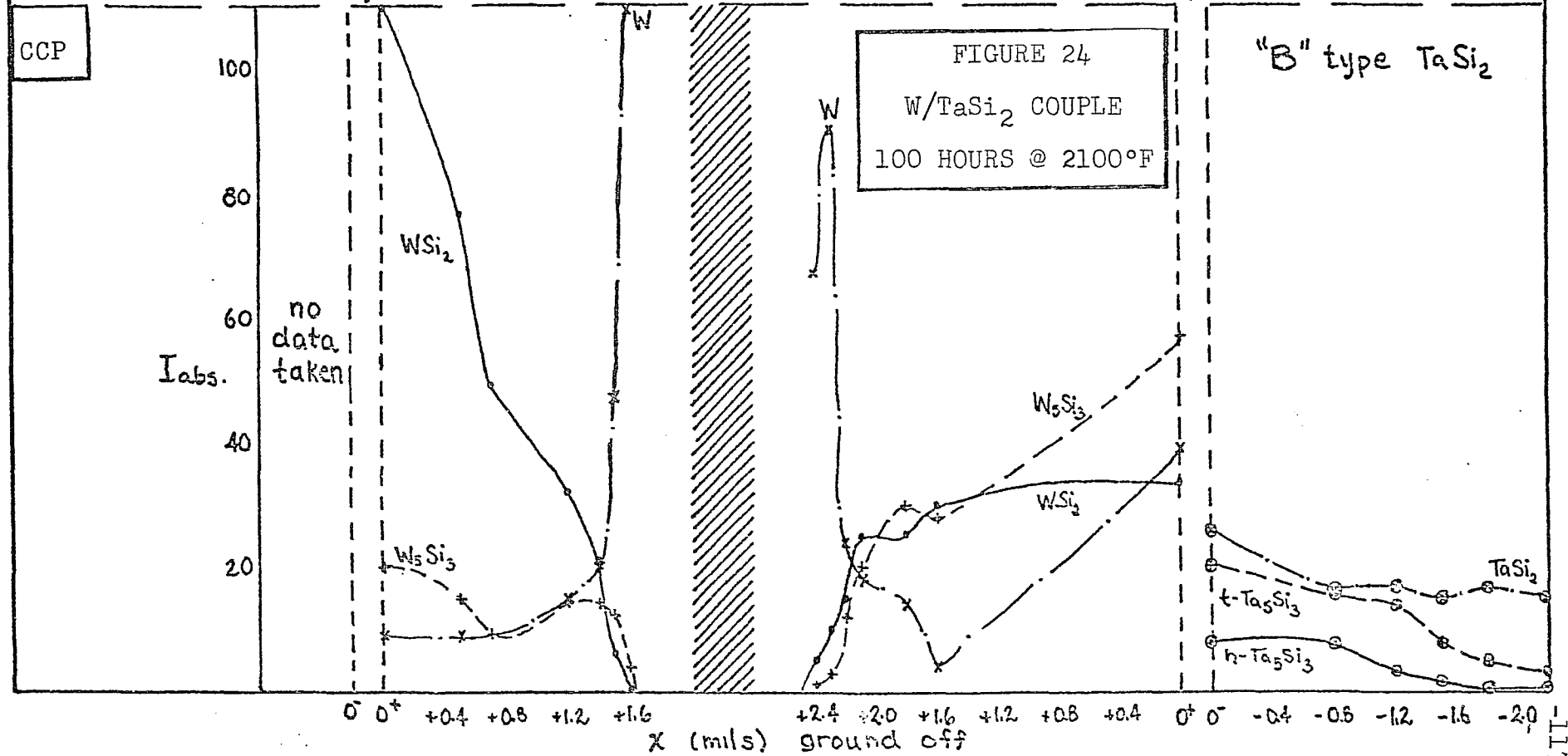
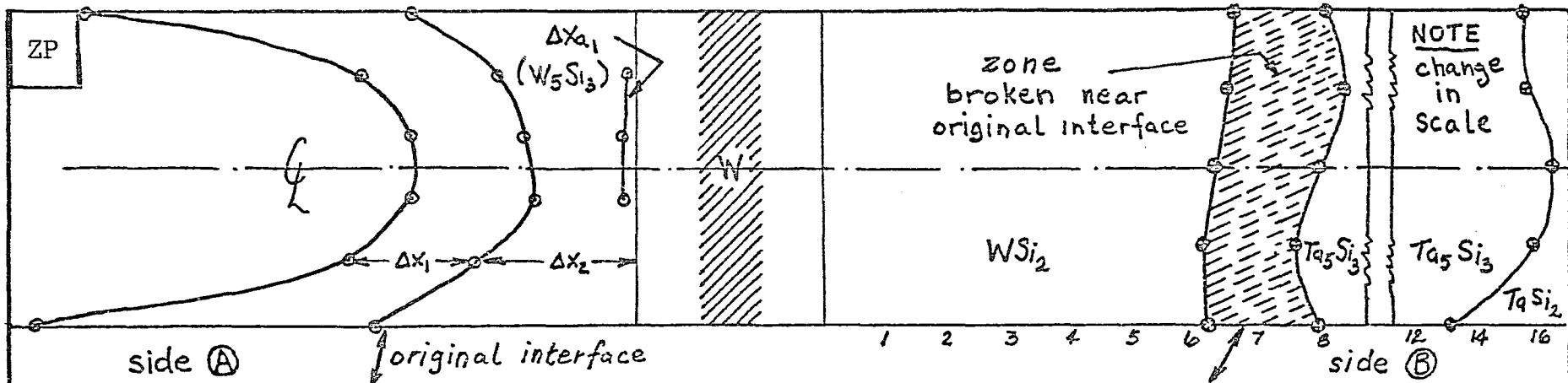


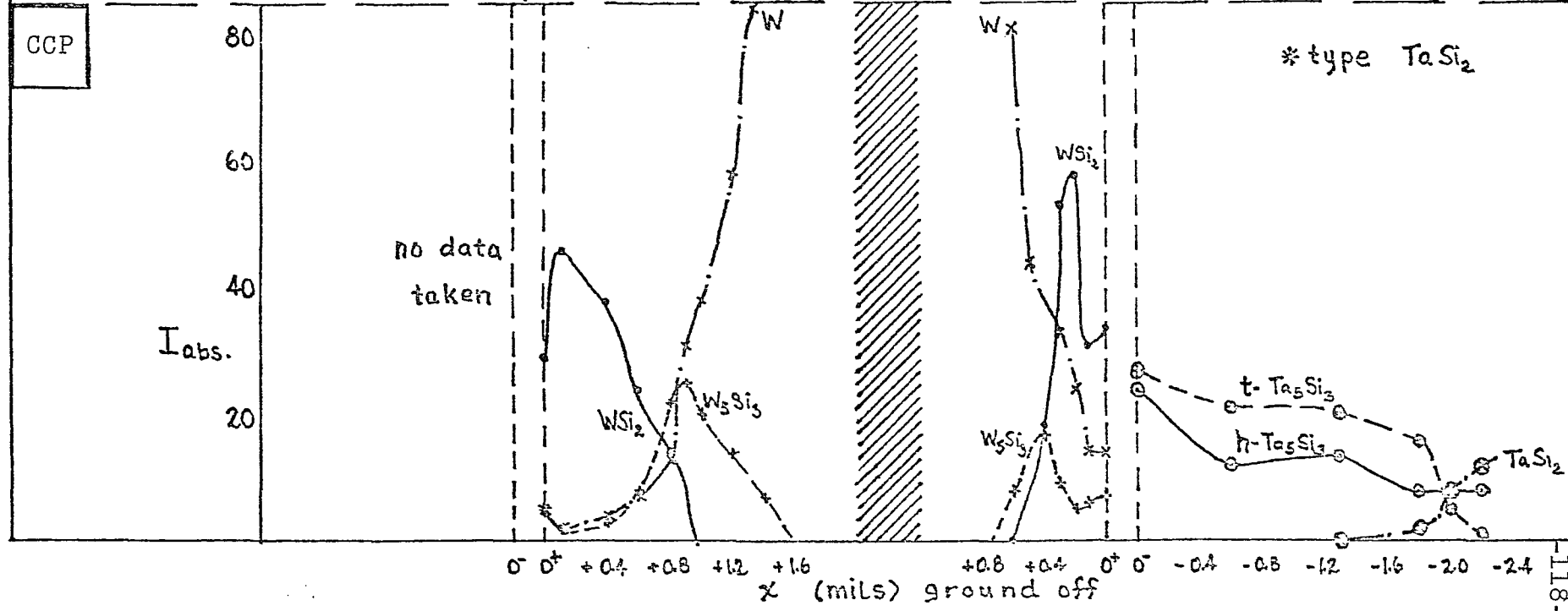
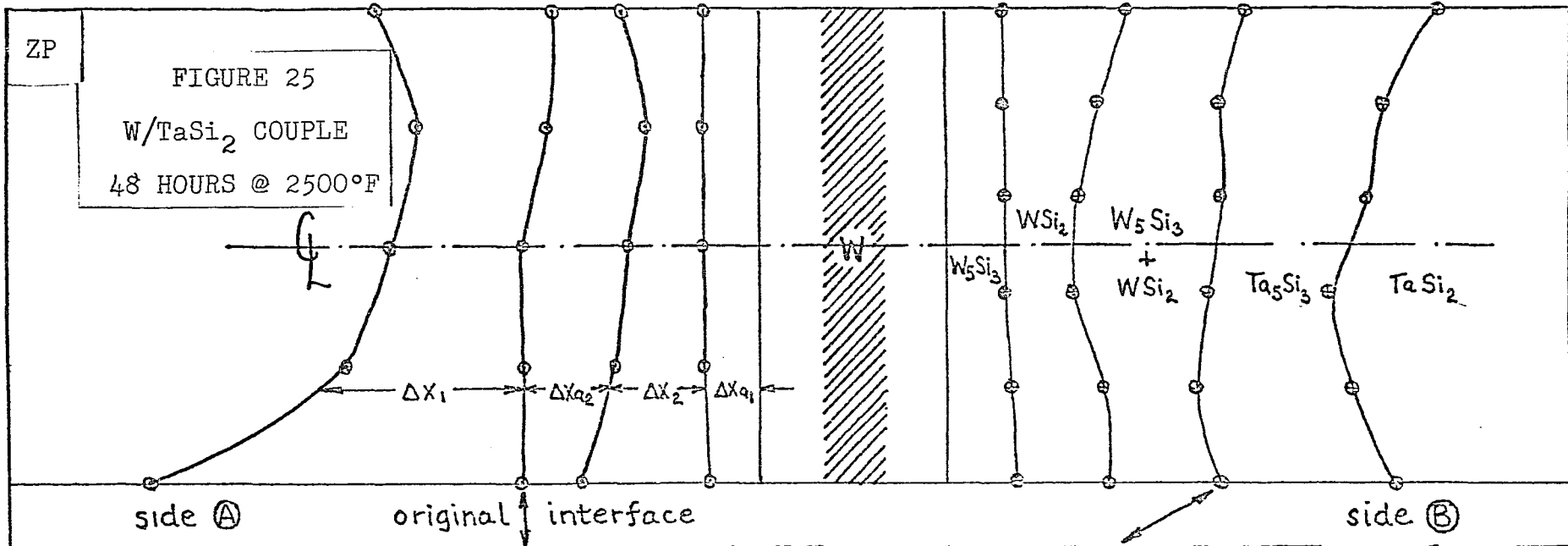
FIGURE 20
 Zr/TaSi₂ COUPLE ANNEALED AT 2500°F FOR 72 HOURS











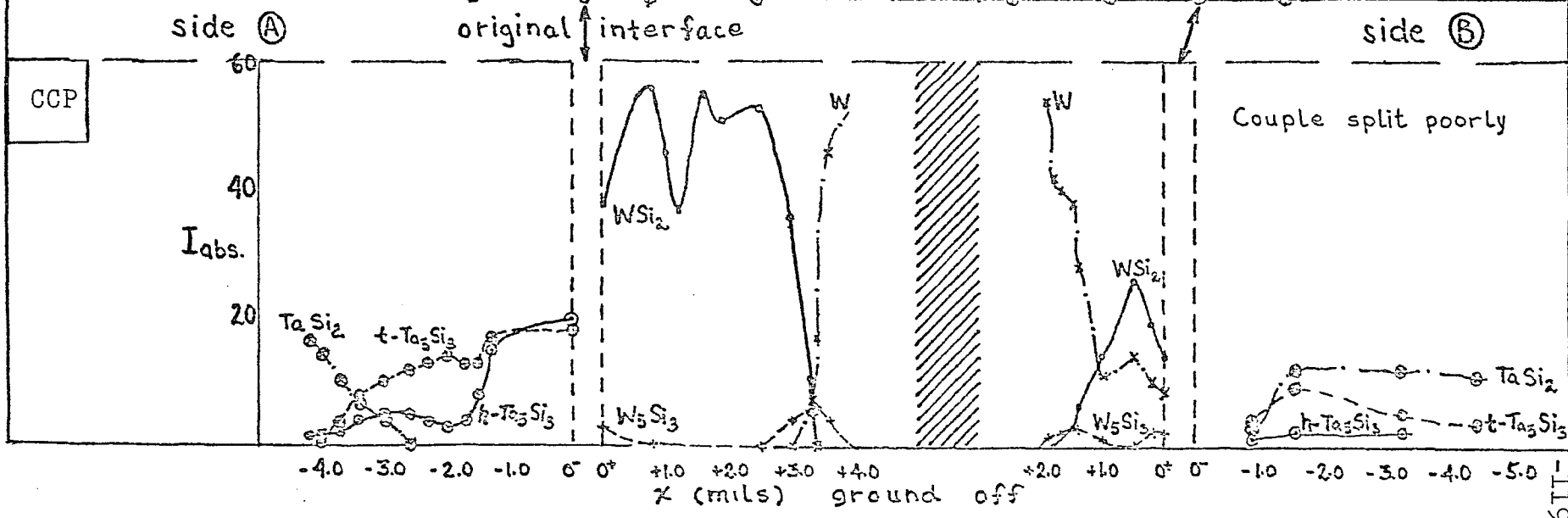
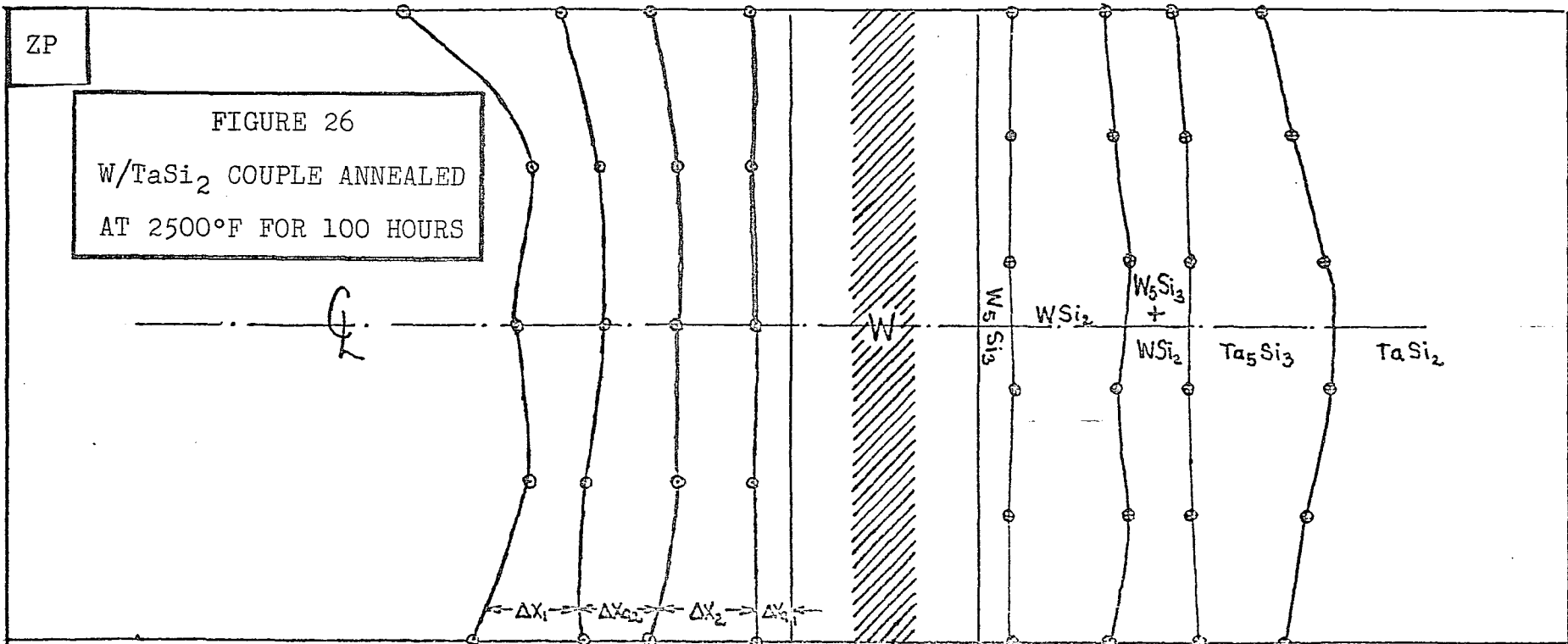
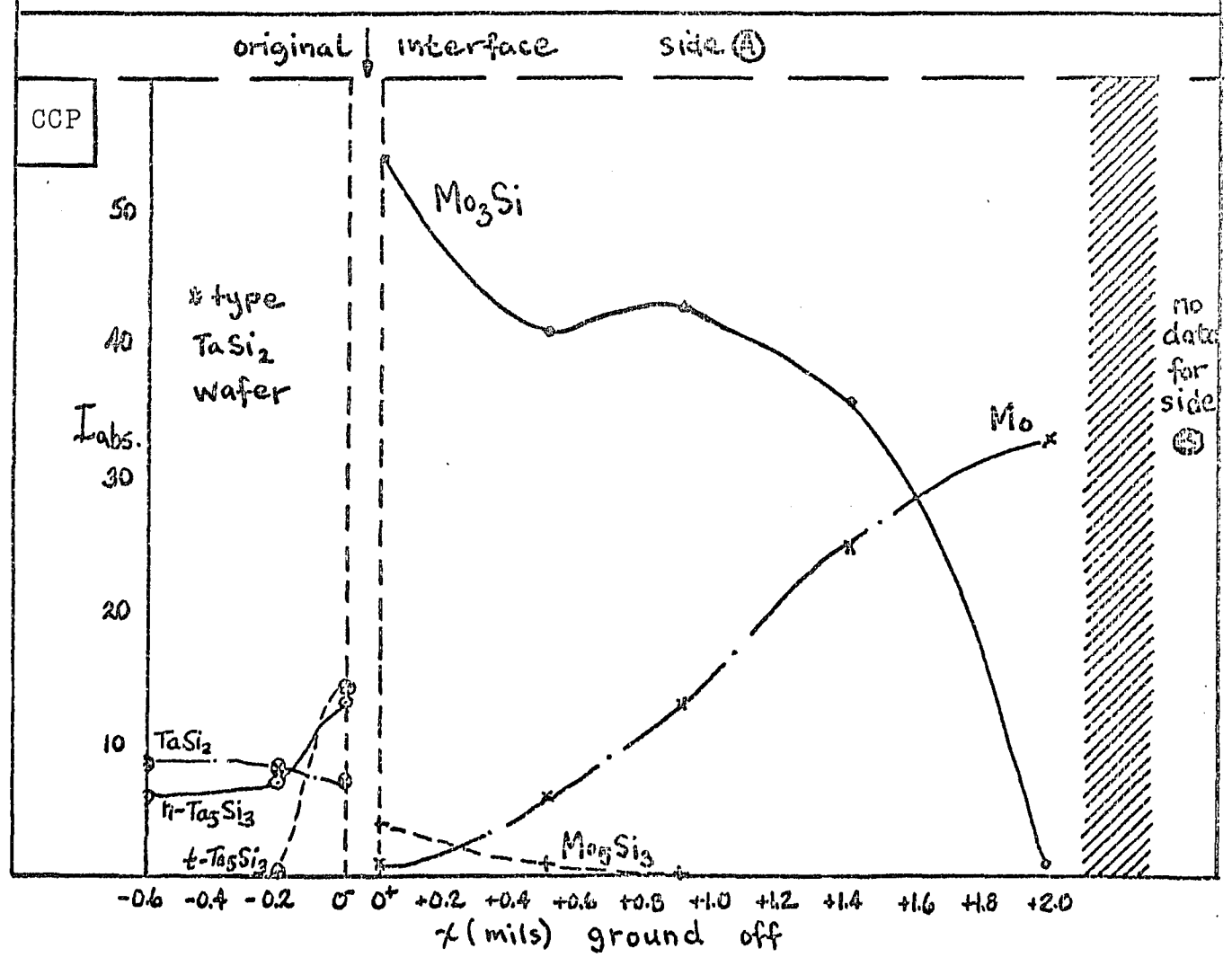


FIGURE 27

Mo/TaSi₂ COUPLE ANNEALED AT 2100°F FOR 24 HOURS

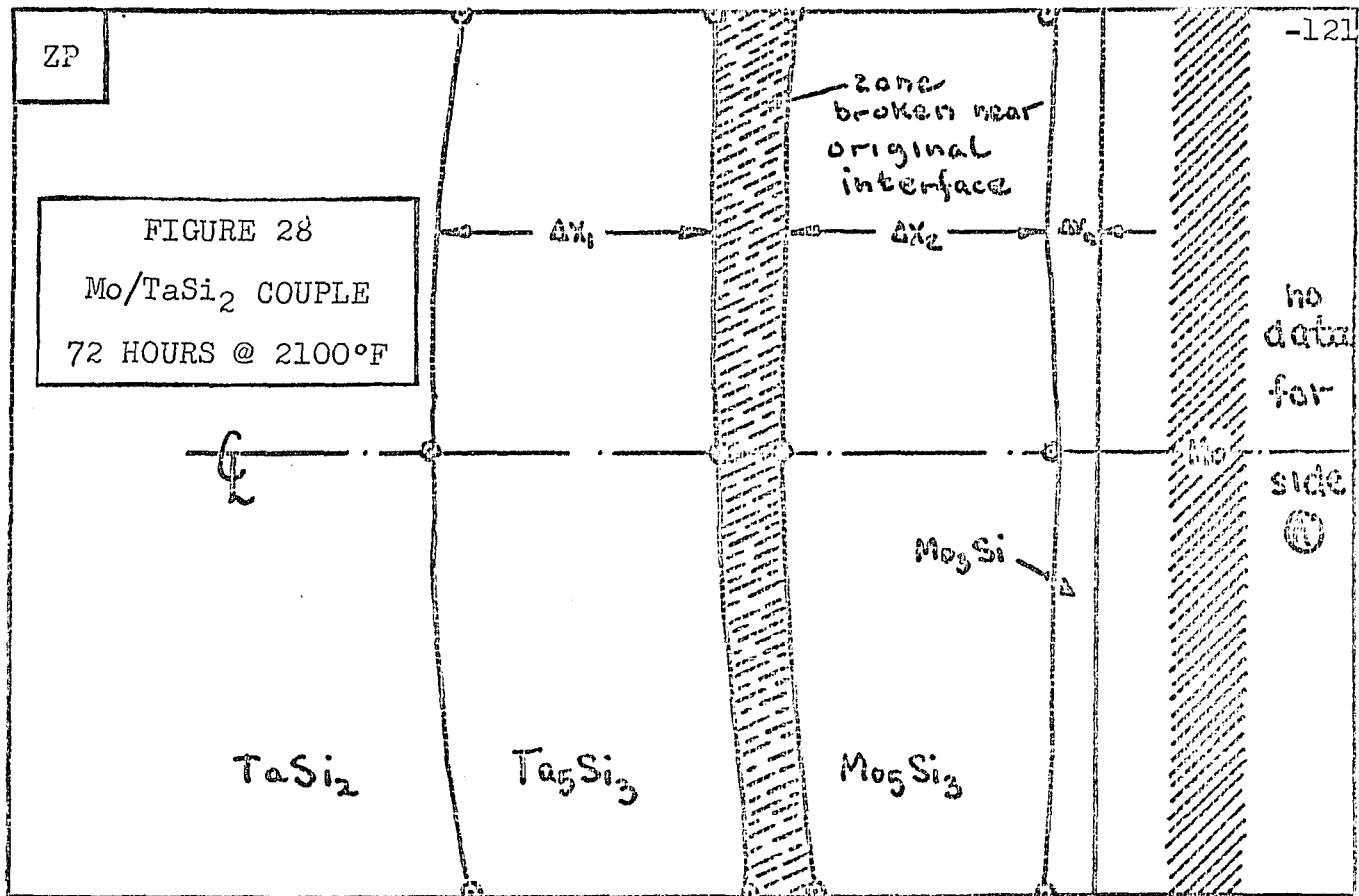
NO ZP

ZONE BROKEN AND CRACKED



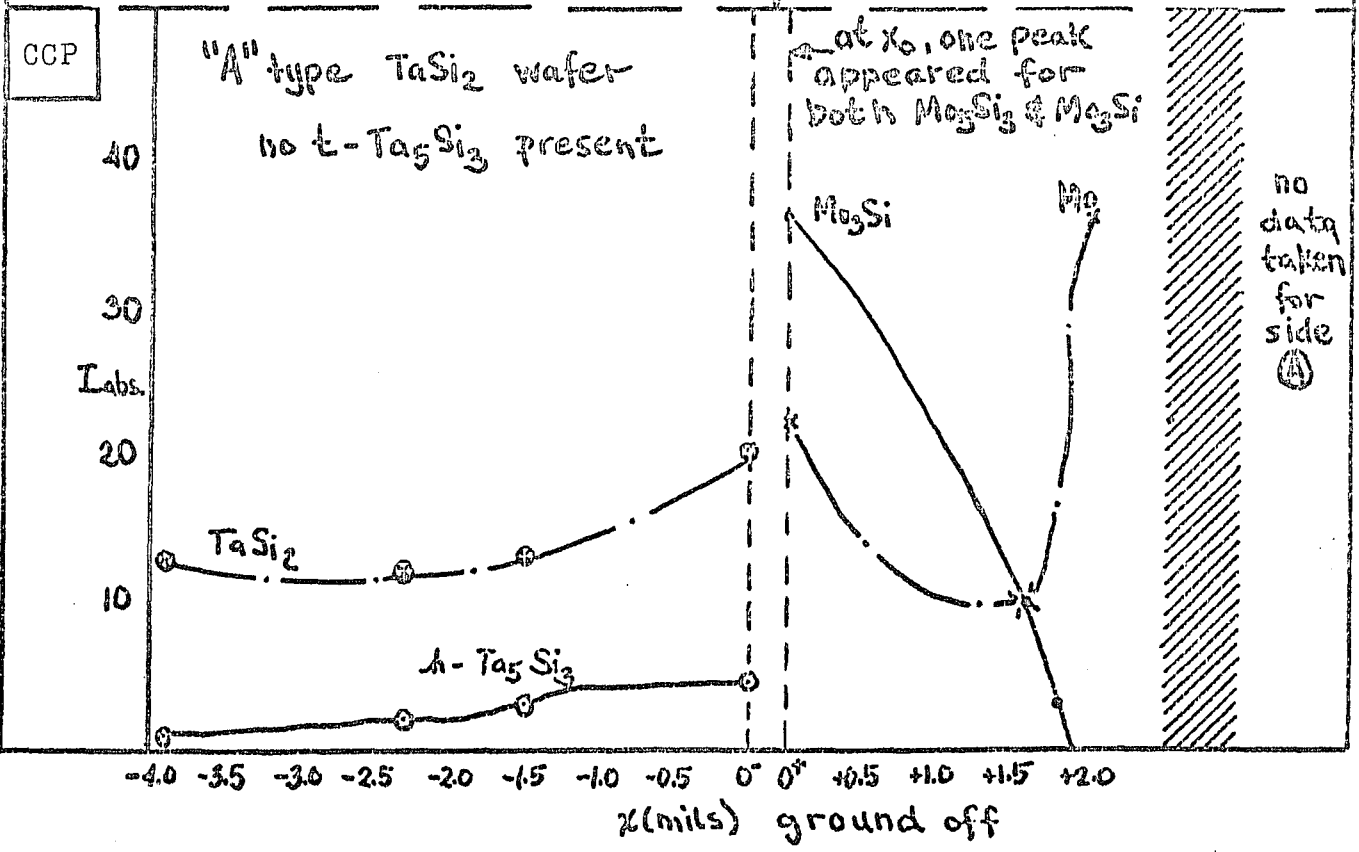
ZP

FIGURE 28
 Mo/TaSi₂ COUPLE
 72 HOURS @ 2100°F



side (B) original interface

CCP



"A" type TaSi₂ wafer
 no t-Ta₅Si₃ present

at x₀, one peak
 appeared for
 both Mo₅Si₃ & Mo₃Si

no data
 taken
 for
 side
 (A)

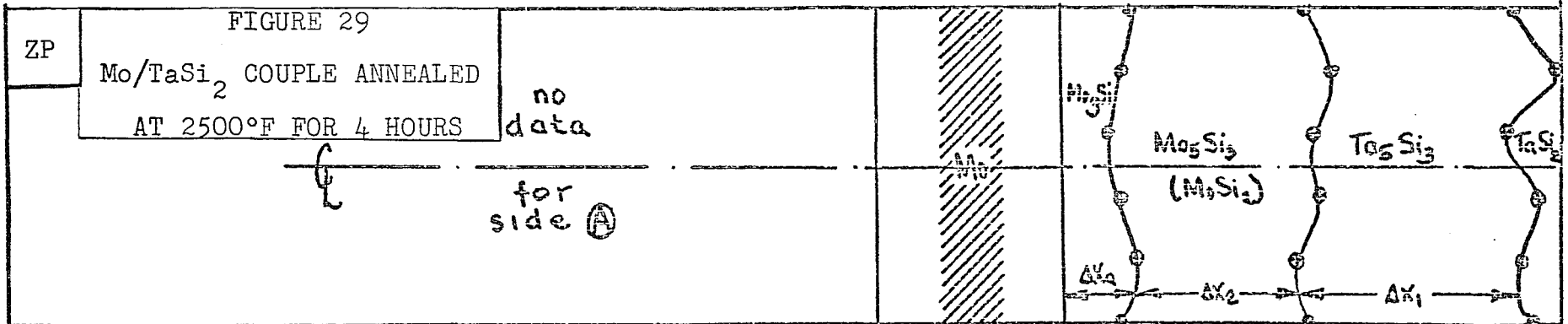
-4.0 -3.5 -3.0 -2.5 -2.0 -1.5 -1.0 -0.5 0 0⁺ +0.5 +1.0 +1.5 +2.0
 x(mils) ground off

FIGURE 29

Mo/TaSi₂ COUPLE ANNEALED
AT 2500°F FOR 4 HOURS

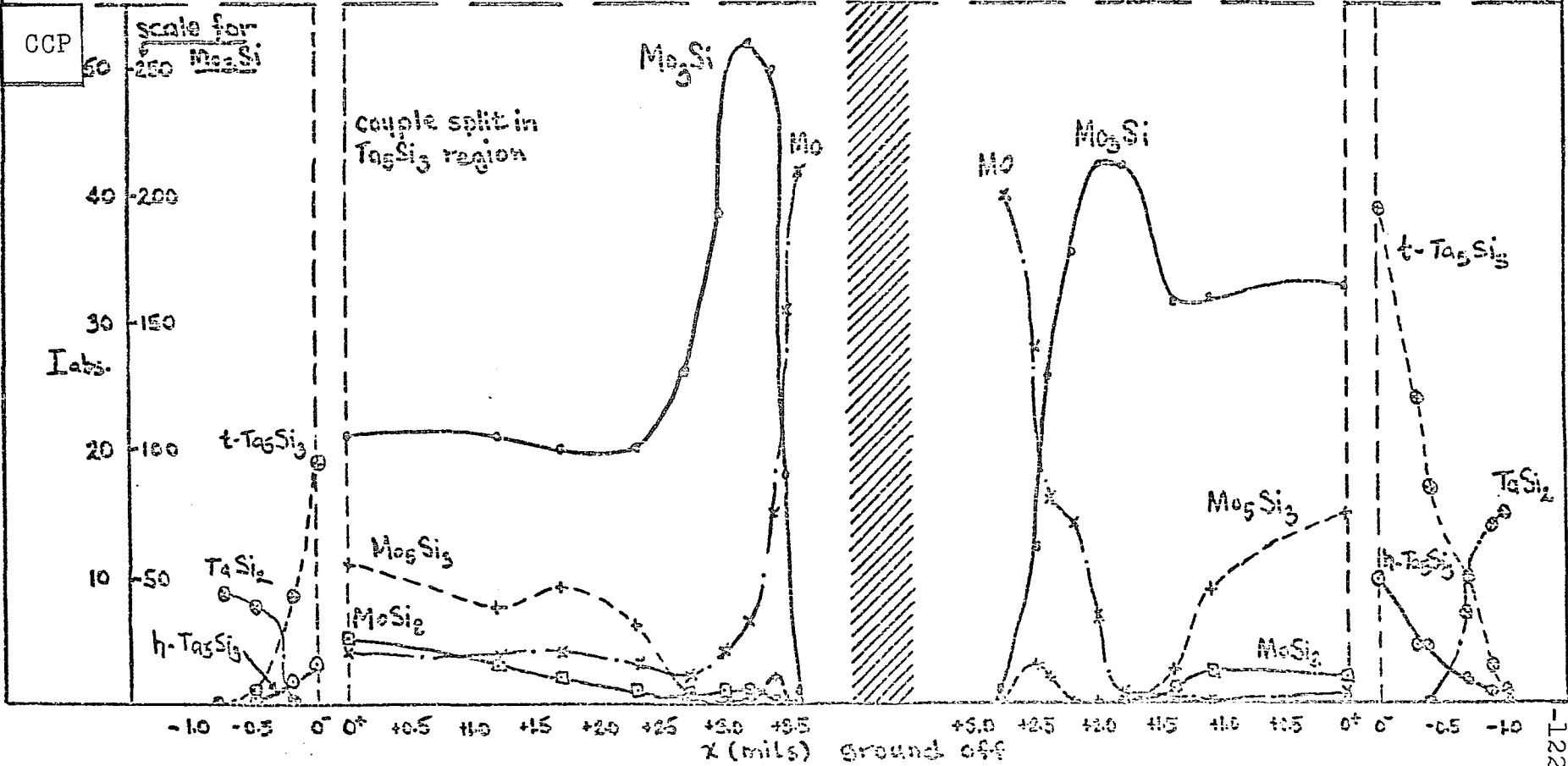
no
data

for
side (A)



original | interface | side (A)

side (B)



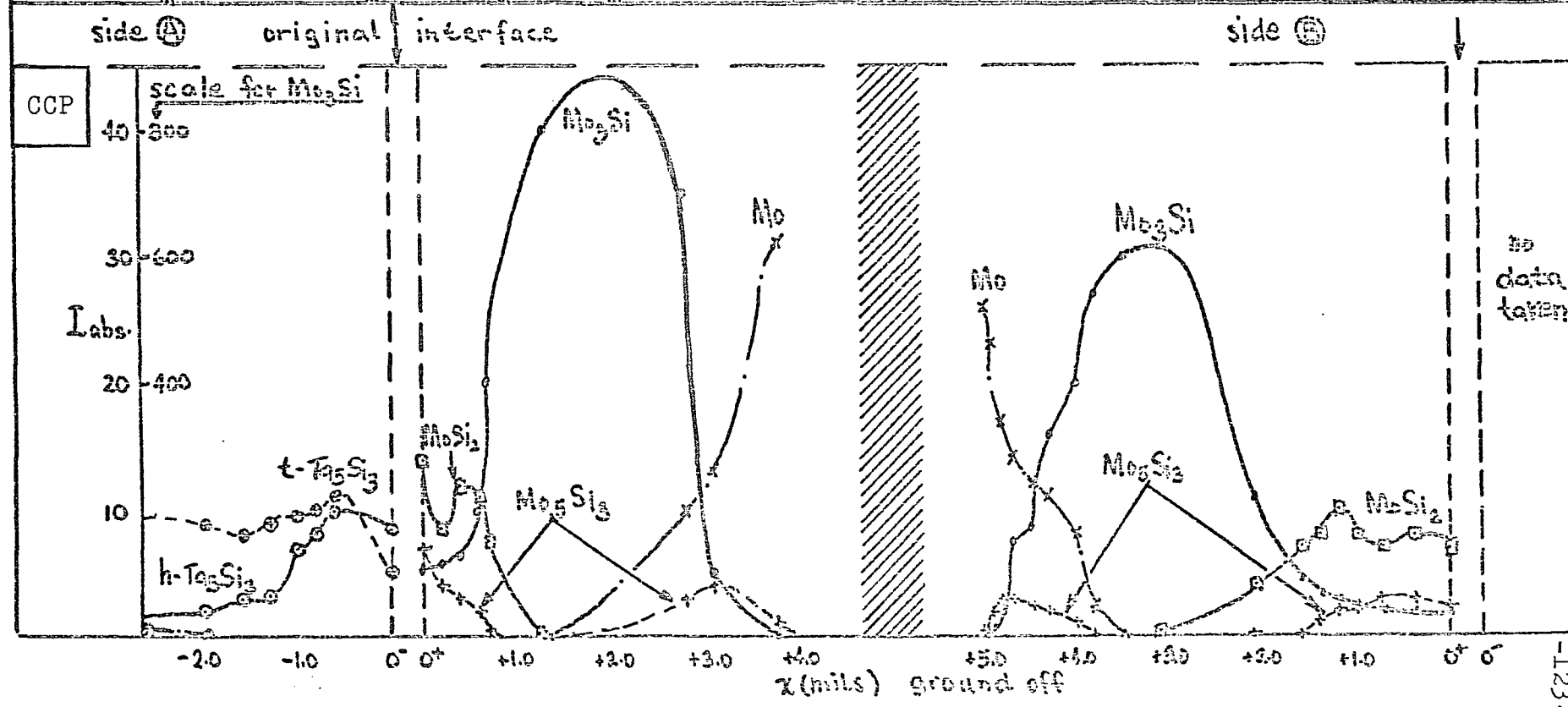
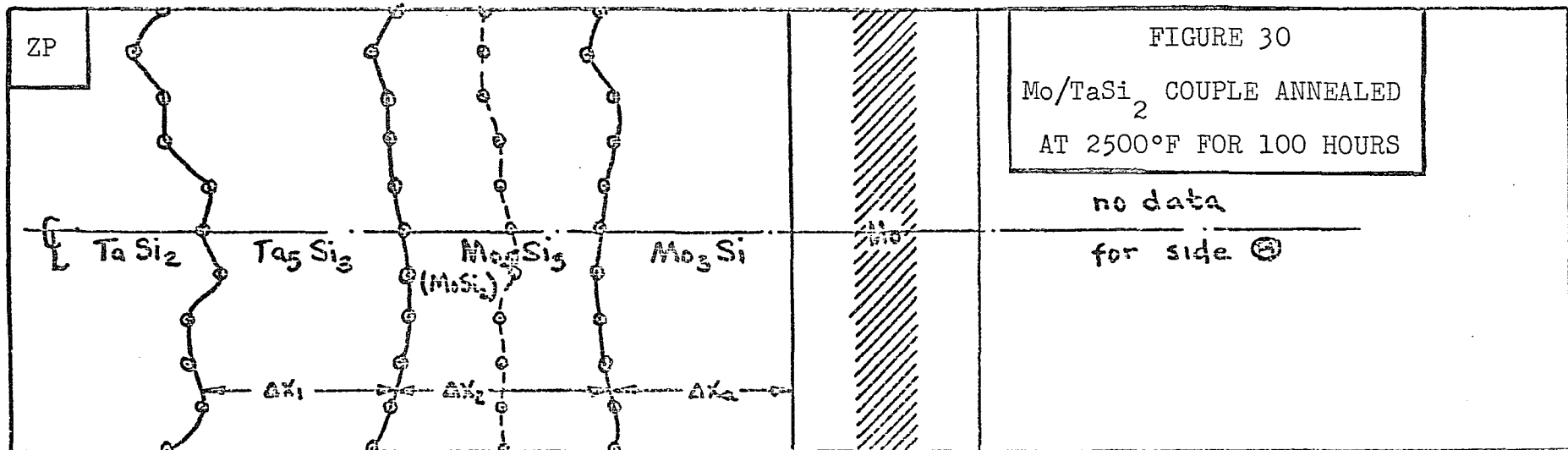
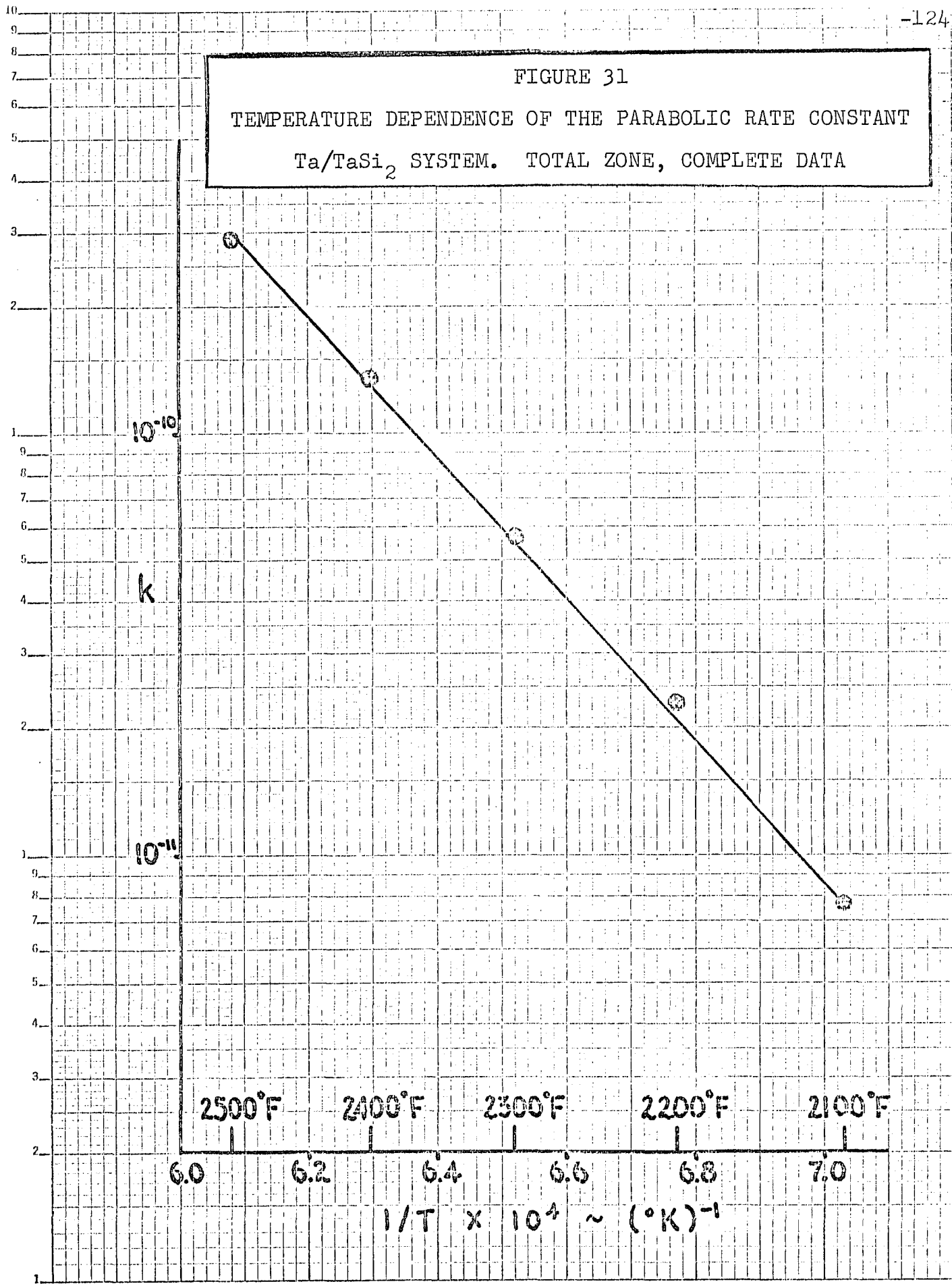


FIGURE 31
TEMPERATURE DEPENDENCE OF THE PARABOLIC RATE CONSTANT
Ta/TaSi₂ SYSTEM. TOTAL ZONE, COMPLETE DATA



SEMI-LOGARITHMIC 46 5490
3 CYCLES X TO DIVISIONS MADE IN U.S.A.
KEUFEL & ESSER CO.

FIGURE 32a
THE EFFECT OF TEMPERATURE ON PARABOLIC RATE CONSTANTS
TOTAL ZONES, COMPLETE DATA

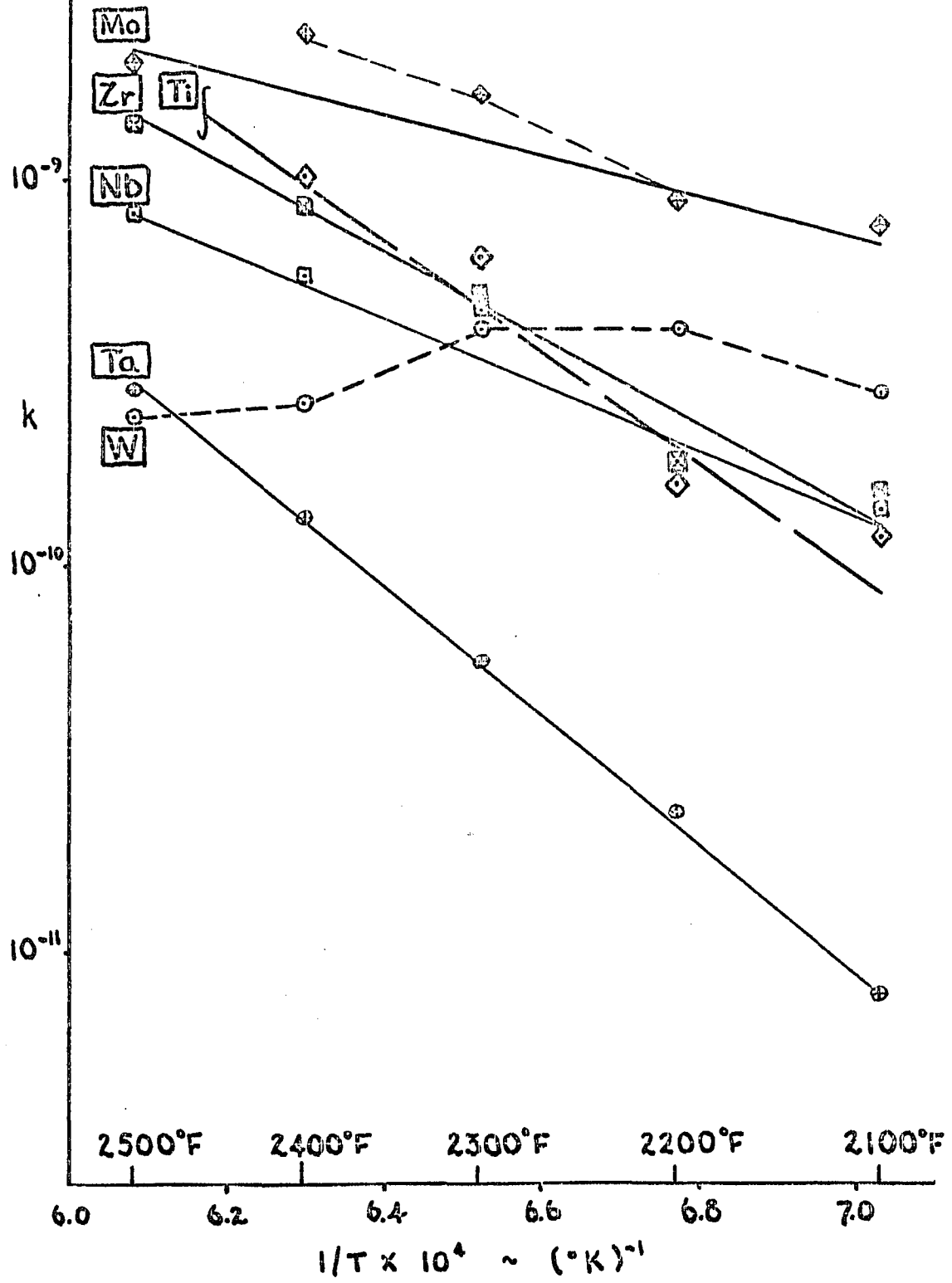
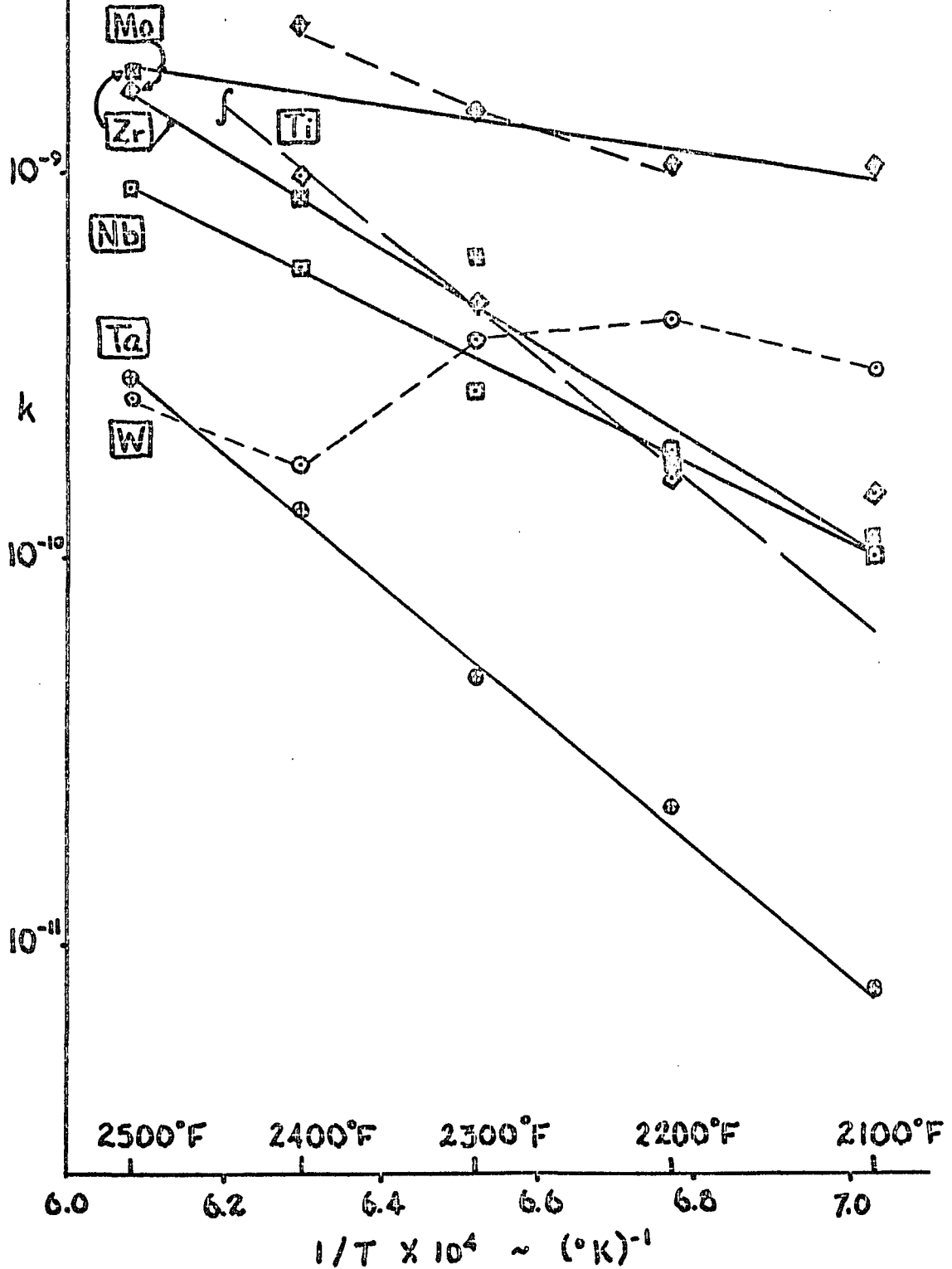


FIGURE 32b
THE EFFECT OF TEMPERATURE ON PARABOLIC RATE CONSTANTS
TOTAL ZONES, INCOMPLETE - GOOD WAFERS ONLY



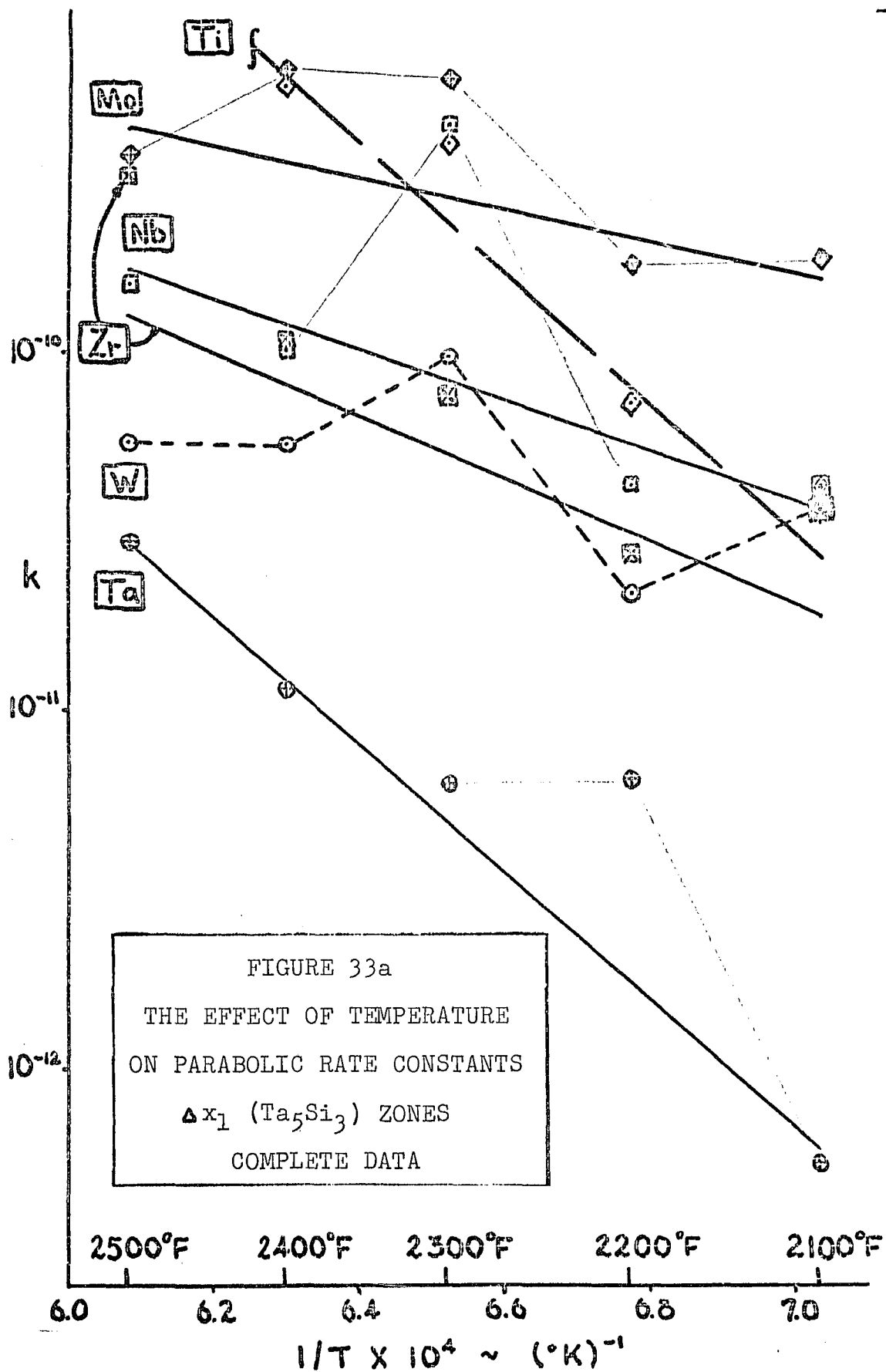
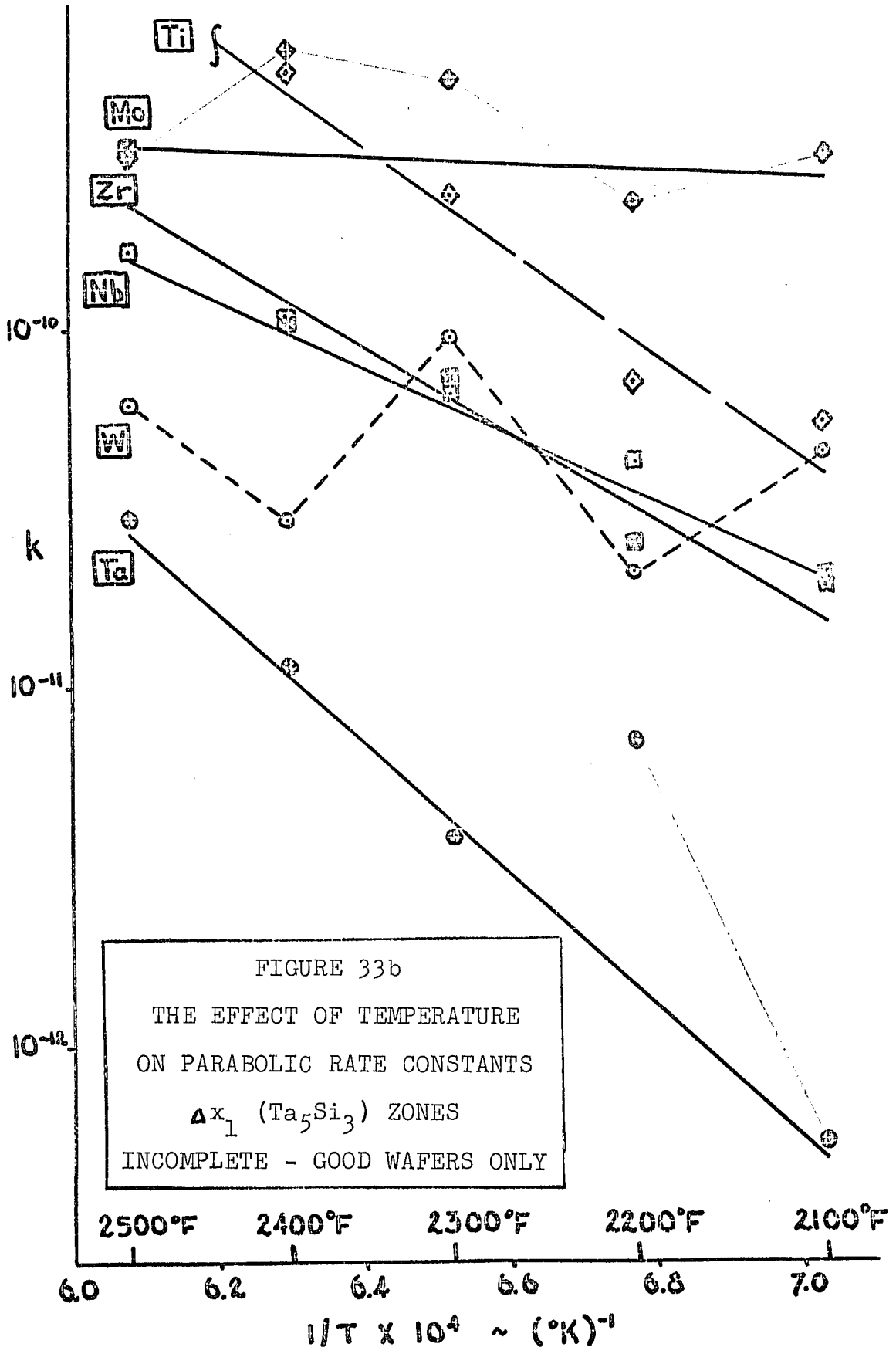


FIGURE 33a
THE EFFECT OF TEMPERATURE
ON PARABOLIC RATE CONSTANTS
Δx₁ (Ta₅Si₃) ZONES
COMPLETE DATA



IV PHOTOMICROGRAPHS (PLATES)

Page 129 follows

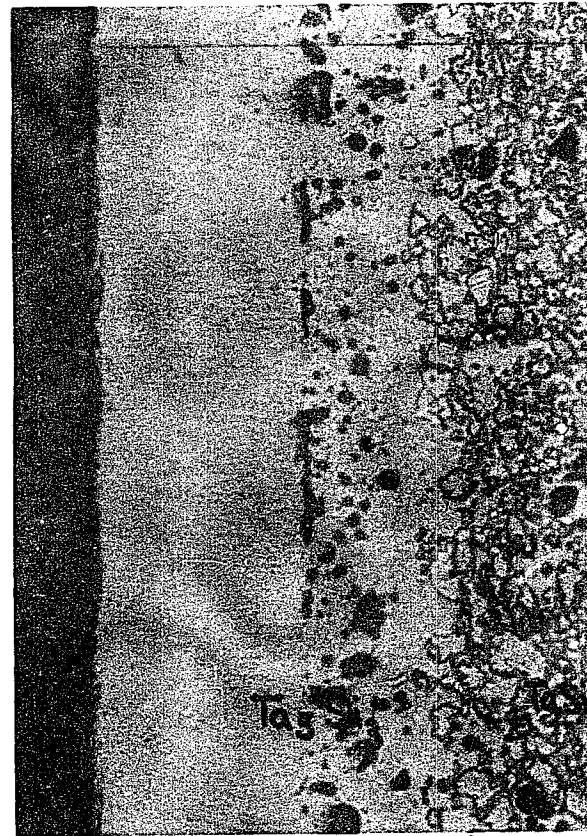
Plate I

Ta Ta₅Si₃ TaSi₂

$\frac{|\Delta X_2|}{X_M X_0}$

Ta/TaSi₂ Couple After 48 Hrs.
at 2300°F. Unetched. (300x)

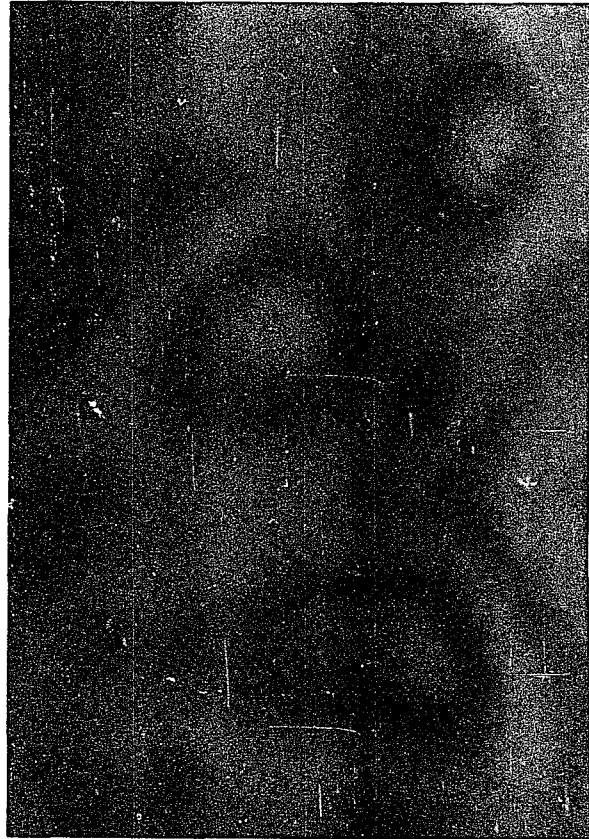
Plate II



X_M ΔX_2 X_0 ΔX_1 X_{TS}

Ta/TaSi₂ Couple Employing *-type
TaSi₂ Wafer after 48 hrs. at 2500 F.
Etched. (700x)

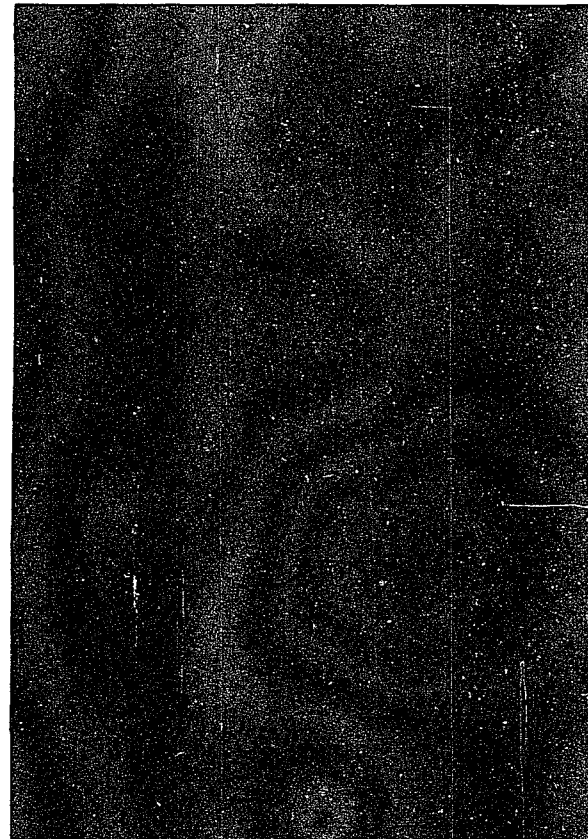
Plate III



x_M $x_a(x_{rs})$ x_o

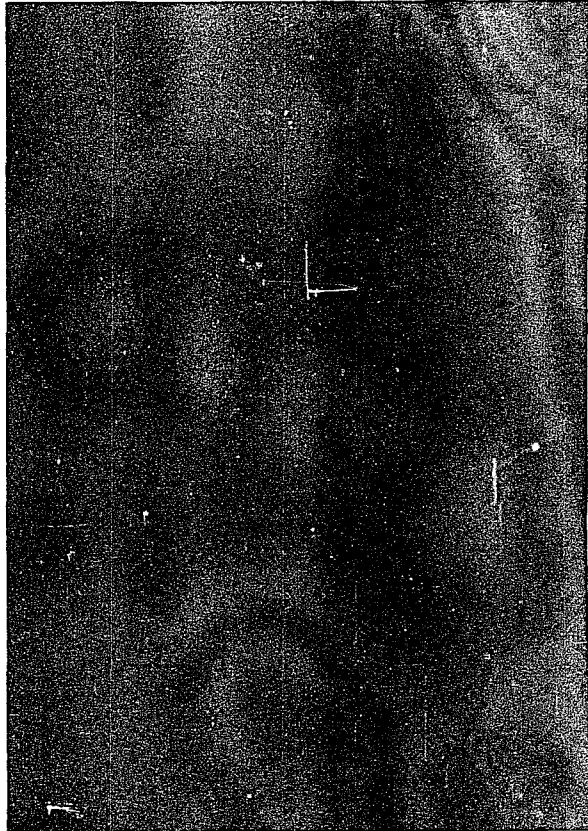
Atypical Ta/TaSi₂ Couple Employing
"A" Type TaSi₂ Wafer after 72 Hrs.
at 2500°F. Etched. (700x)

Plate IV



Surface of "A" Type TaSi₂ Wafer
Polished and etched. (1000x)

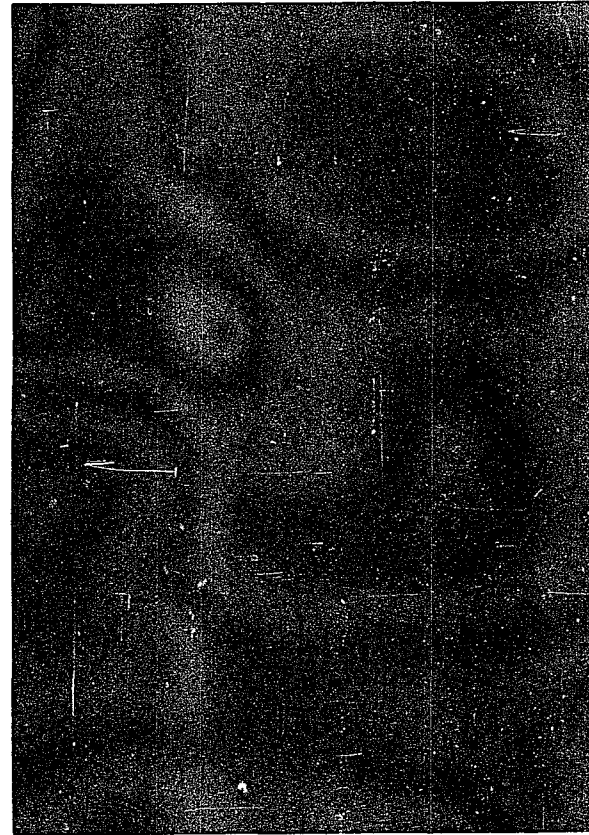
Plate V



x_M Δx_2 x_0 Δx_1 x_{TS}

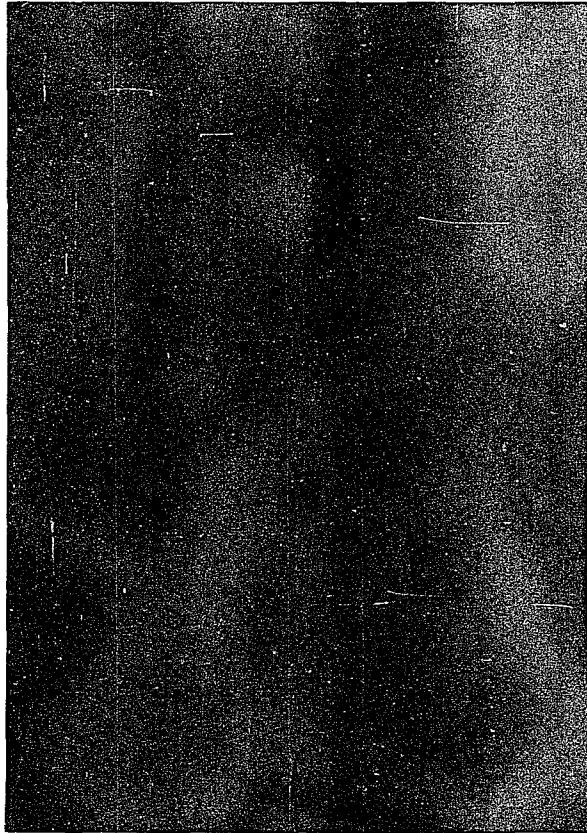
Ta/TaSi₂ Couple Employing "B" Type
TaSi₂ Wafer after 72 Hrs. at 2500°F.
Etched. (700x)

Plate VI



Surface of "B" Type TaSi₂ Wafer
Polished and etched. (1000x)

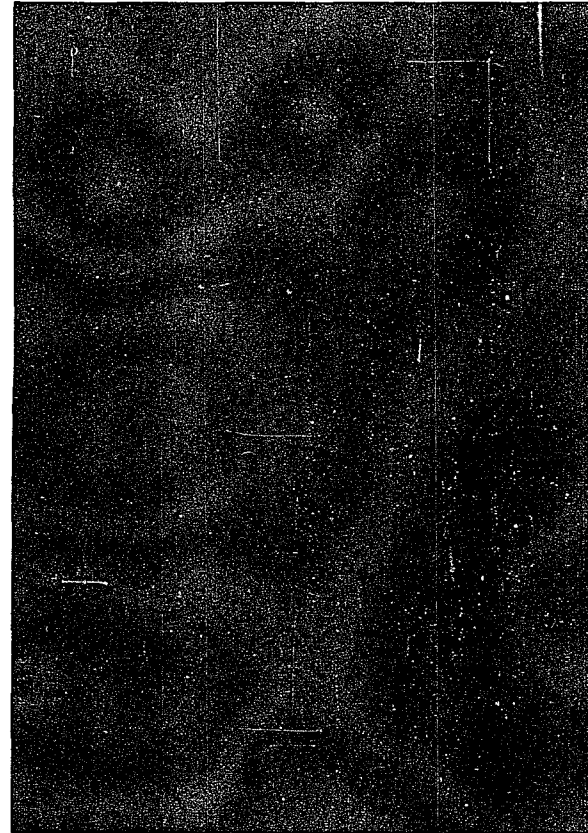
Plate VII



X_M X₀

Ta/TaSi₂ Couple after 4 Hrs. at
2100°F. Etched. (700x)

Plate VIII



X_M ΔX₂ X₀ ΔX₁ X_{T5}

Ta/TaSi₂ Couple after 100 Hrs. at
2400°F. Etched. (700x)

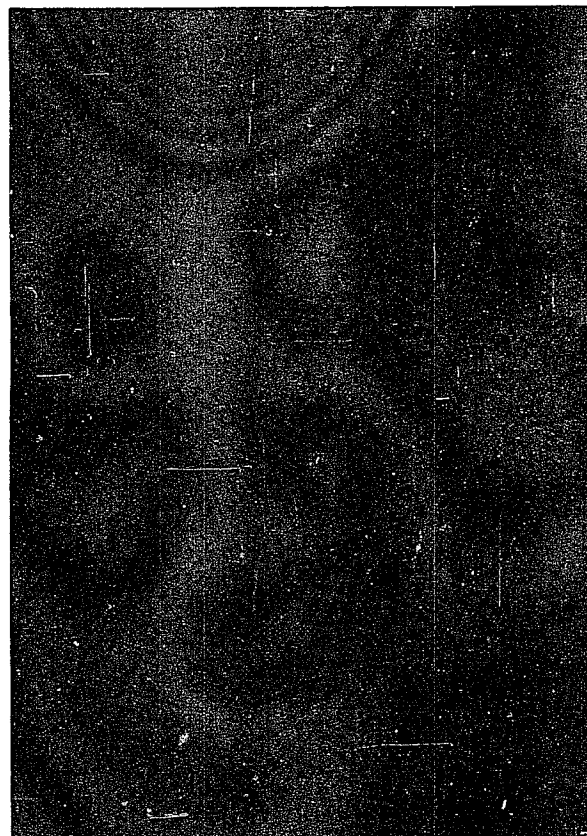
Plate IX



X₁ X₂ X₀ XTS

Nb/TaSi₂ Couple after 4 Hrs. at 2100°F. Etched. (700x)

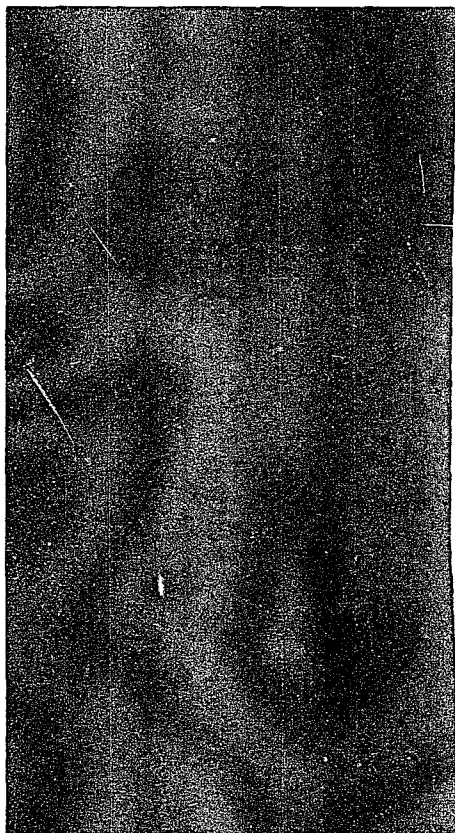
Plate X



ΔX₂ ΔX₁ X₁ X₂ X₀ XTS

Nb/TaSi₂ Couple after 4 Hrs. at 2500°F. Etched. (700x)

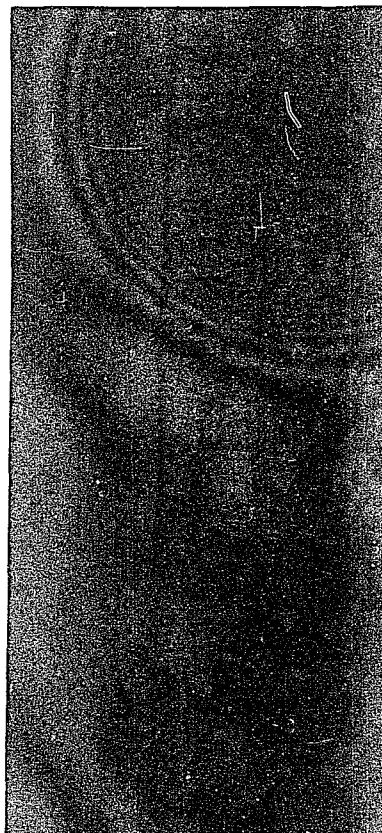
Plate XI



ΔX_2 | ΔX_1 | ΔX_0 | X_{TS}
 X_M | X_a | X_0 | X_{TS}

Nb/TaSi₂ Couple after 24
Hrs. at 2200°F. Etched.
(700x)

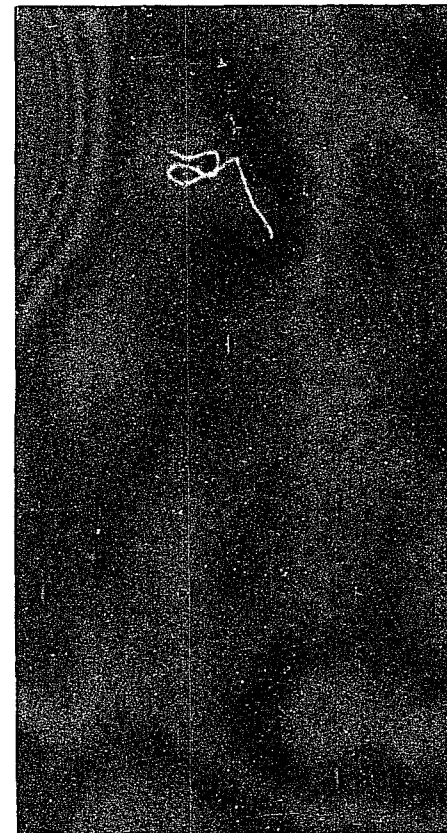
Plate XII



ΔX_2 | ΔX_1 | ΔX_0 | X_{TS}
 X_M | X_a | X_0 | X_{TS}

Nb/TaSi₂ Couple after
48 Hrs. at 2200°F.
Etched. (700x)

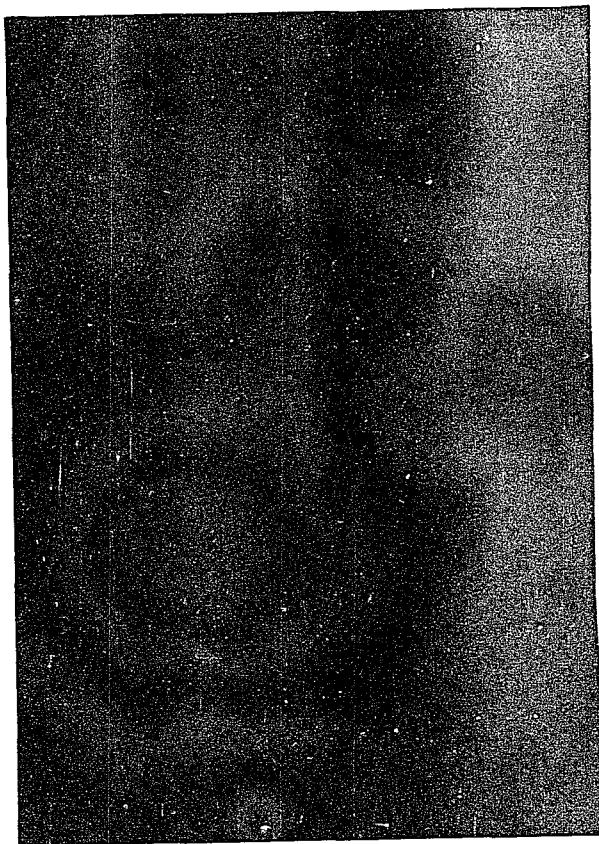
Plate XIII



ΔX_2 | ΔX_1 | ΔX_0 | X_{TS}
 X_M | X_a | X_0 | X_{TS}

Nb/TaSi₂ Couple after 72
Hrs. at 2200°F. Etched.
(700x)

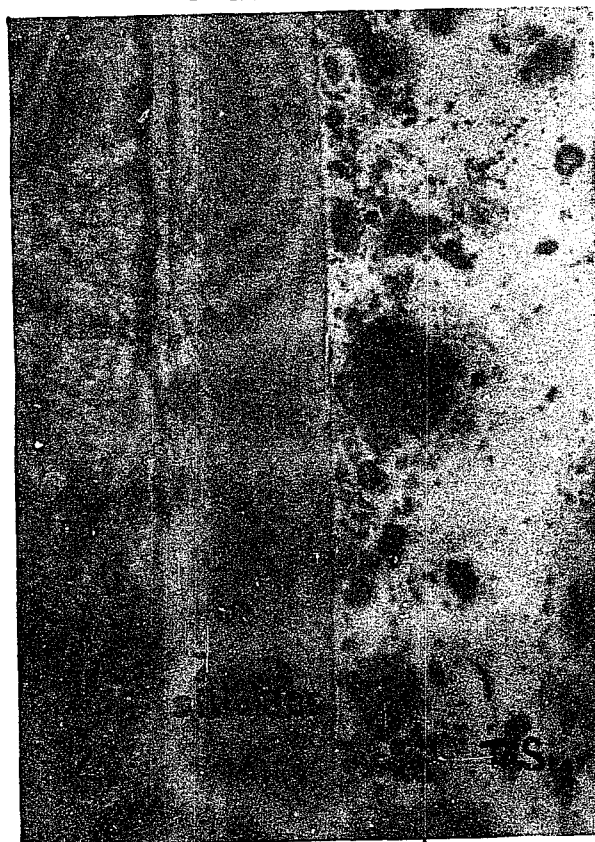
Plate XIV



X_1 X_2 X_0

Zr/TaSi₂ Couple after 4 Hrs.
at 2100°F. Lightly etched.
(700x)

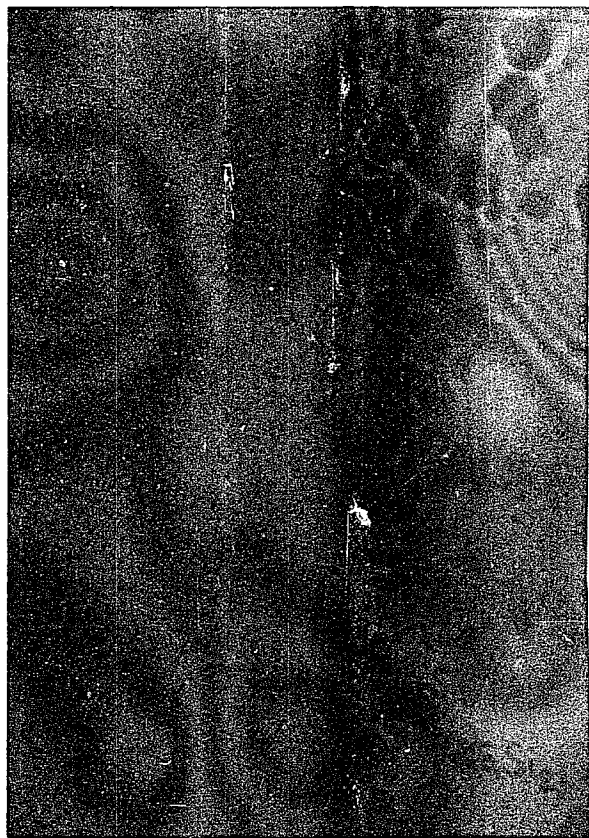
Plate XV



ΔX_1 ΔX_2 X_1 X_2
 X_1 X_2 X_0 X_{TS}

Zr/TaSi₂ Couple after 48 Hrs.
at 2200°F. Lightly etched. (700x)

Plate XVI



X_M X_a ΔX_2 X_0 ΔX_1 X_{TS}

Zr/TaSi₂ Couple after 4 Hrs.
at 2400°F . Lightly etched.
(700x)

Plate XVII



X_M ΔX_a X_a ΔX_2 X_0 ΔX_1 X_{TS}

Zr/TaSi₂ Couple after 72 Hrs.
at 2500°F. Etched. (300x)

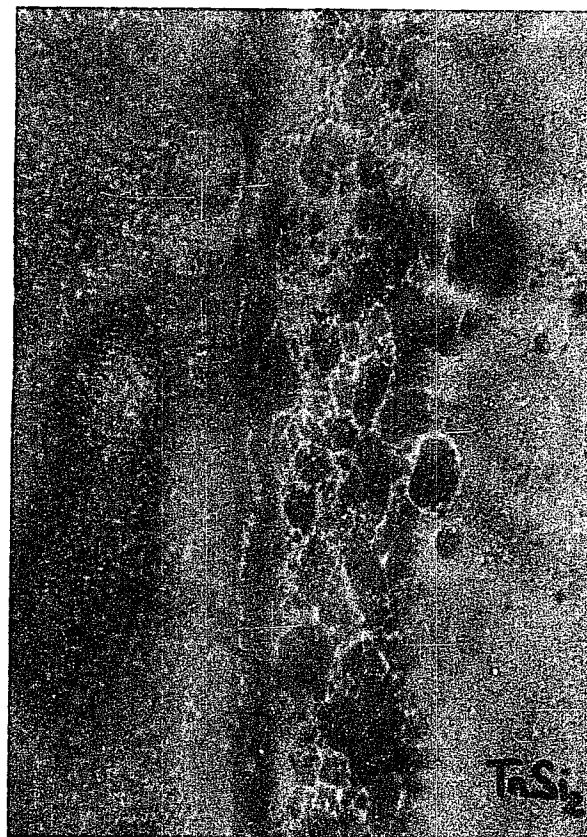
Plate XVIII



X49

Ti/TaSi₂ Couple after 4 Hrs.
at 2100°F. Lightly etched.
(700x)

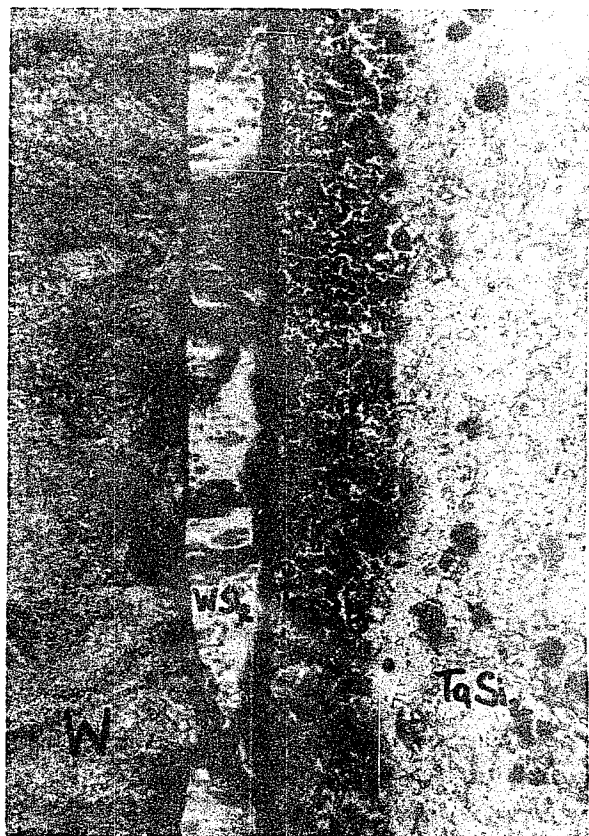
Plate XIX



ΔX_2 ΔX_1 \downarrow
X49 X6 X75

Ti/TaSi₂ Couple after 24 Hrs.
at 2400°F. Etched. (300x)

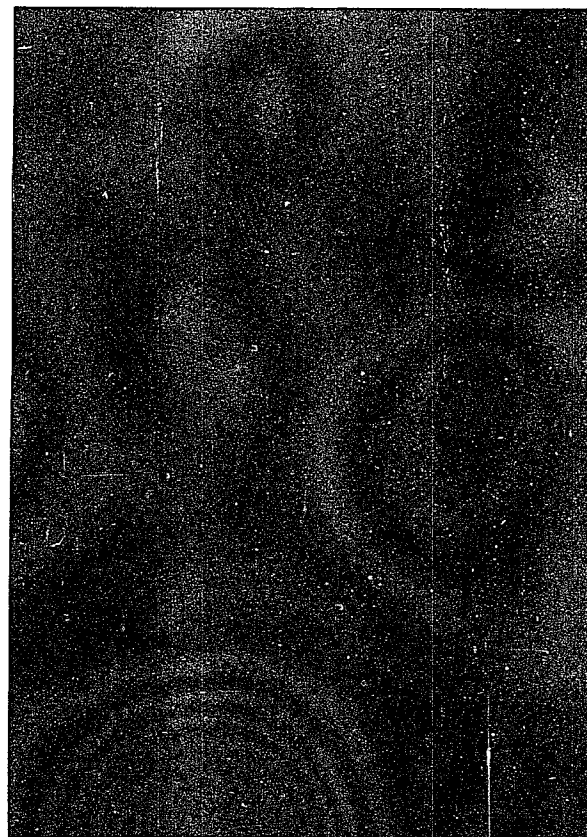
Plate XX



ΔX_2 | ΔX_1 |
 X_M | X_0 | X_{TS}

W/TaSi₂ Couple after 48 Hrs.
at 2100°F. Etched. (300x)

Plate XXI



ΔX_2 | ΔX_1 |
 X_M | X_{a1} | X_{a2} | X_0 | X_{TS}

W/TaSi₂ Couple after 100 Hrs.
at 2400°F. Etched. (700x)

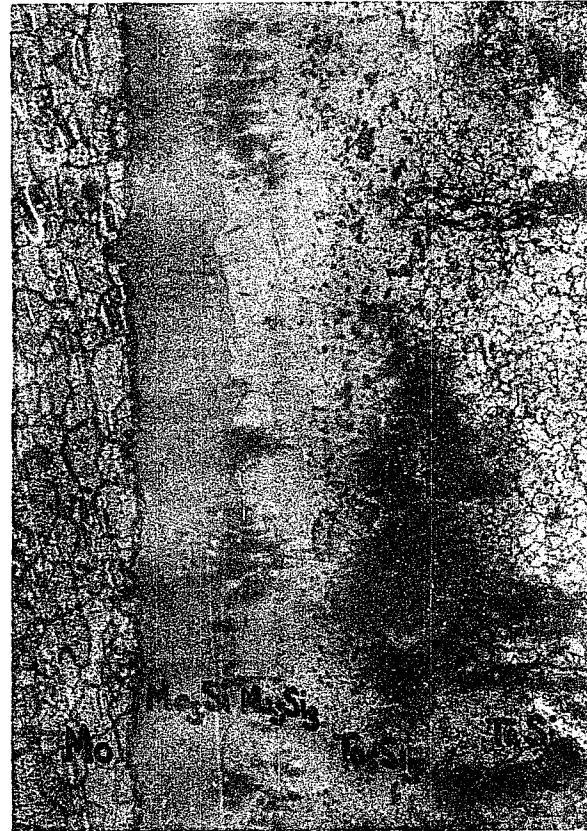
Plate XXII



X_M | ΔX_2 | X_0 | ΔX_1 | X_{TS}

Mo/TaSi₂ Couple after 48 Hrs.
at 2100°F. Etched. (300x)

Plate XXIII



X_M | ΔX_2 | X_0 | ΔX_1 | X_{TS}

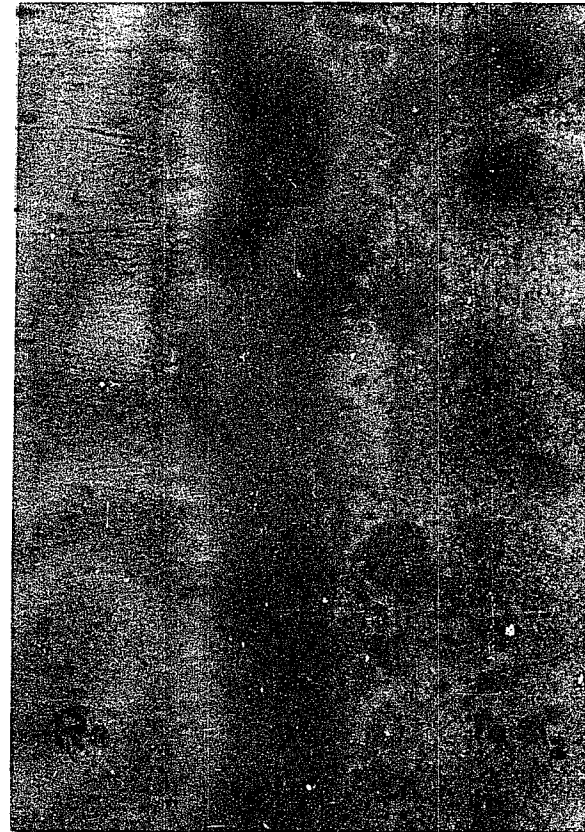
Mo/TaSi₂ Couple after 100 Hrs.
at 2500°F. Etched. (300x)

Plate XXIV



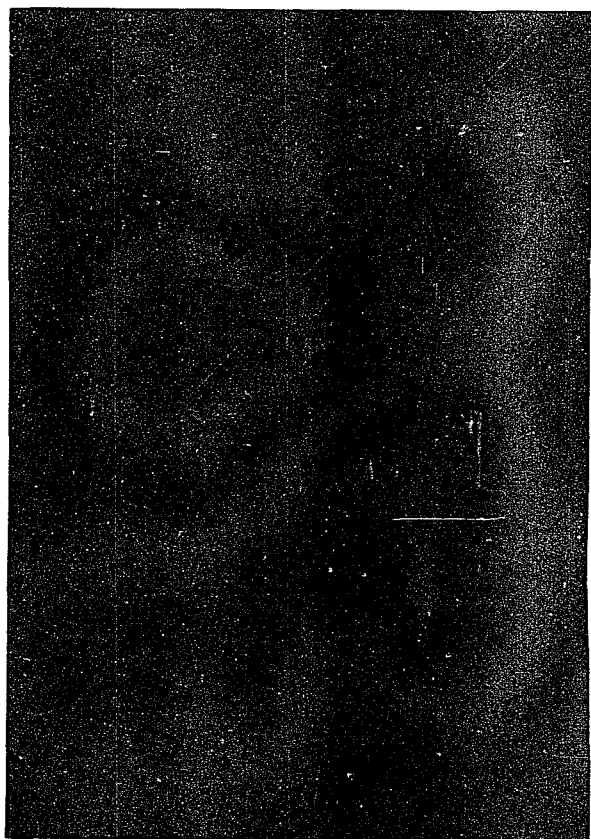
Re/TaSi₂ Couple after 100 Hrs.
at 2100°F. Etched. (300x)

Plate XXV



Re/TaSi₂ Couple after 100 Hrs.
at 2500°F. Etched. (300x)

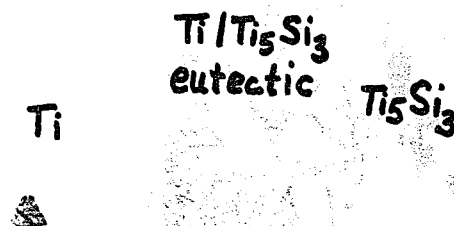
Plate XXVI



x_m | Δx_1 | x_a Δx_2 | x_0

Appearance of Ti/Ti₅Si₃ Eutectoid in a Ti/TaSi₂ Couple Annealed at 2100°F for 72 Hrs. Etched. (1600x)

Plate XXVII



Ti

Ti/Ti₅Si₃
 eutectic Ti₅Si₃

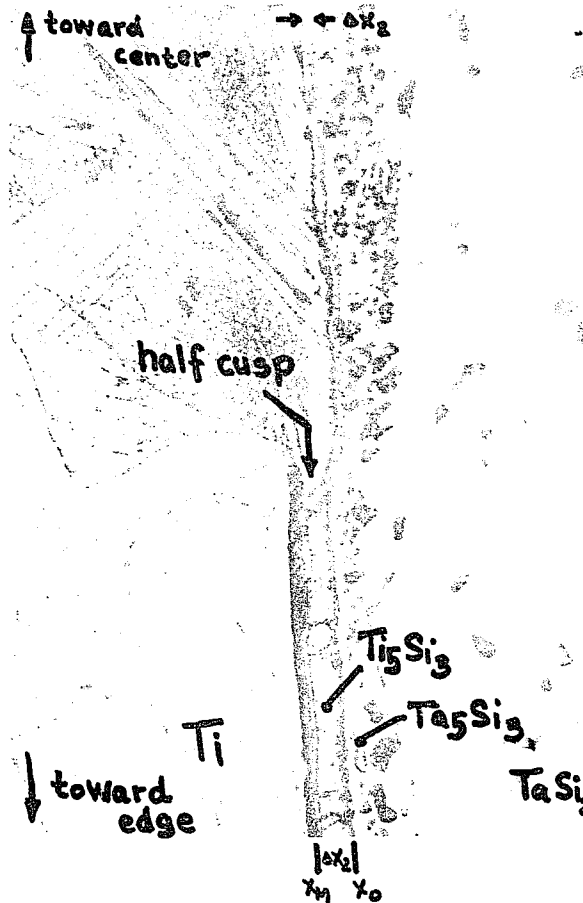
Appearance of Ti/Ti₅Si₃ Eutectic Formed from the Melt in a Ti/TaSi₂ Couple Annealed at 2500°F. Unetched. (63x)

Plate XXVIII



Attack of Eutectic on Ti in a Ti/TaSi₂ Couple after Annealing at 2500°F. Unetched. (30x)

Plate XXIX



Example of Cusp Formation in the Ti/TaSi₂ System. Etched. (300x)

V DISCUSSION

A. The Ta/TaSi₂ Couple

1. Comparison of Results

In this work the growth rate of Ta₅Si₃ in the Ta/TaSi₂ system has been accurately measured. In the Arrhenius form the parabolic growth constant is

$$k = 5e^{-77,000/RT}$$

where the activation energy is known with 95% confidence to be between 74,000 and 80,000 cal/mole and the pre-exponential constant is known with the same confidence to be between 2 and 11 cm²/sec. This may be compared with the result obtained by Bartlett (24) who expressed his diffusion constant as

$$\tilde{D} \Delta C = 0.3e^{-58,000/RT}$$

which becomes

$$k = 36.6e^{-58,000/RT}.$$

There appears to be a substantial discrepancy between the pre-exponential constant in Bartlett's equation and his graphical data. The graphical data yields a pre-exponential constant approximately 10⁻³ times that shown in the equation. In his paper, Bartlett gives no indication of the accuracy of his data. The reasons for the difference between the two results are based on differences in experimental procedure, which are listed below:

a. Bartlett used coated samples rather than solid wafers, thereby limiting the time of the diffusion anneal.

b. Quality of the $TaSi_2$ coatings could not be as carefully controlled as with $TaSi_2$ wafers.

c. Although Bartlett's temperature range was close to that used in this investigation, he used only four conditions.

d. The number of runs at each temperature was not more than three and only two were annealed for more than four hours. Therefore, it is doubtful that steady-state was reached.

e. Electron-microprobe analysis rather than the optical microscope was used to identify phases and locate phase boundaries.

In addition, Bartlett identified the Ta_5Si_3 as pure tetragonal, whereas both hexagonal and tetragonal Ta_5Si_3 were found to grow in the present study.

The rate of degradation of $TaSi_2$ in the $Ta/TaSi_2$ system has also been measured separately. This is identical with the growth rate of Ta_5Si_3 on the $TaSi_2$ side of the original interface (Δx_1) and may be expressed in terms of its parabolic growth constant as

$$k_1 = 2e^{-81,000/RT}$$

where the activation energy is known with 95% certainty to be between 74,000 and 88,000 cal/mole and the pre-exponential constant to be between 0.2 and 16. There are no corresponding results to compare with this since Bartlett did not identify the original interface.

The results of the marker experiments indicate that only silicon diffuses. Therefore, there should be only one activation energy for diffusion for k_1 , k_2 and k , and the pre-exponential constants should be related through the ratio of k_2/k_1 from equations (21) and (22) in Section I. The differences in these experimentally determined constants is then a result of experimental error.

2. Significance of Results

TABLE XII

CALCULATED TIMES TO GROW A 1 MIL LAYER OF Ta₅Si₃ AND LOSE 1 MIL TaSi₂
 (For Layers Other Than 1 Mil, Multiply Times by Square of Layer Thickness in Mils)

TEMPERATURE	1500°F	2000°F	2500°F
1. Time to grow 1 mil Ta ₅ Si ₃ :			
a) This work	10 ⁶ hrs.	600 hrs.	5.25 hrs.
b) Bartlett	18 hrs.	5 min.	8 sec.
c) Ratio $\frac{t \text{ present work}}{t \text{ Bartlett}}$	50,000	7,500	2,400
2. Lifetime of 1 mil coating of TaSi ₂ :			
a) Using result of k_1	1.4x10 ⁷ hrs.	6,600 hrs.	45 hrs.
b) Using $k_1 = \frac{1}{7} k \text{ total}$	7x10 ⁶ hrs.	4,200 hrs.	37 hrs.

In Table XII, times are calculated from the experimentally determined Arrhenius equations which indicate the practical service lifetimes of a $TaSi_2$ coating at 1500°F, 2000°F and 2500°F if the coating could be applied in a dense form similar to the wafers fabricated in this work. The first and second lines are the times required to grow the total Ta_5Si_3 zone 1 mil thick using the equations from this work and Bartlett's work respectively. The ratio, next line, indicates that a dense $TaSi_2$ layer has a considerably longer lifetime than the porous coating used in Bartlett's work. The total Ta_5Si_3 zone grows both from degradation of $TaSi_2$ and consumption of Ta metal and, therefore, the time required to grow 1 mil Ta_5Si_3 is less than the service lifetime of 1 mil of $TaSi_2$. On the last line (2b) the lifetime of a 1 mil layer of $TaSi_2$ has been computed from the results on line 1 assuming the theoretical relationship between k_2 and k_1 from equations (21) and (22) in Section I. From these equations, k_2 should be approximately six times k_1 and the time to grow a 1 mil Δx_1 zone (or deplete 1 mil $TaSi_2$) would be seven times the time to grow 1 mil total Ta_5Si_3 . This may be compared with the lifetime of a 1 mil $TaSi_2$ layer calculated directly from the experimentally determined equation for the growth rate of the Δx_1 zone (2a). The agreement is fairly good and is best at higher temperatures. As previously stated, statistical analysis of the results shows that the equations

for the total and Δx_1 zones may have the same activation energies. Also, the confidence limits on the pre-exponential constants indicate that the growth constant for the Δx_1 zone (degradation of TaSi_2) may very well be one-seventh of the growth rate of the total zone.

In a practical application, lifetimes of about 1000 hours are desired at a temperature of 2500°F. This work shows that it would be necessary to use a minimum coating thickness of about 5 mils merely to compensate for loss of TaSi_2 by diffusion. The total thickness would need to be much greater, making the application at 2500°F quite doubtful.

B. Barriers

1. Effectiveness of Metals Tested

Inspection of Tables IX and X and Figures 32 through 33 clearly indicates that none of the metals tested would serve as barriers to the degradation of TaSi_2 . The test metals may be listed in order of decreasing effectiveness.

- a. W
- b. Nb and Zr
- c. Ti and Mo

The low temperature data for W is meaningless in terms of solid state diffusion and even the growth at high temperatures has been affected by early vapor transport of silicon. The usefulness of Ti against TaSi_2 is limited by the melting point of the Ti- Ti_5Si_3 eutectic and, therefore, Ti should not be used above 2400°F.

2. Factors Influencing the Effectiveness of Test Metals

The order given above for the effectiveness of the metals tested as barriers to the degradation of $TaSi_2$ does not yield simple correlations or obvious reasons for the results. Rather, it has become apparent from the results of this work that the criteria for choosing appropriate barriers to diffusion are quite complex. In addition to growth rate of intermediate layers, there are two factors that must be considered in choosing a barrier material: compatability with the substrate and coating and the amount of pore formation. These factors were not investigated in this work, in order to more fully study the chemical kinetics and diffusional behavior of the silicide systems. In certain systems, all three factors are strongly interdependent during the course of the diffusion anneals. Although the effects of pore formation on growth rates were not evident, the role of mechanical compatability on growth in the $W/TaSi_2$ and $Re/TaSi_2$ systems is most important. This will be accounted for after some discussion of the factors which inherently effect the growth rates in the $M/TaSi_2$ system.

a. Phases Formed

It is obvious that the growth rates of intermediate phases in a $M/TaSi_2$ system will depend on the composition (in this case stoichiometry) of the phases formed.

What might not be as obvious is that phases growing near the original interface in amounts too small to be measured under the microscope may very strongly affect the growth rate of the Ta_5Si_3 phase across the original interface as well as that of the M silicide adjacent to the thin phase. Table XIII is a summary of the phases found to exist between the metal and $TaSi_2$ in the diffusion zone. It may be noted that in each system but the Zr/ $TaSi_2$ system, the trisilicide (M_5Si_3) grew as a measurable zone. This is designated Z in the table. Phases labeled X were not noticeable microscopically, but were observed by X-ray diffraction analysis. The Ta_2Si phase, shown as X*, grew only under special conditions, previously discussed, near the metal interface. The cross-hatched areas represent phases not reported on the phase diagrams and should, therefore, be non-existent. The double cross-hatched areas are silicides reported in the literature but not represented on the accepted phase diagrams and, therefore, their existence is questionable. Only boxes marked X or Z represent silicides that were found to be present in the diffusion couples studied in this work. Identification of the Zr silicides was difficult and the compositions of the growing zones could not be deduced. Also, although there was evidence of Zr_2Si in the diffusion zone, identification was not conclusive: Nonetheless, X-ray diffraction analysis was fairly conclusive in showing that no Zr_5Si_3 or higher Zr silicides existed in the

TABLE XIII
SUMMARY OF INTERMEDIATE PHASES FOUND

M	MSi ₂	MSi	M ₃ Si ₂	M ₅ Si ₃	M ₂ Si	M ₃ Si	M ₄ Si	M _{4.5} Si
Ta	—	Diagonal lines (top-left to bottom-right)	Diagonal lines (top-left to bottom-right)	Z	X*	Diagonal lines (top-left to bottom-right)	Diagonal lines (top-left to bottom-right)	—
W	Z	Diagonal lines (top-left to bottom-right)	Cross-hatch	Z	Diagonal lines (top-left to bottom-right)	Diagonal lines (top-left to bottom-right)	Diagonal lines (top-left to bottom-right)	Diagonal lines (top-left to bottom-right)
Mo	X	Diagonal lines (top-left to bottom-right)	Diagonal lines (top-left to bottom-right)	Z	Diagonal lines (top-left to bottom-right)	Z	Diagonal lines (top-left to bottom-right)	Diagonal lines (top-left to bottom-right)
Nb	X	Diagonal lines (top-left to bottom-right)	Cross-hatch	Z	Diagonal lines (top-left to bottom-right)	Cross-hatch	—	Diagonal lines (top-left to bottom-right)
Ti	—	—	Diagonal lines (top-left to bottom-right)	Z	Diagonal lines (top-left to bottom-right)	Diagonal lines (top-left to bottom-right)	Diagonal lines (top-left to bottom-right)	Diagonal lines (top-left to bottom-right)
Re	Z	Cross-hatch	Diagonal lines (top-left to bottom-right)	Z	Diagonal lines (top-left to bottom-right)	Cross-hatch	Diagonal lines (top-left to bottom-right)	Diagonal lines (top-left to bottom-right)
Zr	—	—	Cross-hatch	—	?	Cross-hatch	No X-ray data	Diagonal lines (top-left to bottom-right)

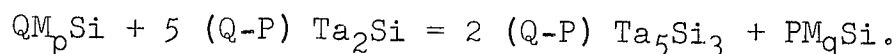
diffusion zone. Of the other systems investigated, only Ta, Mo and Nb have silicides lower than the trisilicide according to their phase diagrams. Only in the Mo system does the lowest silicide grow as a zone. The growth of the Mo_3Si zone is probably the reason for the unexpectedly high growth rate in that system. It may also be seen that in the W and Re systems, the highest silicide (MSi_2) grows as a zone, whereas in the Mo and Nb systems, the disilicide appears only in small amounts near the original interface. In the Ti and Zr systems, neither the di nor monosilicides were found.

Thermodynamic data indicate that the trisilicides are the most stable silicides in the systems studied and it is therefore not surprising that the M_5Si_3 zone grows in each system (but the Zr/TaSi₂ system). Using the free energy data of Levine (45) for the Ta silicides and using enthalpy data for the other M silicides (43) to approximate free energy, the activities of most of the silicides encountered may be calculated. Although the data used in this calculation were not accurately known, the general magnitudes of the activities may be compared. Enthalpies of formation at room temperature (298°K) were used in the approximation $a \approx e^{-\Delta H_r/RT}$ at 1000°K because, for solids, ΔH_{298}^0 is a good approximation to ΔG at any temperature. ΔH_r , the heat of reaction per mole of silicon, was calculated for at least two reactions for each silicide yielding at least two activities:

one for the compound in equilibrium with the next highest silicide and one for equilibrium with the next lowest silicide or metal. For instance, for Ta_5Si_3 in equilibrium with $TaSi_2$ the result may be expressed as \tilde{a}_{Si} for Ta_5Si_3 ($TaSi_2$) = 0.565. Similarly, \tilde{a}_{Si} for Ta_5Si_3 (Ta_2Si) = 0.011, and \tilde{a}_{Si} for Ta_5Si_3 (Ta) = 7×10^{-6} . Activities calculated in such a manner range as low as 5×10^{-12} for Zr_4Si (Zr). High values for M trisilicides are approximately 10^{-2} for W and 10^{-3} for Nb and Mo (all in equilibrium with MSi_2); but the highest value for \tilde{a}_{Si} of a M trisilicide is 0.14 for Ti_5Si_3 ($TiSi$). When these activities are compared with that for Ta_5Si_3 (Ta_2Si), it may be predicted that in a general system $TiSi$ (and therefore $TiSi_2$) would not be expected to grow. W_5Si_3 (WSi_2) and Re_3Si [$ReSi(ReSi_2)$] have activities almost equal to Ta_5Si_3 (Ta_2Si) and, therefore, WSi_2 and $ReSi_2$ may grow only under certain conditions, whereas $MoSi_2$ and $NbSi_2$ should be expected to grow stably. The driving force for diffusion should be related to the chemical activity. It was shown that Ti_5Si_3 ($TiSi$) is the only growing M silicide whose approximate activity is higher than that calculated for Ta_5Si_3 (Ta_2Si). This indicates that the driving force for silicon diffusion in the general system shown in Section I is considerably lower in the $Ti/TaSi_2$ system than in the other $M/TaSi_2$ systems.

The same analysis may be presented differently. If the existence of Ta_2Si is taken into account,

an overall equilibrium reaction taking place at the M silicide/
Ta silicide interface may be written



The direction in which the above reaction is spontaneous should depend on the sign of ΔG_r (in this case, ΔH_r). During the course of diffusion, it may be expected that the lowest stable silicide forms first and higher silicides form from this. All reactions involving the gain of silicon showed that the reaction to the next highest silicide was spontaneous, except for Zr_2Si going to Zr_5Si_3 . The result is again evident from the table below in which the direction of the generalized equation above is determined from ΔH_r . The table indicates that the highest silicides thermodynamically stable in the M/TaSi₂ couples for Ti and Zr are Ti₅Si₃ and Zr₂Si. This explains the fact that, although Zr₅Si₃ is the most stable Zr silicide when formed from the elements, the trisilicide does not grow in the Zr/TaSi₂ diffusion zone.

Also of interest is the fact that the ΔH_r for the W reaction is zero or, as previously shown, the approximate silicon activity for WSi₂ (W₅Si₃) equals that for Ta₅Si₃ (Ta₂Si). Therefore, because of the relative thermodynamic properties of Ta and W silicides, a delicate balance exists at the W silicide/Ta₅Si₃ interface which affects the stability of the WSi₂ phase. This balance might be upset by any number of variables. If there were poor contact in the

TABLE XIV
THERMODYNAMICALLY STABLE PHASES

M	M_pSi	M_qSi	ΔH_f (kcal/mole Si)	Direction toward
W	WSi_2	W_5Si_3	0	$WSi_2 = W_5Si_3$
Re	$ReSi_2$	ReSi (no data for Re_5Si_3)	- 2	ReSi
Mo	Mo_5Si_3	Mo_3Si	+ 14	Mo_5Si_3
Mo	$MoSi_2$	Mo_5Si_3	+ 3.7	$MoSi_2$
Nb	$NbSi_2$	Nb_5Si_3	+ 3.4	$NbSi_2$
Ti	TiSi	Ti_5Si_3	- 5	Ti_5Si_3
Zr	Zr_5Si_3	Zr_2Si	-103	Zr_2Si

W/TaSi₂ couple, W metal could be in contact with silicon vapor (in equilibrium with Ta₅Si₃) rather than solid Ta₅Si₃. The activity of the vapor could be high enough to form WSi₂. When contact improved (as the metal deformed) silicon activity of the solid Ta₅Si₃ might be too low for WSi₂ to continue growing and the equilibrium reverses.

Although thermodynamic considerations were useful in explaining some of the resulting phase compositions in the diffusion zones, the reasons for the existence of others are still unknown. Table XV lists the crystal structures of the metals and of the possible silicides in each of the systems as well as the predominant silicides actually formed in the chronological order of their appearance

TABLE XV
STRUCTURAL CORRELATION OF SILICIDE FORMATION

METAL (C.S.)	POSSIBLE SILICIDES (C.S.)	PREDOMINANT
Ta (cubic)	Ta ₅ Si ₃ (hexagonal & tetragonal) Ta ₂ Si (tetragonal) Ta _{4.5} Si (hexagonal)	Tetragonal Ta ₅ Si ₃ lowest silicide: Ta ₂ Si, not Ta _{4.5} Si
W (cubic, a=3.2)	WSi ₂ (tetr.; a=3.21, c=7.88) W ₅ Si ₃ (tetr.; a=9.6, c=5.0)	I WSi ₂ II W ₅ Si ₃
Mo (cubic)	MoSi ₂ (tetragonal) Mo ₅ Si ₃ (tetragonal) Mo ₃ Si ₃ (cubic)	I Mo ₃ Si II Mo ₅ Si ₃
Nb (cubic)	NbSi ₂ (hexagonal) Nb ₅ Si ₃ (tetr. & hex.) Nb ₃ Si ₂ (?) Nb ₄ Si ₂ (hex.)	I tetr. Nb ₅ Si ₃ II Nb ₃ Si ₂
Zr (hex. cubic above 860°C)	ZrSi (rhombohedral) ZrSi ₂ (rhombohedral) Zr ₅ Si ₃ (hex.) Zr ₆ Si ₅ Zr ₂ Si (tetr.) Zr ₄ Si ₃ Zr ₃ Si (hex.)* Zr ₄ Si ₃	I Zr ₂ Si? II Zr ₃ Si + Zr/Si S.S. + ?
Ti (hex. cubic above 860°C)	TiSi (rhombohedral) TiSi ₂ (rhombohedral) Ti ₅ Si ₃ (hex.)	Ti ₅ Si ₃
Re (hexagonal)	ReSi ₂ (tetr.) ReSi (cubic) Re ₅ Si ₃ (tetr.) Re ₃ Si (cubic)	I ReSi ₂ II Re ₅ Si ₃ ?

in the diffusion zone. It is possible that the structure of the first-formed silicide best matches the structure of the metal from which it grows and that epitaxial growth plays an important role in determining phase compositions. Although the epitaxial growth mechanism only controls growth for very thin layers, if conditions are proper for the stability of the first-formed silicide, it may retain its original structure many microns from the metal interface.

b. Compatibility

It has been shown that even in predicting growth rates under ideal conditions of pure solid state diffusion, extensive knowledge of phase diagrams, thermodynamic data and crystal structures is needed, as well as stoichiometry ranges and fundamental diffusivities. Under non-ideal conditions, other factors come into play, such as mechanical compatibility. One of the effects of incompatibility between metal wafer and $TaSi_2$ wafer has been to decrease the mechanical contact between the wafers in the W and Re systems. The extent of true contact between brittle $TaSi_2$ and any metal should depend on the deformability of the metal. Rhenium exhibits the lowest deformability (as indicated by the highest elastic modulus) of the metals used in this work as shown in Table XVI.

TABLE XVI
ELASTIC MODULI OF SOME REFRACTORY METALS (46)

METAL	E (psi x 10 ⁶)	
	AT ROOM TEMPERATURE	AT 2000°F
Re	70	-
W	55	50
Mo	48	38
Ta	28	21
Nb	15	8.5
Zr	10	-
Ti	10	-

Therefore, from the data above and in light of the results of this work, the effect of poor contact can be seen to be greatest in the Re/TaSi₂ system, important in the W/TaSi₂ system, of possible significance in the Mo/TaSi₂ system, and of no significance in the remaining systems.

C. Relationship of D's to k's

The results presented in Tables III through X represent experimental growth rates rather than fundamental diffusivities. The values of these parabolic rate constants (k) are necessary for computing the actual thicknesses of TaSi₂ as a function of time and temperature and thereby comparing the effectiveness of barrier metals. The quantity \tilde{D} (containing D_{Si} and D_M) is the more basic diffusion coefficient.

For any solid, \tilde{D} is a constant dependent only on temperature, whereas k also depends on the environment of other compounds about the growing phase. Therefore, if \tilde{D} can be determined from k , fundamental diffusion knowledge about the solids under investigation could be obtained which could be used in later studies independent of the system in which the material is growing.

In this work, it has been shown that in all of the systems but Ti/TaSi₂ only silicon diffuses. Therefore, \tilde{D} is directly related to D_{Si} by: $\tilde{D} = N_M D_{Si}$. In the simplest system, Ta/TaSi₂, k is directly related to D_{Si} according to equation (17) in Section I, and

$$D_{Si} \Delta N_{Si} = 0.7e^{-77,000/RT}.$$

As previously mentioned, ΔN_{Si} is not known but can be assumed to be independent of temperature. Once this quantity is accurately measured in the Ta/TaSi₂ system, D_{Si} in Ta₅Si₃ will be explicitly known in any system.

For systems of TaSi₂ versus metal, equations (44) and (66) show that, under the assumptions stated, k and $(D \Delta N)_{Si}$ are proportional for the Ta₅Si₃ phase. Therefore, since D_{Si} will be the same in the Ta₅Si₃ phase for each system, it is the differences in ΔN which account for the different growth rates of Ta₅Si₃. Nonetheless, if ΔN is independent of temperature in the M/TaSi₂ systems as well as in the Ta/TaSi₂ system, the activation energies should all be

the same for the growth of the Ta_5Si_3 phase. Comparison of the Δx_1 (Ta_5Si_3 zone) data in Tables IX and X clearly shows that, of the M/ $TaSi_2$ systems studied, only Ti/ $TaSi_2$ has an activation energy comparable to that for Ta/ $TaSi_2$. This means that ΔN for Ta_5Si_3 in the other systems cannot be considered independent of temperature. Indeed, in the Nb, Zr and Mo systems the CCP plots indicate that the compositions of the Δx_2 zones change with temperature, particularly near the original interface. This would cause N_{Si} on the Ta_5Si_3 side of the original interface to vary, producing a ΔN_{Si} across the Ta_5Si_3 which would depend on temperature in a complicated manner. In fact, in the W/ $TaSi_2$ system, the compositional changes are even more complex, causing ΔN_{Si} in Ta_5Si_3 to vary with time as well as temperature. Only in the Ti/ $TaSi_2$ system do the zone compositions remain constant and, although the mechanism is complicated by the diffusion of Ti, the activation energy for the growth of Ta_5Si_3 is comparable to that in the Ta/ $TaSi_2$ system.

The Ti/ $TaSi_2$ system may be analyzed as outlined in Part 4 of Section IC, since the Δx_a zone has been shown to be an extremely thin eutectoid mixture at all conditions. Because the Ta_5Si_3/Ti_5Si_3 interface could not be located (due to considerable porosity in the zone) the diffusion properties of Ti in Ti_5Si_3 cannot be calculated, although it has been shown that Ti does indeed diffuse. Nonetheless, the diffusion

constant of Si in Ti_5Si_3 is directly related to k for the Δx_2 zone through equation (68). Therefore, the activation energy listed for the Δx_2 zone in Tables IX and X should be the activation energy for silicon diffusion in Ti_5Si_3 .

The remaining M/ $TaSi_2$ systems must be considered as more complicated since at least two M silicide zones grew simultaneously. Therefore, the Q 's listed for the Δx_2 and Δx_a zones are not true activation energies, but rather the result of the coupling of the D 's and k 's for the two zones. True activation energies can be derived from the values of $D \Delta N$ computed from equations (49) and (50) for the Nb/ $TaSi_2$ and Mo/ $TaSi_2$ systems. In the W/ $TaSi_2$ system, the data are insufficient to totally describe the basic diffusion characteristics of the growing phases due to the complexity of the pattern of growth. The zone compositions in the Zr/ $TaSi_2$ system were not satisfactorily determined in this investigation and, therefore, the analysis to be used below cannot be applied. For the Nb/ $TaSi_2$ and Mo/ $TaSi_2$ systems, the Δx_2 zones were considered pure Nb_3Si_2 and Mo_5Si_3 respectively and the Δx_a zones Nb_5Si_3 and Mo_3Si . Equations (49) and (50) were used to compute $D_{Si} \Delta N_{Si}$ from k_0 values listed in Tables IV and VIII for the Δx_2 and Δx_a zones. Figures 34 and 35 are plots comparing the temperature dependence of the $D_{Si} \Delta N_{Si}$ values and the k_0 values from which they were derived. The data here were not treated statistically. It may be noted

FIGURE 34

COMPARISON OF k_0 AND $D\Delta N$ VALUES IN A COUPLED SYSTEM

Nb/TaSi₂ SYSTEM

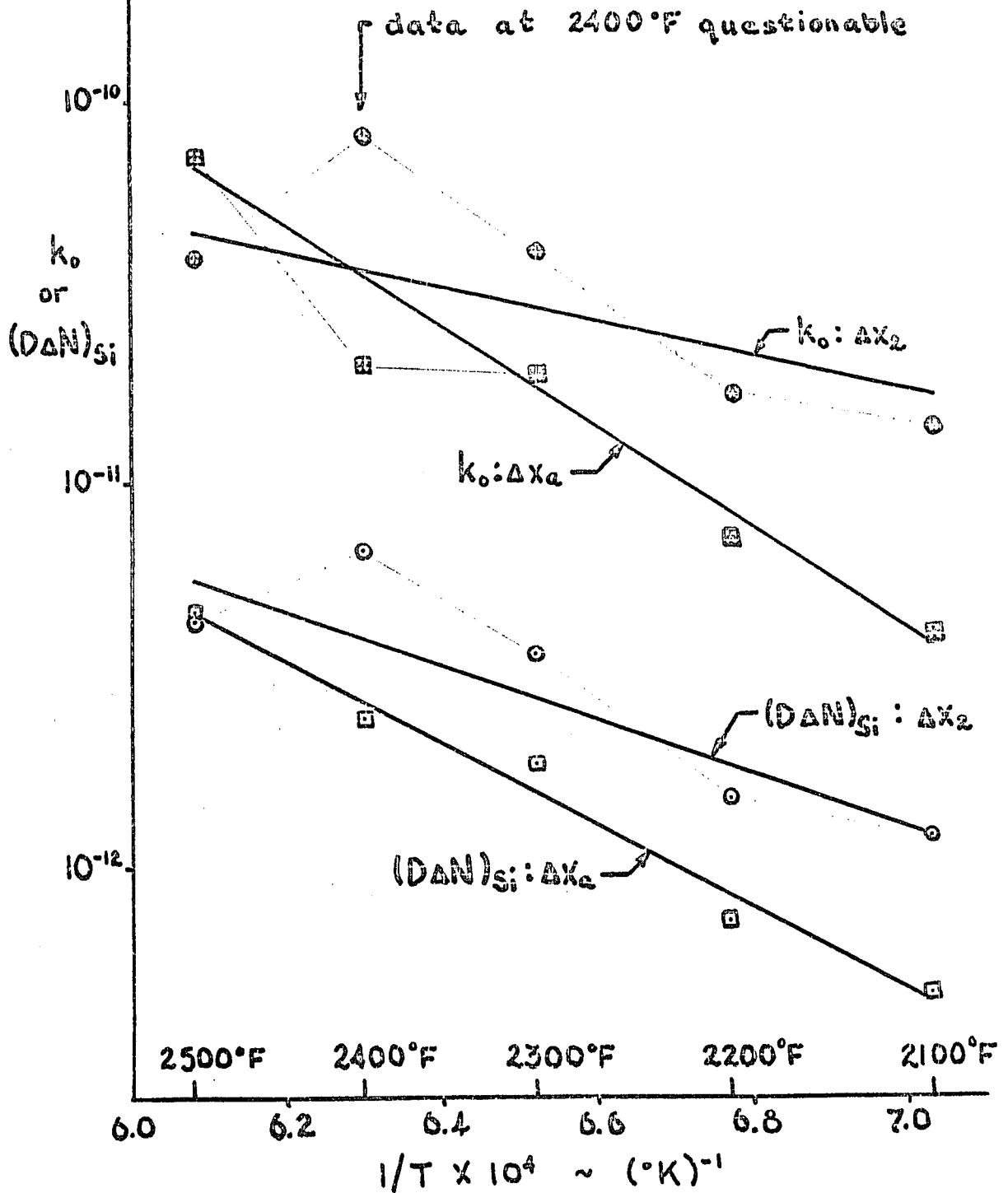
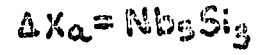
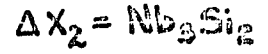
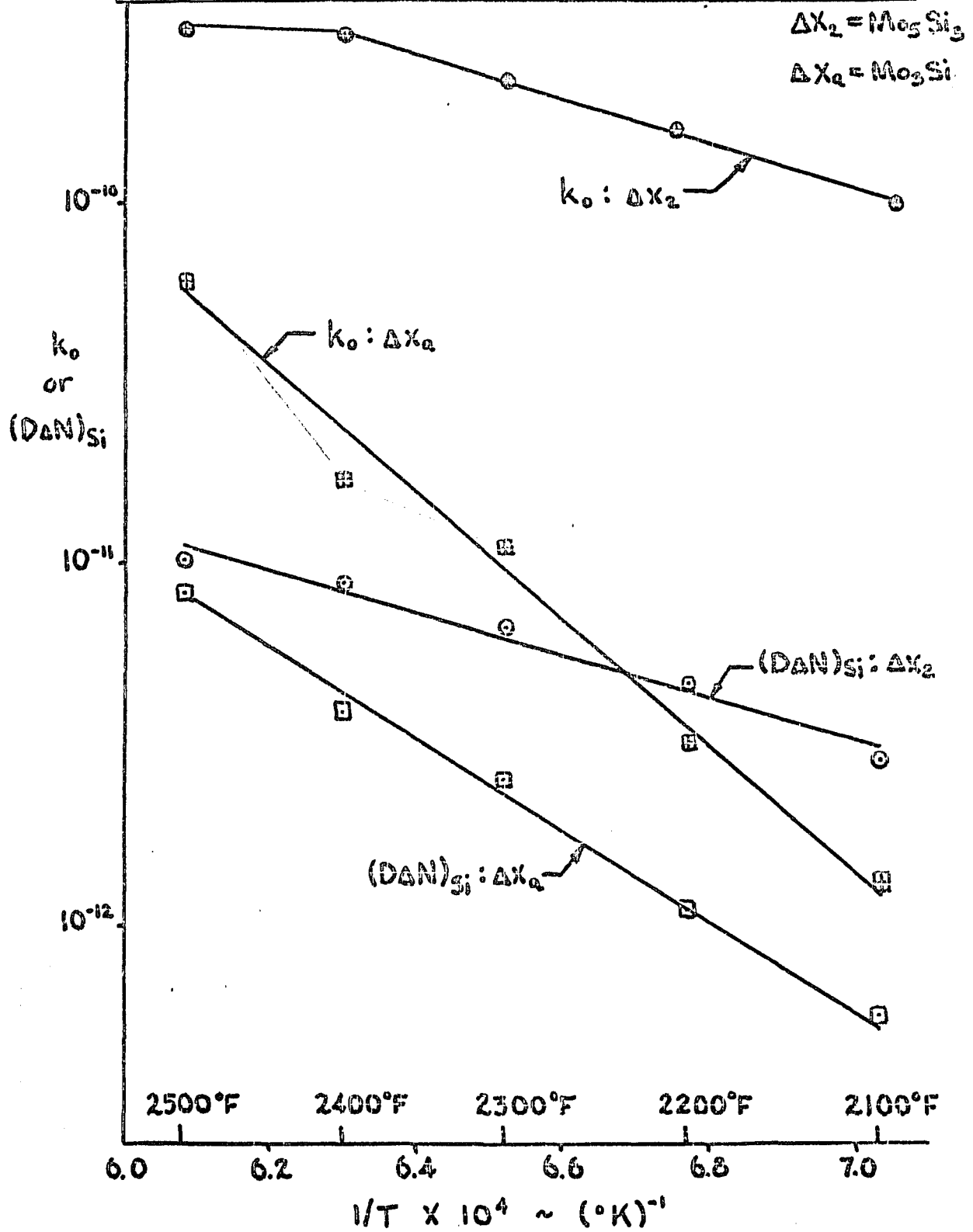


FIGURE 35

COMPARISON OF k_0 and $D\Delta N$ VALUES FOR A COUPLED SYSTEM

Mo/TaSi₂ SYSTEM



in the figures that the points for $(D \Delta N)_{Si}$ better fit a straight line than do the points for k_0 , particularly for the Δx_a zone. Also, the slopes of the lines for Δx_2 and Δx_a are closer for $(D \Delta N)_{Si}$ than for k_0 . Comparison of Q's calculated from the slopes of the lines in Figures 34 and 35 and from Tables IX and X appears in Table XVII.

TABLE XVII

COMPARISON OF ACTIVATION ENERGIES (kcal/mole)

ZONE	FROM: TABLE IX	TABLE X	k_0 PLOT	$D_{Si} \Delta N_{Si}$ PLOT
Mo (Δx_2)	30 ± 10	6 ± 17	24	27
Mo (Δx_a)	75 ± 7	86 ± 9	82	58
Nb (Δx_2)	36 ± 9	39 ± 9	27	33
Nb (Δx_a)	55 ± 7	58 ± 6	59	49

Q values from the slopes of the k_0 plots are directly comparable to the values arrived at statistically (Tables IX and X). For the Δx_a zones, activation energies from $D_{Si} \Delta N_{Si}$ plots are lower than the associated Q's from k_0 plots; but although the Q's for Δx_2 are slightly increased, they cannot be considered different from the statistically calculated values. It must be remembered that slight changes in composition near the original interface in the Δx_2 zone resulted in erroneous activation energies for the Δx_1 zones. Surely the activation energies for the growth of the Δx_2

zones are similarly erroneous. Therefore, the Q's of basic significance which result from the analysis above are:

$$Q \text{ for Mo}_3\text{Si} = 58,000 \text{ cal/mole}$$

and $Q \text{ for Nb}_5\text{Si}_3 = 49,000 \text{ cal/mole}.$

These may be compared with the values reported for Mo_3Si by Bartlett, Gage and Larssen (27) and those for Nb_5Si_3 reported by Bartlett (24) and Lavendel and Elliot (25).

$$Q \text{ for Mo}_3\text{Si} = 78,000 \text{ cal/mole}$$

$$Q \text{ for Nb}_5\text{Si}_3 = 58,000 \text{ (24) and } 49,000 \text{ (25) cal/mole}.$$

The values for Nb_5Si_3 are comparable to those reported in this work. Q for Mo_3Si is considerably higher than reported here, but is the same as that from statistical analysis of the simple k values. It appears that Bartlett, et.al. (27) did not take the coupling of diffusivities and rate constants into account and reported an apparent rather than a fundamental activation energy.

D. Unusual Behavior

During the course of this investigation, certain unusual or unexpected phenomena became evident which were not directly related to the reaction kinetics or diffusion mechanisms in the silicide systems. These will be discussed below.

1. Atypical Diffusion Zone in the Ta/TaSi₂ System

Plate III shows the appearance of the atypical diffusion zone which resulted when Ta was coupled

with a particular type of poor TaSi₂ wafer, designated "A" type. Both microscopic and X-ray diffraction analyses confirmed the existence of TaSi₂ on the Ta side of the original interface for each of the four Ta/TaSi₂ couples employing "A" type TaSi₂ wafers. TaSi₂ is apparently present on both sides of the original interface and the Ta₅Si₃/TaSi₂ interface appears within the zone previously designated Δx_2 . Operation of a solid state mechanism of growth must produce Ta₅Si₃ on both sides of the original interface and, therefore, another mechanism must be operating. "A" type TaSi₂ wafers contained many minute pores which were probably interconnected to form a network which exposed a large amount of internal surface. At the annealing temperatures silicon from the interior of the wafer may diffuse as vapor through the pores to the original interface maintaining a high supply of silicon for diffusion through Ta₅Si₃ to the Ta interface. In this way the Ta₅Si₃ layer is formed only by reaction of Si with Ta and the presence of Si vapor maintains TaSi₂ on both sides of the original interface.

2. Cusps in the Ti/TaSi₂ System

Plate XXIX shows a microscopic feature which was peculiar to the Ti/TaSi₂ system. The half cusp shown results when the thickness of the Δx_2 zone changes abruptly due to a change in the position of x_M (the Ti/Ti₅Si₃ interface). This type of behavior is a result of two factors, the

first of which is unique to the Ti/TaSi₂ system.

- a. Both Ti and Si may diffuse.
- b. Regions of poor contact may exist near the edges of the sample (where the half cusps are always found) due to the manner in which the couple sandwiches were set up.

Poor contact disallows solid state transport of silicon or titanium across the original interface, but Si may now be transported as a vapor across the original interface. Therefore, the upper portion of Plate XXIX represents the normal condition in which both Si and Ti diffuse in the solid state forming Ti₅Si₃ on both sides of the original interface and accounting for the thinness of the Δx_2 layer. Near the center of the photomicrograph, contact is disrupted and only silicon may diffuse via vapor transport forming Ti₅Si₃ only on the Ti side of the original interface.

VI CONCLUSIONS

The growth rate of Ta_5Si_3 in the Ta/TaSi₂ system has been accurately measured. The rate of degradation of TaSi₂ has been measured separately. Six metals have been tested to determine their efficacy as barriers to the degradation of TaSi₂. None of the metals tested was effective in lowering the rate of loss of TaSi₂ by diffusion. Some of the metals investigated have previously been shown to increase the oxidation resistance of TaSi₂ coatings when used as additives in the Ta/TaSi₂ system. It may, therefore, be concluded that these additive metals operate by participating in the oxidation reaction to form more protective glasses rather than as barriers to the growth of less protective lower silicides.

As a result of this work, fundamental activation energies for diffusion of silicon in four silicides have been determined. The four compounds are:

Ta_5Si_3 ; $Q_{Si} = 77,000$ cal/mole
 Mo_3Si ; $Q_{Si} = 58,000$ cal/mole
 Nb_5Si_3 ; $Q_{Si} = 49,000$ cal/mole
and Ti_5Si_3 ; $Q_{Si} = 44,000$ cal/mole.

VII AREAS OF FURTHER INVESTIGATION

As a result of questions raised during the course of this work, many areas for further investigation have been made apparent. Some of these areas follow:

- A. Similar kinetic studies on some M/Si systems.
- B. More complete short time data for the W/TaSi₂ and Mo/TaSi₂ systems.
- C. Studies at higher temperatures in the Re/TaSi₂, W/TaSi₂ and Mo/TaSi₂ systems.
- D. Morphology studies on silicides, both parallel and perpendicular to the diffusion direction with the aid of the electron microscope.
- E. Electron microprobe analysis on most of the diffusion zones to confirm the results of X-ray diffraction analysis.
- F. Radioactive tracers studies in the silicide systems.
- G. Phase studies and detailed X-ray diffraction analysis on the Zr/Si system and the low silicon content end of the Nb/Si system, as well as the confirmation of the existence of Nb₃Si₂ and determination of its crystal structure.
- H. Ternary phase studies in the silicide systems.
- I. Silicon vapor pressure studies to help determine the silicon activities in the silicide systems.

APPENDIX I

PHASE DIAGRAMS

FIGURE I-1
Ta-Si PHASE DIAGRAM (49)

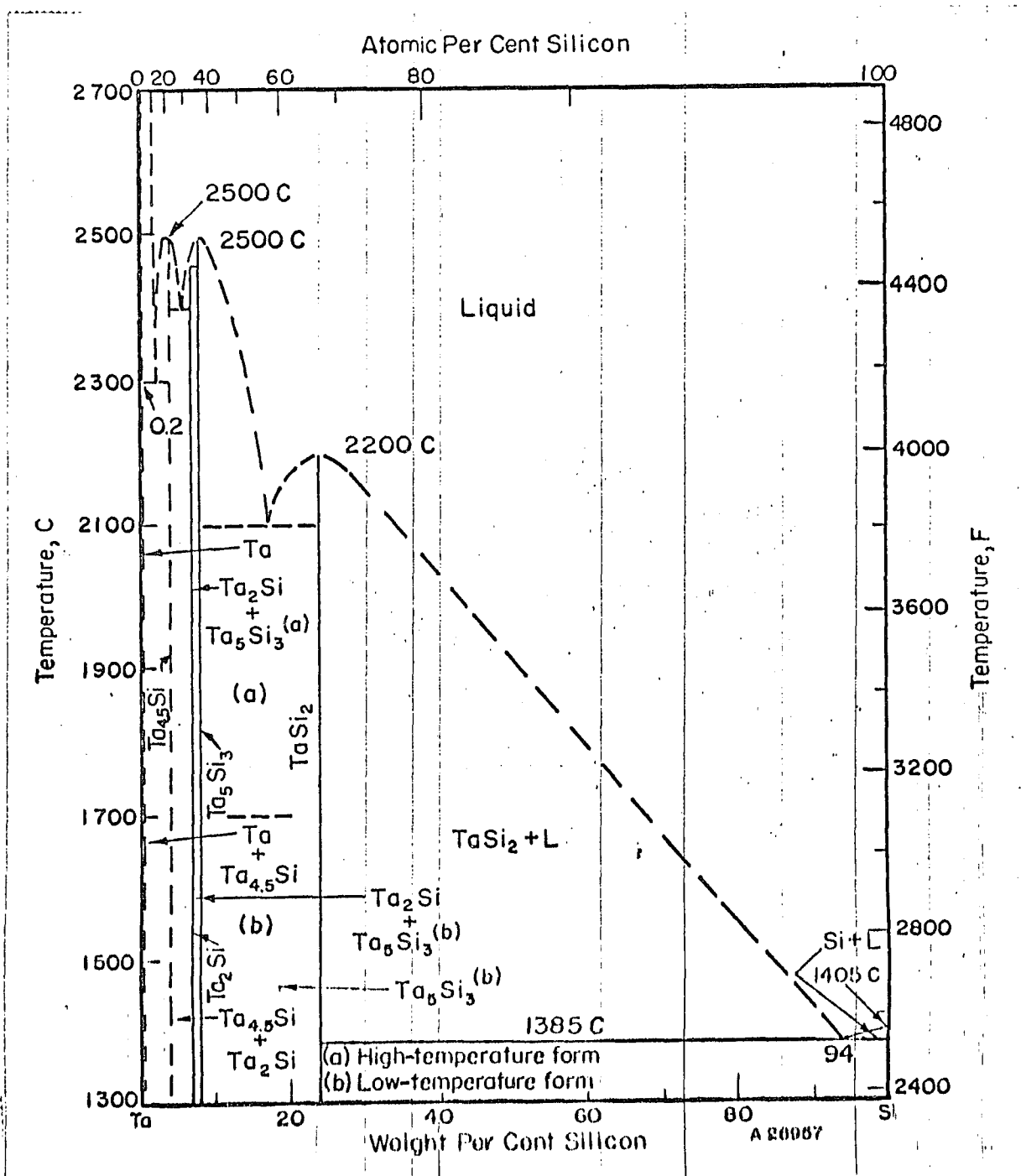


FIGURE I-2

Nb-Si (Cb-Si) PHASE DIAGRAM (49)

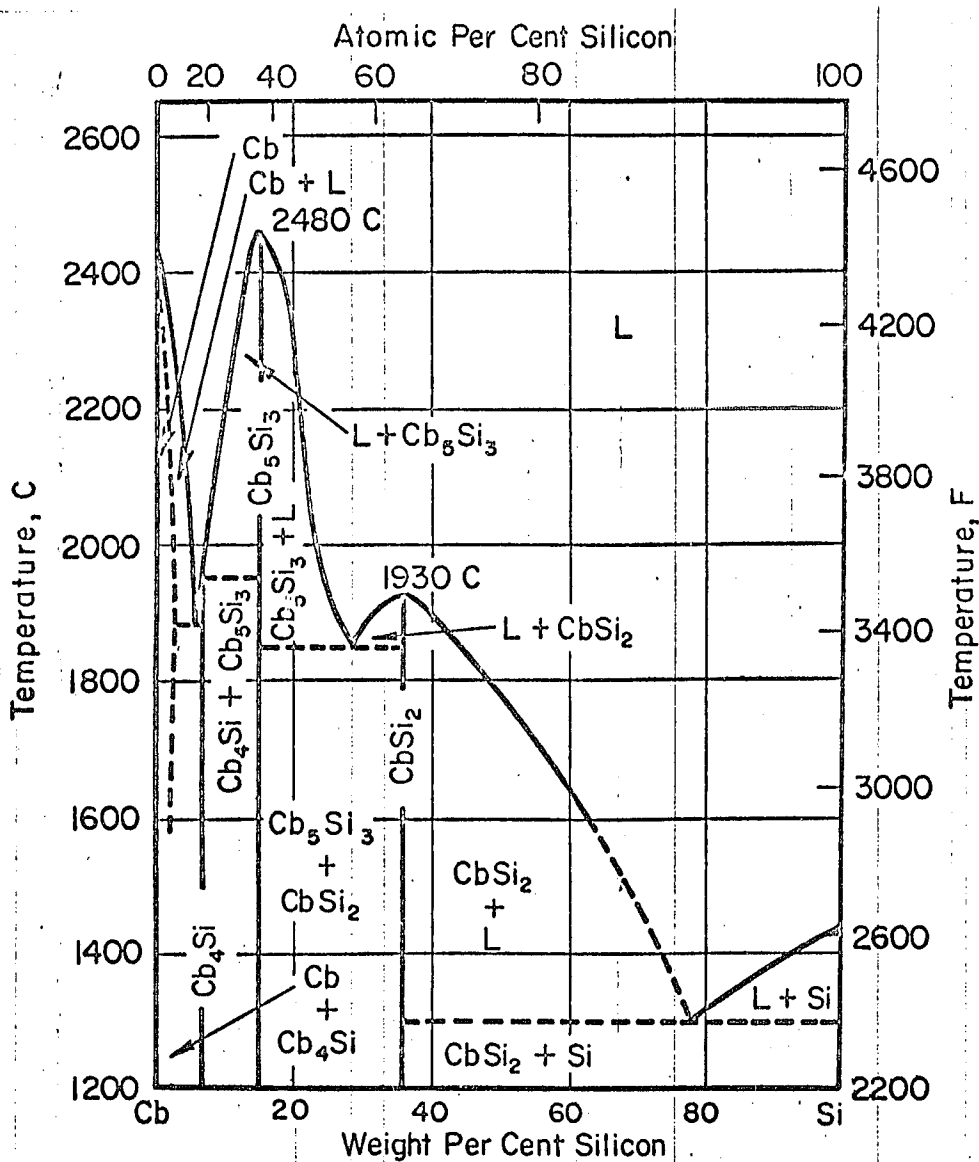


FIGURE I-3
Zr-Si PHASE DIAGRAM (42)

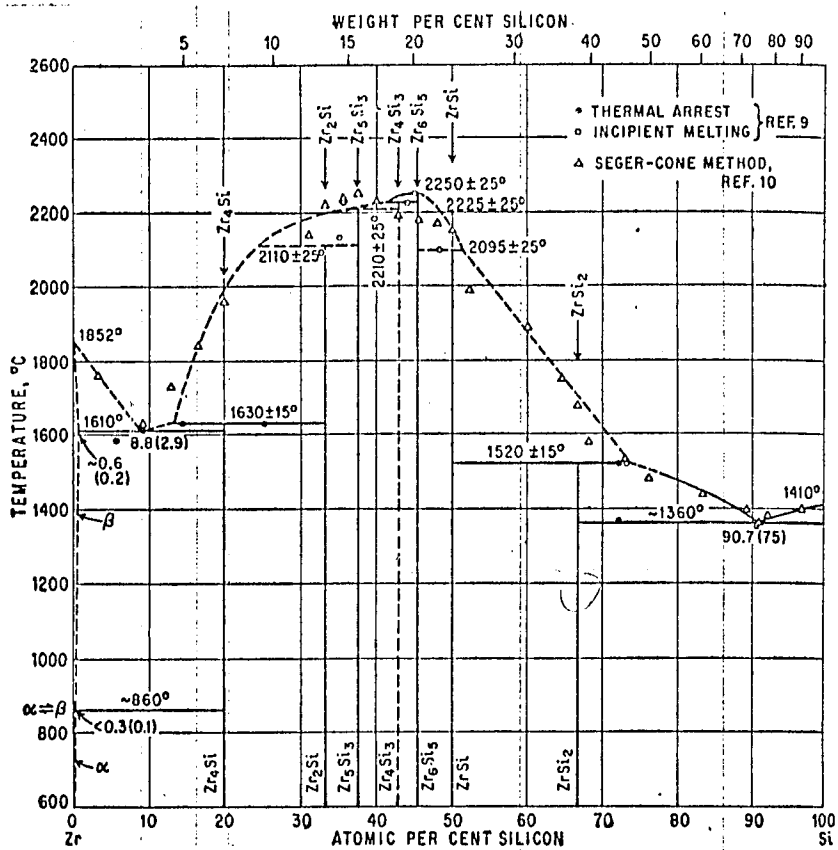


FIGURE I-4
Ti-Si PHASE DIAGRAM (42)

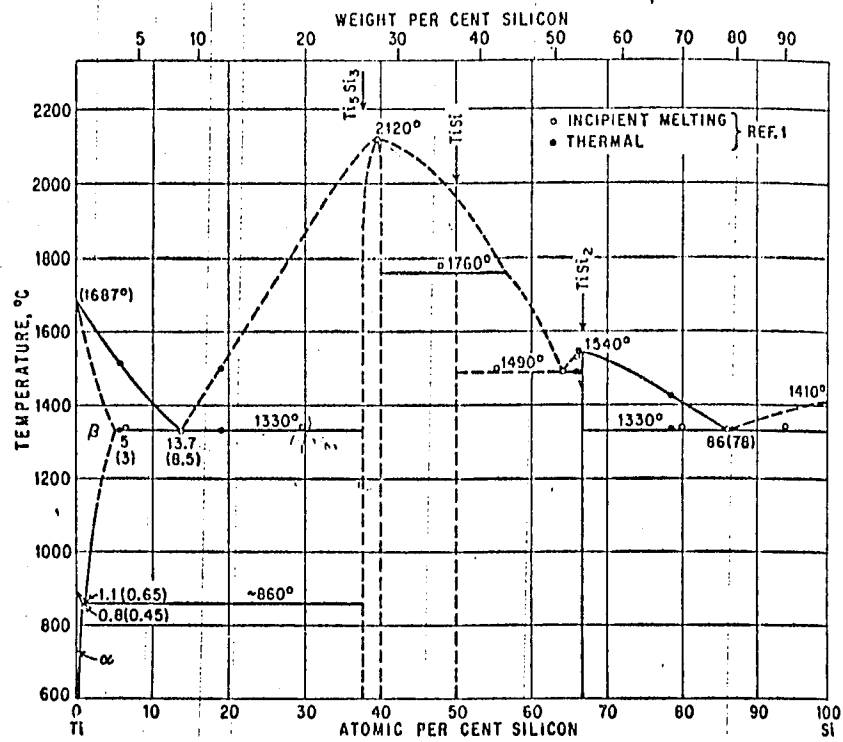


FIGURE I-5

W-Si PHASE DIAGRAM (49)

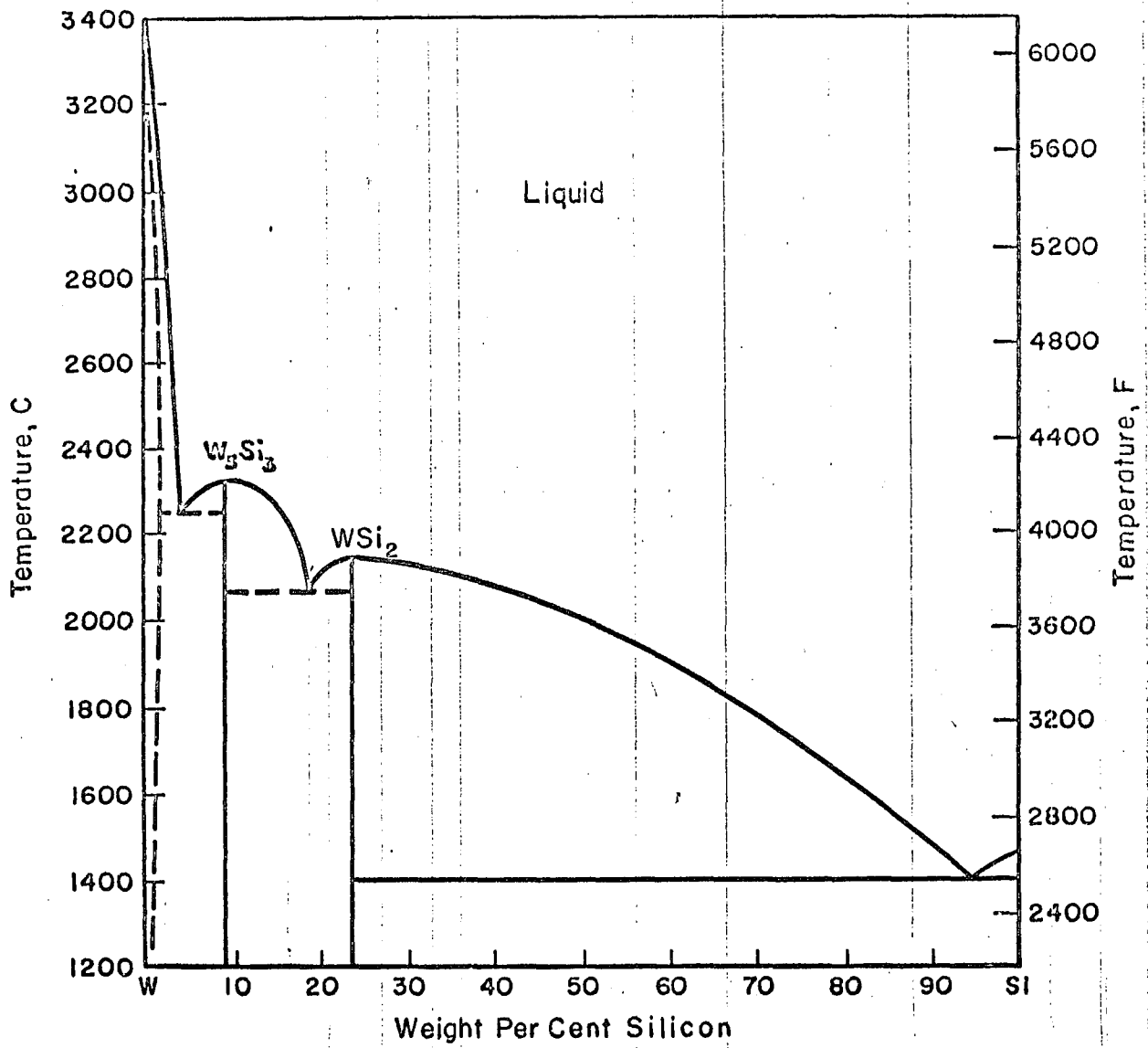
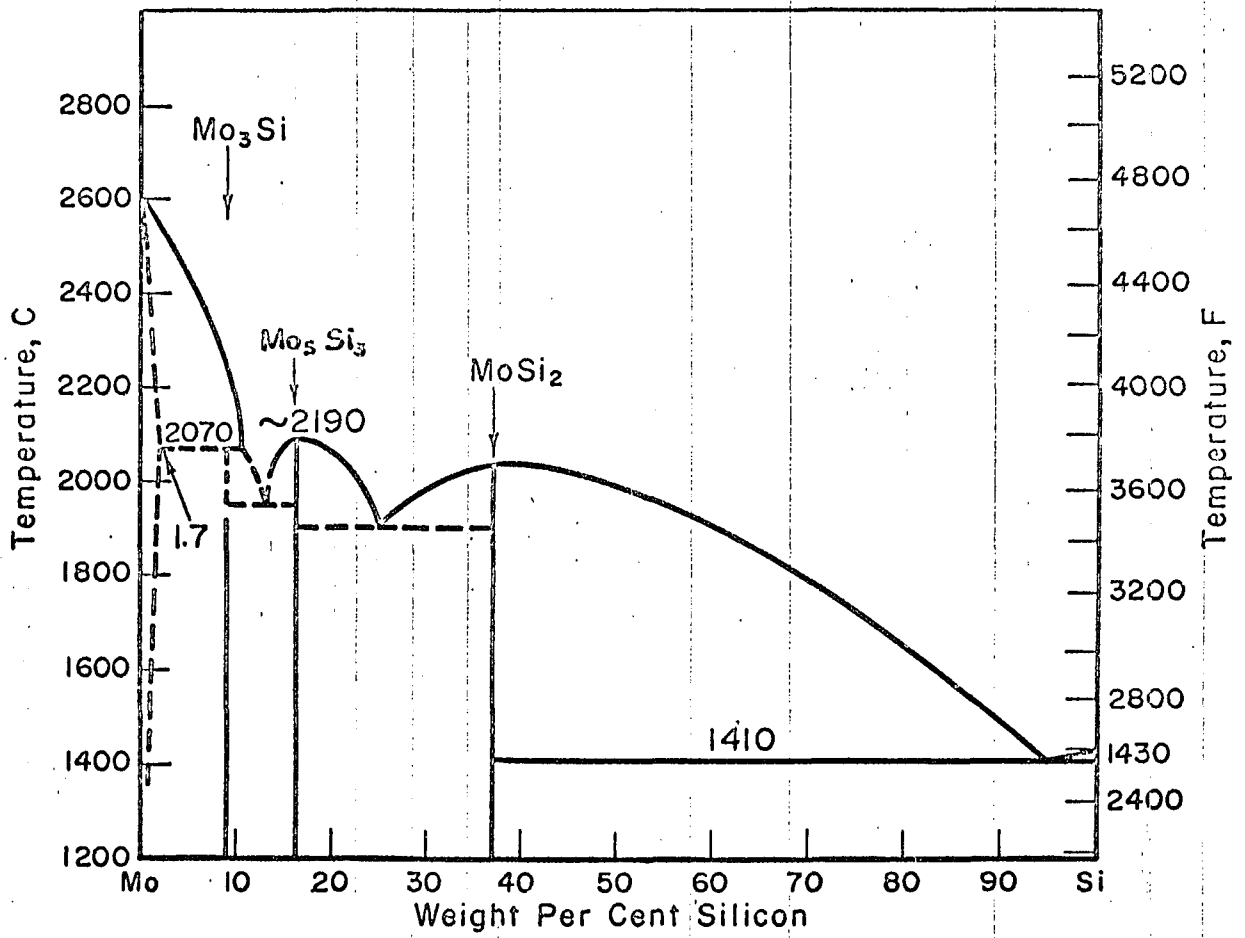


FIGURE I-6
Mo-Si PHASE DIAGRAM (49)



APPENDIX II

MATERIALS AND ETCHING REAGENTS

Page 175 follows

MATERIAL SOURCES AND SPECIFICATIONS

Material	Form	Specifications	Source
TaSi ₂	Powder	No purity spec., -325 mesh	Cerac Corp.
TaSi ₂	Powder	No purity spec., -325 mesh	Shieldalloy Corp.
Silicon	Powder	99.99% pure, -325 mesh	United Mineral & Chemical
Tantalum	Powder	1) Met. Grade (99.9% min) L # MG-50 2) Met. Grade (99.9% min) L # ZM #750	Fansteel Corp. Fansteel Corp.
Nickel	Powder	No specifications	Charles Hardy
Tantalum	Rod	99.90% min:, Vacuum melted	Fansteel Corp.
Tantalum	Sheet	99.95% pure, 0.05" thick	United Mineral & Chemical
Titanium	Sheet	99.5% pure, 0.077" thick	Titanium Corp. of America
Zirconium	Sheet	99.99% pure, 1/16" thick	Materials Research Corp.
Molybdenum	Sheet	99.95+% pure, 1/16" thick	Materials Research Corp.
Niobium	Rod	99.82% pure	United Mineral & Chemical
Rhenium	Wafers	99.97% pure, 0.02" thick	Cleveland Refractories
Tungsten	Wafers	99.9% pure, 1/16" thick	Kulite Tungsten Co.

ETCHING REAGENTS

Etchant for	Contents	Treatment
Ta Silicides	7.5 parts HF 2.5 parts HNO ₃ 100 parts H ₂ O	Immersion 3 to 4 minutes at room temperature
Ti, Zr	Above diluted	2 to 5 seconds
Ta silicides (chemical polish for TaSi ₂ wafers)	5 ml. HF 15 ml. 5% chromic acid 40 ml. 1% KMnO ₄ 10 ml. H ₂ O	Swab 2 minutes
Ta Nb	30 ml. lactic acid 10 ml. HNO ₃ 10 ml. HF	10 minutes 30 seconds-5 minutes
	<u>Murakami's Reagent</u>	
Re W, Mo	10 grams K ₃ Fe (CN) ₆ 10 grams KOH (or NaOH) 100 ml. H ₂ O	5 minutes 1 minute

APPENDIX III

DETAILS OF TaSi₂ WAFER PRODUCTION

Page 177 follows

PROCEDURE FOR THE PRODUCTION OF DENSE TaSi₂ WAFERS

1. Synthesis

a. Tantalum and silicon powders were ball-milled together for one day in stoichiometric amounts plus 1% excess silicon to account for evaporation losses. Ball-milling was done using 100 gram batches (24.67 gms. Si + 75.33 gms. Ta) in a rubber-lined, 3" D mill containing 1/4" and 1/8" stainless steel balls.

b. Reaction wafers were pressed in a 1" diameter hardened steel die at an optimum load of 15 thousand pounds. Wafers weighed between 10 and 15 grams and were pressed for about five minutes. Upward ejection was used to release the wafers from the die.

c. Five reaction wafers were reacted at a time producing a yield of about 60 grams of usable TaSi₂. Reaction took place in an induction furnace in a vacuum contained by a Vycor tube. The reaction wafers were stacked so that only the lower wafer was in contact with the alumina support ring inside an alumina crucible with a tantalum foil susceptor and a tantalum cover. Temperature was measured with an optical pyrometer. No corrections were made for black-body radiation or losses through the sight glass. Therefore, true temperatures were probably higher than those recorded. Reaction took place below 1200°C and was always violently exothermic, no matter how slowly the mass was brought up to temperature. After reaction and subsequent cool-down

(approximately half an hour), the reacted wafers were removed from the crucible and visually examined for staining. Due to the violence of reaction some pieces came in contact with tantalum or alumina which might have had a contaminating effect. These pieces became discolored from the contact and could be visually distinguished from the pure TaSi_2 . The stained surfaces were rubbed off and discarded. The majority of the TaSi_2 was in the form of hard solid agglomerates and was ground in a mortar and pestle to be stored for processing into wafers. X-ray diffraction patterns of this powder showed the material to be pure TaSi_2 .

2. Wafer Preparation and Pressing

a. To 60 grams of TaSi_2 previously sintered was added 0.5% nickel powder as a sintering aid. This was ground and mixed together in a ball mill for 24 hours.

b. The mixture was put in 15 gram batches into a mortar and 1% binder (polymethylmethacrylate solution) was added. After mixing and drying, the mixture was ground to a uniform powder with a pestle and screened through a 100 mesh nylon screen to be stored for pressing.

c. 1.5 grams of TaSi_2 (with binder and sintering aid) were weighed out and carefully charged into a 1/2" diameter hardened steel die which had previously been lubricated with a stearic acid solution. The wafer was then pressed under a 10 thousand pound load for about a minute.

Upward ejection was used to release the wafer from the die.

3. Presintering

Freshly pressed wafers were loaded into the presintering rig, two wafers in each alumina dish. The rig accommodated ten alumina dishes and hung inside a quartz tube which was inserted in a resistance-wound pot furnace. The tube was evacuated using a mechanical pump and the temperature slowly raised to 1000°F as measured by a Chromel-Alumel thermocouple. After holding the temperature at 1000°F for about an hour, the furnace was slowly cooled to room temperature overnight. The presintering step removed the binder and left the wafers with very low mechanical strength, so that the presintered wafers had to be handled very carefully.

4. Sintering

Final sintering was done in a tantalum resistance furnace atop a vacuum pumping station, capable of pressures of 10^{-5} Torr. Up to four wafers could be sintered at one time in each furnace. The wafers were supported on alumina rings. After evacuating the furnace, the temperature was raised to about 1600°C (as measured by an optical pyrometer) and held for ten minutes. The furnace was then slowly cooled to room temperature and the sintered wafers removed. After rough grinding on a diamond wheel to remove the outer crust of Ta_5Si_3 , X-ray diffraction analysis showed the wafers to contain only $TaSi_2$ and trace amounts of Ta_5Si_3

(less than 5%). Density measurements on wafers sampled at random showed none to be below 95% of theoretical density.

Grinding and polishing on diamond discs produced mirror finishes on the wafers.

APPENDIX IV

DETAILS OF X-RAY DIFFRACTION ANALYSIS

Page 181 follows

A. X-Ray Diffraction Data

The following tables present the X-ray diffraction data recorded for some interesting samples encountered in this research. In all the tables but Table IV-V, the results shown are diffractometer data in which I is the height above background of the peak recorded. In Table IV-V, a powder sample was analyzed in a film camera and the intensities recorded as S (strong), M (medium) and W (weak), with V (very) indicating degree and B referring to the breadth of the arc. In all of the tables D represents a doublet; and an asterisk indicates that a peak is either enhanced by a nearby strong reflection or that the peak is a result of more than one phase having similar d values.

Table IV-I shows the changes in the X-ray diffraction data for a typical good TaSi₂ wafer at various stages in the fabrication procedure. The TaSi₂ can be seen to be pure, trace amounts of Ta₅Si₃ appearing only after final sintering. Table IV-II compares the X-ray diffraction data for tetragonal Ta₅Si₃ formed on the surfaces of TaSi₂ wafers as a result of silicon vaporization during sintering at different conditions. Non-uniform intensities and additional unknown peaks are a result of unusual strain produced in the lattice. This is most evident in the completely exposed upper surfaces (columns 1 and 2). Also, the higher temperature used in sintering the porous wafer introduced many more "strain" peaks. The data in columns 2, 3 and 4 are

for one particular TaSi₂ wafer and it can therefore be seen that resintering the wafer produced an annealing effect and greatly reduced the strain in the lattice.

The implications of the data presented in Table IV-III, showing the complete analysis of the surfaces of some wafers when split near the original interfaces, have already been discussed. The layers of Ta₅Si₃ are generally thin in these couples and the TaSi₂ peaks being refracted from beneath the Ta₅Si₃ layers have been omitted for clarity. Peaks for hexagonal Ta₅Si₃ and tetragonal Ta₅Si₃ have been separated so that they may be easily compared to the ASTM data (column 1). Columns 2 and 3 are data for the surfaces of the Ta wafer (Δx_2 zone) and TaSi₂ wafer (Δx_1 zone) respectively from a Ta/TaSi₂ couple annealed at 2200°F for 6 hours. The remaining columns contain data for TaSi₂ wafer surfaces from the following couples:

Column 4: W/TaSi₂, 2300°F for 6 hours.

Column 5: Re/TaSi₂, 2100°F for 7 hours.

Column 6: Mo/TaSi₂, 2100°F for 72 hours.

Column 7: Nb/TaSi₂, 2100°F for 72 hours.

and Column 8: Zr/TaSi₂, 2100°F for 7 hours.

Table IV-IV presents X-ray diffraction data for the Re silicides in a Re/TaSi₂ couple annealed for 7 hours at 2100°F. The six reflections listed in the ASTM File for ReSi₂ account for the strongest peaks, but the data in

the ASTM file does not contain any peaks of intensity lower than 50. The remaining peaks may be ReSi_2 or a lower Re silicide. By following the growth and shrinkage of peaks as a Re silicide zone was transversed in the manner which produced the concentration change profiles, it was deduced that only the last two triplets contained reflections for ReSi_2 . Therefore, it was assumed that the other peaks indicated the presence of Re_5Si_3 , since none of the other Re silicides listed in the ASTM file matched the results. Knapton (44) reported this compound as being tetragonal with $a = \sim 9.53$ and $c = \sim 4.81$; but using these parameters did not yield appropriate d values. A value for $a = 8.81$ was calculated for the lattice parameter from the X-ray data. Because only two of the peaks were accounted for using an l value not zero, the c parameter could not be checked and was taken as that reported by Knapton. The d values calculated using the lattice parameters $a = 8.81$, $c = 4.81$ and the values for h , k , l are shown in the last two columns of the table. All of the remaining peaks are accounted for in this manner. It may also be inferred that the compound is not Re_3Si since this compound has a cubic structure.

Tables IV-V, IV-VI and IV-VII list some X-ray diffraction data for the Zr/TaSi_2 system. In Table IV-V, the two types of patterns formed on the film strip are

separated. The full arcs were identified as Zr_3Si from the ASTM file and the spotty arcs as α Zr, whose lattice has been distorted by the solid solution of silicon. Some of the peaks for Zr_3Si and Zr_2Si appear in Tables IV-VI and IV-VII for Zr/TaSi₂ couples annealed for four hours at 2100°F and 2500°F respectively, but positive identification was impossible. The data shown in these tables are an example of the type of results obtained for the Zr silicide zones as well as the manner in which the data, which later yielded CCP plots, were recorded.

B. Calculation of Depth of Penetration

The contribution of zones beneath the primary zone to the diffraction of X-rays may be estimated by calculating the depth of penetration of the X-rays in the different materials. This depth may be computed from the equation given in Cullity (38).

$$G_x = (1 - e^{-2\mu x / \sin\theta})$$

where G_x is the fraction of total intensity contributed by a surface layer of depth x , μ is the absorption coefficient and θ is the angle of refraction. Absorption coefficients are listed in tables as $\frac{\mu}{\rho}$ for most metals and the values for compounds can be calculated from the relationship

$$\frac{\mu}{\rho} = w_1 \left(\frac{\mu}{\rho} \right)_1 + w_2 \left(\frac{\mu}{\rho} \right)_2$$

where w_1 and w_2 are the weight fraction of component 1 and 2 respectively in the compound and ρ is the density. There-

fore, the thickness of the layer contributing to 95% of the total intensity can be calculated for the metals and their silicides below by setting $G_x = 0.95$. θ may be taken to be 20° , since most of the characteristic peaks are in the range $2\theta = 35^\circ$ to 45° .

Material	μ	X (to absorb 95% of X-rays)		% X-rays re- fracted through a 0.3 mil layer
		mils	microns	
Ta	2720	0.2	5	1.6
W	3300	0.2	5	0.7
Zr	930	0.6	15	24
Ti	918	0.7	17	25
TaSi ₂	1250	0.5	12	15
Ta ₅ Si ₃	1950	0.3	8	5
W ₅ Si ₃	1980	0.3	8	5
ZrSi ₂	550	1.1	27	43
TiSi ₂	554	1.1	27	43
Ti ₅ Si ₃	708	0.8	20	34

From the table above, it may be seen that 0.3 mils of Ta₅Si₃ will effectively allow only 5% of the X-rays passing through it to be refracted from a lower layer. To be as effective, it would take more than 1 mil of TiSi₂ or ZrSi₂. It may also be seen that whereas 5% of the X-rays passing through a 0.3 mil layer of Ta₅Si₃ or W₅Si₃ will contribute to the total intensity of the refracted beam, 43% of the total intensity would be refracted from a layer the same distance below a TiSi₂ or ZrSi₂ layer.

TABLE IV-I
X-RAY ANALYSIS OF GOOD TaSi₂ WAFERS AT DIFFERENT STAGES
OF FABRICATION

Fresh Pressed			Presintered			Final Wafer			ASTM (TaSi ₂)	
d	I	I/I ₁	d	I	I/I ₁	d	I	I/I ₁	d	I/I ₁
4.13	19	17	4.13	18	16	4.147	-	-	4.13	22
3.50	111	100	3.498	114	100	3.504	81	100	3.50	100
2.57	47	42	2.57	45	39	2.574	40	49	2.57	58
2.390	11	10	2.389	14	12	2.390	11	14	2.389	17
2.246	71	64	2.246	71	62	2.247	57	70	2.246	94
2.188	25	23	2.188	28	25	2.189	16	20	2.187	32
2.069	28	25	2.069	29	26	2.071	22	27	2.070	36
1.932	49	44	1.932	52	46	1.933	39	48	1.932	63
1.614	5	5	1.614	6	5	1.615	6	7	1.615	10
1.565	2	2	1.566	3	3	1.564	2	2	1.565	6
1.526	10	10	1.525	10	9	1.527	8	10	1.525	21
1.523	16	14	1.522	18	16	1.523	15	19	1.523	27
1.504	15	13	1.504	15	13	1.505	11	14	1.505	24
1.412	9	8	1.413	10	9	1.413	8	10	1.413	17
1.380	2	2	1.380	2	2	1.380	2	2	1.380	4
1.353	13	12	1.353	12	11	1.355	11	14	1.353	21
1.351	16	14	1.351	17	15	1.351	12	15	1.351	25
									Strong Ta ₅ Si ₃ (h)	
3.218	1					3.218	1		3.21	50
						3.025	2		3.02	70
						2.437	2		2.44	70
									2.41	70
						2.206	6*		2.21	100
						2.153	1.5		2.15	50
2.13	<1					2.126	3		2.13	100
						1.520	6*		1.52	70
1.409	5*		1.409	2*		1.410	5*		1.48	50B
									1.41	70
* enhanced by TaSi ₂ peaks										

TABLE IV-II

X-RAY ANALYSIS OF TaSi₂ SURFACES AFTER SINTERING

Good Wafer			Porous Wafer (Sintered at Higher Temp)									ASTM (t-Ta ₅ Si ₃)	
			Top Surface			Bottom Surface			Resintered (Top)				
d	I	I/I ₁	d	I	I/I ₁	d	I	I/I ₁	d	I	I/I ₁	d	I/I ₁
3.616	6	10	3.63	4	14	3.624	2-	16	3.63	8+	12	3.63	30
3.229	<2	3	—	—	—	3.241	1+	9	3.245	2	3	3.256	10
2.969	62	105	2.968	18	67	2.966	1+	9	2.972	19+	28	2.956	20
2.846	9	15	2.860	5	18	2.848	1+	9	2.853	9+	13	2.862	40
2.816	17	29	2.824	8	30	2.819	4	33	2.823	21	31	2.816	70
2.493	31	53	2.494	12	44	2.493	5	42	2.494	16	24	2.490	50
2.340	59	100	2.323	27	100	2.340	12+	100	2.344	67	100	2.340	100
2.292	4	7	2.301	4	15	2.295	1+	9	2.301	5+	8	2.305	30
2.193	29	49	2.193	18	67	2.192	3	25	2.194	21	31	2.192	60
2.13	<2	3	—	—	—	—	—	—	—	—	—	2.132	10
2.051	13	22	2.057	7	26	2.056	4-	33	2.057	19	28	2.054	70
1.983	>100	200	1.983	37	137	1.980	2+	17	1.981	28	42	1.978	40
—	—	—	—	—	—	1.951	6	50	—	—	—	1.948	10
1.691	2+	4	1.693	1	4	—	—	—	1.692	2-	3	1.693	10
—	—	—	1.628	2	7	—	—	—	1.627	3	4	1.629	10D
1.561	4	7	1.564	2+	8	1.563	1	8	1.566	3+	5	1.565	60
1.531	2	3	1.532	1	4	—	—	—	1.534	2	3	1.533	40
1.519	1	2	—	—	—	—	—	—	—	—	—	1.521	35
1.488	18	30	1.485	6	22	—	—	—	1.485	5+	8	1.484	50
1.467	20	34	1.468	20	74	1.464	3+	25	1.466	26	39	1.467	80
1.452	2	3	—	—	—	1.454	1+	9	1.455	2+	3	1.455	50
1.428	11	19	1.427	9	33	1.427	6	50	1.427	13+	20	1.428	70
D1.414	2	3	—	—	—	—	—	—	—	—	—	1.413	30
1.361	4	7	1.362	2+	8	1.361	1	8	1.363	6	9	1.363	70
+1 unknown			+18 unknown			+7 unknown			+2 unknown				

TABLE IV-III

X-RAY ANALYSIS OF Ta₅Si₃ ZONES NEAR THE ORIGINAL INTERFACE
IN DIFFERENT M/TaSi₂ COUPLES

ASTM		Ta Side(Ta/TaSi ₂)			TaSi ₂ Side(Ta/TaSi ₂)			TaSi ₂ Side(W/TaSi ₂)		
d	I/I ₁	d	I	I/I ₁	d	I	I/I ₁	d	I	I/I ₁
<u>t-Ta₅Si₃</u>										
3.63	30	3.627	10	18	3.642	11	16	3.624	7	11
3.256	10	3.245	8	14	3.25	2	3	3.245	3	5
2.956	20	—	—	—	2.975	5	7	2.965	4	6
2.862	40	2.848	20	35	2.856	13	18	2.846	9	14
2.816	70	2.822	66	116	2.830	26	37	2.821	22	35
2.490	50	2.493	3	5	2.499	17	24	2.491	13	21
2.340	100	D2.342	57	100	2.348	71	100	2.342	63	100
2.305	30	2.299	19	33	2.302	6	8	2.296	5	8
2.192	60	2.194	7	12	D2.196	20	28	2.191	21	33
2.132	10	—	—	—	2.128*	4	6	2.133*	7	11
2.054	70	2.056	80	140	D2.060	23	32	2.056	23	37
1.978	40	B1.98	1	2	1.984	8	11	1.979	8.5	13
1.948	10	B1.95	1	2	—	—	—	1.931	1	2
1.693	10	—	—	—	—	—	—	1.686	1	2
1.629	10D	1.623*	3	5	—	—	—	—	—	—
1.565	60	1.564	15	26	1.566*	6	8	1.564*	4.5	7
1.533	40	1.533	7	12	D1.53	2.5	4	1.533	2.5	4
1.521	35	—	—	—	D1.524*	8	11	1.516*	1.5	2
1.484	50	1.485	3	5	D1.48*	2	3	1.485*	3	5
1.467	80	1.466	20	35	D1.466	14	20	D1.465	15	24
1.455	50	1.456	6	11	1.46	2	3	1.455	3	5
1.428	70	1.423	7	12	D1.428*	10	14	1.427*	10	16
1.413	30	1.414*	1	2	D1.414*	5	7	D1.411*	3	5
1.363	70	1.363	7	12	D1.363	5	7	1.363	6	10
1.353	20	—	—	—	D1.355*	4	6	—	—	—
<u>h-Ta₅Si₃</u>										
3.68	40	—	—	—	—	—	—	—	—	—
3.21	50	—	—	—	D3.22	3	33	3.220	4	40
3.02	70	3.029	1	50	3.027	5	56	3.023	5	50
2.60	30	2.58	1	50	2.6	1.5	17	2.593	1.5	15
2.44	70	—	—	—	2.44	4	44	2.438	6	60
2.41	70	2.415	2	100	D2.40	3	33	2.409	5	50
2.21	100	2.25	1	50	2.209	9	100	2.209	10	100
2.15	50	—	—	—	2.15	3	33	2.153	10	100
2.13	100	2.13	2	100	2.128*	4	44	2.133	7	70
1.87	20	—	—	—	—	—	—	—	—	—

(continued)

TABLE IV-III (Continued)

h-Ta ₅ Si ₂ (Continued)														
			TaSi ₂ Side (Re/TaSi ₂)			TaSi ₂ Side (Mo/TaSi ₂)			TaSi ₂ Side (Nb/TaSi ₂)			TaSi ₂ Side (Zr/TaSi ₂)		
d	I	I/I ₁	d	I	I/I ₁	d	I	I/I ₁	d	I	I/I ₁	d	I	I/I ₁
1.67	20	—	—	—	—	—	—	—	—	—	—	—	—	—
1.62	30	—	1.623*	3	150	1.616	2.5	28	—	—	—	—	—	—
1.57	40	—	—	—	—	1.566*	6	67	1.564*	4.5	45	—	—	—
1.48	50B	—	—	—	—	D1.48*	2	22	1.485*	3	30	—	—	—
1.43	40	—	—	—	—	D1.428*	10	110	1.427*	10	100	—	—	—
1.41	70	—	1.414*	2	100	D1.414*	5	56	D1.411*	3	30	—	—	—
1.38	50	—	—	—	—	—	—	—	—	—	—	—	—	—
1.52	70	—	—	—	—	D1.524*	8	89	1.516*	1.5	15	—	—	—
Unidentified peaks →			2.58 [2]				2.695 [2]				2.564 [2]			
			2.521 [4]				2.26 [3]				2.520 [2]			
			2.415 [2]				2.17 [1]							

TaSi ₂ Side (Re/TaSi ₂)			TaSi ₂ Side (Mo/TaSi ₂)			TaSi ₂ Side (Nb/TaSi ₂)			TaSi ₂ Side (Zr/TaSi ₂)		
d	I	I/I ₁	d	I	I/I ₁	d	I	I/I ₁	d	I	I/I ₁
3.624	4	11	3.636	8	11	3.641	4	12	3.623	3	10
3.248	2	5	3.241	4	5	—	—	—	3.241	1	3
2.966	3	8	2.968	5	7	2.966	2	6	2.966	4	13
2.848	7	18	2.855	11	15	2.854	4	12	2.851	4	13
2.822	15	39	2.829	24	32	2.826	9	28	2.823	10	32
2.493	12	32	2.499	15	20	2.494	6	19	2.493	8	26
2.342	38	100	2.348	75	100	2.345	32	100	2.341	31	100
2.296	4	11	2.302	6	8	2.299	2	6	2.297	2.5	8
2.191	12	32	2.194	23	31	2.195	10	31	2.190	9	29
2.136*	5	13	2.135*	5	7	—	—	—	2.140	2	6
2.056	17	45	2.061	24	32	2.057	9	28	2.056	13	42
1.979	6	16	1.982	12	16	1.982	5	16	1.977	6	19
—	—	—	1.943	1	1	—	—	—	—	—	—
—	—	—	1.694	1	1	—	—	—	—	—	—
1.625*	1	3	B1.625*	1	1	—	—	—	—	—	—
1.564	4	11	1.566	7	9	1.565	3	9	1.564	3	10
1.534	2	5	1.536	3	4	—	—	—	B1.534	2	6
1.529	3	8	B1.518*	1	1	1.518*	2	6	—	—	—
1.485	2	5	1.487	4	5	1.483*	1.5	5	1.485	2	6
1.466	11	29	D1.466	21	28	1.467	6	19	D1.464	10	32
1.455	2	5	1.456	3	4	—	—	—	1.454	1	3
1.427	7	18	1.428	14	19	1.428*	5	16	D1.427	7	23
1.413*	2	5	1.414*	2	3	1.413*	5	16	—	—	—
D1.362	4	11	D1.363	9	12	1.363	2	6	D1.362	5	16

(continued)

TABLE IV-III (Continued)

hex. Ta ₅ Si ₂									
3.238*	2	50	—	—	—	3.223	2	29	Barely
3.025	3	75	3.025	4	50	3.025	3	43	
B2.605	1	25	2.597	3	37	2.597	1.5	22	
2.442	2	50	2.447	4	50	2.440	3	43	
2.415	4	100	2.415	3	37	2.409	2.5	36	
B2.210	4	100	2.215	8	100	2.205	7	100	
2.152	3	75	2.156	17	212	2.158	8	114	
2.136*	5	125	2.135*	5	63	2.130	4	57	
—	—	—	—	—	—	—	—	—	
—	—	—	—	—	—	—	—	—	
1.625*	1	25	B1.625	1-	12	—	—	—	Discernible
1.569*	2	50	1.569	3	37	1.570	1	14	
1.518*	1+	25	B1.518*	1-	12	1.581*	2	29	
1.481*	1-	25	1.483*	1.5	19	1.483*	1.5	22	
—	—	—	—	—	—	1.428*	5	71	
1.413*	2	50	1.414*	2	25	1.409*	2.5	36	
1.376	2	50	—	—	—	—	—	—	
—	—	—	—	—	—	—	—	—	
—	—	—	—	—	—	—	—	—	
—	—	—	—	—	—	—	—	—	
2.562 [2]			3.948 [2] 2.569 [7] 2.800 [7] 2.288 [9] 2.696 [2] 2.260 [2] 2.597 [3] 1.321 [3]			3.191 [3] 2.300 [3] 2.794 [3] 2.258 [7] 2.688 [7] 2.034 [3] 2.552 [6] + 7 more			2.673 [4] 1.872 [10]

TABLE IV-IV

X-RAY ANALYSIS OF THE Re SIDE OF A Re/TaSi₂ COUPLE
ANNEALED AT 2100°F FOR 7 HOURS

2θ	I	d	ASTM I/I, d	$d = \frac{8.81}{\sqrt{h^2+k^2+3.43l^2}}$	h, k, l
23.16	35	3.837	ReSi ₂ 100 3.82		
27.86	2	3.12		3.12	220
30.88	100	2.893	ReSi ₂ 100 2.90		
33.7	1	2.66		2.60	221
35.2	2	2.55		2.444	320
36.66	1	2.449		2.223	112
40.44	11	2.229		2.21	400
40.74	65	2.213}	ReSi ₂ 100 2.21		
40.86	34	2.207}		2.138	410
42.14	2	2.143}			
42.22	2	2.139}			
45.72	51	1.983	ReSi ₂ 50 1.97		
47.34	32	1.919	ReSi ₂ 50 1.915		
58.84	17	1.568}	ReSi ₂ 100 1.56		
59.00	10	1.564}		1.56	440
59.14	16	1.561}			
59.32	8	1.557}			
64.10	11	1.452}		1.448	610
64.32	13	1.447}	ReSi ₂ (?)		
64.50	7	1.444}			
67.91	16	1.380}		1.377	540
68.14	18	1.375}	ReSi ₂ (?)		
68.32	5	1.372}			

TABLE IV-V

RESULTS OF X-RAY ANALYSIS ON A POWDER SAMPLE
 REMOVED FROM THE SURFACE OF A Zr WAFER
 AFTER ANNEALING AGAINST TaSi₂ FOR 72 HOURS AT 2100°F

Phase I (Full Arcs)			Phase II (Spctty Arcs)		
d	I	ASTM Zr ₃ Si (24% Si)	d	I	ASTM αZr
3.508	VW	3.506 [40]	2.823	S	2.798 [33]
2.979	M	2.965 [40]	2.468	S	2.459 [100]
2.553	VS	2.551 [100]	1.912	M	1.894 [17]
2.468	M	2.460 [70]	1.628	M	1.616 [17]
2.062	S	2.060 [40]	1.475	M	1.463 [18]
1.875	M	1.882 [40]	1.380	S	1.399 [3]
		1.866 [60]			1.368 [18]
1.585	W	1.582 [100]	1.375	S	1.350 [12]
1.525	VVW		1.294	W	1.287 [4]
1.494	M	1.489 [100]	1.237	W	1.230 [4]
1.308	W	1.322 [70]	1.093	M	1.084 [4]
1.213	VVW		1.046	M	1.036 [6]
1.178	M	1.174 [100]	1.018	M	1.006 [3]
1.117	W		0.984	M	0.978 [2]
1.080	W	further d	0.975	W	0.966 [4]
1.018	W	values not	0.938	W	0.933 [3]
0.995	VVW	listed on	0.910	MB	0.900 [5]
0.958	VVW	card.	0.884	MB	0.877 [3]
0.938	W		0.814	WB	0.820 [2]
0.878	M(VB)				
0.839	M(B)				
0.808	W(VB)				
0.795	M(VVB)				

Substitution of a smaller atom (such as Si) into Zr lattice would cause d values to be shifted up.

TABLE IV-VI

X-RAY DATA FOR THE Zr SIDE OF A
Zr/TaSi₂ COUPLE ANNEALED AT 2100°F.

+0.0 mil		+0.4 mil		+0.5 mil		+0.8 mil	
2θ	I	2θ	I	2θ	I	2θ	I
31.65	4	31.6	4	31.7	4	31.76	4
32.05	69	32.05	28	32.08	14	32.02	12
33.6	2.5	_____	_____	_____	_____	_____	_____
34.9	4.5	35.0	13	35.0	13	34.9	19
37.1	1	36.57	19	36.6	19	36.6	28
38.8	2	_____	_____	38.6	2	_____	_____
39.6	1	40.3	2B	_____	_____	_____	_____
44.1	1	_____	_____	_____	_____	_____	_____
45.7	1	_____	_____	_____	_____	_____	_____
48.1	1	48.0	2	48.1	3.5	48.1-48.2	5B
_____	_____	50.0	1	_____	_____	_____	_____
54.57	1.5	_____	_____	_____	_____	_____	_____
57.0	3	56.92	15	57.1	10	57.0	10
57.4	2	_____	_____	_____	_____	_____	_____
60.9	2	_____	_____	_____	_____	_____	_____
62.3	4	_____	_____	_____	_____	_____	_____
62.63	3	D62.5	3	_____	_____	_____	_____
63.64	61	63.58	37	63.58	14	63.6	27
66.9	7	66.8	6	66.9	3	66.9	4
68.8	2B	68.37	6	68.5	4	68.5	7B

TABLE IV-VII

X-RAY DATA FOR THE Zr SIDE OF A Zr/TaSi₂ COUPLE
ANNEALED AT 2500°F.

+ 0.0 mil		+ 0.5 mil		+ 1.0 mil		+ 1.4 mil		+ 2.1 mil		+ 2.5 mil	
2θ	I	2θ	I	2θ	I	2θ	I	2θ	I	2θ	I
<p>Note: at ~ 27.4° background jumps from 14 to 19</p>											
29.16	21	29.12	7	29.5	3	29.55	3	—	—	—	—
30.02	10	30.02	10	30.05	5	30.6	5	30.3	1	—	—
31.9	16	32.08	13	32.1	10	32.1	12	32.0	10	32.0	11
33.7	5	33.64	14	33.6	43	33.55	372	33.6	90	33.6	2
35.08	10	35	3B	35.03	4.5	35.0	10	34.96	10	35.0	14
36.4	15	36.5	6	36.5	6	36.65	16	36.56	27	36.6	31
—	—	39.05	2	39.0	2	—	—	—	—	—	—
43.8	26	43.75	5.5	43.75	1B	—	—	—	—	—	—
—	—	—	—	—	—	48.06	5	48.0	5	48.0	6
48.2	11	48.27	7	—	—	—	—	—	—	—	—
48.65	39	48.63	79	48.67	100	—	—	—	—	—	—
—	—	—	—	56.95	3	56.9	8	57.0	8	57.0	9
57.7	5	—	—	—	—	—	—	—	—	—	—
59.35	7	59.2	3	—	—	—	—	—	—	—	—
60.1	2	—	—	—	—	—	—	—	—	—	—
60.55	3	—	—	60.7	2	—	—	—	—	—	—
61.22	8	61.27	4.5	61.3	5	—	—	61.3	3	—	—
61.77	19	—	—	—	—	—	—	—	—	—	—
—	—	62.04	4	62.0	3	—	—	—	—	—	—
63.6	13	63.58	65	63.6	90	63.56	136	63.6	114	63.6	15
—	—	—	—	64.7	3	—	—	—	—	—	—
66.4	2	—	—	—	—	—	—	—	—	—	—
66.9	3	—	—	—	—	—	—	66.7	2	—	—
68.58	296	68.57	308	68.58	264	68.52	100	68.5	61	68.5	5B
70.35	2	70.37	5	70.38	16	70.35	63	70.35	12	—	—
71.24	11	—	—	—	—	—	—	—	—	All peaks above fit ASTM Zr but 33.6°	

APPENDIX V

PLAN FOR THE STATISTICAL ANALYSIS
OF THE DATA

Page 195 follows

The data in this work may be analyzed statistically by linearizing the equations expressing the time and temperature dependencies of the thickness measurements:

$$(\Delta x)^2 = k_0 t \text{ or } (\Delta x)^2 = k_s t + b$$

and $(\Delta x)^2/t = k = k^0 e^{-Q/RT}$.

The general linear equation is

$$Y_{ij} = A_2 + A_1 X_j.$$

In the first form of the parabolic rate equation A_2 is assumed equal to zero and, therefore, $Y_{ij} = (\Delta x)^2$,

$A_1 = k_0$ and $X_j = t$. In the second form, $A_1 = k_s$ and $A_2 = b$, where b must be negative to have physical significance. The

temperature dependence of the Arrhenius form may be linearized by letting $Y_{ij} = \ln (\Delta x)^2/t$, $A_2 = \ln k^0$, $A_1 = -Q/R$

and $X_j = 1/T$. Therefore, once the measured data (Δx) has been operated on to linearize the time and temperature re-

lationships, a least-squares analysis may be easily performed on the data. This analysis will yield parabolic rate con-

stants, k_0 and k_s , and an incubation period, b (when significant), when operating on $Y_{ij} = (\Delta x)^2$ and $X_j = t$; and

the activation energy, Q , and pre-exponential constant, k^0 , when operating on $Y_{ij} = \ln (\Delta x)^2/t$ and $X_j = 1/T$.

The following scheme has been prepared using equations presented in Hicks (47) and from private consultation with Professor C. Anderson (48) of the Mechanical Engineering Department, The City College of New York.

A. Least Squares Analysis

1. A_1 , assuming $A_2 = 0$

$$a) \quad \bar{X} = \frac{\sum_j n_j X_j}{\sum_j n_j}$$

where n_j = number of Y values at each X.

$$b) \quad \bar{Y} = \frac{\sum_j \sum_{ij} Y_{ij}}{\sum_j n_j}$$

$$c) \quad A_1 = \bar{Y}/\bar{X}$$

2. A_1 and A_2

$$a) \quad A_1 = \frac{\sum_j \sum_{ij} (X_j - \bar{X}) Y_{ij}}{\sum_j (X_j - \bar{X})^2}$$

$$b) \quad A_2 = \bar{Y} - A_1 \bar{X}$$

3. Variance, s .

$$s^2 = \frac{\sum_j \sum_{ij} [Y_{ij} - (A_2 + A_1 X_j)]^2}{\sum_j n_j - 2}$$

4. Confidence Intervals, C.I.

a) for A_1 :

$$C.I. = \frac{s}{\sqrt{\sum_j (X_j - \bar{X})^2}} t_{\alpha/2, N-2}$$

b) for A_2 :

$$C.I. = st_{\alpha/2, N-2} \sqrt{\frac{1}{\sum_j n_j} + \frac{\bar{X}^2}{\sum_j (X_j - \bar{X})^2}}$$

in which t is a variable of the form $t = Z/\sqrt{\chi^2/\nu}$ which

relates the unit normal variable, Z , to the χ^2 variable of ν degrees of freedom and $N = \sum_j n_j$. t 's are listed in tables as a function of N and the probability level α . For a 95% confidence interval $\alpha = 0.05$.

B. Departure from Linearity

1. Linear Regression (Sum of Squares)

$$L.R. = A_1^2 \sum_j n_j (X_j - \bar{X})^2$$

2. Departure from Linearity (Sum of Squares)

a) $Y_{.j} = \sum_i Y_{ij}$

b) $\bar{Y}_{.j} = Y_{.j}/n_j$

c) $D.L. = \sum_j n_j [\bar{Y}_{.j} - \bar{Y} - b_1 (X_j - \bar{X})]^2$

3. Residual (Sum of Squares)

$$R = \sum_{ij} (Y_{ij} - \bar{Y}_{.j})^2$$

4. Mean Squares

a) $MS_L = L.R.$

b) $MS_D = D.L./q-2$

where $q =$ number of j levels.

c) $MS_R = R/\sum_j n_j - q$

5. F tests

F is a variable relating the χ^2 variables and degrees of freedom, ν , by

$$F = \frac{\chi_1^2/\nu_1}{\chi_2^2/\nu_2}$$

F values are listed in tables as a function of ν_1 , ν_2 and a probability level, which is taken as 0.05.

$$a) \quad F_L = \frac{MS_L}{MS_R}$$

$$b) \quad F_D = \frac{MS_D}{MS_R}$$

If F_L or F_D are larger than $F_{\nu_1, \nu_2, \alpha}$ from the table, the linear factor or higher order factor respectively is significant. When both F_L and F_D are significant, a ratio, C_{test} , may be formed indicating the relative significance of the linear factor.

$$C_{test} = \frac{F_L}{F_L + F_D}$$

The closer C_{test} is to unity, the higher the relative significance of the linear factor and, therefore, the closer is the behavior of the data to the theoretical behavior expressed by the equations.

BIBLIOGRAPHY

1. G. V. Samsonov: "Silicides and Their Uses in Engineering", 1959. Translation AFSC FTD-TT-61-409, 1962.
2. L. S. Castleman: "An Analytical Approach to the Diffusion Bonding Problem", Nucl. Sci. and Eng., 4, 209 (1958).
3. G. V. Kidson: "Some Aspects of Growth of Diffusion Layers in Binary Systems", J. Nuclear Mat., 3(1), 21 (1961).
4. L. S. Darken: "Diffusion, Mobility and Their Interrelation Through Free Energy in Binary Metallic Systems", Trans. AIME, 175, 184 (1949).
5. A. C. Smigelskas and E. O. Kirkendall: "Zinc Diffusion in Alpha Brass", Trans. AIME, 171, 130 (1947).
6. M. M. F. Janssen and G. D. Rieck: "Reaction Diffusion and Kirkendall Effect in the Ni-Al System", Trans. Met. Soc. AIME, 239, 1372 (1967).
7. G. B. Gibbs: "Diffusion Layer Growth in a Binary System", J. Nuclear Mat., 20, 303 (1966).
8. U. Roy: "Phase Boundary Motion and Polyphase Diffusion in Binary Metal - Interstitial Systems", Acta Met., 16, 243 (1968).
9. R. Resnick, R. Steinitz and L. Seigle: "Determination of the Diffusivity of C in Ta and Cb Carbides by Layer-Growth Measurements", Trans. Met. Soc. AIME, 233, 1915 (1965).
10. G. Kimmel, A. Bar-or and A. Rosen: "Interdiffusion Between Ni and U", Trans. ASM, 61, 703 (1968).
11. B. N. Arzamasov: "Determination of the Diffusion Reaction Coefficient", Met. Term. Ob. Metallov, 3, 49 (1967).
12. C. Wagner: "The Evaluation of Data Obtained with Diffusion Couples of Binary Single-phase and Multiphase Systems", Acta Met., 17, 99 (1969).
13. C. E. Birchenall: "Mechanisms of Diffusion in the Solid State", Met. Reviews, 3(11), 235 (1958).

14. H. A. Domian and H. I. Aaronson: "Simultaneous Diffusion of Ag and Mg in B-AgMg", Chapter 14 in "Diffusion in Body-Centered Cubic Metals, ASM, Metals Park, Ohio, 1965.
15. L. V. Azaroff: "The Role of Crystal Structure in Diffusion", J. Appl. Phys., 32, 1658 (1961).
16. P. Wynblatt: "Diffusion Mechanisms in Ordered Body-Centered Cubic Alloys", Acta Met., 15, 1453 (1967).
17. W. C. Hagel: "Diffusion in Intermetallic Compounds", G.E. Res. Lab. Report No. 63-RL-3320 M (1963).
18. N. S. Gorbunov: "Diffuse Coatings on Iron and Steel", The Academy of Sciences of the U.S.S.R., Moscow, 1958.
19. A. D. LeClaire: "Application of Diffusion Theory to BCC Structures", Chapter 1 in "Diffusion in Body-Centered Cubic Metals", ASM, Metals Park, Ohio, 1965.
- 19a. C. S. Hartley, J. E. Steedly and L. D. Parsons: "Binary Interdiffusion in BCC Transition Metal Systems", Chapter 4 in "Diffusion in Body-centered Cubic Metals", ASM, Metals Park, Ohio, 1965.
20. O. B. Sherby and M. T. Simnad: "Prediction of Atomic Mobility in Metallic Systems", Trans. ASM, 54, 227 (1961).
21. W. Jost: "Diffusion in Solids, Liquids and Gases", Academic Press, New York, 1952.
22. J. Crank: "Mathematics of Diffusion", Oxford University Press, Fairlawn, N.J., 1956.
23. R. M. Barrer: "Diffusion In and Through Solids", Cambridge Press, Cambridge, Mass., 1951.
24. R. W. Bartlett: "Kinetics of Ta₅Si₃ and Cb₅Si₃ (Growth in Disilicide Coatings on Ta and Cb)", Trans. Met. Soc. AIME, 236, 1230 (1966).
25. H. W. Lavendel and A. C. Elliot: "Investigation of Modified Silicide Coatings for Refractory Metal Alloys with Improved Low-Pressure Oxidation Behavior", AFML-TR-65-344 (1965).

26. D. M. Koffman and R. E. Ogilvie: "Diffusion Studies in the Co-Si and W-Si Binary Systems", AFML-TR-65-34 (1965).
27. R. W. Bartlett, P. R. Gage and P. A. Larssen: "Growth Kinetics of Intermediate Silicides in the MoSi₂/Mo and WSi₂/W Systems", Trans. Met. Soc. AIME, 230, 1528 (1964).
28. P. R. Gage and R. W. Bartlett: "Diffusion Kinetics Affecting the Formation of Silicide Coatings on Mo and W", Trans. Met. Soc. AIME, 233, 832 (1965).
29. Norikazu Hashimoto: "Kinetics of WSi₂ Growth on Si", Trans. Met. Soc. AIME, 239, 1109 (1967).
30. G. V. Samsonov, et.al.: "Diffusion of Si in Ti, Ta, Mo and Fe", Dop. Akad. Nauk Ukr SSR, 1, (1959). Translation FTD-TT-63-262 (1963).
31. E. M. Passmore, J. E. Boyd, L. F. Neal, C. A. Anderson and B. S. Lement: "Investigation of Diffusion Barriers for Refractory Metals", WADD T.R. 60-343 (1960).
32. E. M. Passmore, J. E. Boyd and B. S. Lement: "Investigation of Diffusion Barriers for Refractory Metals", ASD-TDR-62-432 (1962).
33. "Powder Diffraction File", Compiled by the Joint Committee on Powder Diffraction Standards, American Society for Testing and Materials.
34. H. Nowotny, H. Schachner, R. Kiefer and F. Benesovsky: Monatsh. Chem., 84, 1 (1953).
35. A. G. Knapton: Nature, 175, 730 (1955).
36. E. Parthé, H. Nowotny and H. Schmid: Monatsh. Chem., 86, 385 (1955).
37. E. Parthé, B. Lux and H. Nowotny: Monatsh. Chem., 86, 459 (1955).
38. B. D. Cullaby: "Elements of X-ray Diffraction", Addison-Wesley Pub. Co., Mass., 1956.
39. S. I. Alyamovskii, P. V. Gel'd, F. P. Shveikin and I. I. Matveenko: "Lower Silicide of Nb, Nb₃Si", Izv. Akad. Nauk SSSR, Neorg. Mat., 3(#4), 729 (1967).

40. E. Parthé, H. Schachner and H. Nowotny: Monatsh. Chem., 86, 182 (1955).
41. O. G. Karpinskii and B. A. Evseev: "Crystal Structure of the Compound Zr_5Si_4 ", Izv. Akad. Nauk SSSR, Neorg. Mat., 4 (#8), 1248⁴ (1968).
42. M. Hansen: "Constitution of Binary Alloys", Second Edition, McGraw Hill, N.Y., 1958.
43. P.T.B. Shaffer: "Handbook of High-Temperature Materials, No. 1: Materials Index", Plenum Press, N.Y., 1964.
44. A. G. Knapton: Plansee Proc., 3rd Seminar, 1958, 42 (1959).
45. S. Levine: "The Thermodynamics of Refractory Metal Silicides by an EMF Method", Doctoral Dissertation, The City University of New York, 1969.
46. M. Semchyshen and J. J. Harwood: "Refractory Metals and Alloys", Interscience Pub., N.Y., 1961.
47. C. R. Hicks: "Fundamental Concepts in the Design of Experiments", Holt, Rinehart and Winston, N.Y., 1964.
48. Private communication with Professor C. Anderson, Department of Mechanical Engineering, The City University of New York.
49. J. J. English: "Binary and Ternary Phase Diagrams of Columbian, Molybdenum, Tantalum and Tungsten", DMIC Report 152, 1961.